Carnegie Mellon University

CARNEGIE INSTITUTE OF TECHNOLOGY

THESIS

SUBMITTED IN PARTIAL FULFILLMENT OF THE REQUIREMENTS

FOR THE DEGREE OF Doctor of Philosophy

TITLE Biophysical Characterization of the Dynamic Regulation of Chromatin Structure and Rheology in Human Cell Nuclei

PRESENTED BY Stephen T. Spagnol

ACCEPTED BY THE DEPARTMENT OF

Chemical Engineering

KRIS NOEL DAHL	5/4/15
ADVISOR	DATE
LORENZ BIEGLER	5/4/15
DEPARTMENT HEAD	DATE

APPROVED BY THE COLLEGE COUNCIL

VIJAYAKUMAR BHAGAVATULA	5/4/15
DEAN	DATE

Biophysical Characterization of the Dynamic Regulation of Chromatin Structure and Rheology in Human Cell Nuclei

Submitted in partial fulfillment of the requirements for the degree of

Doctor of Philosophy

in

the Department of Chemical Engineering

Stephen T. Spagnol

B.S., Chemical Engineering, The Pennsylvania State University,
Schreyer Honors College

Carnegie Mellon University
Pittsburgh, PA

May, 2015

Acknowledgements

I would like to thank each of the members of the Dahl Laboratory for their technical and moral support during the course of my Ph.D. work.

In particular, I would like to thank the Senior Dahl Laboratory Members for their support at the early critical points during my graduate work:

Elizabeth A. Booth (Ph.D.) for her dedication to my success as well as training me and providing much of the critical groundwork for my Thesis project.

Agnieszka Kalinowski (M.D., Ph.D.) for never pulling any punches… ever… on any topic, technical or otherwise. It was a character-building exercise I will never forget and will always appreciate [in hindsight].

Peter Yaron (Ph.D.), our Postdoctoral Fellow when I entered the group, for his level-headed insight and support during my preparation for the Ph.D. Qualifying Exam. This was embodied in his refrain: “Keep it simple, stupid.”

Brian Holt (Ph.D.), the longest tenured senior Ph.D. student during my time here. He trained me in confocal and fluorescence lifetime imaging microscopy with his seemingly infinite knowledge on microscopy.

I would like to thank several Undergraduate Students in the Dahl Laboratory:

James Weltz (B.S., Carnegie Mellon and Ph.D. Candidate, University of Colorado Boulder) who was the first undergraduate who I had the pleasure of developing a project for and working with during my Thesis. He was a remarkable Undergraduate Researcher operating at the level of a graduate student and destined for great things (now a Ph.D. Candidate himself). I can only hope I had even the smallest hand in it.

Matt Biegler (B.S., Carnegie Mellon and Ph.D. Candidate, Duke University) and Kelli Coffey (B.S., Carnegie Mellon) who worked as Undergraduate Researchers for Agnieska Kalinowski, and with whom I had the pleasure of working alongside.

Last among members of the Dahl Laboratory, but certainly not least, the Junior Ph.D. Students:

Travis Armiger (Ph.D. Candidate, Carnegie Mellon), Stefanie Baker (Ph.D. Candidate, Carnegie Mellon) and Sarah Robb (Ph.D. Candidate, Carnegie Mellon). These three provided the Dahl Laboratory with some much needed enthusiasm and energy through organizing Dahl Group events and providing no small amount of support during the critical end of my Thesis work (including the best cupcakes I have ever had). Their technical feedback has been greatly appreciated. Their personal support during Thesis writing cannot be overstated. I

am confident that the Dahl Laboratory is left in the hands of great people – intellectually, professionally and personally. I hope to have at least bequeathed to these three some measure of perspective, guidance and insight that may help them going forward, though they would be successful just the same.

I would like to thank several close friends within the Department for their support over the years:

Patrick Boyer (Ph.D.), a fellow Dahl lab member, and John Goldman (Ph.D.) who entered the Ph.D. program with me. We made it through every step of the program together, and having their support as we went through this together enhanced this experience beyond words. Their support, as both colleagues and best friends, has made this an incredible experience. I would also like to thank John Riley (Ph.D. Candidate, Carnegie Mellon) and Ben Yezer (Ph.D. Candidate, Carnegie Mellon). Though they came a year after we started, they have been two of the best friends I could have asked for, despite Ben Yezer's insistence of being merely "likeable coworkers". I would like to thank several friends of mine who were already in the program when I arrived and imparted the great culture of this Department to us: Chris Wirth, Stacey Wirth, Ethan Demeter, Anita Lee, Matt Reichert, Sharon Vuong, Steve Istivan, Kaytlin Henry and Ben Murphy.

I would like to thank two faculty members from the Chemical Engineering Department:

Professor Lynn Walker for recruiting me into the program, inspiring my interest in polymers and rheology from her courses as well as providing me with vital personal, technical and professional insight throughout the course of my Thesis work.

Professor Kathryn Whitehead, who I met from her first visit as a faculty candidate and knew from the start she would be a perfect fit for this Department. Since arriving here, she has helped me immensely both personally and professionally, striving to make me a better communicator.

I would like to thank all of the members of this Department, including the students, *incredible* staff (Shannon Young, Janet Latini, Larry Hayhurst and Julie Tilton) and faculty who have made this the best learning experience I have ever had on every level. I would like to thank the Chemical Engineering Graduate Student Association for all that it does for this Department and providing me with so many opportunities to give back to it as President, Graduate Student Assembly Representative and through the Industrial Career Seminar. This Department has been very much a family to me, making it such a fun experience even during the toughest stretches of my Thesis work. If I could impart one final thought on to ChEGSA and the Department it is to remember, “A rising tide lifts all boats.” Work every day to make this a better place and you will reap the benefits of those

experiences all the more. From a Department that I gained so much from, I hope to always continue to return the favor.

Finally, I would like to thank my Thesis Advisor, Professor Kris Noel Dahl. She was my top pick as an Advisor before I even arrived, and without her none of this would have been possible. I have leaned on her immensely over the years as a Thesis Advisor and as an exceptional mentor. The wealth of technical expertise I gained from her is best evinced through the course of this Thesis, but unfortunately the true learning experiences I gained from her cannot be measured. However, I will carry them with me throughout my career and personal life, and I will be eternally grateful for having had such an amazing person to serve as my Advisor.

Beyond Carnegie Mellon University, I would like to thank my family for their strong support and encouragement over the years. In particular my Mother, Barbara; Stepfather, Scott; my twin Sister, Steph; and my Uncle Tommy. I have depended on them in more ways than I can count, and I am very grateful for all that they have done to help get me here.

I would like to acknowledge my Funding Sources for their support:
This research was supported the Achievement Rewards for College Scientists (ARCS) Foundation (Stephen T. Spagnol), Bertucci Fellowship (Stephen T. Spagnol), and James C. Meade Fellowship (Stephen T. Spagnol) as well as the NSF (NSF-CBET-0954421 and CMMI-1300476 to Kris Noel Dahl).

Doctoral Committee:

I would like to thank my Ph.D. Thesis Committee members in particular for their insight and feedback during the course of my work at Carnegie Mellon University. Their insight, both intellectual and professional, proved invaluable to my success as a doctoral student, and no doubt will do so over the course of my career.

Kris Noel Dahl, Ph.D.

Committee Chair

Associate Professor of Chemical Engineering and Biomedical Engineering, Carnegie Mellon University

Lynn M. Walker, Ph.D.

Professor of Chemical Engineering, Carnegie Mellon University

Kathryn A. Whitehead, Ph.D.

Assistant Professor of Chemical Engineering, Carnegie Mellon University

Yu-li Wang, Ph.D.

R. Mehrabian Professor and Head of the Department of Biomedical Engineering, Carnegie Mellon University

Tom Misteli, Ph.D.

Associate Director, Center for Cancer Research, National Cancer Institute, National Institutes of Health

Abstract

Out of the growing body of evidence demonstrating the role of higher-order chromatin organization within the nucleus in regulating the functions of the linear sequence of DNA emerges the genome as a physical entity. DNA packs into hierarchical levels of chromatin condensation, which then tailor accessibility to the linear sequence for nuclear processes while also serving as a central feature of nuclear organization. Further, varying condensation state alters the physical properties of the chromatin fiber. These may then exert or facilitate forces aiding in the spatial organization within the nucleus. Yet, this complex concept of nuclear structure even neglects the dynamic aspects of the genome continuously fluctuating and undergoing structural remodeling within the nucleus. Thus, while chromatin position within the nucleus is critical for biological functions including transcription, we must reconcile a particular position of a gene locus with the dynamic and physical nature of chromatin. Here we characterize the physical aspects of the genome associated with its dynamic properties that aid in regulation. We focus on developing techniques that measure the evolution of physical properties associated with nuclear processes. We leverage these techniques, capable of quantifying and spatially resolving its structural state within the nucleus and elucidating the underlying physics of its dynamics, to illuminate physical features associated with cellular processes. Specifically, we investigate the nuclear structural changes associated with growth factor stimulation on primary human cells known to impact large scale gene expression pathways. We also demonstrate dysfunction associated with these physical

mechanisms accompany disease pathologies. Thus, we unify the biological understanding of cellular processes within the context of physical features of genome structure, organization and dynamics that are critical to human health and disease.

Table of Contents

Acknowledgements ii

Abstract..... viii

Table of Contents x

List of Figures..... xvii

Chapter I: Introduction……..…….……1

Nuclear Organization of Genome Function…….2

Nuclear Structure and Mechanics are Implicated in Function……6

Chromatin Dynamics and the 4D Nature of Genome Function…….10

Stimulation and Gene Expression……..14

Disease and Dysfunction……15

Thesis Objectives……...17

References……..20

Chapter II: Spatially Resolved Quantification of Chromatin Condensation through Changes in Local Rheology in Cell Nuclei using Fluorescence Lifetime Imaging……..25

Introduction……...…….25

Materials and Methods……..…….29

Cell Culture and Transfection……29

Drug Treatments……30

Cell Fixation and Staining….……30

Preparation of DNA *in vitro* Solutions……..31

Fluorescence Lifetime Imaging Microscopy…….31

Statistics…….33

Results……33

Differential Fluorescence Lifetime in Human Cell Nuclei……33

Fluorescence Lifetime Sensitivity of λ-DNA Condensation…….39

Spatially-Resolved *in situ* Chromatin Condensation State……45

Discussion……..……49

Physical Effectors Influencing the Fluorescence Lifetime Dependence of Chromatin Condensation State *in situ* and *in vitro*…….…...50

FLIM to Measure Chromatin Structure and Mechanics *in situ*….54

Acknowledgements……57

References……..……57

Chapter III: Active Cytoskeletal Forces and Chromatin Condensation Independently Modulate Chromatin Fluctuations……...…60

Introduction……...……60

Materials and Methods……..……62

Cell Culture and Transfection……62

Drug Treatments……63

Particle Tracking and Image Analysis...……63

Cell Fixation and Fluorescence Microscopy……..65

Statistics……66

Results……66

Different Bound Nuclear Probes Reveal Similar Chromatin Fluctuations…….....……66

MSD Prefactor is Impacted Primarily by Chromatin Condensation……..69

MSD Diffusive Exponent is Impacted by Force Propagation…...70

ATP Depletion: Loss of Motors and Chromatin Hypercondensation……74

Discussion……..……75

Particle Tracking Using Network-Bound Probes in the Nucleus……..75

Nuclear Viscoelasticity from Particle Tracking…….....….76

Nuclear Fluctuations and Mechanics of the Nuclear Interior in the Context of Cytoskeletal Mechanics….…….….80

Physiological Implications of Altered Chromatin Fluctuations……...….81

Acknowledgements……85

References……..……86

Chapter IV: Physical Mechanisms of Chromatin Dynamics and Reorganization in Vascular Endothelial Growth Factor Stimulation...…….89

Introduction……...…….89

Materials and Methods……...93

Cell Culture, Transfection and Drug Treatments...……93

Particle Tracking and Image Analysis...……93

Cell Fixation and Fluorescence Microscopy……..95

Three-Dimensional Length Scales of Endothelial Cells……97

Nuclear Fluctuations.……98

Kymographs…..……99

Statistics……99

Results……...…100

Chromatin Fluctuations from VEGF-Stimulated Genome Reorganization.....100

Altered Chromatin Condensation State During Stimulated Gene Expression……....102

VEGF Stimulation Increases Actin Stress Fiber Colocalization with the Nucleus……..…105

VEGF Stimulation Increases Nuclear Envelope Fluctuations……..108

Discussion……111

Acknowledgements……..…115

References……..……..…116

Chapter V: Nuclear Stiffening and Chromatin Softening with Progerin Expression Leads to an Attenuated Nuclear Response to Force……...…120

Introduction……...……...120

Materials and Methods…….…....122

Cell Culture and Transfection……...……...…122

Micropipette Aspiration……...123

Shear and Compressive Force……..124

Data Analysis……...125

Results…….,,,,……...…126

Exogenous Progerin Expression Stiffens Nuclei..……..…126

Progerin Expression Reduces Chromatin Condensation and Softens the Nuclear Interior……..128

Progerin Expression Reduces Propagation of Cytoskeletal Forces to the Nuclear Interior…..……131

Progerin Expression also Reduces the Intranuclear Response to Extracellular Applied Force.....…….…….133

Discussion……..……..……135

Acknowledgements……..139

References……..……..…139

Chapter VI: Increased Chromatin Fluctuations are Localized to Regions of DNA Damage and Induced by Structural Relaxation……..…142

Introduction……...……...142

Materials and Methods…….…....146

Cell Culture, Transfection and Drug Treatments..……...…146

Particle Tracking and Image Analysis...……..148

Cell Fixation and Fluorescence Lifetime Imaging Microscopy……..149

Statistics……...151

Results……..…152

DNA Damage Induces Decoupling of Chromatin Dynamics Coincident with Structural Relaxation...……..152

FACT Complex Subunit SSRP1 and SIRT6 Deacetylase Facilitate Chromatin Relaxation at Sites of Double-Strand Breaks……..158

Discussion……..……..……171

Decoupling of Chromatin Dynamics at DNA DSB Sites through Structural Relaxation Influences Translocation Probability……....171

Models of DNA DSB Dynamics and Repair Probabilities……..174

Mechanistic Effects of Chromatin Remodeling in the Context of Ongoing Repair…….....……...176

Acknowledgements……..……..……..…179

References……..……..…180

Chapter VII: Early Passage Dependence of Mesenchymal Stem Cell Mechanics Influences Cellular Invasion and Migration……...…183

Introduction……...……...183

Materials and Methods…….……....185

Cell Isolation and Culture…….....……...…185

Micropipette Aspiration...……....186

Mechanical Analysis…….....……..…..187

PDMS Micropillars……..…188

Invasion Analysis…….....……188

Cell Labeling and Imaging…….....……...189

Results……..…190

Measuring Mechanics of Primary hMSCs Measured by Micropipette Aspiration……...190

hMSCs Grow into Micropillars…...……..……..…193

Differential Cell Elongation in Micropillars……....196

Increased Cell Passage Alters Cell Mechanics and Invasion Potential……...197

Discussion……..……..……199

Acknowledgements……..……..……..…201

References……..……..…202

Chapter VIII:

Conclusions…….……204

Summation and Conclusions……204

Future Outlook…….210

Appendix: Publications and Conference Proceedings Resulting from Thesis.....216

List of Figures

Chapter I

Figure 1.1: Schematic of nucleoskeleton-cytoskeleton interconnections 7

Chapter II

Figure 2.1: Fluorescence lifetime measurements of chromatin condensation state in human umbilical vein endothelial cell nuclei with Hoechst 33342 35

Figure 2.2: Fluorescence lifetime measurements of chromatin condensation state in human umbilical vein endothelial cell nuclei with PicoGreen 37

Figure 2.3: Dynamic light scattering measurements of in vitro λ-DNA solutions of varying condensation state 40

Figure 2.4: Fluorescence lifetime measurements of in vitro λ-DNA solutions of varying condensation state 41

Figure 2.5: Fluorescence lifetime measurements of in vitro λ-DNA solutions of varying ionic strength solutions 43

Figure 2.6: Fluorescence lifetime measurements of in vitro λ-DNA solutions of varying viscosity 44

Figure 2.7: Fluorescence lifetime spatial distribution around nucleoli in endothelial cell nuclei 47

Figure 2.8: Fluorescence lifetime spatial distribution around of endothelial cells labelled for heterochromatin marker H3K9me3 with immunocytochemistry 48

Figure 2.9: Changes in chromatin condensation state in the nuclear interior impact the local viscosity which strongly influence the fluorescence lifetime 51

Chapter III

Figure 3.1: Extended MSD plots from particle-tracking measurements 65

Figure 3.2: Particle tracking of distinct subnuclear regions in HUVECs 67

Figure 3.3: Global chromatin network mechanics measured by ensemble averaged MSD are probe-independent 68

Figure 3.4: Chromatin decondensation alters nuclear mechanical properties 70

Figure 3.5: Reduced myosin II-based force generation attenuates chromatin dynamics 71

Figure 3.6: Transfection of RFP-KASH constructs in HUVECs 72

Figure 3.7: Cells expressing dominant negative KASH show reduced chromatin dynamics 73

Figure 3.8: Combined effect of chromatin hypercondensation and motor activity inhibition by ATP depletion shows greatest reduction in MSD 75

Figure 3.9: Bounded physiological range of chromatin dynamics in HUVECs....84

Chapter IV

Figure 4.1: Confocal image of fixed endothelial cell allows visualization of cellular dimensions 98

Figure 4.2: Chromatin dynamics from VEGF-stimulated genome reorganization exhibit distinct temporal behavior 102

Figure 4.3: Fluorescence lifetime measurements of chromatin condensation state during stimulated gene activation in VEGF-stimulated endothelial cell nuclei ..104

Figure 4.4: VEGF treatment shows actin stress fibers near the nucleus.....106

Figure 4.5: Colocalization of actin and nuclear fluorescence intensity 107

Figure 4.6: VEGF treatment is associated with fine fluctuations of the nuclear envelope 109

Figure 4.7: VEGF treatment is associated with gross area fluctuations of the nucleus 110

Chapter V

Figure 5.1: Exogenous progerin expression stiffens nuclei 127

Figure 5.2: HGPS patient cells show enhanced chromatin compliance 129

Figure 5.3: Exogenous expression of DsRed-Progerin enhances chromatin compliance in cells.....130

Figure 5.4: Progerin expression reduces cytoskeletal force propagation to the nuclear interior.....132

Figure 5.5: Progerin expression reduces intranuclear mechanical sensitivity to external force application.....134

Chapter VI

Figure 6.1: Particle tracking of nucleolar regions in U2OS cells 152

Figure 6.2: Particle tracking of telomeres in U2OS cells 153

Figure 6.3: Particle tracking of chromatin in bleomycin-treated U2OS cells.....153

Figure 6.4: Chromatin dynamics of nucleolar and telomeric regions measured by ensemble averaged MSD are physically uniform.....155

Figure 6.5: Chromatin dynamics in the presence of DNA double-strand breaks results in a physical decoupling of DNA damage dynamics from control behavior.....157

Figure 6.6: Fluorescence lifetime measurements of global chromatin condensation state in HeLa cell nuclei associated with FACT complex subunit SSRP1 and the DNA damage response from bleomycin treatment.....161

Figure 6.7: Fluorescence lifetime spatial distribution of HeLa cell nucleus treated with the control vector following bleomycin exposure 162

Figure 6.8: Fluorescence lifetime spatial distribution of HeLa cell nucleus with SSRP1 inhibition from short hairpin RNA (shRNA) following bleomycin exposure.....163

Figure 6.9: Fluorescence lifetime measurements of chromatin condensation state of DNA Damage foci in HeLa cells associated with FACT complex subunit SSRP1 activity following bleomycin treatment.....164

Figure 6.10: Fluorescence lifetime measurements of global chromatin condensation state in MEF cell nuclei associated the DNA DSB damage response.....167

Figure 6.11: Fluorescence lifetime spatial distribution of wild type MEF cell nucleus with DNA damage induced by photoactivation of TRF1-KR 168

Figure 6.12: Fluorescence lifetime spatial distribution of SIRT6 knockout MEF cell nucleus with DNA damage induced by photoactivation of TRF1-KR 169

Figure 6.13: Fluorescence lifetime measurements of chromatin condensation state of DNA Damage foci in MEF cells associated with SIRT6 activity at following photoactivation of TRF1-KR 170

Figure 6.14: Probability distribution of 1D random walk displacements for undamaged and damaged chromatin.....175

Chapter VII

Figure 7.1: Schematics of methodologies for cellular analysis 189

Figure 7.2: Micropipette aspiration of hMSCs 191

Figure 7.3: Quantification of creep compliance of hMSCs for three patient samples.....192

Figure 7.4: Mechanical parameters of hMSCs determined from creep compliance data.....193

Figure 7.5: hMSCs and fibroblasts grown on flat surfaces and 8 μm spaced micropillars 194

Figure 7.6: Entry of cells into differentially spaced micropillars 195

Figure 7.7: Persistence length of cells within 8 μm micropillar.....197

Figure 7.8: Increased passage alters cell mechanics and invasion into micropillars 198

Chapter VIII

Figure 8.1: Summary of previous control studies of nuclear particle tracking and discrete impacts on chromatin compliance and system forces 206

Chapter I

Introduction

Cellular processes are carried out by collections of proteins, each born of a unique linear sequence of DNA within the genome. Yet, the expression of each gene is nested within layers of complex, higher-order structural and spatial organization within the nucleus as well as dynamic genome regulation.[1-3] It is within this dynamic, physical context that the entirety of genome functionality observed in the nucleus may be revealed; these features cannot, at least at present, be recapitulated *in vitro*. However, much of our understanding of the physical properties of chromatin has emerged independently from the observations that biological functions are related to chromosome organization and position within the nucleus. Unfortunately, observed biological phenomena cannot be extricated from the physical model of chromatin as a polymer, and unifying theories of structure, organization and dynamics in the biological regime and polymer physics regime is necessary to illuminate the full complement of factors giving rise to function. For instance, chromatin structural changes that facilitate loop formation are biologically associated with coordinated regulation of transcription or other processes. These changes are driven by protein complexes as well as physical effects including macromolecular crowding and depletion attraction. Further, chromatin mobility is tightly regulated by a delicate balance of driving forces and viscoelastic resistances that govern the physical principles of all polymer reptation in an entangled mesh. Yet, these movements are critical to

evolving functional needs that demand reorganization for genomic processes. Investigation of such dynamic changes requires techniques for visualization at the appropriate length and time scales as well as physical understanding to elucidate the underlying mechanisms. The physics of dynamics focuses on the effects of forces (applied and frictional) on underlying motion as in classical mechanics, but here the forces are derived from the functional components of biology. Thus, developing biophysical techniques and models capable of measuring these dynamics and bridging the physical underpinnings of chromatin within the biological context becomes critical to discovering genome function in all its complexity.

Here, we review the current knowledge of the genome and its organization with respect to nuclear structure and function. We highlight the physical aspects associated with its dynamic nature and its spatial arrangement within the nucleus. We also demonstrate how the genome dynamically evolves to meet new functional needs during physiological changes, and how dysfunction arises in disease pathologies associated with nuclear organization. What emerges is a clear picture of genome function derived in no small part by physical properties that facilitate its organization and dynamic function, the investigation of which is the objective of this Thesis.

Nuclear Organization of Genome Function

DNA winds around histones to pack a genome that spans meters into the nucleus while still leaving regions accessible for transcription. The DNA-histone

complex, called the nucleosome, is a 100 kDa, 10 nm histone octamer (made of histone proteins H2A, H2B, H3 and H4) complexed with a DNA molecule which folds two-times around.[4] Condensed nucleosome structures form chromatin. Expanded chromatin reconstituted from histones and DNA has the appearance of 10 nm thick beads on a string, but with higher-order structures from additional folding and organization.

Chromatin is then arranged in the nucleus with loose spatial specificity. This corresponds to decondensed, gene-rich regions of euchromatin preferentially located at the interior where gene expression is high and condensed, gene-poor regions of heterochromatin primarily at the periphery where gene activity is low.[5-8] As 98% of human DNA does not code for protein, this noncoding DNA is believed to aid regulation through hierarchical organization.[9] A variety of chromatin modifications cause heterochromatin formation. These include DNA methylation patterns, histone modifications that enhance DNA-histone interactions (and consequently increase condensation)[3] and the binding of other proteins.[9] Additionally, regions of heterochromatin commonly bind to the lamin proteins of the nucleoskeleton at the nuclear periphery (Figure 1), which aids in repression and organization.[10-12]

This hierarchical organization of DNA into varying levels of condensation serves many functions. By virtue of being less condensed, DNA in euchromatin is more readily transcribed with accessible binding sites to transcription or other factors[13] and even heightened mobility.[14, 15] In this way DNA serves to nucleate *de novo* formation of functional sites within the nucleus. In fact, many of the

nuclear functional sites, or nuclear bodies, have been observed to assemble *de novo* upon the initiation of activity,[16, 17] leading to the idea that the nucleus is a self-organizing system.[1, 2] The most heavily studied example is the formation of the nucleolus, where ribosomal biogenesis occurs.[18] Nucleolar disassembly and assembly during cell division mechanistically depends on the suspension and re-initiation of ribosomal biogenesis, respectively.[19-21] The formation of nucleoli occurs via the coalescing of necessary proteins and ribosomal genes from the five different pairs of homologous chromosomes containing them[21] by complex mechanisms that are likely facilitated by physical properties of chromatin in addition to protein binding. Assembly can be induced by extrachromosomal ribosomal DNA,[22] and disassembly by inhibition of ribosomal gene transcription.[23] Self-organization is further supported by the fact that nucleolar proteins are continuously exchanged with the nucleoplasm and that nucleolar size is correlated with ribosomal production.[24] The nucleolus is the most understood nuclear body, but others are believed to function similarly. The most analogous example is evidence pointing to the emergence of specific transcription hubs, called transcription factories, that may act to service other genes and function much the way the nucleolus does for ribosomal gene transcription and biogenesis.[25]

What emerges as a dominant feature of nuclear organization is the centrality of function to the formation of nuclear bodies. Proteins, and even protein complexes, readily diffuse through even the densest chromatin packing.[26, 27] This leaves a reservoir of available components upon the initiation of any

nuclear process. As observed in the nucleolus, nuclear bodies experience a constant flux of protein components, continuously evolving in response to functional needs. Thus, rapid turnover in function is possible because the nucleus maintains this capacity for dynamic change rather than equilibrium or steady-state function. Consequently, gene expression is not simply an on and off process, but one of varying degrees. This is most evident in comparing the stochastic single cell gene expression profiles[28] with the population, exposing the "myth of the average cell".[29]

Part of the stochastic nature of nuclear functions arises from the assembly of processing complex. This occurs in a complementary fashion if the necessary factors are available within the residence time of binding, implying the need of function for formation. In this way, the protein flux into and out of nuclear bodies serves to take advantage of the available reservoir by allowing function to dictate need. As this is an inherently inefficient process, recurring and continuous processes often keep the machinery intact. The inefficiency of *in vitro* transcriptional complex assembly[30] has been a hypothesis put forth for the possible presence of intact transcription factories within the nucleus[25] to allow quick changes in gene expression. These potential transcription factories may contain several active polymerases simultaneously transcribing multiple genes.[25] Each factory, by virtue of a distinct protein composition, would confer unique environments that help regulate the expression of genes in shared factories.[25] In this way, the cell tailors expression in a manner unique to genes and co-regulated gene groups. By contrast, sporadic but exigent nuclear processes such as DNA

repair would necessitate rapid signaling and response to form repair complexes upon the initiation of damage, for which the large reservoir of freely diffusion components becomes critical.

Nuclear Structure and Mechanics are Implicated in Function

The nucleus is neither an isolated structural nor mechanical system.[31, 32] The nucleus, being the largest and stiffest organelle,[33, 34] has been shown to play a role in balancing the contractile forces associated with cell adhesion and motility.[35] The actin filaments of the cytoskeleton play a prominent role in this process.[35, 36] This is of particular importance for endothelial cells which line the blood vessels, where actin is a direct modulator of nuclear height, elongation and polarization during cell migration as part of the pro-angiogenic response.[37] Thus, there is a mutual dependence between the cytoskeleton and the nucleus for both structure and mechanics.

Each of the cytoskeletal filaments are linked to the nucleus through a series of proteins that span the outer and inner nuclear membranes and that are collectively called the Linker of Nucleoskeleton and Cytoskeleton, or LINC, complex as shown in Figure 1.[38, 39] The LINC complex, composed of SUN-domain and nesprin proteins, interconnects these cytoskeletal structures with the nucleoskeleton of the cell. Large, multi-domain nesprin proteins are found on the outer nuclear membrane and connect to actin via the N-terminal actin binding of nesprins 1 and 2. Nesprin -3 contains a site that binds to plectin, which associates to intermediate filaments.[40, 41] Nesprin 4, present in specialized cells, interacts

with the microtubule motor protein, kinesin and is suggested to be involved in microtubule-dependent movement.[42]

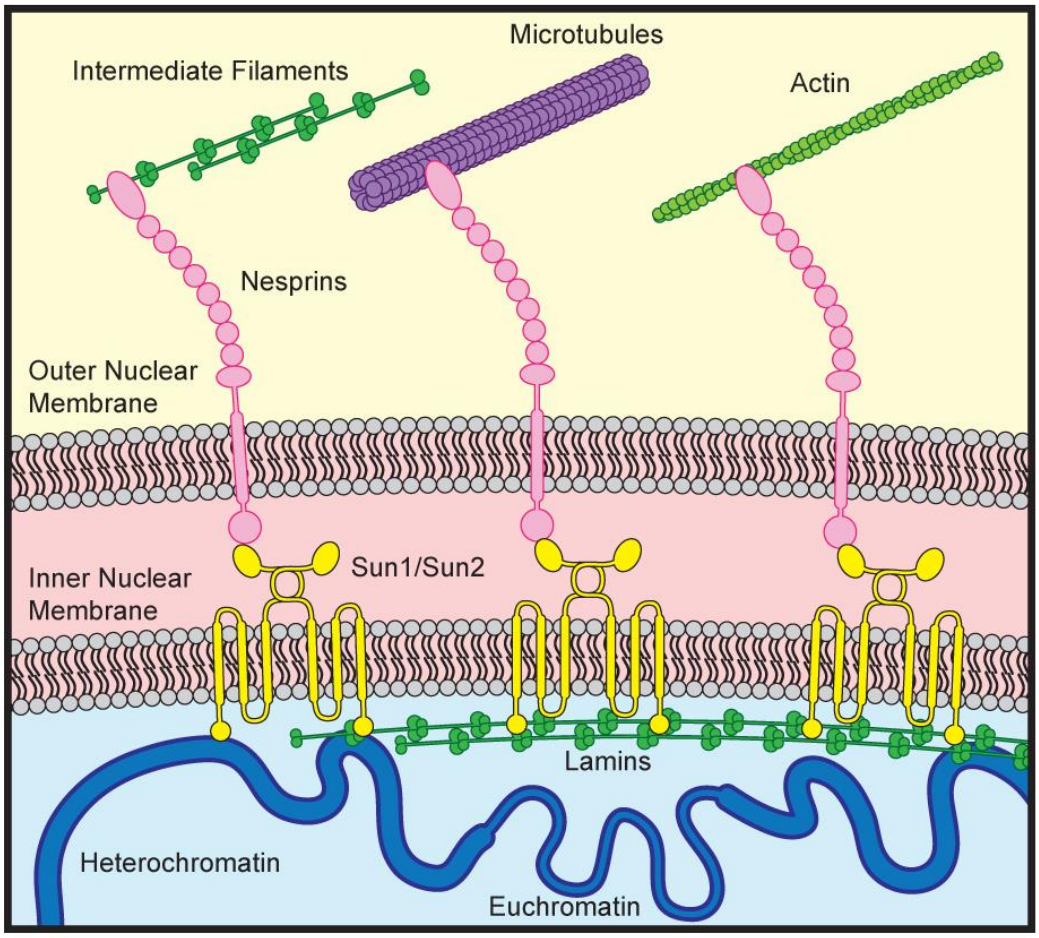

Figure 1.1. Schematic of nucleoskeleton-cytoskeleton interconnections. *Cytoskeletal filament systems connect to the outer nuclear membrane via nesprin proteins. The direct connection is then maintained through SUN 1/2 protein complexes, which bind to inner nuclear membrane nesprins, transmembrane proteins and lamins. Lamins then bind directly and indirectly to chromatin in the nuclear interior.*

Within the nucleus, SUN1 and SUN2 proteins interact with the nucleoskeleton composed primarily of two types of lamin proteins as well as lamin binding proteins, nuclear pore complexes and other proteins.[31, 43, 44] The lamin proteins then provide the nucleoskeleton with its dominant mechanical characteristics and help to integrate cytoskeletal mechanical signals by connecting to nuclear protein complexes and chromatin.[31] Lamins are type V intermediate filament proteins with a rod-shaped domain flanked by globular domains on the N and C termini. The C-terminal domain of lamins are much larger than cytoplasmic intermediate filaments and contain the nuclear localization sequence and an Ig-fold structure.[45, 46] The tail domain is also the site of protein-protein and protein-DNA binding.

Lamins assemble into coiled-coil dimers that assemble both linearly head-to-tail and laterally into staggered rope-like structures and form the mostly-disorganized meshwork of the nuclear lamina. In standard intermediate filament assembly, dimers form staggered lateral associations to create an intermediate filament.[47, 48] Due to the head-to-tail assembly method of the coiled-coils, lamin filaments lack polarity and the large tail domains which extend from the central structures allows for multiple binding sites along the lamina.

There are two main types of lamin proteins. A-type lamins, primarily lamin A and lamin C, are splice variants of the same gene LMNA. B-type lamins, primarily lamin B1 and lamin B2, are encoded from different genes. Lamin A is primary contributor to the mechanical stability of the nucleus.[49] Loss of lamin A causes nuclear weakness and rupture.[50] Conversely, association of lamin A in

model nuclear systems induces sheets of thicker filaments on the nuclear lamina, significantly increasing the rigidity of the nucleus.[51] There are hundreds of mutations in LMNA, which lead to a host of disorders. By contrast, loss of B-type lamins is usually lethal for organisms and for cells.[52] However, B-type lamins are thought to regulate gene expression, and model systems with loss of these lamins do not show altered nuclear mechanics.[53]

A-type lamins and B-type lamins form primarily autonomous networks that assemble independently and appear to have different nuclear functions. Lamin filaments are homopolymers of either lamin A or lamin B.[54] A- and B-type lamins also have different binding partners at the inner nuclear membrane. In nuclear envelope reassembly after mitosis, B-type lamins are incorporated into the nucleoskeleton earlier than A-type lamins.[55] A-type lamin filaments are 15 nm in diameter and form thick sheets and bundles whereas B-type lamins are 7 nm in diameter assemble into more regular, dispersed structures.[56]

The lamin proteins can bind to DNA both directly and indirectly through complexes of proteins, including transcriptional repressors and regulators.[57] During development and differentiation, chromatin formation and association with the nuclear lamina are believed to alter the mechanics of cells at later states of differentiation.[10, 58] Genes associated with the lamina are generally repressed.[31, 57] However, the loss of chromatin-lamina association is not in itself a means of gene activation, but instead serves as a necessary part of a multistep mechanism for stochastic gene activation.[10, 11] This highlights the probabilistic nature of gene expression and repression, with the association and dissociation of several factors

being necessary but not sufficient for either outcome, which exposes the lack of deterministic organization.

Chromatin Dynamics and the 4D Nature of Genome Function

The static view of linear DNA for gene expression and condensed chromatin for silencing allows for simplistic demonstration, but obscures the reality of dynamic chromatin activity within the nucleus. Much like other aspects of nuclear function, chromatin condensation occurs by the predominance of numerous sequential and stochastic steps over competing factors.[3] Thus, chromatin in the nucleus is continuously remodeling between the varying degrees of condensation. Evidence of this is provided by the presence of opposing bivalent (i.e. both activating and repressing) histone modifications at most sites, with one set dominating the behavior.[59] Each step of condensation (or decondensation and activation) occurs through a multitude of protein-DNA and protein-protein binding events associated with different residence times.[24] This wide divergence of characteristic binding time scales results in another layer of stochastic control. Additionally, these factors may be cooperative or inhibitory by altering residence times of others[60] to favor certain outcomes. Along these lines, recent work on the binding of chromatin regulators (CRs) to DNA exposed different patterns of CR combinations for specific chromatin environments, genes of common functions and regulatory elements.[59] The cumulative result of these effects is transiently stabilized sites of hierarchical organization within the nucleus resulting from the stochastic interactions among chromatin domains and

with protein complexes, which highlights the importance of chromatin physical properties to this probabilistic behavior.

When not bound to stable complexes, chromatin fluctuates and diffuses through the nucleus.[14, 61] In yeast, GFP-tagged regions of chromatin move ~0.5 μm, or half the radial length of the nucleus, in 10 seconds.[62] Yet individual chromosomes occupy distinct territories within the nucleus, with these movements corresponding to regions of ~1/1000th of the nuclear volume in humans,[63] though overlap and incursion by loops from other chromosomes is frequent.[61] The nature of such chromatin remodeling and movements as well as the physical mechanisms and the biological factors regulating these dynamic processes, particularly with evolving functional changes, are a primary focus of this Thesis and revealed at length in later Chapters. We do know that the presence of many dense chromosome territories results in highly restricted motion within the human nucleus. This confers another advantage through molecular crowding, which enhances stochastic interactions by increasing effective concentrations and the collision frequency of interactions, while decreasing the probability of less favorable conformations (preferring native structure to more variety).[64-66]

The organization of chromosome territories within the nucleus is nonrandom and cell-type specific,[6, 67, 68] with more gene dense chromosomes concentrated at the interior as discussed previously. This is believed to aid in gene regulation, with implications for incidence of chromosomal translocations in cancer mutation rates.[69, 70] Additionally, protein concentrations within the nucleus are heterogeneous, allowing for individual genes to be positioned in unique

protein environments that play a role in expression patterns.[68] In this light, the dynamic repositioning of chromatin can serve to facilitate functional changes by moving to regions for specialized function dictated by their protein composition. The function of the nucleolus again provides a useful analogy, where the presence of protein components specific to ribosomal biogenesis bestows an environment specially tailored for its function.

Transcription sites are envisioned to service their neighborhood of genes in a mechanism similar ribosomal biogenesis in the nucleolus. This has been hypothesized for the observation of gene repositioning during differential expression.[62, 71-73] Some genes even form loops out from their chromosome territory to allow access to transcriptional machinery and differential regulation from the rest of the chromatin within the territory, as well as to bring distantly located portions of chromatin for co-regulation.[1] This is also observed in colocalization of distal genes to potential transcription factories and the associated activation-dependent movement, which demonstrates a need for these unique environments and established transcription factories.[73] The result is the ability to regulate the expression of genes on distant regions of the same chromosome or of different chromosomes, thereby coordinating genes of related functions as observed in the nucleolus.[1] Thus, not only are chromosomes themselves organized based on gene density, but movements of single genes facilitate this regulation.

While the correlation of radial position with chromosomal translocations and gene expression as well as positional correlation with gene density of chromosomes shows statistical significance across populations of cells of the

same type,[8, 67] it is important to recognize that these average positions give no indication of the true position within a single cell, as consistent with the ideas and application of the ensemble from statistical mechanics.[74-77] The reason is due to the probabilistic nature of this organization and the lack of deterministic guarantors of gene and chromosomal position, which is instead driven by physical properties of chromatin and probabilistic nature of biological interactions guiding this organization. The best evidence of this involves photobleaching experiments during cell division in which daughter cells partially maintained chromosome positioning.[67] The lack of complete conservation of chromosome position or complete randomization shows the degree to which probabilistic mechanisms successfully maintain positioning patterns without deterministic control.

Physical models have attempted to recapitulate aspects of chromatin organization and dynamics with some success. The loop models accurately depict the spatial organization of the genome in the nucleus emanating from fluorescence *in situ* hybridization (FISH) experiments. By contrast, the fractal model finds concurrence with chromosome conformation capture (3C) experiments that yield information about chromosomal interactions.[78] Additionally, conventional polymer dynamics models of de Gennes reptation or the Rouse chain model have been applied strictly to chromatin dynamics.[79-81] However, the mere consistency of data with underlying models obscures what is likely much more complex phenomena.[82] The lack of congruence across experimental techniques demonstrates these models are likely oversimplifications of the observed phenomena. The failures likely point to faults in the underlying

assumptions of these models, which generally assume some form of equilibrium or static state whether it be with respect to chromatin remodeling, evolving transcriptional status or others.

Stimulation and Gene Expression

While the stochastic control of genome function aids regulation of expression, at first glance it appears to pose a problem for the large scale transitions in transcriptional activity known to accompany major physiological events. These changes in gene expression are best exemplified in the different stages of stem cell potency (its ability to differentiate into various cell types), which is determinant of the number of genes that have the potential to be expressed.[10] When cells become more terminally differentiated, and therefore unable to become cells of other tissue types, they no longer need access to the entire genome. Instead they express a certain subset of genes necessary for tissue-specific function. Thus, differentiation provides the most dramatic example of gene expression changes, but is by no means the only one. Cells often attain a quiescent state in normal tissue that, upon stimulation by certain factors, causes extensive turnover in gene expression such as in the pro-angiogenic stimulation of endothelial cells discussed in Chapter IV.

At the scale of a single gene, stimulated transcriptional activation involves the binding of transcription factors to specific genes for regulated expression. This requires large scale chromatin decondensation to open up binding sites for access to proteins, and the coalescing of genes and required processing factors. The

signaling cascades have been well studied, but the mechanisms that give rise to this global reorganization of proteins and genes remains to be determined and is a focus of this Thesis.

It is understood that at the nuclear scale assembly of genes at transcription sites and chromatin remodeling and reorganization must occur with certain spatial and temporal integrity. Recent evidence suggests active cytoskeletal stresses on the nucleus play a role in enhancing the necessary turnover within the nucleus for the appropriate chromatin remodeling and reorganization.[83, 84] We show later that these imposed stresses likely act globally and nonspecifically to increase chromatin agitation and, therefore, the probability of expression by enhancing the kinetic events of binding, remodeling, and the mobility of components.[82-84] Additionally, transcription factor nuclear signaling in response to mechanical stimuli has been shown to depend on actin polymerization states.[83, 85, 86] Even in processes free of external mechanical effects the necessary chromatin dynamics and reorganization are also found to depend on imposed cytoskeletal stresses that act to reposition heterochromatin during development.[84, 85]

Disease and Dysfunction

Given the integral role of proteins in organizing the genome, dysfunction associated with any number of proteins and the subsequent alterations in nuclear organization can cause aberrant expression. This is particularly true of the peripheral organization of the genome along the nucleoskeleton. Since lamins bind repressed regions of chromatin, laminopathies associated with mutations in

lamin proteins can alter gene function.[5, 11] The result is a perturbation of chromatin-lamina associations,[11] changes in expression,[11] and differential nuclear mechanical properties.[5] This suggests a role for aberrant gene regulation in laminopathies.

In Chapter V, we focus on one type of laminopathy in particular called Hutchinson-Gilford progeria syndrome (HGPS) that arises from a mutation in LMNA resulting in a truncated lamin A protein, D50 lamin A or progerin, that lacks 50 internal amino acids near its C-terminus.[87, 88] Due to incorrect post-translational processing[89] progerin is more strongly localized to the nuclear membrane. The results are structural changes in the nucleus such as loss of interior chromatin condensation, changes in heterochromatin organization, nuclear envelope blebbing and increased thickness of the nuclear lamina.[90] Mechanically, this over-accumulation of progerin at the nuclear envelope decreases the lamina network's ability to deform,[91] and cells expressing progerin are less able to adapt to shear stress.[92] Endothelial cells and smooth muscle cells are particularly sensitive in HGPS, and histological sections of elderly patients show high levels of progerin expression.[93]

The most notable effects of disease on nuclear structure and organization arise in cancer. Altered nuclear function associated with cancer metastasis include defects in histones,[94] heterochromatin-inducing proteins,[95] several DNA-binding proteins involved in higher-order organization[96] and transcription factors.[97] These mutations dramatically alter nuclear organization.[98] The result is changes to the mechanical and structural properties that affect nuclear shape, heterochromatin

formation and organization as well as nucleolar assembly and function.[99] Thus, nuclear stains still serve as the basis for many biopsies today. In Chapter II we demonstrate fluorescence lifetime imaging microscopy (FLIM) as a technique that may provide additional quantification and spatial information to these conventional methods as an indicator of irregularities in genome organization. However, it is likely that the series of random mutations that lead to aberrant genome organization provide selective advantages for further gene mutation and aberrant expression associated with cancer. To that end, understanding the physical mechanisms associated with DNA repair processes is imperative.[100] This is particularly true for DNA damage that gives rise to the complete severing of DNA ends, termed double-strand breaks (DSBs), where the mobility of severed ends may be implicated in the probability of successful repair as investigated in Chapter VI. What we find is an obvious role for proper higher-order organization of the genome to precisely regulate genome function.

Thesis Objectives

It is evident that the dynamic processes of chromatin are critical to satisfying the functional needs of the human genome. Structural remodeling of chromatin directly impacts transcription, replication and repair. Further, given the strong correlation of chromosome location with differential nuclear function, the role of chromatin mobility cannot be discounted as we progress from a static picture of genome organization to a more realistic dynamic one. This is particularly true during transition states accompanying physiological or

pathological changes, including large scale stimulated transitions in gene expression.

The overarching objective of this thesis is to build a physical understanding of chromatin in human nuclei as it relates to biological processes. To that end, we investigate chromatin *in situ* as a physical entity using dynamic measurements related to its mechanical state, including particle-tracking microrheology and fluorescence lifetime imaging microscopy (FLIM). What has long been the limitation of mechanics-based measurements in biology is the careful elucidation of the precise relationship between the mechanical state and the underlying biological functional state.

Thus, here we aim to build a conceptual understanding of how distinct biological changes associated with chromatin impact its physical properties as quantified through the accompanying mechanical changes. In Chapter II we demonstrate that varying chromatin condensation states can be quantified and spatially resolved for assaying functionally-derived structural changes of chromatin using FLIM. We show that this arises through the unique dependence of the fluorescence lifetime on chromatin mechanical states associated with differential condensation. We illuminate the precise physical mechanisms that regulate chromatin dynamics in human cell nuclei in Chapter III. Specifically, we show a decoupling of mechanical parameters associated with condensation state from active molecular motor protein processes that serve to enhance this motion beyond simple thermal energy.

These findings demonstrate that chromatin dynamics can be precisely tuned through modulation of chromatin condensation state or molecular motor forces (derived primarily from the cytoskeleton and propagated through the LINC complex) to meet physiological needs. Prominent roles for the proper regulation of chromatin high-order organization and dynamics are demonstrated in response to chemically-stimulated genome reorganization known to accompany large scale changes in gene expression in Chapter IV. The effects of chromatin dynamics and structure in disease pathologies, including progeria discussed above and the DNA damage repair processes implicated in cancer, are highlighted in Chapters V and VI, respectively. We close with a clinically-relevant investigation of global cell mechanics (including nuclear and cytoskeletal) on human mesenchymal stem cell injection therapies and their subsequent migration to wound sites in Chapter VII.

Thus, through our work we develop imaging and tracking techniques as well as a physical understanding of chromatin in human cell nuclei from which we build on to illuminate a more complete picture of genome function. The coupled investigation of genome function as both a biological and physical entity enables us to reveal the complex role of higher-order genome organization in facilitating the functions of the linear sequence. This physical understanding of our dynamic measurements allows us to resolve underlying features of nuclear processes that have dramatic implications for human health and disease.

References

1. T. Misteli, *Cell*, 2007, **128**, 787-800.
2. M. R. Hubner and D. L. Spector, *Annu Rev Biophys*, 2010, **39**, 471-489.
3. C. A. McQueen and Knovel (Firm), Elsevier, Oxford, 2nd edn., 2010.
4. B. Alberts, *Molecular biology of the cell*, 4th edn., Garland Science, New York, 2002.
5. K. N. Dahl, E. A. Booth-Gauthier and B. Ladoux, *Journal of biomechanics*, 2010, **43**, 2-8.
6. E. Fedorova and D. Zink, *Current opinion in genetics & development*, 2009, **19**, 166-171.
7. P. K. Geyer, M. W. Vitalini and L. L. Wallrath, *Current opinion in cell biology*, 2011, **23**, 354-359.
8. K. Kupper, A. Kolbl, D. Biener, S. Dittrich, J. von Hase, T. Thormeyer, H. Fiegler, N. P. Carter, M. R. Speicher, T. Cremer and M. Cremer, *Chromosoma*, 2007, **116**, 285-306.
9. J. C. Knight, *Clinical science*, 2003, **104**, 493-501.
10. D. Peric-Hupkes, W. Meuleman, L. Pagie, S. W. M. Bruggeman, I. Solovei, W. Brugman, S. Graf, P. Flicek, R. M. Kerkhoven, M. van Lohuizen, M. Reinders, L. Wessels and B. van Steensel, *Mol Cell*, 2010, **38**, 603-613.
11. N. Kubben, M. Adriaens, W. Meuleman, J. W. Voncken, B. van Steensel and T. Misteli, *Chromosoma*, 2012, **121**, 447-464.
12. L. Guelen, L. Pagie, E. Brasset, W. Meuleman, M. B. Faza, W. Talhout, B. H. Eussen, A. de Klein, L. Wessels, W. de Laat and B. van Steensel, *Nature*, 2008, **453**, 948-U983.
13. R. M. Martin and M. C. Cardoso, *FASEB journal : official publication of the Federation of American Societies for Experimental Biology*, 2010, **24**, 1066-1072.
14. J. R. Chubb, S. Boyle, P. Perry and W. A. Bickmore, *Curr Biol*, 2002, **12**, 439-445.
15. G. Mearini and F. O. Fackelmayer, *Cell Cycle*, 2006, **5**, 1989-1995.
16. J. Rino and M. Carmo-Fonseca, *Trends in cell biology*, 2009, **19**, 375-384.
17. M. Dundr and T. Misteli, *Csh Perspect Biol*, 2010, **2**.
18. R. Schneider and R. Grosschedl, *Gene Dev*, 2007, **21**, 3027-3043.
19. A. K. L. Leung, D. Gerlich, G. Miller, C. Lyon, Y. W. Lam, D. Lleres, N. Daigle, J. Zomerdijk, J. Ellenherg and A. I. Lamond, *Journal of Cell Biology*, 2004, **166**, 787-800.
20. V. Sirri, S. Urcuqui-Inchima, P. Roussel and D. Hernandez-Verdun, *Histochem Cell Biol*, 2008, **129**, 13-31.
21. A. Nemeth and G. Langst, *Trends Genet*, 2011, **27**, 149-156.
22. D. Hernandez-Verdun, *Histochem Cell Biol*, 2006, **126**, 135-148.
23. D. A. Sinclair and L. Guarente, *Cell*, 1997, **91**, 1033-1042.
24. T. Misteli, *Science*, 2001, **291**, 843-847.
25. P. R. Cook, *J Mol Biol*, 2010, **395**, 1-10.

26. A. Bancaud, S. Huet, N. Daigle, J. Mozziconacci, J. Beaudouin and J. Ellenberg, *Embo Journal*, 2009, **28**, 3785-3798.
27. A. Belmont, *Current opinion in cell biology*, 2003, **15**, 304-310.
28. M. B. Elowitz, A. J. Levine, E. D. Siggia and P. S. Swain, *Science*, 2002, **297**, 1183-1186.
29. J. M. Levsky and R. H. Singer, *Trends in cell biology*, 2003, **13**, 4-6.
30. C. M. Bral, J. W. Steinke, C. J. Kang and D. O. Peterson, *Gene expression*, 1998, **7**, 191-204.
31. K. N. Dahl and A. Kalinowski, *Journal of cell science*, 2011, **124**, 675-678.
32. D. N. Simon and K. L. Wilson, *Nat Rev Mol Cell Bio*, 2011, **12**, 695-708.
33. K. N. Dahl, A. J. Engler, J. D. Pajerowski and D. E. Discher, *Biophysical journal*, 2005, **89**, 2855-2864.
34. A. J. S. Ribeiro and K. N. Dahl, *Engineering in Medicine and Biology Society (EMBC), 2010 Annual International Conference of the IEEE*, 2010, 831-834.
35. J. Borrego-Pinto, T. Jegou, D. S. Osorio, F. Aurade, M. Gorjanaacz, B. Koch, I. W. Mattaj and E. R. Gomes, *Journal of cell science*, 2012, **125**, 1099-1105.
36. S. B. Khatau, C. M. Hale, P. J. Stewart-Hutchinson, M. S. Patel, C. L. Stewart, P. C. Searson, D. Hodzic and D. Wirtz, *Proceedings of the National Academy of Sciences of the United States of America*, 2009, **106**, 19017-19022.
37. T. J. Chancellor, J. Lee, C. K. Thodeti and T. Lele, *Biophysical journal*, 2010, **99**, 115-123.
38. K. N. Dahl, A. J. S. Ribeiro and J. Lammerding, *Circulation research*, 2008, **102**, 1307-1318.
39. E. A. Booth-Gauthier, S. Spagnol and K. N. Dahl, *Mechanobiology of the Endothelial Nucleus*, CRC Press, 2015.
40. M. Crisp, Q. Liu, K. Roux, J. B. Rattner, C. Shanahan, B. Burke, P. D. Stahl and D. Hodzic, *Journal of Cell Science*, 2006, **172**, 41-53.
41. M. Ketema, K. Wilhelmsen, I. Kuikman, H. Janssen, D. Hodzic and A. Sonnenberg, *Journal of Cell Science*, 2007, **120**, 3384-3394.
42. K. J. Roux, M. L. Crisp, Q. Liu, D. Kim, S. Kozlov, C. L. Stewart and B. Burke, *Proceedings of the National Academy of Sciences of the United States of America*, 2009, **106**, 2194-2199.
43. M. S. Zastrow, S. Vlcek and K. L. Wilson, *Journal of Cell Science*, 2004, **117**, 979-987.
44. D. Razafsky and D. Hodzic, *Journal of Cell Biology* 2009, **186**, 461-472.
45. H. Herrmann and R. Foisner, *Cell Mol Life Sci*, 2003, **60**, 1607-1612.
46. H. Herrmann, M. Hesse, M. Reichenzeller, U. Aebi and T. M. Magin, *Int Rev Cytol*, 2003, **223**, 83-175.
47. R. D. Goldman, B. Grin, M. G. Mendez and E. R. Kuczmarski, *Current Opinion in Cell Biology* 2008, **20**, 28-34.
48. M. J. Buehler and T. Ackbarow, *Computer Methods in Biomechanics and Biomedical Engineering* 2008, **11**, 595-607.

49. Y. Gruenbaum, K. L. Wilson, A. Harel, M. Goldberg and M. Cohen, *J Struct Biol*, 2000, **129**, 313-323.
50. J. Lammerding, P. C. Schulze, T. Takahashi, S. Kozlov, T. Sullivan, R. D. Kamm, C. L. Stewart and R. T. Lee, *J Clin Invest*, 2004, **113**, 370-378.
51. K. N. Dahl, P. Scaffidi, M. F. Islam, A. G. Yodh, K. L. Wilson and T. Misteli, *Proceedings of the National Academy of Sciences of the United States of America*, 2006, **103**, 10271-10276.
52. J. Harborth, S. M. Elbashir, K. Bechert, T. Tuschl and K. Weber, *J Cell Sci*, 2001, **114**, 4557-4565.
53. J. Lammerding, L. G. Fong, J. Y. Ji, K. Reue, C. L. Stewart, S. G. Young and R. T. Lee, *J Biol Chem*, 2006, **281**, 25768-25780.
54. E. Delbarre, M. Tramier, M. Coppey-Moisan, C. Gaillard, J. C. Courvalin and B. Buendia, *Human Molecular Genetics*, 2006, **15**, 1113-1122.
55. R. D. Moir, M. Yoon, S. Khuon and R. D. Goldman, *Journal of Cell Biology* 2000, **151**, 1155-1168.
56. M. W. Goldberg, I. Huttenlauch, C. J. Hutchison and R. Stick, *Journal of Cell Science*, 2008, **121**, 215-225.
57. K. L. Wilson and R. Foisner, *Csh Perspect Biol*, 2010, **2**.
58. M. W. Goldberg, I. Huttenlauch, C. J. Hutchison and R. Stick, *Journal of cell science*, 2008, **121**, 215-225.
59. O. Ram, A. Goren, I. Amit, N. Shoresh, N. Yosef, J. Ernst, M. Kellis, M. Gymrek, R. Issner, M. Coyne, T. Durham, X. L. Zhang, J. Donaghey, C. B. Epstein, A. Regev and B. E. Bernstein, *Cell*, 2011, **147**, 1628-1639.
60. A. Agresti, P. Scaffidi, A. Riva, V. R. Caiolfa and M. E. Bianchi, *Mol Cell*, 2005, **18**, 109-121.
61. N. Tokuda, T. P. Terada and M. Sasai, *Biophysical journal*, 2012, **102**, 296-304.
62. S. M. Gasser, *Science*, 2002, **296**, 1412-1416.
63. J. R. Chubb and W. A. Bickmore, *Cell*, 2003, **112**, 403-406.
64. A. P. Minton, *Current opinion in structural biology*, 2000, **10**, 34-39.
65. D. Marenduzzo, K. Finan and P. R. Cook, *Journal of Cell Biology*, 2006, **175**, 681-686.
66. A. Dhar, K. Girdhar, D. Singh, H. Gelman, S. Ebbinghaus and M. Gruebele, *Biophysical journal*, 2011, **101**, 421-430.
67. L. A. Parada, J. J. Roix and T. Misteli, *Trends in cell biology*, 2003, **13**, 393-396.
68. L. Meldi and J. H. Brickner, *Trends in cell biology*, 2011, **21**, 701-708.
69. P. J. Wijchers and W. de Laat, *Trends Genet*, 2011, **27**, 63-71.
70. L. A. Parada, P. G. McQueen, P. J. Munson and T. Misteli, *Molecular biology of the cell*, 2002, **13**, 246a-246a.
71. C. Lanctot, T. Cheutin, M. Cremer, G. Cavalli and T. Cremer, *Nature reviews. Genetics*, 2007, **8**, 104-115.
72. S. Ahmed, D. G. Brickner, W. H. Light, I. Cajigas, M. McDonough, A. B. Froyshteter, T. Volpe and J. H. Brickner, *Nature cell biology*, 2010, **12**, 111-118.

73. C. S. Osborne, L. Chakalova, K. E. Brown, D. Carter, A. Horton, E. Debrand, B. Goyenechea, J. A. Mitchell, S. Lopes, W. Reik and P. Fraser, *Nature genetics*, 2004, **36**, 1065-1071.
74. A. Hakkinen and A. S. Ribeiro, *Comput Biol Chem*, 2012, **37**, 11-16.
75. H. G. Garcia, L. Bintu, J. Kondev and R. Phillips, *Biophysical journal*, 2005, **88**, 569a-569a.
76. L. Bintu, N. E. Buchler, H. G. Garcia, U. Gerland, T. Hwa, J. Kondev, T. Kuhlman and R. Phillips, *Current opinion in genetics & development*, 2005, **15**, 125-135.
77. L. Bintu, N. E. Buchler, H. G. Garcia, U. Gerland, T. Hwa, J. Kondev and R. Phillips, *Current opinion in genetics & development*, 2005, **15**, 116-124.
78. B. Albert, I. Leger-Silvestre, C. Normand and O. Gadal, *Bba-Gene Regul Mech*, 2012, **1819**, 468-481.
79. I. Bronstein, Y. Israel, E. Kepten, S. Mai, Y. Shav-Tal, E. Barkai and Y. Garini, *Physical review letters*, 2009, **103**, 018102.
80. H. Hajjoul, J. Mathon, H. Ranchon, I. Goiffon, J. Mozziconacci, B. Albert, P. Carrivain, J. M. Victor, O. Gadal, K. Bystricky and A. Bancaud, *Genome Res*, 2013, **23**, 1829-1838.
81. S. C. Weber, A. J. Spakowitz and J. A. Theriot, *Physical review letters*, 2010, **104**.
82. S. T. Spagnol and K. N. Dahl, *Integr Biol-Uk*, 2014, **6**, 523-531.
83. K. V. Iyer, S. Pulford, A. Mogilner and G. V. Shivashankar, *Biophysical journal*, 2012, **103**, 1416-1428.
84. B. Hampoelz, Y. Azou-Gros, R. Fabre, O. Markova, P. H. Puech and T. Lecuit, *Development*, 2011, **138**, 3377-3386.
85. F. Miralles, G. Posern, A. I. Zaromytidou and R. Treisman, *Cell*, 2003, **113**, 329-342.
86. M. K. Vartiainen, S. Guettler, B. Larijani and R. Treisman, *Science*, 2007, **316**, 1749-1752.
87. A. De Sandre-Giovannoli, R. Bernard, P. Cau, C. Navarro, J. Amiel, I. Boccaccio, S. Lyonnet, C. L. Stewart, A. Munnich, M. Le Merrer and N. Levy, *Science*, 2003, **300**, 2055.
88. M. Eriksson, W. T. Brown, L. B. Gordon, M. W. Glynn, J. Singer, L. Scott, M. R. Erdos, C. M. Robbins, T. Y. Moses, P. Berglund, A. Dutra, E. Pak, S. Durkin, A. B. Csoka, M. Boehnke, T. W. Glover and F. S. Collins, *Nature*, 2003, **423**, 293-298.
89. B. Korf, *New Engl. J. Med.*, 2008, **358**, 552-555.
90. R. D. Goldman, D. K. Shumaker, M. R. Erdos, M. Eriksson, A. E. Goldman, L. B. Gordon, Y. Gruenbaum, S. Khuon, M. Mendez, R. Varga and F. S. Collins, *Proc. Natl. Acad. Sci. USA*, 2004, **101**, 8963-8968.
91. K. N. Dahl, P. Scaffidi, M. F. Islam, A. G. Yodh, K. L. Wilson and T. Misteli, *Proc. Natl. Acad. Sci. USA*, 2006, **103**, 10271-10276.
92. J. T. Philip and K. N. Dahl, *J. Biomech.*, 2008, **41**, 3164-3170.
93. S. T. Spagnol, J. S. Weltz, Y. Q. Xue and K. N. Dahl, *Cellular and molecular bioengineering*, 2014, **7**, 225-230.

94. T. Sjoblom, S. Jones, L. D. Wood, D. W. Parsons, J. Lin, T. D. Barber, D. Mandelker, R. J. Leary, J. Ptak, N. Silliman, S. Szabo, P. Buckhaults, C. Farrell, P. Meeh, S. D. Markowitz, J. Willis, D. Dawson, J. K. V. Willson, A. F. Gazdar, J. Hartigan, L. Wu, C. S. Liu, G. Parmigiani, B. H. Park, K. E. Bachman, N. Papadopoulos, B. Vogelstein, K. W. Kinzler and V. E. Velculescu, *Science*, 2006, **314**, 268-274.
95. G. K. Dialynas, M. W. Vitalini and L. L. Wallrath, *Mutat Res-Fund Mol M*, 2008, **647**, 13-20.
96. H. J. Han, J. Russo, Y. Kohwi and T. Kohwi-Shigematsu, *Nature*, 2008, **452**, 187-193.
97. M. Eilers and R. N. Eisenman, *Gene Dev*, 2008, **22**, 2755-2766.
98. E. Lever and D. Sheer, *J Pathol*, 2010, **220**, 114-125.
99. D. Zink, A. H. Fischer and J. A. Nickerson, *Nat Rev Cancer*, 2004, **4**, 677-687.
100. V. Dion and S. M. Gasser, *Cell*, 2013, **152**, 1355-1364.

Chapter II

Spatially Resolved Quantification of Chromatin Condensation through Changes in Local Rheology in Cell Nuclei using Fluorescence Lifetime Imaging

Introduction

The structural state of DNA in the nucleus, corresponding to varying levels of chromatin condensation, is integral to its function. DNA itself forms the basis of much of the intranuclear structure and function. DNA is packaged with an octamer of histone proteins (two each of the core histones H2A, H2B, H3 and H4) to form nucleosomes. Nucleosomes are connected by linker DNA to form the 10 nm fiber that may bind linker histones (H1 and H5) for further condensation with other nucleosomes for more compact chromatin.[1] This varying of hierarchical condensation is thought to allow or prevent access of transcription factors to the linear sequence[2, 3] while serving as a central feature of nuclear organization.[4] Chromatin states are broadly categorized into heterochromatin and euchromatin, owing to their historical association with the density of their appearance with light[5] or electron microscopy.[6] Heterochromatin is generally associated with highly condensed, gene-poor stretches of chromatin consistent with repression.[7] This dense packing of heterochromatin is driven in part by histone modifications particularly at lysine residues, including deacetylation and specific methylation patterns.[8] These modifications enhance the binding of histones and other

chromatin architectural proteins that drive further condensation, such as heterochromatin protein 1 (HP1). Heterochromatin is further classified into constitutive heterochromatin that is very highly condensed and repressed, and facultative heterochromatin that is condensed but may become activated in response to environmental signals.[8] By contrast, euchromatin is gene-rich and largely decondensed, allowing for active processes including transcription.[9] Chromatin remodeling associated with decondensation is an active, ATP-dependent process that involves modification as well as movement or ejection of histone proteins.[10] The subtleties associated with these and other varying chromatin modification processes lead to gradations in condensation. Thus, the binary assignment of chromatin state is largely an oversimplification that obscures the reality of highly dynamic chromatin structure with rapid and frequent remodeling between intermediate states of condensation providing an element of plasticity to chromatin function.[8, 11, 12]

In addition to chromatin condensation state, there is a non-random three-dimensional arrangement of chromatin within the nucleus with euchromatin preferentially located to the interior and heterochromatin to the periphery, which is thought to impact genome function and gene expression.[13, 14] Proteins are heterogeneously distributed throughout the nucleus, giving rise to protein complexes that form distinct functional environments including Cajal bodies, PML bodies, nucleoli, transcription sites and many other subnuclear bodies wherein the spatial arrangement of chromatin becomes critical.[4] As such, the differential condensation state of chromatin throughout the nucleus is integral to

and serves to nucleate these functional sites upon initiation of activity;[15-17] *e.g.*, the interior of the nucleolus consists of decondensed chromatin enveloped by a border of heterochromatin.[18] By contrast, the spatially resolved condensation states of chromatin associated with other functional sites – including the appropriate length scales to be measured – remains to be determined. Of particular consequence is the inability to spatially resolve chromatin condensation state as it varies temporally with evolving processes, including the dynamic chromatin mobility that is intimately related to its condensation state.[19, 20]

There are complementary ways to quantify and spatially resolve chromatin condensation state in human cell nuclei, but most have significant limitations. Resolution itself is typically restricted for intensity-based light microscopy methods[21] since electron microscopy often requires damaging fixation procedures. Fixation and disruption of structures can similarly reduce resolution, quantification and reproducibility for utilizing immunocytochemistry[22] and *in situ* hybridization techniques. Major advances in quantifying chromatin structure have been made using specialized cell lines with fluorescently labelled nucleosomal elements.[21] These methods have proven very useful, particularly when coupling fluorescence intensity measurements with other fluorescence-based measurements (including fluorescence anisotropy[23], fluorescence lifetime and/or Förster resonance energy transfer[24]) that enhance spatial resolution. However, the use of specialized cell lines hinders its application to primary human cell lines where chromatin condensation and organization is tightly regulated most similarly to that observed *in vivo*.

Mechanical measurements that leverage the inherent relationship between mechanical-structural coupling of chromatin condensation states[19, 25-27] as related to chromatin mobility experiments noted above have similarly been used to quantify chromatin condensation state *in situ*. Current mechanics-based methods, including particle tracking of fluorescent probes[19, 28] or bulk mechanical measurements,[25-27] overcome the limitation of specialized cell lines and can be used in live cells, but they are generally low-throughput and provide mostly ensemble information.

Here we utilize fluorescence lifetime imaging microscopy (FLIM) of a membrane permeable, DNA-binding fluorophore for quantifying and spatially resolving chromatin condensation state in primary human endothelial cells. The phenomena of fluorescence lifetime measures the exponential decay rate (via time) of a fluorophore from the its excited state to the radiative fluorescence emission.[29] The fluorescence lifetime is highly sensitive to the multiple aspects of local fluorophore environment within a length scales of angstroms and up to <10 nm.[29, 30] We show that differential chromatin condensation states within the nucleus uniquely contribute to the fluorescence lifetime. Further, through *in vitro* measurements of DNA solutions we demonstrate that fluorescence lifetime is acutely sensitive to local solution viscosity, which varies most significantly with DNA condensation state even in the absence of binding proteins. We show the high spatial resolution of FLIM through co-labeling distinct functional sites within the nucleus and resolving the characteristic chromatin condensation state around those regions. The spatial resolution and ability to quantify chromatin

condensation state changes *in situ* makes FLIM a promising technique for measuring large scale chromatin decondensation and reorganization in response to chemically-stimulated changes in gene expression or other physiological changes associated with changes to condensation state as we will show in subsequent Chapters. The establishment of FLIM for quantifying the spatial organization of chromatin condensation in primary human cell nuclei provides a potentially high-throughput technique for assaying the functionally-derived structural changes of chromatin through its unique dependence on mechanics. This will enable large-scale measurements of chromatin condensation state changes, including their temporal evolution, to better understand functional changes of nuclear processes.

Materials and Methods

Cell Culture and Transfection

For our cell experiments, we used human umbilical vein endothelial cells (HUV-EC-C [HUVEC], ATCC CRL-1730^{TM}, Manassas, VA) that were cultured in endothelial basal media with endothelial growth supplements (Lonza, Hopkinton, MA). This particular HUVEC line is cultured minimally commercially to maintain consistency; these HUVECs are a non-continuous line being pooled from multiple individuals, but these cells are not immortalized and, thus, is suitable for a limited number passages in culture. Here, cells were used between passages 2-8. Cells were passaged onto glass slides (VWR International, Radnor, PA) in 35 mm tissue culture dishes (Corning Inc., Corning, NY). For transfection experiments, cells were transfected using the endothelial cell-specific

Lipofectin transfection reagent (Life Technologies, Grand Island, NY) in Opti-MEM I Reduced Serum Medium (Life Technologies, Grand Island, NY). For these experiments we used rDNA of GFP-Fibrillarin (kind gift from D. Discher, University of Pennsylvania). Cells were incubated for transfection for five hours, at which time we changed to normal growth media and incubated the cells for an additional 24-72 hours prior to experiments to allow for adequate expression and proliferation to confluency.

Drug Treatments

Chromatin condensation experiments were run using either trichostatin A (TSA, 200 ng/mL for 24 hours) for decondensation or sodium azide (NaN_3, 10 mM) and 2-deoxyglucose (2-DG, 50 mM) for one hour for ATP depletion-induced chromatin condensation.

Cell Fixation and Staining

Cell fixation was done using 3.7% formaldehyde in phosphate buffered saline (PBS). Cell permeabilization was done using 0.2% Triton X-100 in PBS. For fluorescence lifetime imaging microscopy (FLIM) experiments, cells were stained with 5 μg/mL Hoechst 33342 (Life Technologies, Grand Island, NY) in PBS. For immunocytochemistry labeling experiments, cells were blocked with 0.2% bovine serum albumin (BSA, Sigma Aldrich, St. Louis, MO) in PBS. We labeled the constitutive heterochromatin marker Histone H3K9me3 with the primary rabbit polyclonal antibody (ab8898, Abcam, Cambridge, England) and a

secondary donkey anti-rabbit antibody (sc-362291, Santa Cruz Biotechnology, Dallas, TX).

Preparation of DNA *in vitro* Solutions

For the DNA *in vitro* solution experiments, double-stranded λ-DNA was obtained from New England Biolabs (Ipswich, MA). All solutions were sterile-filtered. The base buffer was 20 μg/mL of λ-DNA with Hoechst 33342 in 60 mM $MgCl_2$ in 10 mM Tris-HCl. For the ψ-condensation (Polymer-and-Salt-Induced-condensation) experiments, poly(ethylene glycol) 6000 (PEG 6000) was used (M_n 6,000, Sigma-Aldrich, St. Louis, MO) and serially diluted to the proper solution concentration with the base buffer. Dynamic light scattering (DLS) experiments of DNA-PEG 6000 solutions were run using a Malvern Zetasizer Nano ZSP (Malvern, Worcestershire, UK). The fluorescence lifetime dependence experiments with varying ionic strength were done using serial dilutions of $MgCl_2$ in 10 mM Tris-HCl for the indicated concentrations. The fluorescence lifetime viscosity dependence experiments were done using serial dilutions of glycerol-ethylene glycol. Viscosity measurements of glycerol-ethylene glycol solutions were made using Discovery Hybrid Rheometer-2 (TA Instruments, New Castle, DE) using a shear rate sweep of 0.1-10,000 s^{-1}.

Fluorescence Lifetime Imaging Microscopy

Our FLIM setup utilized a Leica TCS SP5 inverted laser scanning confocal microscope and a 100x (1.4 NA) oil immersion objective. For excitation

in the FLIM experiments, a Ti:sapphire mode-locked, pulsed infrared laser (Chameleon, Coherent) system was utilized as the multiphoton excitation source (1 W, average) tuned to 825 nm with pulse-widths of <140 fs delivered at 90 MHz. For emission, a FLIM-specific photomultiplier tube (PMT) was used and collected the spectra from 404-536 nm. Fluorescence lifetime data was acquired and analyzed using previously published methods[19, 31] with a suite of software from Becker & Hickl SPC-830 for time-correlated single photon counting (TCSPC) with 10 ps resolution along with 220 time channels and a 10.8 ns measurement window.

The decay rate of the fluorescence lifetime can be modeled as a summation of exponential decays (Equation 1), where τ_n and a_n are the lifetime and normalized amplitude of the n^{th} exponential decay, respectively. I(t) is the number of photons detected per unit time, t, and I_0 is the offset for the background. The mean fluorescence lifetime is defined as shown in Equation 2.

$$I(t) = I_0 + \sum_n a_n e^{-t/\tau_n} \quad (1)$$

$$\tau_m = \frac{\sum_n a_n \tau_n}{\sum_n a_n} \quad (2)$$

The heat map creation and data analysis of the fluorescence lifetimes were performed in Becker & Hickl SPCImage software. For cell experiments, we segmented the nuclei in each field of view to isolate only nuclear pixel signal for data analysis using MATLAB. We analyzed the fluorescence lifetime fits using a χ^2 test, where Hoechst 33342 was best modeled by a double exponential decay.

Statistics

Magnitudes of the mean fluorescence lifetimes were statistically compared using Student's t-test. Fits of the fluorescence lifetime exponential decay were verified using a χ^2 test. The fit of the fluorescence lifetime dependence of Hoechst 33342 bound to λ-DNA with varying viscosity was tested using ANOVA ($p<<0.001$).

Results

Differential Fluorescence Lifetime in Human Cell Nuclei

The fluorescence lifetime is mostly insensitive to properties of the initial excitation such as the exposure time, intensity and wavelength of the incident light as well as the emission artifacts including fluorophore concentration and photobleaching.[29] Instead, the fluorescence lifetime depends on the local environment of the fluorophore.[29] We first aimed to investigate the fluorescence lifetime sensitivity to chromatin condensation state in human umbilical vein endothelial cell (HUVEC) nuclei for the minor groove DNA-binding fluorophore Hoechst 33342. In control HUVECs, we observe a heterogeneous distribution of fluorescence lifetimes within the nuclei using both Hoechst 33342 (Figure 2.1A, bottom middle panel) and PicoGreen (Figure 2.2A, bottom left panel), which indicates that differential fluorophore environments correspond to varying levels of chromatin condensation. While Hoechst 33342 exhibits selectivity for dsDNA and its fluorescence is largely unaffected by the presence of proteins,[32] PicoGreen allows for confirmation of the FLIM results due to its high sensitivity and the strong linearity of its detection range.[33] We decondensed chromatin with the

histone deacetylase inhibitor Trichostatin A (TSA) and induced chromatin condensation by depleting ATP using sodium azide (NaN_3) and 2-deoxyglucose (2-DG). Treatment with NaN_3+2-DG lead to condensation of chromatin and a more homogeneous distribution of mean fluorescence lifetimes trending towards lower values (Figure 2.1A, bottom left panel). Decondensation of chromatin by treatment with TSA also resulted in a more homogeneous distribution of spatially resolved mean fluorescence lifetimes in the heat maps, but conversely trending towards higher mean fluorescence lifetimes (Figure 2.1A, bottom right panel, and Figure 2.2A, bottom right panel). By contrast, the control cell nucleus exhibited a wide distribution of high and low fluorescence lifetime values ranging between both extremes (Figure 2.1A, bottom middle panel, and Figure 2.2A, bottom left panel). We quantified these changes by calculating the mean fluorescence lifetime using Equation 2 for all segmented nuclei throughout each field of view. Chromatin condensation resulted in a reduction in the mean fluorescence lifetime, while chromatin decondensation resulted in a significant increase (Figure 2.1B and Figure 2.2B). Additionally, TSA treatment resulted in a statistically significant reduction in variance (Figure 2.1C and Figure 2.2C), indicating more uniform chromatin condensation state throughout the nucleus as measured by the mean fluorescence lifetime. Thus, the fluorescence lifetime of chromatin-bound Hoechst 33342 indicates local chromatin condensation state in human cell nuclei.

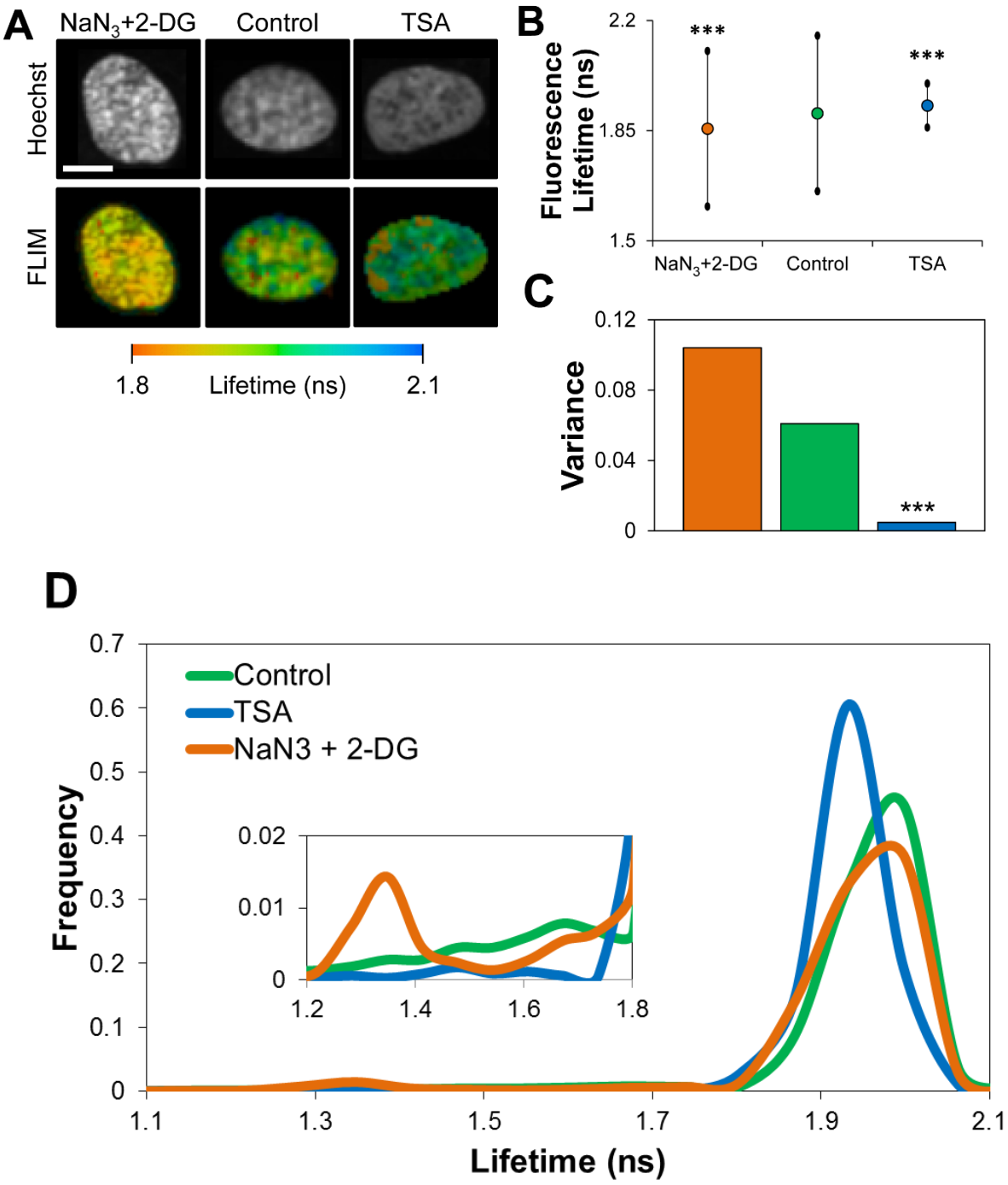

Figure 2.1: Fluorescence lifetime measurements of chromatin condensation state in human umbilical vein endothelial cell nuclei with Hoechst 33342. *(A) Fluorescence intensity confocal images (top) and mean fluorescence lifetime heat maps (bottom) of chromatin is measured in endothelial cell nuclei labeled with*

Hoechst 33342. Cells are treated with NaN_3+2-DG for chromatin hypercondensation or with TSA for chromatin decondensation. Altered fluorescence intensity with treatments show differential chromatin condensation state, with more intense fluorescence arising from highly concentrated condensed chromatin. Mean fluorescence lifetime heat maps similarly indicate spatial arrangement of local fluorophore environments for labeled chromatin consistent with varying chromatin condensation state. Treatment with NaN_3+2-DG results in more punctate regions of fluorescence intensity and shorter mean fluorescence lifetime (orange) relative to untreated controls, while TSA resulted in a significant reduction in punctate regions and longer mean fluorescence lifetime (blue). (B) The mean fluorescence lifetime of segmented nuclei for the various treatment conditions was calculated using Equation 2. Treatment with NaN_3+2-DG resulted in a strong reduction in the mean fluorescence lifetime relative to untreated controls ($p<<0.001$). By contrast, TSA treatment resulted in a dramatic increase in the mean fluorescence lifetime relative to untreated controls ($p<<0.001$) as well as a large reduction in the variance ($p<<0.001$) (C) which indicated an increase in chromatin condensation state homogeneity throughout the cell nucleus. (D) Frequency distribution of the mean fluorescence lifetimes for the three treatment conditions show altered lifetime around 1.9 ns and the presence of a second mode at 1.4 ns for NaN_3+2-DG (inset). Analysis was done using 60-80 segmented nuclei for each treatment condition. Error bars indicate standard deviation of pixel-to-pixel mean fluorescence lifetime differences of segmented nuclei under each treatment condition. Standard deviation was used in place of

standard error of the mean to emphasize the reduction in the fluorescence lifetime variance from chromatin decondensation from TSA treatment (p<<0.001). Scale bar is 10 μm.

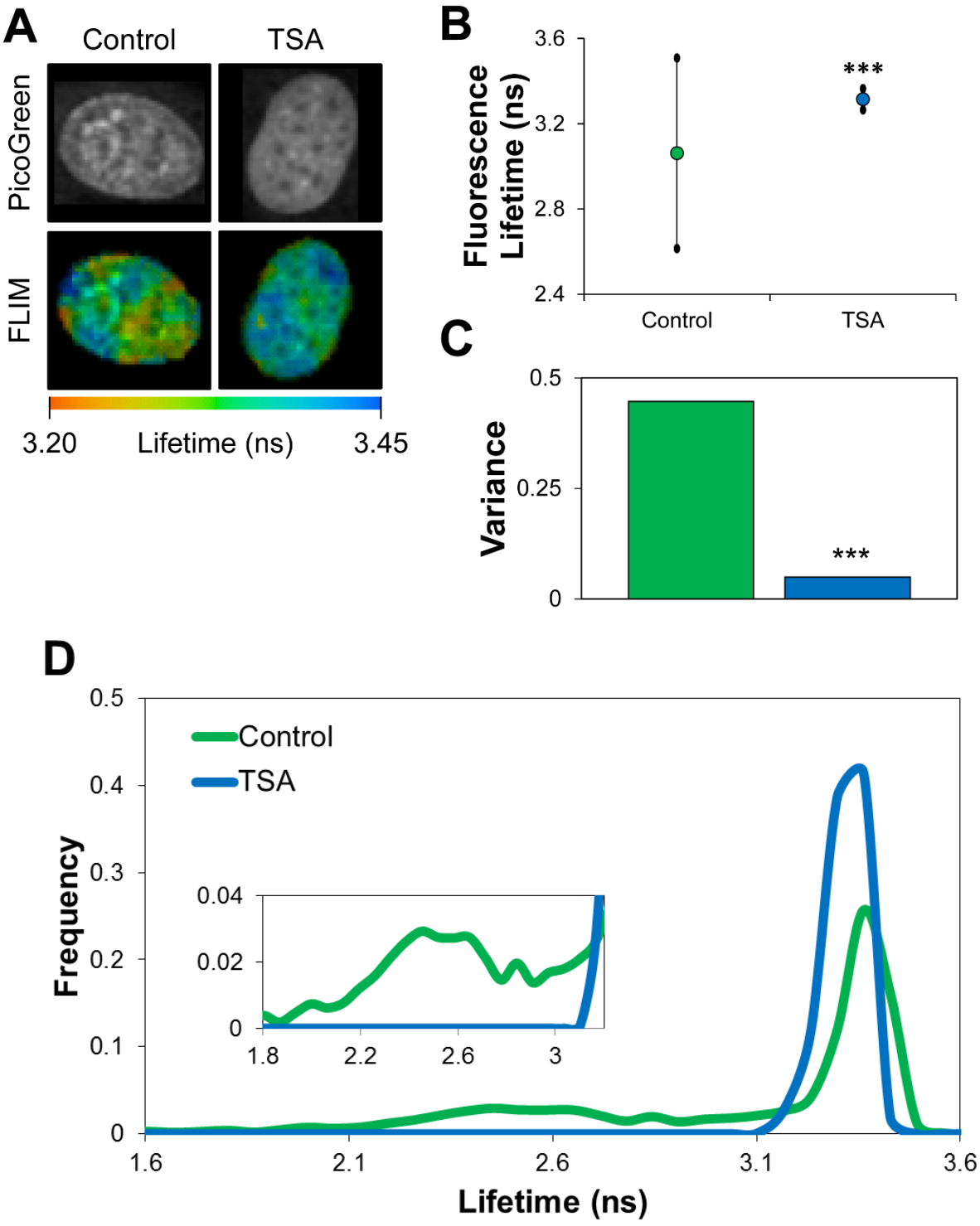

Figure 2.2: Fluorescence lifetime measurements of chromatin condensation state in human umbilical vein endothelial cell nuclei with PicoGreen. *(A) Fluorescence intensity confocal images (top) and fluorescence lifetime heat maps (bottom) of chromatin is measured in endothelial cell nuclei labeled with PicoGreen. Cells are treated with TSA for chromatin decondensation. Altered fluorescence intensity with treatments show differential chromatin condensation state, with more intense fluorescence arising from highly concentrated condensed chromatin. Fluorescence lifetime heat maps similarly indicate spatial arrangement of local fluorophore environments for labeled chromatin consistent with varying chromatin condensation state. Treatment with TSA resulted in a significant reduction in punctate regions and longer fluorescence lifetime (blue). (B) The fluorescence lifetime of segmented nuclei for the various treatment conditions was calculated using Equation 2. Treatment with TSA resulted in a dramatic increase in the fluorescence lifetime relative to untreated controls ($p<<0.001$) as well as a large reduction in the variance ($p<<0.001$) (C) which indicated an increase in chromatin condensation state homogeneity throughout the cell nucleus. (D) Frequency distribution of the fluorescence lifetimes for the two treatment conditions. Analysis was done using 60-80 segmented nuclei for each treatment condition. Error bars indicate standard deviation of pixel-to-pixel fluorescence lifetime differences of segmented nuclei under each treatment condition. Standard deviation was used in place of standard error of the mean to emphasize the reduction in the fluorescence lifetime variance from chromatin decondensation from TSA treatment ($p<<0.001$). Scale bar is 10 μm.*

Fluorescence Lifetime Sensitivity of λ-DNA Condensation

Having established a relationship between chromatin condensation and fluorescence lifetime, we aimed to determine the condensation-dependent environmental effectors driving the change in the fluorescence lifetime of the fluorophore. The fluorescence lifetime is known to depend on factors such as viscosity, polarity, temperature and the presence of quenchers in the surrounding medium local to the fluorophore.[29] We examined the fluorescence lifetime dependence on environmental factors associated with condensation for λ-DNA, which notably corresponds with altered DNA conformation and local viscosity.

We induced condensation of λ-DNA by macromolecular crowding using the inert, neutral flexible polymer poly(ethylene glycol) (M_n 6000, PEG 6000) in the presence of a divalent cation (Mg^{2+}) often called polymer-and-salt-induced (psi or ψ) condensation.[34] This allowed us to remove *in situ* nuclear artifacts of DNA-binding proteins (particularly histones) and the resulting ionic interactions from the direct effect of condensation-induced changes on structure and mechanics that influence the fluorescence lifetime. Above a threshold concentration of PEG in the presence of divalent cations, DNA condenses due to depletion forces between PEG and DNA through the entropically-favored increase in excluded volume for PEG associated with this condensation.[35, 36] We characterized the onset of DNA condensation using dynamic light scattering (DLS), where we observed a reduction in diffusivity consistent with DNA condensation for [PEG] of 50 mg/mL (Figure 2.3).[37] Further addition of PEG, including beyond the overlap concentration,[37] results in a greater reduction in the

diffusivity that likely indicates the reduced diffusivity of multi-molecular aggregates[38] of condensed DNA from the increased solution viscosity or production of larger multi-molecular aggregates (Figure 2.3).

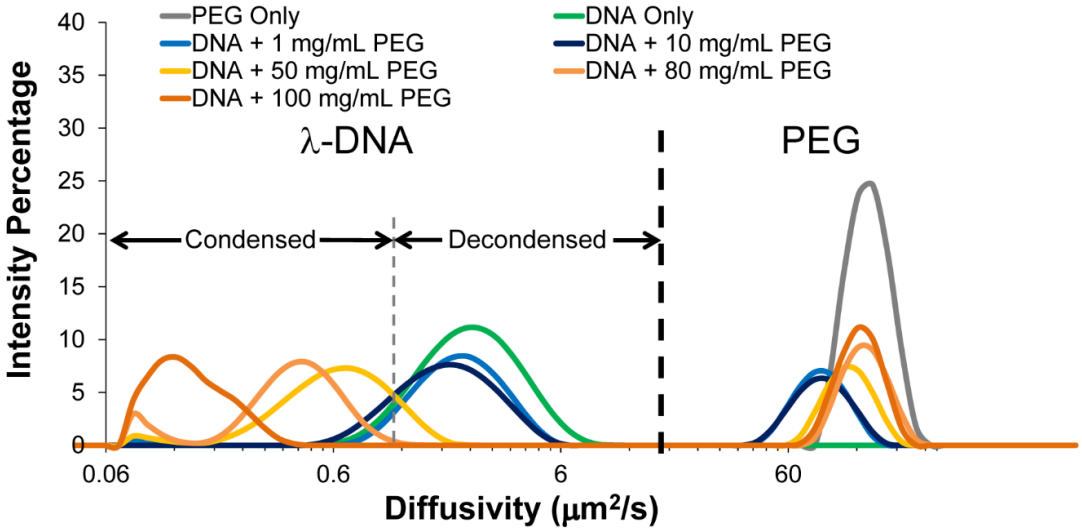

Figure 2.3: Dynamic light scattering measurements of *in vitro* λ-DNA solutions of varying condensation state. *Measurements of PEG 6000 (gray) and λ-DNA (green) alone indicate their location within the combined solutions. As we increase PEG concentration, initially we see a negligible effect on the λ-DNA diffusivity distribution (shades of blue). At 50 mg/mL, the solution is above a threshold concentration of PEG 6000 and we observe a reduction in the λ-DNA diffusivity distribution, including a sharp decrease beyond the overlap concentration for PEG 6000 at 100 mg/mL (shades of yellow-orange). The initial reduction stems from the polymer-and-salt-induced (psi or ψ) condensation by macromolecular crowding-induced depletion forces. We show the regime over which λ-DNA is condensed and decondensed along with the location of the PEG*

population. Distributions are derived from 10-15 runs per individual measurements and averages of several measurements.

We measured the mean fluorescence lifetime associated with the PEG-induced DNA condensation and observed a significant reduction in the mean fluorescence lifetime for [PEG] of 50 mg/mL or greater (Figure 2.4). This is consistent with the *in situ* experiments of induced chromatin condensation in HUVEC nuclei where it resulted in a reduced mean fluorescence lifetime (Figure 2.1 and 2.2). Interestingly, following DNA condensation there was no further change in the mean fluorescence lifetime despite increasing solution viscosity associated with higher [PEG] including the sharp increase beyond overlap concentration[37] at 100 mg/mL. Thus, upon DNA condensation, the fluorescence lifetime seemingly becomes largely insensitive to further changes in viscosity.

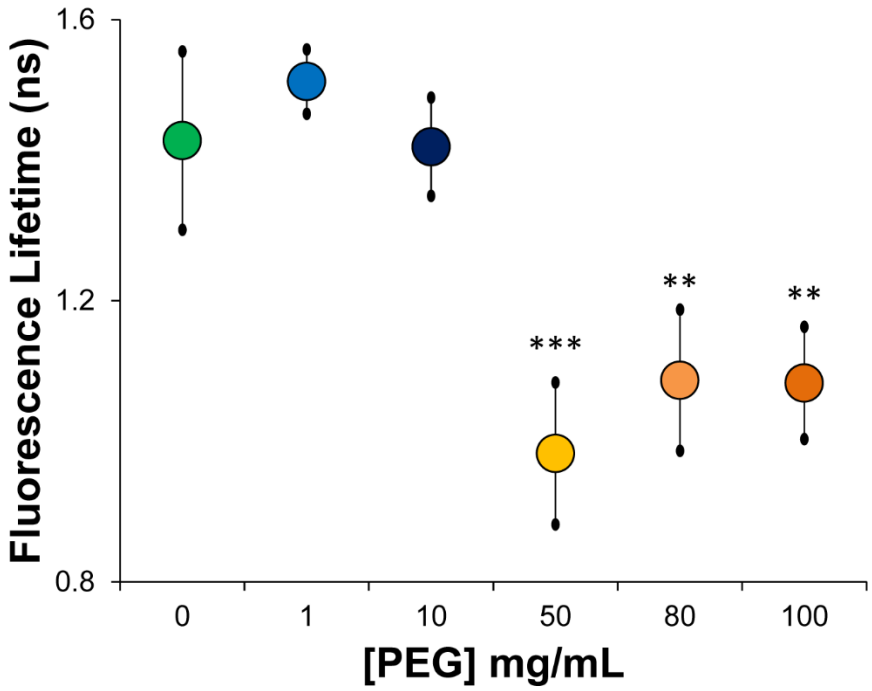

Figure 2.4: Fluorescence lifetime measurements of *in vitro* λ -DNA solutions of varying condensation state. *As in the DLS experiments, we observe a dramatic reduction in the mean fluorescence lifetime above the threshold PEG 6000 concentration (~50 mg/mL; p<0.01) that is maintained at higher concentrations (shades of yellow-orange symbols). Interestingly, despite the increase in viscosity that occurs with increasing PEG concentration (including the sharp increase in trend above the overlap concentration at 100 mg/mL) we see no further statistical change in the mean fluorescence lifetime despite the dependence of the fluorescence lifetime on local viscosity. Error bars reflect standard deviation. Statistical significance based on Student's t-test with the 0 mg/mL PEG, with **p<0.025 and ***p<0.01.*

While PEG allows for investigation of the role of DNA condensation in the absence of polarity effects associated with binding proteins near sites of Hoechst 33342 binding, it simultaneously increases solution viscosity while reducing the dielectric constant of the solution (though only moderately reducing the dielectric constant over this range of concentration[39]) with increasing [PEG]. We aimed to delineate the exact roles of ionic strength and solution viscosity on the fluorescence lifetime of Hoechst 33342-bound DNA. We varied solution polarity using solutions of varying [$MgCl_2$] since local polarity changes in the cell likely stem predominately from ion flux. We observed no statistically significant change in the mean fluorescence lifetime with increasing $MgCl_2$ concentration by over three orders of magnitude from 0 M to more than 1 M (Figure 2.5). This is

consistent with the relative insensitivity of the fluorescence intensity of bis-benzimide (Hoechst family) dyes with salt concentration upon binding DNA.[32]

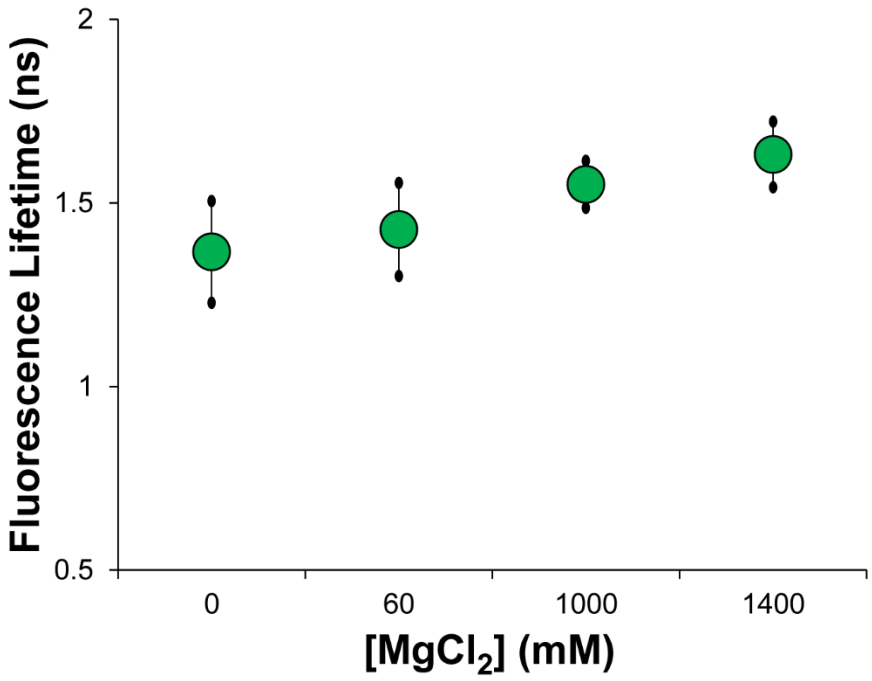

Figure 2.5: Fluorescence lifetime measurements of *in vitro* λ -DNA solutions of varying ionic strength solutions. *The mean fluorescence lifetime of solutions of λ-DNA with varying concentration of $MgCl_2$ shows no statistical dependence on ionic strength. Across a wide distribution of salt concentration varying over three orders of magnitude we see no statistically significant effect on the mean fluorescence lifetime, indicating it is not strongly influenced by salt concentration. Statistical comparisons made by Student's t-test, with no statistical difference between solutions.*

Using glycerol-ethylene glycol solutions of varying concentration, we controlled for media polarity changes due to the similarity of their dielectric constants[29] thereby allowing us to effectively isolate the fluorescence lifetime

dependence on viscosity alone. We observed a statistically significant increase in fluorescence lifetime magnitudes with viscosity, and confirmed the significance of the power-law trend ($\sim\eta^{0.2}$) of fluorescence lifetime with solution viscosity (Figure 2.6). The strong statistical significance of the power-law fit ($p<<0.001$) indicates the dominant role of viscosity on the fluorescence lifetime of Hoechst 33342 bound to DNA. However, the dependence of the fluorescence lifetime on solution viscosity appeared to be less significant than the dependence on DNA condensation state. In aggregate, these experiments indicate that Hoechst 33342 bound to DNA is mostly insensitive to local solution ionic strength, but acutely dependent on viscosity particularly with respect to the viscosity change associated with varying DNA condensation state.

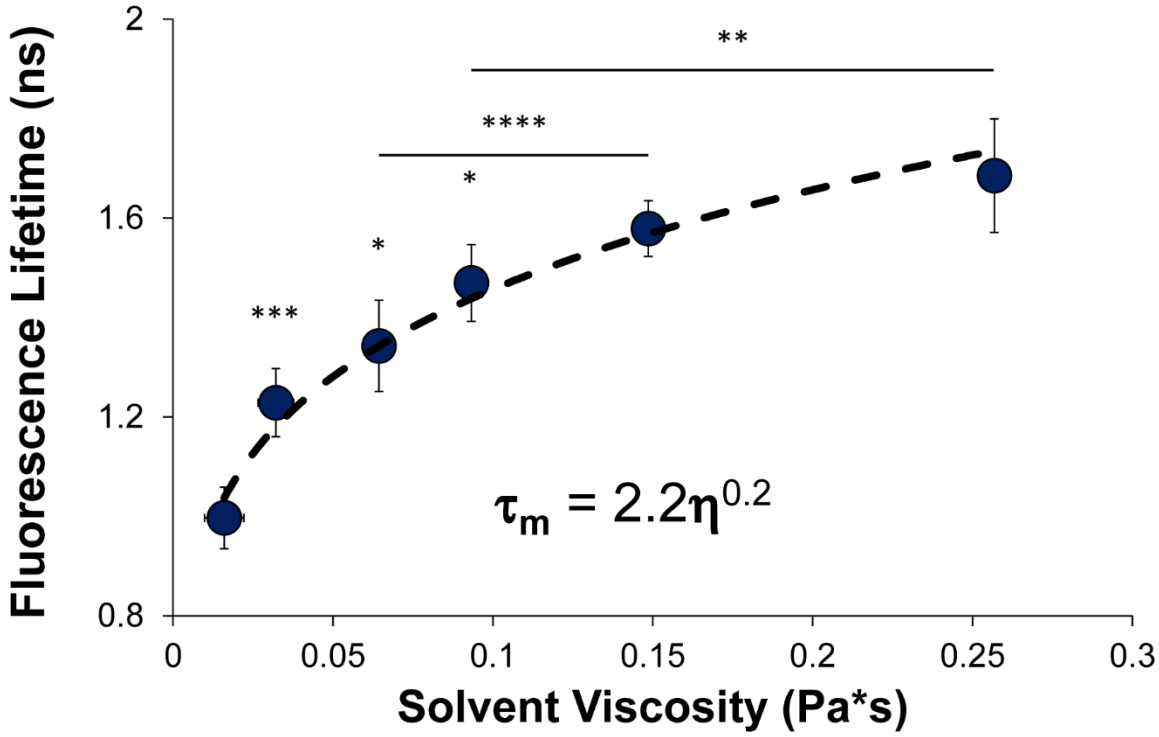

Figure 2.6: Fluorescence lifetime measurements of *in vitro* λ -DNA solutions of varying viscosity. *We determine the mean fluorescence lifetime dependence of*

*Hoechst 33342 bound to λ-DNA in solutions of varying viscosity glycerol-ethylene glycol solutions. We see a strong dependence of the mean fluorescence lifetime on viscosity over the range shown here. Viscosity measurements for the glycerol-ethylene solutions were determined using a Discovery Hybrid Rheometer-2. Statistical comparisons made by Student's t-test, with *p<0.05, **p<0.025, ***p<0.01 and ****p<0.001. All statistical comparisons of the magnitudes are with the previous point unless otherwise indicated by lines. The viscosity power-law fit dependence of the mean fluorescence lifetime, based on the known phenomenological relationship between fluorescence lifetime and viscosity, was determined using ANOVA (p<<<0.001).*

Spatially-Resolved *in situ* Chromatin Condensation State

In addition to quantifying and spatially resolving chromatin condensation state during physiological and pathological changes, the ability to investigate chromatin condensation state in the context of ongoing functional processes enables us to study the role of these deeper layers of genome function in facilitating nuclear organization. Previous work has highlighted the role of chromatin in serving to nucleate *de novo* formation of functional sites within the nucleus, thereby lending credibility to the idea that the nucleus is a self-organizing system.[4] FLIM provides the means to investigate the interrelation of chromatin structure and organization with function in the nucleus through the enhanced spatial resolution.

We transfect HUVECs with the nucleolar protein GFP-Fibrillarin as our indicator of nucleolar location since it is present at active ribosomal gene transcription centers.[1, 40] The chromatin organization associated with the nucleolus, being a functional site of very low internal chromatin composition[41] as well as mostly homogenous chromatin structural state associated with decondensation for active ribosomal gene transcription on the interior that is then bounded by dense heterochromatin[18], makes it an ideal candidate for testing the spatial resolution of FLIM for assaying chromatin condensation state. Consistent with the known organization of chromatin condensation state of nucleoli, we see the internal nucleolar regions are associated with some of the highest mean fluorescence lifetime regions of the nuclear interior in the mean fluorescence lifetime heat maps indicating highly decondensed chromatin (Figure 2.7). Further, we observe that these regions are bounded by a noticeable amount of very low mean fluorescence lifetimes associated with tightly condensed heterchromatin domains that bound the nucleolus. The slight overlap of lower mean fluorescence lifetime over a portion of the GFP-Fibrillarin signal likely results from known chromatic aberrations and z-plane differences associated with the near infrared[42] (high wavelength of 825 nm) multiphoton excitation of Hoechst 33342 utilized for FLIM relative to the visible laser (low wavelength of 488 nm) excitation of GFP.

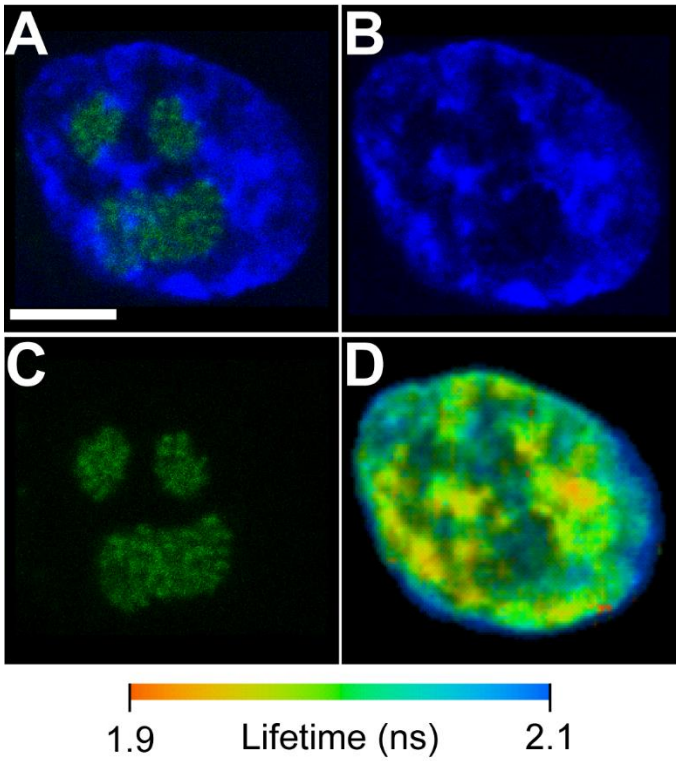

Figure 2.7: Fluorescence lifetime spatial distribution around nucleoli in endothelial cell nuclei. *(A) An overlay of a confocal image of HUVECs labelled for chromatin with Hoechst 33342 (blue, B) and nucleoli with transfected nucleolar protein GFP-Fibrillarin (green, C). (D) The spatially resolved mean fluorescence lifetime of the same nucleus shows largely decondensed chromatin within the interior of the nucleolus (deep blue regions). Further, the nucleoli are bounded by condensed chromatin (yellow-orange regions) consistent with heterochromatin-bound nucleolar regions. Other condensed chromatin regions show correspondence with the brighter, more punctate regions of chromatin fluorescence (B) consistent with heterochromatin. Scale bar is 5 μm.*

We also compare the fluorescence lifetime measurement of chromatin condensation state with the constitutive heterochromatin marker H3K9me3

labeled by immunocytochemistry (Figure 2.8). While the heterochromatin marker provides for a decently punctate image of heterochromatin regions, the reliance solely on the fluorescence intensity of the measurement with limited spatial resolution obfuscates clear delineation of the gradations of heterochromatin regions since it merely denotes the presence or absence of H3K9me3 (as discussed previously). Nonetheless, we qualitatively observe reduced mean fluorescence lifetimes associated with the most prominent regions of the heterochromatin label (Figure 2.8), indicating the fluorescence lifetime is measuring the levels of chromatin condensation as consistent with the chemically-induced chromatin condensation and decondensation discussed previously (Figure 2.1). However, the heat maps of the mean fluorescence lifetimes allow us to visualize and quantify intermediate states of chromatin condensation associated with the constitutive heterochromatin marker.

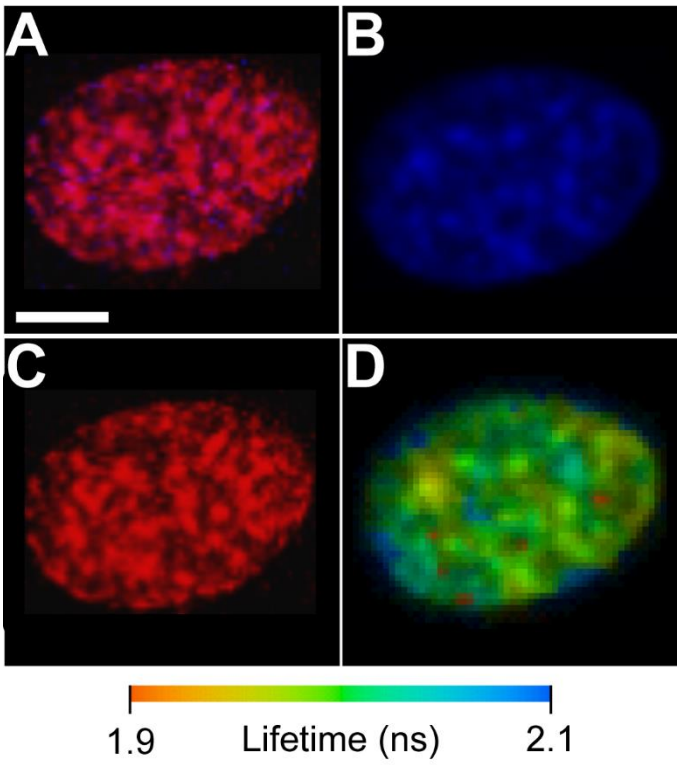

Figure 2.8: Fluorescence lifetime spatial distribution around of endothelial cells labelled for heterochromatin marker H3K9me3 with immunocytochemistry. *(A) An overlay of a confocal image of HUVECs labelled for chromatin with Hoechst 33342 (blue, B) and constitutive heterochromatin marker histone H3 tri-methylated at lysine residue 9 (H3K9me3) by immunocytochemistry (red, C). (D) The spatially resolved mean fluorescence lifetime of the same nucleus shows qualitative agreement with the heterochromatin marker corresponding to more condensed chromatin (green-orange regions). Scale bar is 5 μm.*

Discussion

The quantitative visualization of chromatin structure and organization within the nucleus, including its condensation state and spatial arrangement, remains a major obstacle to understanding genome function. The capacity to spatially resolve chromatin condensation state throughout the nucleus has major bearing on understanding both the functional attributes associated with those states and the dynamics of chromatin through the nuclear interior. Our emerging understanding of stem cell differentiation[43] as well as cancer pathology[44] related to DNA repair[20] has highlighted the integral role of chromatin structural modifications and repositioning associated with these functional processes. Yet, questions still remain as to the causal relationship of chromatin organization with these functions including the influence of the structural state and dynamic movements. Here we aimed to address the limitation of quantification of

chromatin condensation *in situ* through the development of a technique for high-throughput quantification of chromatin condensation state and it spatial arrangement in a primary human cell line using only a cell-permeable, DNA-binding fluorophore via fluorescence lifetime and its unique dependence on the mechanical-structural interrelation of chromatin. This method does not require transfection, fixation, permeabilization or disruption of large scale chromatin structure to allow in large macromolecules (e.g., antibodies, hybridization partners) and provides submicron-scale resolution of DNA and chromatin condensation states.

Physical Effectors Influencing the Fluorescence Lifetime Dependence of Chromatin Condensation State *in situ* and *in vitro*

We show the dependence of fluorescence lifetime on chromatin condensation state in primary human cell nuclei using chemically-induced global changes. Our results indicate an increase in the fluorescence lifetime corresponds to chromatin decondensation and *vice versa* (Figure 2.9A and 2.9B). Further, using macromolecular crowding-induced DNA condensation (ψ condensation) for *in vitro* solutions, we demonstrate that the fluorescence lifetime change is dependent on the altered structural state associated with condensation independent of the presence of binding proteins. We highlight that the physical parameter impacting the fluorescence lifetime change upon condensation is the stark transition in the sensitivity to viscosity associated with these two states of DNA condensation. Decondensed λ-DNA, being a largely flexible polymer (L_C~ 16.2 μm >> L_P ~0.05μm[45]), maintains a compliant mechanical state undergoing large

length scale (relative to the Hoechst 33342 minor groove-binding site of ~2 nm[1, 46]) Brownian polymeric fluctuations that render the fluorescence lifetime sensitive to local solution viscosity (Figure 2.9C). After condensation, these large length scale λ-DNA fluctuations are reduced, diminishing the sensitivity to the viscosity as well as the local solution viscosity due to the simultaneous condensation of other λ-DNA molecules. Within the context of the nucleus (Figure 2.9A and 2.9B), chromatin condensation similarly corresponds to a less viscous environment relative to decondensed chromatin. This "switch" sensitivity upon condensation renders the fluorescence lifetime sensitive to the condensation state and intermediates via the viscosity when not condensed. Previous works have similarly demonstrated chromatin decondensation results in more viscous and deformable cell nuclei.[26, 27]

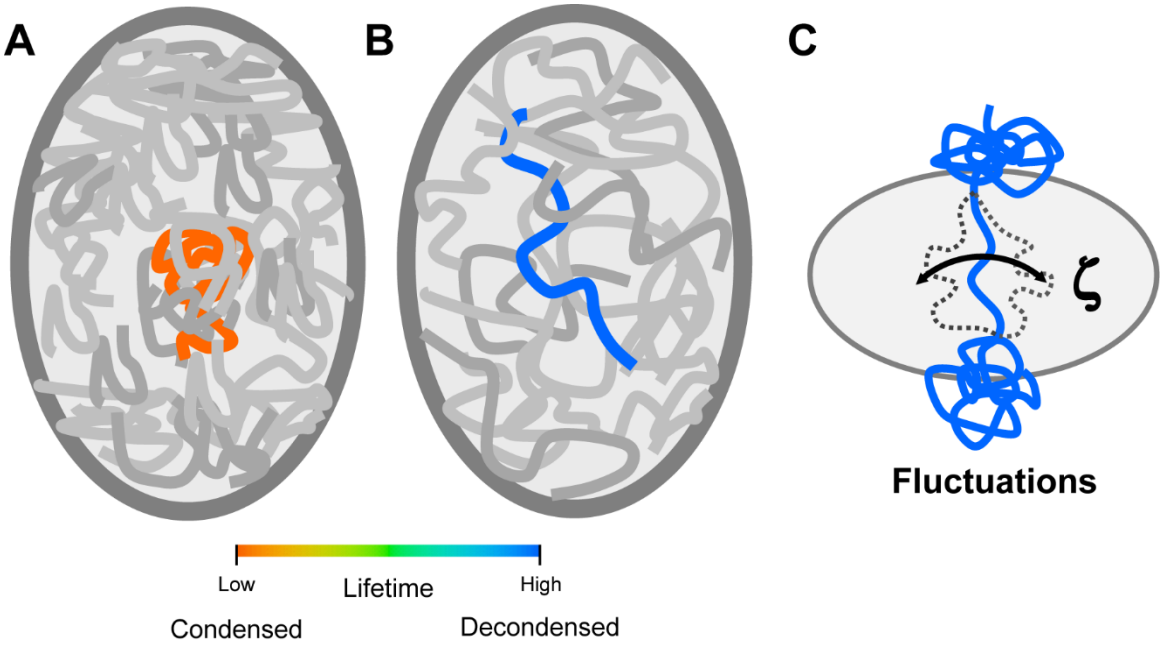

Figure 2.9: Changes in chromatin condensation state in the nuclear interior impact the local viscosity which strongly influence the fluorescence lifetime. *In most cells, the nucleus has regions of highly condensed chromatin (A). While the concentration of chromatin in the nuclear interior is unchanged upon decondensation, the nuclear interior becomes more viscous due to the reduction in densely packed chromatin (B). As such, the chromatin in condensed regions has a low fluorescence lifetime (orange in A) and chromatin in decondensed regions has a high fluorescence lifetime (blue in B). (C) Decondensed chromatin undergoes fluctuations influenced by frictional drag (ζ) from the surrounding environment. Regions of higher viscosity arising from chromatin decondensation have increased mean fluorescence lifetimes.*

The lack of a strong influence of [$MgCl_2$] on the fluorescence lifetime is somewhat surprising given the general association of fluorescence lifetime of molecules in solution on ionic strength through polarity.[29] However, we suggest that the minor-groove binding of Hoechst 33342 to DNA[46] makes the fluorophore sensitivity to the media ionic strength relatively negligible likely due to the presence of interactions with the base pairs themselves (where hydrogen bonds[47] and possibly aromatic ring interactions may occur). This idea is supported by the reduced sensitivity of bis-benzimide (Hoechst family) dyes to pH (over a broad range) upon binding to DNA as well as the relative insensitivity of the fluorescence to [$MgCl_2$] and [NaCl] over broad ranges[48] in the bound state. Thus, upon the binding of Hoechst 33342 to chromatin, the chromatin structural state

and its resulting effect on local viscosity and as well as the sensitivity of its fluctuations to viscosity proves the dominating environmental characteristic influencing fluorescence lifetime. This is consistent with the known effect of increased viscosity on increasing the fluorescence lifetime of the Hoechst family of dyes, including a dramatic increase upon binding DNA.[29]

Previous work has demonstrated that the viscosity dependence of the fluorescence lifetime can be considerable depending on the internal flexibility of the fluorophore structure, where those that more freely undergo internal rotations (often termed "molecular rotors") have strong fluorescence lifetime dependence on viscosity.[29] In this case, the binding of Hoechst 33342 to DNA renders the fluorescence lifetime susceptible to both the structural state of the DNA and the viscosity of the surrounding medium, which would influence the ability of DNA to reptate or fluctuate. Further, since we observe the same results with PicoGreen, it suggests this is likely not a fluorophore-specific phenomena. Thus, the dependence of the fluorescence lifetime on chromatin condensation and viscosity may not depend appreciably on structure-specific behavior of the fluorophore associated with internal rotations, but instead local structure associated with the binding state of that fluorophore and the molecule it binds to. Thus, given the length scale dependence of fluorescence lifetime being on the order of angstroms up to <10 nm and the lack of effect over dramatic ranges of ionic strength, the condensation state of DNA in the context of Brownian fluctuations and the associated viscous drag becomes paramount to the fluorescence lifetime dependence (Figure 2.9C). Since these Brownian fluctuations depend on both the

structural state of the polymer itself and the resistance in the surrounding medium (viscosity), the "switch" sensitivity of the fluorescence lifetime enables us to quantify chromatin condensation state through the reduced mechanical flexibility and viscosity associated with increasing condensation. This dependence of the fluorescence lifetime on chromatin condensation state through mechanics provides a high-throughput technique for quantifying and spatially resolving condensation state throughout the nucleus.

FLIM to Measure Chromatin Structure and Mechanics *in situ*

The utility of the fluorescence lifetime measurement of chromatin condensation lies in its ability to be done *in situ* and with spatial resolution for a variety of cell nuclei under varying physiological and pathological conditions. Where previous methods have failed to provide the proper resolution or be utilized for primary cell lines, the fluorescence lifetime proves capable of surmounting these limitations through its dependence on mechanical chromatin compliance as related to its condensation state.

Leveraging mechanical measurements for use in understanding dynamic cellular processes has yielded strong success.[2, 19, 23, 27, 49, 50, 51] The critical obstacle of mechanics-based measurements depends on the elucidation of the precise relationship between the mechanical state and the underlying biological functional state. Here, through both *in vitro* and *in situ* fluorescence lifetime measurements of DNA and chromatin, respectively, we identify the coupling of the fluorescence lifetime to the condensation state-dependent sensitivity to local solution viscosity.

We show the utility of these measurements for large scale changes in chromatin structure and organization as well as spatially resolved chromatin condensation at distinct functional sites. Resolving the chromatin structure within and around nucleoli highlights the capability of FLIM for determining the role of chromatin condensation in the context of functional organization. While ribosomal biogenesis in the nucleolus is a continuous process in interphase nuclei, FLIM can similarly be utilized to capture snapshots of chromatin condensation with respect to the progression of other functional processes. This affords the opportunity to monitor the role of chromatin hierarchical organization (higher-order structural state and spatial arrangement) in the context of genome function during physiological changes.

In Chapter III we will demonstrate the use of particle tracking to measure chromatin condensation state *in situ*.[19] Particle tracking measurements boast the benefit of additional biological information associated with the driving forces of chromatin fluctuations (and, thus, motor activity),[19] while FLIM allows for mapping of the spatial distribution of chromatin condensation states as well as high-throughput capacity relative to other mechanical methods. Particle tracking experiments yield results of many particles, but often only capture a limited number of cells per experiment[25, 52, 53] and require long duration experiments to capture evolving phenomena of biological processes.[19, 52] By contrast, FLIM measurements allow up to 30-40 nuclei in a single field of view (pending cell density) to be sampled in <10 min (in some cases 1 min). This, coupled with the capacity to resolve rapid condensation state changes on these shorter time scales

and within the context of other labeled functional sites, provides an ideal technique for understanding chromatin structural state changes and positioning effects as they are directly related to function.

Using FLIM to quantify changes in chromatin condensation state in cells under various physiological or pathological conditions provides the means to investigate the hierarchical layers of chromatin organization in this context *in situ*. Recent efforts aimed at understanding the physiology of cell lineage determination during stem cell differentiation hinge in part on the ability to determine how the cell nucleus organizes the genome during these changes, including epigenetic modifications for chromatin remodeling and altered chromatin association with the nuclear periphery.[43] FLIM proves capable of simultaneously monitoring both as well as the temporal evolution. This would also enable better understanding of cellular reprogramming for potential therapies, where the same phenomena are at play.[53] Another potential application is the identification of[54] or investigation of[55] cancerous cell types, which are hallmarked by aberrant nuclear organization and dysregulation of the genome. Determining whether structural defects in chromatin organization cause the observed phenotypes or if they are symptomatic of altered gene expression from local changes at a particular gene is current obstacle in cancer pathology for which FLIM would be useful. These future applications of FLIM for assaying hierarchical chromatin organization in human cell nuclei highlight the utility of this high-throughput mechanical technique that provides a promising tool for investigating these deeper layers of genome function.

Acknowledgements

We gratefully acknowledge use of the multiphoton confocal imaging system from Mohammad Islam and help with use and analysis by Brian Holt (Carnegie Mellon, Materials Science and Engineering). Additional thanks to Lynn Walker for her insight into the polymer characterization and rheology as well as Melissa Dao for help with the rheometry experiments (Carnegie Mellon Chemical Engineering). This work is supported by the NSF (NSF-CBET-0954421, CMMI-1300476 to KND and DMR-0619424 to Mohammad Islam) and the ARCS Foundation (STS), Bertucci Fellowship (STS), and James C. Meade Fellowship (STS).

References

1. B. Alberts, J. H. Wilson and T. Hunt, *Molecular biology of the cell*, 5th edn., Garland Science, New York, 2008.
2. L. Bintu, T. Ishibashi, M. Dangkulwanich, Y. Y. Wu, L. Lubkowska, M. Kashlev and C. Bustamante, *Cell*, 2012, **151**, 738-749.
3. R. M. Martin and M. C. Cardoso, *FASEB journal : official publication of the Federation of American Societies for Experimental Biology*, 2010, **24**, 1066-1072.
4. T. Misteli, *Cell*, 2007, **128**, 787-800.
5. E. Heitz, *Jahrb Wiss Botanik.*, 1928, **69**, 762-818.
6. E. Fedorova and D. Zink, *Bba-Mol Cell Res*, 2008, **1783**, 2174-2184.
7. K. N. Dahl, E. A. Booth-Gauthier and B. Ladoux, *Journal of biomechanics*, 2010, **43**, 2-8.
8. C. L. Woodcock and R. P. Ghosh, *Csh Perspect Biol*, 2010, **2**.
9. Y. J. Wang, S. Maharana, M. D. Wang and G. V. Shivashankar, *Sci Rep-Uk*, 2014, **4**.
10. C. J. Burd, J. M. Ward, V. J. Crusselle-Davis, G. E. Kissling, D. Phadke, R. R. Shah and T. K. Archer, *Mol Cell Biol*, 2012, **32**, 1805-1817.
11. O. Ram, A. Goren, I. Amit, N. Shoresh, N. Yosef, J. Ernst, M. Kellis, M. Gymrek, R. Issner, M. Coyne, T. Durham, X. L. Zhang, J. Donaghey, C. B. Epstein, A. Regev and B. E. Bernstein, *Cell*, 2011, **147**, 1628-1639.
12. N. C. Riddle, A. Minoda, P. V. Kharchenko, A. A. Alekseyenko, Y. B. Schwartz, M. Y. Tolstorukov, A. A. Gorchakov, J. D. Jaffe, C. Kennedy,

D. Linder-Basso, S. E. Peach, G. Shanower, H. Y. Zheng, M. I. Kuroda, V. Pirrotta, P. J. Park, S. C. R. Elgin and G. H. Karpen, *Genome Res*, 2011, **21**, 147-163.
13. P. K. Geyer, M. W. Vitalini and L. L. Wallrath, *Current opinion in cell biology*, 2011, **23**, 354-359.
14. E. Fedorova and D. Zink, *Current opinion in genetics & development*, 2009, **19**, 166-171.
15. L. Meldi and J. H. Brickner, *Trends in cell biology*, 2011, **21**, 701-708.
16. J. Rino and M. Carmo-Fonseca, *Trends in cell biology*, 2009, **19**, 375-384.
17. M. Dundr and T. Misteli, *Csh Perspect Biol*, 2010, **2**.
18. S. van Koningsbruggen, M. Gierlinski, P. Schofield, D. Martin, G. J. Barton, Y. Ariyurek, J. T. den Dunnen and A. I. Lamond, *Molecular biology of the cell*, 2010, **21**, 3735-3748.
19. S. T. Spagnol and K. N. Dahl, *Integr Biol-Uk*, 2014, **6**, 523-531.
20. V. Dion and S. M. Gasser, *Cell*, 2013, **152**, 1355-1364.
21. F. Mora-Bermudez and J. Ellenberg, *Methods*, 2007, **41**, 158-167.
22. T. Seidal, A. J. Balaton and H. Battifora, *Am J Surg Pathol*, 2001, **25**, 1204-1207.
23. K. V. Iyer, S. Pulford, A. Mogilner and G. V. Shivashankar, *Biophysical journal*, 2012, **103**, 1416-1428.
24. D. Lleres, J. James, S. Swift, D. G. Norman and A. I. Lamond, *Journal of Cell Biology*, 2009, **187**, 481-496.
25. K. N. Dahl, A. J. Engler, J. D. Pajerowski and D. E. Discher, *Biophysical journal*, 2005, **89**, 2855-2864.
26. J. D. Pajerowski, K. N. Dahl, F. L. Zhong, P. J. Sammak and D. E. Discher, *Proceedings of the National Academy of Sciences of the United States of America*, 2007, **104**, 15619-15624.
27. K. J. Chalut, M. Hopfler, F. Lautenschlager, L. Boyde, C. J. Chan, A. Ekpenyong, A. Martinez-Arias and J. Guck, *Biophysical journal*, 2012, **103**, 2060-2070.
28. A. Zidovska, D. A. Weitz and T. J. Mitchison, *Proceedings of the National Academy of Sciences of the United States of America*, 2013, **110**, 15555-15560.
29. M. Y. Berezin and S. Achilefu, *Chem Rev*, 2010, **110**, 2641-2684.
30. B. J. Bacskai, J. Skoch, G. A. Hickey, R. Allen and B. T. Hyman, *J Biomed Opt*, 2003, **8**, 368-375.
31. P. N. Yaron, B. D. Holt, P. A. Short, M. Losche, M. F. Islam and K. N. Dahl, *Journal of nanobiotechnology*, 2011, **9**, 45.
32. C. Labarca and K. Paigen, *Anal Biochem*, 1980, **102**, 344-352.
33. A. I. Dragan, J. R. Casas-Finet, E. S. Bishop, R. J. Strouse, M. A. Schenerman and C. D. Geddes, *Biophysical journal*, 2010, **99**, 3010-3019.
34. V. A. Bloomfield, *Biopolymers*, 1997, **44**, 269-282.
35. G. Kleideiter and E. Nordmeier, *Polymer*, 1999, **40**, 4025-4033.
36. G. Kleideiter and E. Nordmeier, *Polymer*, 1999, **40**, 4013-4023.
37. K. Hirano, M. Ichikawa, T. Ishido, M. Ishikawa, Y. Baba and K. Yoshikawa, *Nucleic Acids Res*, 2012, **40**, 284-289.

38. N. V. Hud and I. D. Vilfan, *Annu Rev Bioph Biom*, 2005, **34**, 295-318.
39. K. Arnold, A. Herrmann, L. Pratsch and K. Gawrisch, *Biochim Biophys Acta*, 1985, **815**, 515-518.
40. C. Martin, S. Chen, A. Maya-Mendoza, J. Lovric, P. F. Sims and D. A. Jackson, *Journal of cell science*, 2009, **122**, 1551-1562.
41. A. Pliss, A. N. Kuzmin, A. V. Kachynski and P. N. Prasad, *Biophysical journal*, 2010, **99**, 3483-3491.
42. J. K. Streit, S. M. Bachilo and R. B. Weisman, *Analytical chemistry*, 2013, **85**, 1337-1341.
43. D. Peric-Hupkes, W. Meuleman, L. Pagie, S. W. M. Bruggeman, I. Solovei, W. Brugman, S. Graf, P. Flicek, R. M. Kerkhoven, M. van Lohuizen, M. Reinders, L. Wessels and B. van Steensel, *Mol Cell*, 2010, **38**, 603-613.
44. E. Lever and D. Sheer, *J Pathol*, 2010, **220**, 114-125.
45. C. Bustamante, J. F. Marko, E. D. Siggia and S. Smith, *Science*, 1994, **265**, 1599-1600.
46. D. R. Boer, A. Canals and M. Coll, *Dalton T*, 2009, 399-414.
47. C. Zimmer and U. Wahnert, *Prog Biophys Mol Bio*, 1986, **47**, 31-112.
48. C. Labarca and K. Paigen, *Anal Biochem*, 1980, **102**, 344-352.
49. B. Hampoelz, Y. Azou-Gros, R. Fabre, O. Markova, P. H. Puech and T. Lecuit, *Development*, 2011, **138**, 3377-3386.
50. A. J. Engler, S. Sen, H. L. Sweeney and D. E. Discher, *Cell*, 2006, **126**, 677-689.
51. E. A. Booth-Gauthier, T. Alcoser, K. N. Dahl and G. Yang, *Biophysical journal*, 2012.
52. M. Platani, I. Goldberg, A. I. Lamond and J. R. Swedlow, *Molecular biology of the cell*, 2002, **13**, 376a-376a.
53. R. P. Koche, Z. D. Smith, M. Adli, H. C. Gu, M. C. Ku, A. Gnirke, B. E. Bernstein and A. Meissner, *Cell Stem Cell*, 2011, **8**, 96-105.
54. D. Zink, A. H. Fischer and J. A. Nickerson, *Nat Rev Cancer*, 2004, **4**, 677-687.
55. T. Misteli, *Csh Perspect Biol*, 2010, **2**.

Chapter III

Active Cytoskeletal Force and Chromatin Condensation Independently Modulate Chromatin Fluctuations

Introduction

The genome in human cells is a meter of DNA wound into nucleosomes to form chromatin, and further assembled into higher ordered chromatin structures.[1] Expression of genes is correlated with numerous factors including the gene's position inside the nucleus,[2] accessibility to transcription factors,[3] the degree of chromatin condensation,[4] and other aspects of nuclear regulation beyond chemical signaling.[5] Thus, during changes in gene expression from chemical and mechanical stimulus, the genome undergoes global reorganization including chromatin remodeling and movement for the recruitment of genes and transcription factors to form transcription sites or "transcription factories".[6] Thus, both the dynamics remodeling of chromatin and its movements within the nucleus underlie functional changes associated with nuclear processes ranging from transcription and replication to DNA repair following damage.

The nucleus is also an important structural and mechanical element of the cell. The cytoskeleton, nucleoskeleton and nuclear interior are structurally connected by the LINC complex (Linker of Nucleoskeleton and Cytoskeleton). The LINC complex connects cytoskeletal filament networks to nesprin proteins on the outer nuclear membrane. KASH domains of nesprins bind to SUN proteins,

which span the nuclear envelope and bind to the lamins of the nucleoskeleton. Lamins connect directly and indirectly with chromatin and the nuclear interior.[7] Through the LINC complex, the nucleus transmits and balances cytoskeletal forces important for force generation, adhesion and motility.[8] It is also suggested that forces may be propagated via the LINC complex to the nuclear interior where they can facilitate chromatin reorganization.[9, 10]

What remains to be determined are the mechanisms influencing chromatin dynamics necessary for altered gene expression and other nuclear processes in primary human cells. We consider both the resistance of chromatin movement by altering chromatin condensation state as well as the driving forces of chromatin movements, which we observe come primarily from forces generated in the cytoskeleton. Previously, indirect effects of altered chromatin condensation state[11-13] or force propagation[9, 10] on nuclear mechanics and movements have been observed in disparate situations. Here, we examine chromatin fluctuations using particle tracking microrheology in primary human cells with physiologically-relevant nuclear organization. Using various chemical treatments, we find that we are able to effectively decouple the effects of chromatin condensation state and active force generation from the cytoskeleton through the LINC complex. We also show correspondence with our independent quantification of chromatin condensation state using fluorescence lifetime imaging microscopy (FLIM) from Chapter II. These results demonstrate that chromatin condensation state and active forces are effectively partitioned into separate parameters of the ensemble-average mean square displacement (MSD) power-law rheological model. The

ability to decouple and quantify these mechanical effects allow for investigation of their influence in physiological processes, including chemically-stimulated change in gene expression which we demonstrate in Chapter IV. In addition to transcriptional changes, understanding the mechanisms of chromatin remodeling and dynamics also has implications for both mechanotransduction[10] and the DNA damage response involving chromosome translocations and repair.[14, 15]

Materials and Methods

Cell Culture and Transfection

Human umbilical vein endothelial cells (HUV-EC-C, ATCC CRL1730, Manassas, VA) of passages 2-8 were cultured in endothelial basal media with growth supplements (Lonza, Hopkinton, MA). The cells were passaged to 35 mm μ-dishes with ibiTreat (ibidi, Verona, WI) and transfected with rDNA of GFP-Fib (kind gift from D. Discher, University of Pennsylvania) and for KASH experiments rDNA of dominant negative KASH RFP-KASH or the control RFP-KASH-ΔL (kind gift from G. Luxton, University of Minnesota) using Lipofectin transfection reagent (Life Technologies, Grand Island, NY) in Opti-MEM I Reduced Serum Medium (Life Technologies, Grand Island, NY). After five hours of incubation, the media was changed and the cells were incubated for 24-72 hours post-transfection prior to experiments in order to reach confluency and allow for adequate expression levels.

Drug Treatments

For chromatin decondensation experiments, cells were treated with either daunomycin (1 μg/mL for 1 hour and 20 minutes) or trichostatin A (TSA, 200 ng/mL for 24 hours) prior to imaging. Inhibition of myosin-II motor activity was carried out by incubation with blebbistatin (50 μM for 2 hours). Cells were incubated with sodium azide (NaN_3, 10 mM) and 2-deoxyglucose (2-DG, 50 mM) for one hour for ATP-depletion experiments.

Particle Tracking Imaging and Analysis

Imaging for particle tracking experiments was done using a 63x (1.4 NA) oil immersion objective of an inverted microscope (DMI6000, Leica, Buffalo Grove, IL) in a controlled live-cell imaging chamber. Cell nuclei were labeled with 0.5 μg/mL Hoechst 33342 (Life Technologies, Grand Island, NY). Images were taken at multiple positions per plate at 3.0 minute intervals with 1-4 transfected cells per field of view and 4-10 particles per cell for GFP-Fib and 5-35 particles per cell for Hoechst 33342-stained DNA. Cells maintained viability well beyond the duration of the experiment as confirmed by continued imaging for over an hour after the completion of data collection. Two-dimensional tracking of either GFP-Fib or punctate regions of Hoechst 33342-stained DNA was done using custom Laptrack71 programs designed in MATLAB (Natick, MA) as previously published.[16, 17] Briefly, images were cropped and aligned to remove artifacts including imaging drift, nuclear translation, and nuclear rotation. Particles were then detected through statistical algorithms after calibration of

background noise parameters. Particle tracks were then determined by correspondence with succeeding frames. Only persistent tracks of particles present for the full duration of the experiment were used for further analysis.

The ensemble-averaged MSD was calculated from the particle tracks as shown in Equation 1,[18] where τ is the lag time. Sample individual control cell data is shown in Figure 3.1A along with sample error for two data sets in Figure 3.1B. MSD magnitudes were compared at each time point using Student's t-test. Data were fit to a power-law rheological model as consistent for biological systems[19] and the nucleus in particular[11] as shown in Equation 2, where D_{eff} is the effective diffusivity and indicative of mechanical properties and β is the power-law diffusive exponent. Calculation of D_{eff} was done by normalizing lag time, τ, to the sampling time step of three minutes. This allowed for enhanced accuracy in the fit calculation by using interpolation of the data rather than extrapolation. 95% confidence intervals for parameter values were used for statistical comparison. Since the MSD is an inherently positive quantity, outliers with large magnitudes may bias the resultant ensemble average. Consequently, all outliers greater than three standard deviations from the mean were removed and the data were reanalyzed, though with little to no change in the trends. These cells generally had issues with alignment wherein nuclear rotation or translation was not properly removed.

$$MSD(\tau) = \langle (x_{t+\tau} - x_t)^2 + (y_{t+\tau} - y_t)^2 \rangle \quad (1)$$

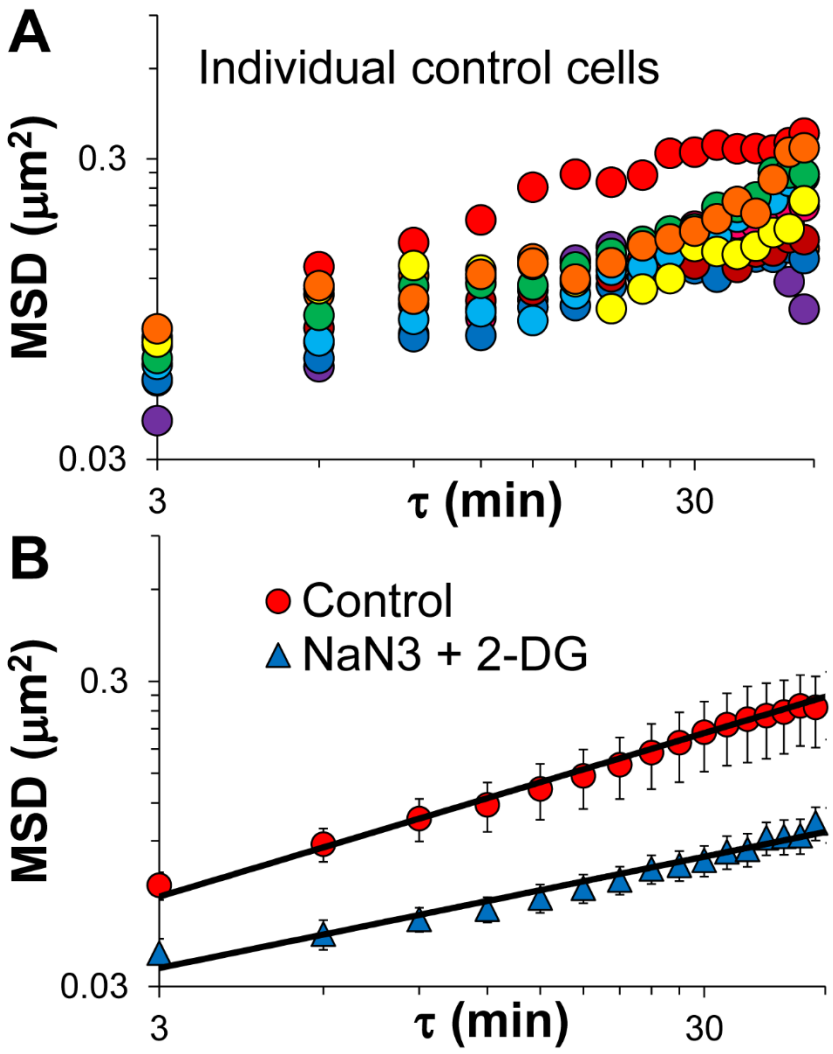

Figure 3.1: Extended MSD plots from particle-tracking measurements. *(A) MSD versus lag time plots of ten individual control cells. (B) Extended plot of Figure 3.8 containing error bars to show their magnitudes for comparison. Error bars reflect SEM.*

Cell Fixation and Fluorescence Microscopy

Following treatment, cells were fixed using 3.7% formaldehyde in phosphate buffered saline (PBS) solution. Cells were then permeabilized using 0.2% Triton X-100 in PBS. DNA was stained using with Hoechst 33342. For

fluorescence imaging, actin was stained using rhodamine phalloidin (Life Technologies, Grand Island, NY) and lamin A/C was immunostained using a primary mouse monoclonal lamin A/C antibody and a secondary goat anti-mouse antibody IgG-CFL Alexa Fluor 488 (Santa Cruz Biotechnology, Santa Cruz, CA).

Statistics

Magnitudes of the ensemble-averaged mean squared displacement were statistically compared using Student's t-test. Fitting parameters and corresponding 95% confidence intervals were determined using the MATLAB for nonlinear least squares regression trust-region algorithm and verified using ANOVA ($p<0.001$). For FLIM experiments, the fits (single or double exponential decays) were determined using a χ^2 test, as discussed above. The mean fluorescence lifetimes were compared using Student's t-test and the variance compared using the F-test.

Results

Different Bound Nuclear Probes Reveal Similar Chromatin Fluctuations

Microrheology studies on *in vitro* biopolymer systems have demonstrated the use of bound probes as a means of capturing the dynamics of polymer network mechanics.[20] We utilize fluorescent molecules bound to chromatin to examine their fluctuations. Specifically, we examine movements of Hoechst 33342-stained DNA and exogenous GFP-tagged fibrillarin (GFP-Fib) in live HUVECs. The probes localize to distinct spatial environments within the nucleus (Figure 3.2B-D). GFP-Fib is located in the nucleolus, which is composed of largely

decondensed DNA and ribonucleoproteins associated with ribosomal biogenesis.[21] In contrast, regions preferentially labeled by Hoechst 33342 show punctate fluorescence intensity associated with highly condensed chromatin domains, which are thought to be primarily regions of heterochromatin.[22] For both probes, we observe power-law behavior for the MSD (Figure 3.3A) and statistically similar magnitudes for the entire duration of the experiment.

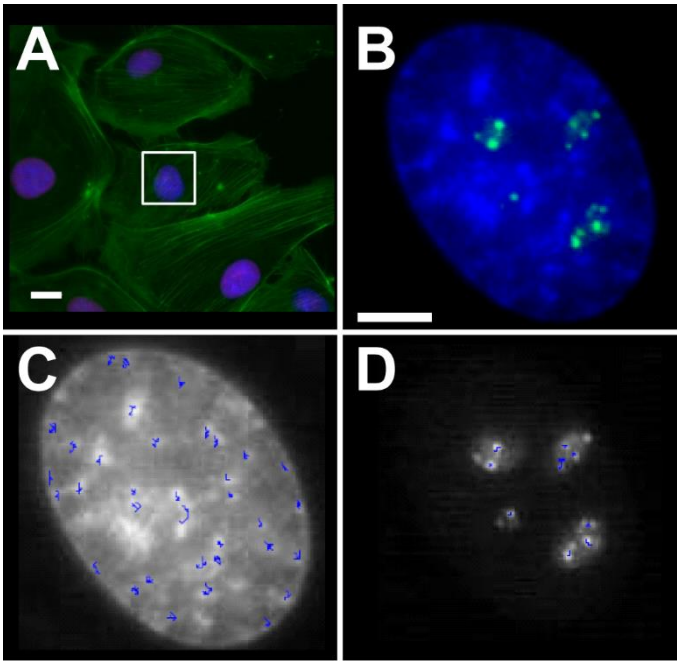

Figure 3.2: Particle tracking of distinct subnuclear regions in HUVECs. *(A) Confluent HUVECs with labeled F-actin (phalloidin, green), lamin A/C (immunostained, red), and DNA (Hoechst 33342, blue) show cytoskeletal and nuclear organization. White inset provides scale of nuclear images. Scale bar is 30 μm. (B) Image from live-cell experiment with DNA (Hoechst, blue) and exogenous GFP-Fib (green) shows disparate localization of imaged puncta. Scale bar is 5 μm. Images obtained every 3 minutes show tracks superimposed on*

fluorescence for (C) Hoechst or (D) GFP-Fib following particle detection, alignment and post-processing (see Methods).

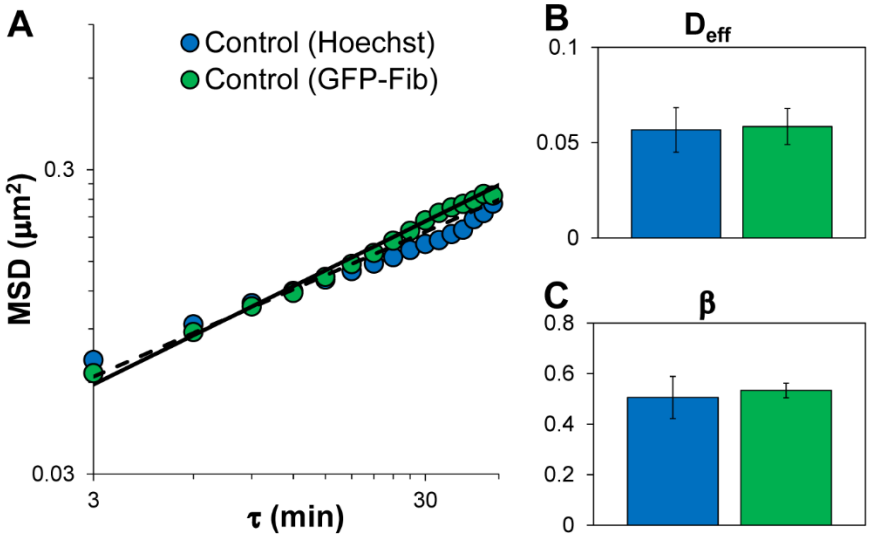

Figure 3.3: Global chromatin network mechanics measured by ensemble averaged MSD are probe-independent. *Particle tracking measurements of punctate regions of Hoechst 33342-stained DNA and GFP-Fib resulted in statistically indistinguishable magnitudes, trends and fits (p>0.05). (A) MSD versus lag time values, (B) the prefactor D_{eff} and (C) the diffusive exponent β. Error bars reflect 95% confidence intervals.*

From analysis of MSD versus lag time (τ), we quantify power-law behavior using Equation (2)

$$MSD = D_{eff}\tau^{\beta} \quad (2)$$

with a decoupled prefactor, D_{eff} (Figure 3.3B), and a diffusive exponent, β (Figure 3.3C). For GFP-Fib and Hoechst 33342, we find that both D_{eff} and β are statistically similar indicating the fluctuations of both probes follow identical

magnitude and time-dependence. This is consistent with our recent work showing that the DNA-binding protein upstream binding factor-1 (GFP-UBF1) and GFP-Fib exhibit equivalent fluctuations in static cells and in response to mechanical stimuli from shear stress for multiple cell lines[17] and our work in Chapter VI extending this to the telomeric protein RFP-TRF1. GFP-Fib is used for all subsequent experiments since punctate regions of DNA labeled by Hoechst 33342 are altered by chromatin treatments.

MSD Prefactor is Impacted Primarily by Chromatin Condensation

Chromatin condensation state has been shown to alter nuclear mechanics and deformability, including the nucleoskeleton and chromatin, as measured by nuclear and cellular stretching[11-13] as well as with FLIM in Chapter II. Our work aimed to study the impact of chromatin condensation state directly on their fluctuations. To examine these effects independent of externally applied forces, we treated cells with different chromatin-modifying agents and performed the particle tracking of probes within chromatin (see Methods). Daunomycin, a DNA-intercalating anthracycline antibiotic, causes a local unwinding of the DNA helix leading to chromatin unfolding and decondensation.[23] Trichostatin A (TSA) is an inhibitor of histone deacetylase (HDAC), which causes a net histone acetylation in the nucleus, decreasing their interaction with DNA and leading to chromatin decondensation[24] as we showed in Chapter II.

In response to both treatments we observe an increase in MSD magnitude compared with controls (Figure 3.4A). When fit to Equation 2, we observe

significant increases in D_{eff} of 190% for daunomycin and 40% for TSA (Figure 3.4B). Interestingly, the diffusive exponent, β, showed no change (Figure 3.4C).

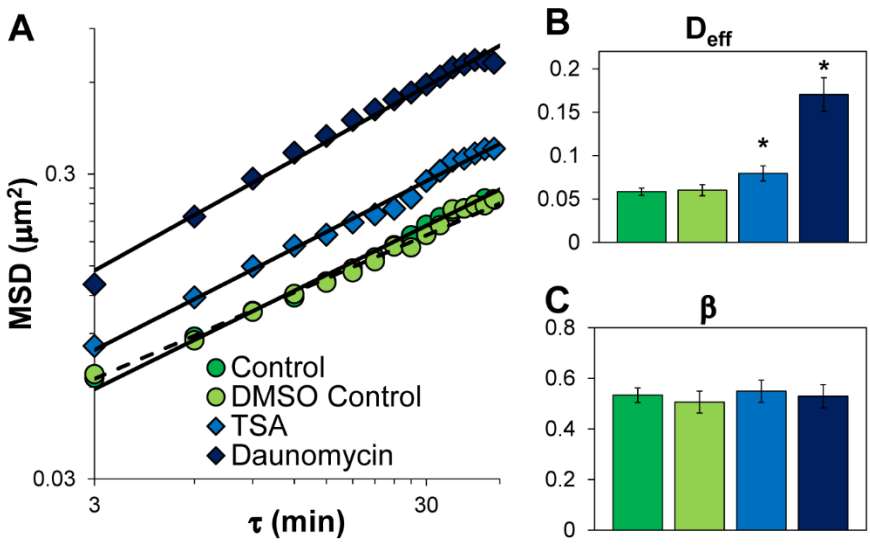

Figure 3.4: Chromatin decondensation alters nuclear mechanical properties. *Cells were treated with chromatin decondensation agents daunomycin, trichostatin A (TSA) or DMSO (TSA control) and imaged for particle tracking of GFP-Fib. (A) Treatment with daunomycin ($p<0.001$) and TSA ($p<0.05$ at early time) increased the magnitudes of the MSDs. Fitting the data to Equation 2 (see Methods) showed (B) a statistically significant increase ($p<0.05$) in the prefactor D_{eff} for both daunomycin and TSA, but (C) no change in the diffusive exponent β. DMSO treatment resulted in no change of MSD, D_{eff} or β. Error bars reflect 95% confidence intervals.*

MSD Diffusive Exponent is Impacted by Force Propagation

Recent work has suggested forces propagated through the cytoskeleton may contribute to chromatin agitation and movement through active forces on the

nucleus.[9, 10] To test the role of active intracellular force generation on chromatin fluctuations, we treat HUVECs with blebbistatin to inhibit the actin motor protein myosin II (see Methods). Blebbistatin treatment results in a reduction in MSD magnitudes (Figure 3.5A) and a dramatic decrease in β of 25% (Figure 3.5C). However, there is no change in D_{eff} (Figure 3.5B). FLIM analysis of nuclei in HUVECs treated with blebbistatin also shows no change in mean fluorescence lifetime, thus for our blebbistatin treatment there is seemingly no effect on chromatin condensation.[25]

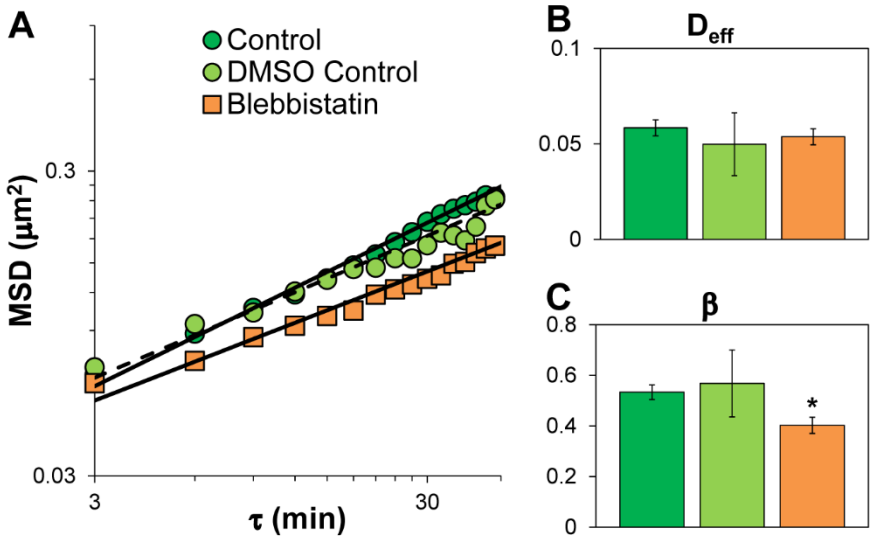

Figure 3.5: Reduced myosin II-based force generation attenuates chromatin dynamics. *(A) Cells were treated with the myosin II inhibitor blebbistatin or DMSO (control) and imaged for particle tracking of GFP-Fib. Blebbistatin treatment reduced magnitudes of MSD ($p<0.05$ for early time). Fitting the data to Equation 2 showed (B) no change in the prefactor D_{eff}, but (C) resulted in a*

reduced diffusive exponent β ($p<0.05$). DMSO treatment showed no change from the control. Error bars reflect 95% confidence intervals.

To confirm these results stemmed from the effect of myosin II on actin and the propagation of these cytoskeletal forces to the nuclear interior, we transfected cells with a dominant negative KASH (RFP-KASH) that displaces nesprins from the nuclear envelope (Figure 3.6) largely decoupling the nucleus from the cytoskeleton.[10, 26] Cells expressing RFP-KASH exhibited reduced magnitudes of MSD (Figure 3.7A) and a reduction in β statistically similar to blebbistatin treatment of 26% (Figure 3.7C) and no corresponding change in D_{eff} (Figure 3.7B). Cells transfected with the control KASH lacking the luminal SUN-binding domain (RFP-KASH-ΔL) showed no effect compared with control (Figure 3.7). Thus, chromatin condensation appears to impact D_{eff} and alteration of motor activity appears to impact β in Equation 2. Further, we highlight the primary cytoskeletal network responsible for these forces is the actin network and its direct mechanical transduction through the LINC complex.

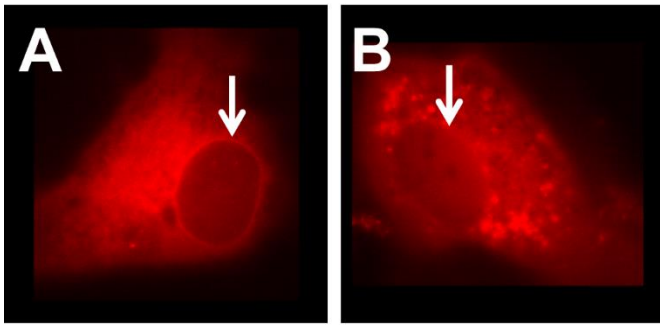

Figure 3.6: Transfection of RFP-KASH constructs in HUVECs. *Images from live-cell experiments of a HUVEC transfected with either (A) the exogenous dominant negative KASH construct RFP-KASH or (B) the exogenous control KASH construct RFP-KASH-ΔL which lacks the luminal SUN binding domains and therefore does not displace the nesprin proteins from the nuclear envelope (indicated with arrows). (A) The RFP-KASH construct shows increased fluorescence intensity at the nuclear envelope compared with no nuclear envelope localization for the RFP-KASH-ΔL construct (B).*

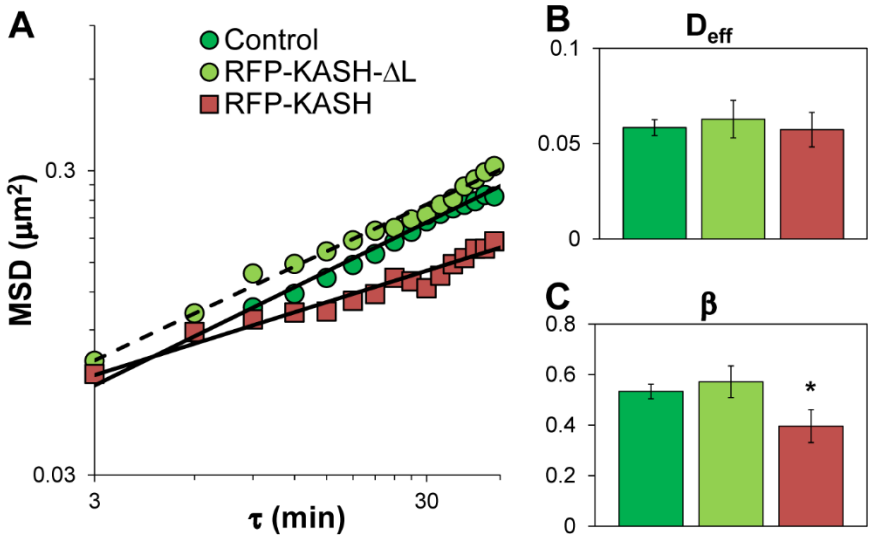

Figure 3.7: Cells expressing dominant negative KASH show reduced chromatin dynamics. *Cells were transfected with either the dominant negative red fluorescent protein-tagged KASH construct (RFP-KASH) that displaces nesprins from the nuclear envelope or a control KASH construct lacking the luminal SUN-binding domain (RFP-KASH-ΔL). (A) Cells were imaged for particle tracking of GFP-Fib. RFP-KASH transfected cells exhibited reduced*

magnitudes of MSD. Fitting the data to Equation 2 showed (B) no change in the prefactor D_{eff}, but (C) resulted in a reduced diffusive exponent β ($p<0.05$). RFP-KASH-ΔL transfected cells showed no change from the control. Error bars reflect 95% confidence intervals.

ATP Depletion: Loss of Motors and Chromatin Hypercondensation

During stimulated nuclear reorganization, including large-scale changes in expression, we expect a compound effect of altered chromatin condensation and active force generation as part of the signal transduction cascade. Removal of ATP using a combination of NaN_3 and 2-DG (see Methods) allows us to examine chromatin hypercondensation and loss of molecular motors. Treatment with NaN_3 and 2-DG led to a dramatic reduction in MSD magnitudes (Figure 3.8A) much like treatment with blebbistatin. Unlike blebbistatin we observed a reduction in both D_{eff} (46%) and β (23%) (Figure 3.8B and 3.8C, respectively), but with the reduction in β being statistically similar to both blebbistatin and RFP-KASH treatment conditions. The loss of motor activity from ATP depletion led to a decrease in active force generation and a reduced β. The reduced D_{eff} is consistent with chromatin hypercondensation associated with the loss of ATP-dependent mechanisms of decondensation as we validated using FLIM in Chapter II.[24] Thus, much like the independent effectors of either chromatin condensation state (daunomycin and TSA) or motor activity (blebbistatin and RFP-KASH), the combined effect of chromatin hypercondensation and loss of motor activity similarly manifest themselves into the parameters D_{eff} and β, respectively.

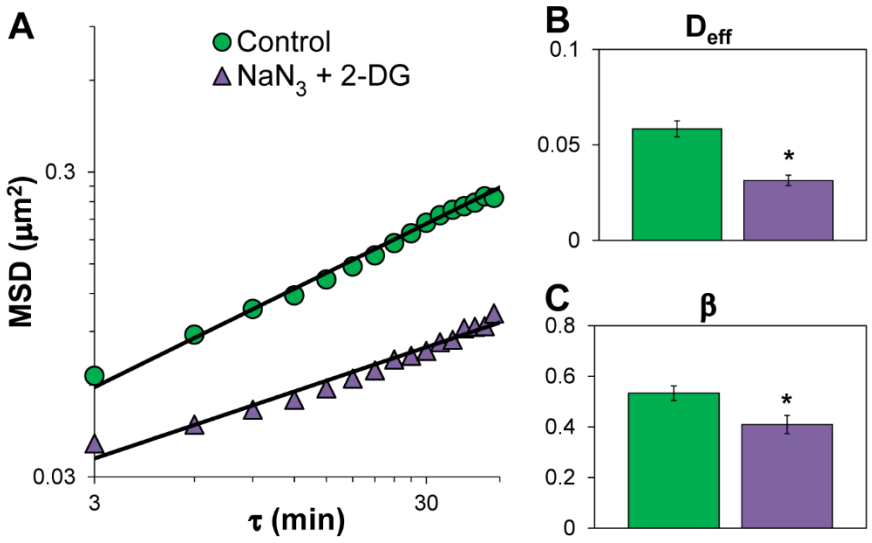

Figure 3.8: Combined effect of chromatin hypercondensation and motor activity inhibition by ATP depletion shows greatest reduction in MSD. *(A) Cells treated with sodium azide and 2-deoxyglucose (NaN_3+2-DG) had greatly reduced magnitudes of MSD ($p<0.001$). Fitting the data to Equation 2 showed (B) a statistically significant reduction in the prefactor D_{eff} ($p<0.05$) and (C) a decrease in the diffusive exponent β ($p<0.05$) indicating reduced active stresses. Error bars reflect 95% confidence intervals.*

Discussion

Particle Tracking Using Network-Bound Probes in the Nucleus

The use of cellular components as probes in this study removes the artifacts associated with foreign probes frequently cited previously including the "cage-like" motion and disruption of the local environment.[27] The identical results from both GFP-Fib and Hoechst 33342-stained DNA indicate the chromatin dynamics measured on these time scales by the ensemble-averaged MSD are probe-independent for these two probes. A requisite condition for this is the

selection of relevant time scales wherein each probe or the ensemble of probes translates over length scales large enough for material heterogeneities to be uniformly sampled and where probe-specific behavior contributes negligibly to the ensemble motion. Given the high mobility and rapid association/disassociation of fibrillarin within the nucleus (on the order of 10 sec),[28] a time step of several minutes effectively mutes these high-frequency, probe-specific events. This holds true for other probes, as we have shown across multiple cell lines previously with GFP-UBF1[17] and as we extend this in Chapter VI to the telomeric protein telomeric repeat-binding factor 1 (RFP-TRF1), but it is not necessarily universal. However, this finding is notable given the drastically different composition and function of these two subnuclear regions: heterochromatin-labeled with Hoechst 33342 and nucleolar GFP-Fib. Heterochromatin contains the highest relative concentration of DNA within the nucleus, whereas the nucleolus is predominately composed of RNA with the balance made almost exclusively of protein.[29] Yet in both cases the network fluctuations of the nuclear interior are nonetheless equivalent because of the crowded, gel-like behavior of the dense nuclear polymer network.

Nuclear Viscoelasticity from Particle Tracking

Determining cellular rheology from particle tracking experiments requires consideration of numerous factors. For equilibrium systems, viscoelasticity manifests as anomalous subdiffusion with MSD ~ τ^{β} and $0<\beta<1$.[30] Material viscoelasticity, binding and obstruction[31] as well as overcrowding[32] similarly form

the basis for anomalous subdiffusion in active cellular systems. However, cells are not equilibrium systems; motor protein activity enhances diffusive motion and fluctuations within cells beyond that of simple thermal fluctuations as part of a phenomenon termed "active diffusion".[33, 34] Previous studies have shown these motors are stochastic and essentially isotropic, making them similar in form to the thermal energy-derived fluctuations.[35, 36] Thus, at longer time scales molecular motor activity averages out to act to globally and nonspecifically to increase the time-dependence of these random fluctuations much like a forcing function, thereby driving this motion beyond that of simple thermal agitation.[34-36] Our results highlight the role of ATP-dependent motor activity in enhancing nuclear diffusive motion and chromatin fluctuations as measured through β.The long time scales (low frequency) of these experiments allows visualization of motor activity on time-dependent influence, as shown previously.[37] Thus, we note that β is truly a measure of system forces, including thermally-driven fluctuations that are supplemented by the presence of molecular motors or external forces enhancing those fluctuations.

By contrast, our work shows chromatin condensation state primarily impacts the prefactor. For typical polymeric systems, modulation of polymer viscoelasticity would affect the exponent, transitioning from elastic ($\beta \rightarrow 0$) to viscous contributions ($\beta \rightarrow 1$) or *vice versa*.[30] Yet, our work shows that changes to chromatin condensation have a limited impact on β, which we suggest stems from active forces playing the dominant role in modulating β[30, 37] (as discussed above). Additionally, the seemingly infinite mechanisms of stress dissipation by

the intranuclear polymer network (including a wide distribution of intermediate and metastable conformations for chromatin, DNA and its binding partners as well as a distribution of binding residence times) results in the characteristic power-law behavior and the absence of any characteristic timescales of relaxation.[11] Thus, the time-dependent effect of altering intranuclear polymer network mechanics would necessarily have a lesser impact on the time dependence of network fluctuations than in classical homogenous polymeric systems.

Previous studies have highlighted that probes bound to a percolated network are capable of capturing network dynamics and mechanics for *in vitro* biopolymer systems,[20, 38] including behavior relevant to the study of mechanobiology. The use of bound probes and the presence of active motors (creating non-equilibrium systems) results in invalidation of the Generalized Stokes-Einstein Relation (GSER) for calculation of the classical material properties. However, in place of the GSER the use of bound probes makes pertinent several models of polymer dynamics for qualitative analysis, including the Rouse chain model and the de Gennes model of reptation depicting polymer dynamics in a crowded environment.[39, 40] Conceptually, changes to local chromatin condensation state and organization can be thought of as altering the effective "tube size" for this reptation[39] which act to change the amplitude of such movements,[40] whereas the motors would primarily affect the time dependence and its enhancement beyond simple thermal agitation. However, it is important to note that the application of these models is convenient to consider these phenomena

conceptually, but their use is neither exact nor definitive. Nonetheless, while determination of the classical material properties is no longer straightforward through the GSER, particularly given the material heterogeneity, D_{eff} still serves as an indicator of material properties for these network fluctuations in a manner conceptually similar to these polymer dynamic models, essentially as an inverse to effective resistance since alterations to condensation state impact the chromatin fiber flexibility. For our experiments, increased D_{eff} reflects a reduced resistance to motion, and therefore an increase in chromatin compliance, that accompanies the chromatin decondensation and *vice versa*.[11-13] We further show the link between chromatin condensation state and D_{eff} using FLIM in Chapter II.[24] Given the strong dependence of D_{eff} on chromatin condensation state through the differential mechanics associated with the chromatin flexibility in those states, we will henceforth refer to D_{eff} as a measure of chromatin compliance.

In summation, there are numerous physical and biological limitations that limit determination of viscoelastic properties from particle tracking microrheology. As such, in this work we have not provided a direct extrapolation of viscoelasticity from measurements of chromatin fluctuations, particularly given the long time steps required to measure small intranuclear movements. This work provides useful comparative data of chromatin condensation and force generation and propagation. However, more appropriate mechanical measurements – such as cell stretching,[13] micropipette aspiration,[11, 12] compression,[41] etc. – can be used to quantify absolute material properties.

Nuclear Fluctuations and Mechanics of the Nuclear Interior in the Context of Cytoskeletal Mechanics

Our work highlights the role of myosin II activity on the actin cytoskeleton in giving rise to the superthermal fluctuations of chromatin within the nucleus through the LINC complex. Myosins are present in the nucleus. However, the extensive actin structural network of the cytoskeleton, including stress fibers, allows myosin II to generate much larger and longer range forces.[42, 43] These forces are capable of propagating into the nuclear interior through the LINC complex as shown here and elsewhere.[9, 10, 42-44] The presence of the vast force-generating apparatus of the cytoskeleton likely explains why our results deviate in behavior from a recent study of chromosomal fluctuations in bacteria and yeast cells devoid of a comprehensive cytoskeleton that exhibited a lower diffusive exponent in control cells and where ATP depletion manifests itself solely in the prefactor.[33]

The statistically similar diffusive exponents observed from blebbistatin treatment and dominant negative KASH show myosin II uniquely contributes to chromatin fluctuations by propagating forces generated from actin and through the LINC complex. Further, the statistical correspondence of these experiments with ATP depletion highlights the prominent role of the actin network and its motor proteins in driving the ATP dependence of chromatin dynamics in live human cells for these longer timescales. This has strong implications for mechanotransduction (pointing to what is likely the primary pathway for force transduction) as well as other nuclear processes associated with chromatin remodeling and dynamics. It also further supports the idea of direct and rapid

signal transduction via mechanical force in mammalian cells,[17, 42, 43] whereby force facilitates chromatin reorganization as a complement to the biochemical signaling.[10]

A recent study highlighted the role of intranuclear ATPase motors (DNA polymerase, RNA polymerase II, and topoisomerase II) in regulating coherent chromatin dynamics of HeLa cells.[15] Interestingly, it seems likely that this short-time coherence on the time scale of seconds likely facilitates the coupling we observe of chromatin dynamics measured by multiple probes at our longer timescales. This coherence of chromatin movement was lost upon inhibition of these ATPases, yet the magnitudes of the local movements increased. These findings suggest that intranuclear ATPases may serve as a means of "elastic coupling" within the nucleus as a possible mechanism for coordinating movements and nuclear processes. However, while they likely play a role in enhancing local chromatin fluctuations of specific loci, our work suggests that at longer time scales cytoskeletal motors are the primary driver of chromatin dynamics beyond that of simple thermal energy particularly for ensemble chromatin dynamics measured by the MSD.

Physiological Implications of Altered Chromatin Fluctuations

Recent work has highlighted the functional role of altered chromatin state within the nucleus: chromatin domains of varying condensation state are differentially affected by force propagation[10] in addition to obvious differences in levels of expression.[4] We suggest that decondensed chromatin serves not only to

increase accessibility of genes to transcription factors, but also to increase the mobility and mechanical sensitivity to promote the reorganization of genes and recruitment of the transcriptional components for associated changes in phenotype or physiological state.[9, 10, 44] Consistent with this, we observe large changes in chromatin fluctuations by altering the condensation state of the chromatin. This is similar to the results observed during heterochromatin formation and nuclear stiffening associated with stem cell differentiation.[12]

Our results with chemical treatments provide a physiological range for functional chromatin dynamics in primary endothelial cells (Figure 3.9). The lower bound corresponds to chromatin hypercondensation and ATP-dependent motor activity inhibition for which the mobility of nuclear components is heavily constrained. Typical chromatin fluctuations of 300-500 nm that occur rapidly in normal physiological conditions[45] are effectively inhibited by such treatment (Figure 3.9). The upper bound results from global chromatin decondensation with normal motor activity. This upper bound may represent a stem cell-like condition with largely decondensed chromatin and phenotypic flexibility prior to lineage commitment.[12, 46] By specifically modulating chromatin condensation state, intranuclear mobility is enhanced by an order of magnitude. Interchromosomal and intrachromosomal interactions for colocalization and coordinated expression occur on the time scale of minutes[47] like these experiments. Thus, local chromatin decondensation along with force-induced agitation may play a role in enhancing the associated transport and kinetics (Figure 3.9). The defined physiological phase space shows that the cell may modulate chromatin condensation state and force-

induced chromatin agitation as a means of enhancing chromatin fluctuations and the turnover in expression. As shown in Figure 3.9, the physiological regime outlines the capacity to enhance chromatin network fluctuations.

Previous work has demonstrated subdiffusion ($\beta < 1$) favors the probability of finding nearby binding targets relative to normal Brownian diffusion ($\beta = 1$).[48] The distance over which subdiffusion exerts this increased probability is defined by a cutoff radius, $R_c \sim MSD(\tau)^{1/2} \sim \tau^{\beta/2}$.[48] For distances below R_c, subdiffusion offers enhanced probability of finding a binding partner. However, R_c critically depends on the characteristic dynamics of the diffusing particle. Thus, through modulation of motor activity (β) or chromatin condensation state (D_{eff}), the cell can effectively control this sampling radius. As $\beta \rightarrow 1$, the advantages of subdiffusion become marginal and R_c increases as we approach normal Brownian diffusion. This can be favorable when binding partners are far apart, as perhaps may be the case with large scale stimulated changes in gene expression necessitating the translocation of transcription factors from the cytoplasm to the nucleus and the binding of specific gene targets. By contrast, one can imagine other scenarios where this probability of escape may be detrimental to cellular processes, as would likely be the case in DNA double-strand break repair where proper pairing of broken ends depends on curtailing long range motion to favor finding the nearby complementary severed end. Thus, this physiological regime of chromatin dynamics that we have defined illuminates new avenues for regulation of nuclear processes through physical mechanisms with wide-ranging implications. Future work leveraging this understanding will

be aimed at investigating how the cell tailors chromatin dynamics for specific physiological changes and cellular processes in succeeding Chapters.

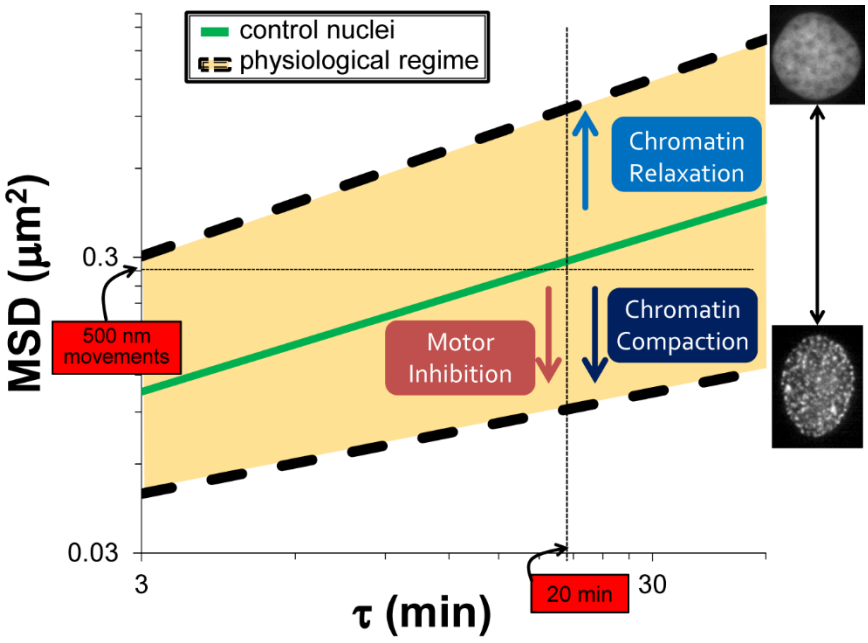

Figure 3.9: Bounded physiological range of chromatin dynamics in HUVECs. *The combination treatment of NaN_3+2-DG provides a lower bound for chromatin fluctuations resulting from global chromatin hypercondensation and motor activity inhibition by ATP depletion. Daunomycin treatment reflects an upper bound on global chromatin decondensation (effective softening) with control levels of active stress generation. The physiological regime (shaded yellow) highlights differences in nuclear state: length scales of fluctuation corresponding to the time scales of physiological events such as initial transcription-mediated chromatin decondensation (~20 minutes) are over three times larger for such a regime, indicating the possibility for much more rapid nuclear reorganization. Common chromatin domain fluctuations of 500 nm (corresponding to 0.25 μm^2)*

are bounded by timescales less than 3 minutes in open chromatin to very long times for tightly condensed chromatin. Further, this physiological regime shows the cell is capable of enhancing chromatin fluctuations during turnover associated with gene expression changes through both chromatin decondensation and cytoskeletal force-induced agitation.

Acknowledgements

We gratefully acknowledge help from Elizabeth Booth-Gauthier (UC Berkeley) for her helpful discussion and input throughout; Ge Yang (Carnegie Mellon Biomedical Engineering, Lane Center for Computational Biology, and Biological Sciences) and Minhua Qui (Carnegie Mellon Biomedical Engineering) for development and assistance with the LAPtrack71 suite of particle tracking programs; Lynn Walker (Carnegie Mellon Chemical Engineering) for her rheological insight; Gant Luxton (University of Minnesota Genetics, Cell Biology and Development) and Nathan Harris (University of Minnesota Genetics, Cell Biology and Development) for providing the KASH constructs and helpful discussion; and Stephanie Wong (Carnegie Mellon Biomedical Engineering) and Yu-li Wang (Carnegie Mellon Biomedical Engineering) for providing blebbistatin as well as insight into treatment conditions. This work is supported by the NSF (NSF-CBET-0954421, CMMI-1300476 to KND and DMR-0619424 to Mohammad Islam) and the ARCS Foundation (STS), Bertucci Fellowship (STS), and James C. Meade Fellowship (STS).

References

1. T. Misteli, *Cell*, 2007, **128**, 787-800.
2. K. Kupper, A. Kolbl, D. Biener, S. Dittrich, J. von Hase, T. Thormeyer, H. Fiegler, N. P. Carter, M. R. Speicher, T. Cremer and M. Cremer, *Chromosoma*, 2007, **116**, 285-306.
3. R. M. Martin and M. C. Cardoso, *FASEB journal : official publication of the Federation of American Societies for Experimental Biology*, 2010, **24**, 1066-1072.
4. J. S. Zhou, J. Y. Fan, D. Rangasamy and D. J. Tremethick, *Nature structural & molecular biology*, 2007, **14**, 1070-1076.
5. K. Luger, M. L. Dechassa and D. J. Tremethick, *Nat Rev Mol Cell Bio*, 2012, **13**, 436-447.
6. A. Ghamari, M. P. C. van de Corput, S. Thongjuea, W. A. van Cappellen, W. van IJcken, J. van Haren, E. Soler, D. Eick, B. Lenhard and F. G. Grosveld, *Gene Dev*, 2013, **27**, 767-777.
7. K. N. Dahl and A. Kalinowski, *Journal of cell science*, 2011, **124**, 675-678.
8. T. J. Chancellor, J. Lee, C. K. Thodeti and T. Lele, *Biophysical journal*, 2010, **99**, 115-123.
9. B. Hampoelz, Y. Azou-Gros, R. Fabre, O. Markova, P. H. Puech and T. Lecuit, *Development*, 2011, **138**, 3377-3386.
10. K. V. Iyer, S. Pulford, A. Mogilner and G. V. Shivashankar, *Biophysical journal*, 2012, **103**, 1416-1428.
11. K. N. Dahl, A. J. Engler, J. D. Pajerowski and D. E. Discher, *Biophysical journal*, 2005, **89**, 2855-2864.
12. J. D. Pajerowski, K. N. Dahl, F. L. Zhong, P. J. Sammak and D. E. Discher, *Proceedings of the National Academy of Sciences of the United States of America*, 2007, **104**, 15619-15624.
13. K. J. Chalut, M. Hopfler, F. Lautenschlager, L. Boyde, C. J. Chan, A. Ekpenyong, A. Martinez-Arias and J. Guck, *Biophysical journal*, 2012, **103**, 2060-2070.
14. V. Roukos, T. C. Voss, C. K. Schmidt, S. Lee, D. Wangsa and T. Misteli, *Science*, 2013, **341**, 660-664.
15. A. Zidovska, D. A. Weitz and T. J. Mitchison, *Proceedings of the National Academy of Sciences of the United States of America*, 2013, **110**, 15555-15560.
16. G. Yang, L. A. Cameron, P. S. Maddox, E. D. Salmon and G. Danuser, *Journal of Cell Biology*, 2008, **182**, 631-639.
17. E. A. Booth-Gauthier, T. Alcoser, K. N. Dahl and G. Yang, *Biophysical journal*, 2012.
18. X. Michalet, *Biophysical journal*, 2011, **100**, 252-252.
19. P. Kollmannsberger and B. Fabry, *Annu Rev Mater Res*, 2011, **41**, 75-97.
20. M. T. Valentine, Z. E. Perlman, M. L. Gardel, J. H. Shin, P. Matsudaira, T. J. Mitchison and D. A. Weitz, *Biophysical journal*, 2004, **86**, 4004-4014.

21. V. Sirri, S. Urcuqui-Inchima, P. Roussel and D. Hernandez-Verdun, *Histochem Cell Biol*, 2008, **129**, 13-31.
22. M. Versaevel, T. Grevesse and S. Gabriele, *Nature communications*, 2012, **3**, 671.
23. L. Sprigg, A. Li, F. Y. Choy and J. Ausio, *Journal of medicinal chemistry*, 2010, **53**, 6457-6465.
24. D. Lleres, J. James, S. Swift, D. G. Norman and A. I. Lamond, *Journal of Cell Biology*, 2009, **187**, 481-496.
25. S. T. Spagnol and K. N. Dahl, *Integr Biol-Uk*, 2014, **6**, 523-531.
26. G. W. Luxton, E. R. Gomes, E. S. Folker, E. Vintinner and G. G. Gundersen, *Science*, 2010, **329**, 956-959.
27. D. Weihs, T. G. Mason and M. A. Teitell, *Biophysical journal*, 2006, **91**, 4296-4305.
28. R. D. Phair and T. Misteli, *Nature*, 2000, **404**, 604-+.
29. A. Pliss, A. N. Kuzmin, A. V. Kachynski and P. N. Prasad, *Biophysical journal*, 2010, **99**, 3483-3491.
30. J. C. Crocker and B. D. Hoffman, *Cell Mechanics*, 2007, **83**, 141-178.
31. M. J. Saxton, *Biophysical journal*, 2007, **92**, 1178-1191.
32. M. Weiss, M. Elsner, F. Kartberg and T. Nilsson, *Biophysical journal*, 2004, **87**, 3518-3524.
33. S. C. Weber, A. J. Spakowitz and J. A. Theriot, *Proceedings of the National Academy of Sciences of the United States of America*, 2012, **109**, 7338-7343.
34. C. P. Brangwynne, G. H. Koenderink, F. C. MacKintosh and D. A. Weitz, *Trends in cell biology*, 2009, **19**, 423-427.
35. A. W. C. Lau, B. D. Hoffman, A. Davies, J. C. Crocker and T. C. Lubensky, *Physical review letters*, 2003, **91**.
36. A. W. C. Lau and T. C. Lubensky, *Phys Rev E*, 2009, **80**.
37. B. D. Hoffman, G. Massiera, K. M. Van Citters and J. C. Crocker, *Proceedings of the National Academy of Sciences of the United States of America*, 2006, **103**, 10259-10264.
38. J. L. McGrath, J. H. Hartwig and S. C. Kuo, *Biophysical journal*, 2000, **79**, 3258-3266.
39. I. Bronstein, Y. Israel, E. Kepten, S. Mai, Y. Shav-Tal, E. Barkai and Y. Garini, *Physical review letters*, 2009, **103**, 018102.
40. H. Hajjoul, J. Mathon, H. Ranchon, I. Goiffon, J. Mozziconacci, B. Albert, P. Carrivain, J. M. Victor, O. Gadal, K. Bystricky and A. Bancaud, *Genome Res*, 2013, **23**, 1829-1838.
41. K. M. Stroka and H. Aranda-Espinoza, *Cellular and molecular bioengineering*, 2011, **4**, 9-27.
42. S. Na, O. Collin, F. Chowdhury, B. Tay, M. X. Ouyang, Y. X. Wang and N. Wang, *Proceedings of the National Academy of Sciences of the United States of America*, 2008, **105**, 6626-6631.
43. S. B. Khatau, C. M. Hale, P. J. Stewart-Hutchinson, M. S. Patel, C. L. Stewart, P. C. Searson, D. Hodzic and D. Wirtz, *Proceedings of the*

National Academy of Sciences of the United States of America, 2009, **106**, 19017-19022.
44. Y. C. Poh, S. P. Shevtsov, F. Chowdhury, D. C. Wu, S. Na, M. Dundr and N. Wang, *Nature communications*, 2012, **3**.
45. M. R. Hubner and D. L. Spector, *Annu Rev Biophys*, 2010, **39**, 471-489.
46. E. Meshorer, D. Yellajoshula, E. George, P. J. Scambler, D. T. Brown and T. Mistell, *Developmental cell*, 2006, **10**, 105-116.
47. R. I. Kumaran, R. Thakar and D. L. Spector, *Cell*, 2008, **132**, 929-934.
48. G. Guigas and M. Weiss, *Biophysical journal*, 2008, **94**, 90-94.

Chapter IV

Physical Mechanisms of Chromatin Dynamics and Reorganization in Vascular Endothelial Growth Factor Stimulation

Introduction

At sites of gene expression, stimulated transcriptional activation involves the coalescing of transcription factors with a particular set of genes for regulated expression. Access to the target genes is provided by dynamic remodeling of the chromatin architecture allowing for decondensation, a process that is tightly regulated by ATP-dependent remodeling complexes.[1] Activation is likely facilitated through non-random chromosome organization within the nucleus,[2, 3] with more gene-dense chromosomes concentrating to the interior and *vice versa*. Additionally, within chromosome territories, actively expressed genes will generally locate to the periphery allowing greater accessibility to nuclear proteins as well as for the intrachromosomal and interchromosomal coregulation of multiple genes by single transcription sites.[2] Given the heterogeneous distribution of nuclear proteins, it is clear that the coalescing of genes with requisite proteins for transcription factories necessitates chromatin mobility. Thus, chromatin dynamics associated with remodeling and repositioning are essential to stimulated activation. However, while chemical signaling cascades are known to facilitate chromatin remodeling and the assembly of transcription factors with specific genome loci, the mechanisms regulating the chromatin dynamics that accompany

stimulated gene expression changes within the context of this strict spatial and temporal integrity are still being elucidated.

We have previously identified the physical mechanisms governing innate chromatin dynamics in human cell nuclei, where we highlighted the unique role of chromatin condensation state (through its effect on mechanical chromatin compliance) and cytoskeletal forces in driving these dynamics and our ability to quantify and measurably decouple them.[4] Our work also suggested a physiological regime over which the cell may effectively modulate chromatin dynamics through this mechanical interplay. Here, we aim to investigate the specific physical mechanisms governing the dynamics of chromatin in response to stimulated changes in expression. We focus on the vascular endothelial growth factor (VEGF) stimulated pro-angiogenic pathway in human umbilical vein endothelial cells (HUVECs).

Angiogenesis is the sprouting of new blood vessels from the preexisting vasculature.[5] It is vital to development and normal physiology and occurs in response to hypoxia or nutrient deficiency in peripheral tissues.[6] It is also implicated in a variety of disease pathologies including cancer metastasis[7] and cardiovascular disease.[8] VEGF itself plays a role in the poor prognosis of breast cancer,[9] rheumatoid arthritis,[10] diabetic retinopathy[11] and macular degeneration.[12] The importance of VEGF to development has also been well documented, including the embryonic lethality linked to the absence of even a single allele.[13] Thus, its role in physiology, including the invasive migration[14] of endothelial cells into the tissues for tubule formation,[15] has been extensively studied. These

physiological events are the result of dramatic changes in gene expression that are stimulated by biochemical signaling cascades that have been a major focus of research for decades.[5-7, 13, 16-25]

While VEGF stimulation involves the upregulation of well over 100 genes,[26, 27] there are distinct temporal dynamics associated with the expression profile. A small subset of genes are directly induced early on by VEGF signal transduction, while the balance are thought to be induced by secondary mechanisms of activation, including by signaling and transcription factors upregulated in the first wave. It seems likely that a large portion of these later genes are buried in tightly condensed chromatin making them less immediately accessible[28] and less mobile for transcriptional activation.[4] It has been suggested that the cytoskeletal structural and mechanical reorganization that accompanies major physiological changes may serve a role in the altered gene expression[29, 30] through their effect on chromatin dynamics in parallel with biochemical signaling.[14] This has been observed previously in other pathways.[31, 32] Along these lines, major structural and mechanical changes occur in the cytoskeleton of endothelial cells in response to VEGF as they go from a quiescent state to an invasive and migratory phenotype. This causes an overhaul of the cytoskeletal architecture.[33, 34] These effects coincide with cytoskeleton-imposed forces that are dominated by actin[35-37] and cause nuclear shape changes[35, 38, 39] that we hypothesized may impact global chromatin dynamics associated with stimulated reorganization.

Here we show distinct temporal regimes of chromatin dynamics in response to VEGF stimulation that correspond to the temporal behavior of the gene expression profiles. Early on, VEGF stimulation results in enhanced chromatin dynamics driven primarily by cytoskeletal forces and accompanied by a moderate level of chromatin decondensation that increases chromatin compliance relative to control cells. These coincide with actin reorganization for increased nuclear colocalization as well as increased nuclear deformations at these time scales. Later in the response we find these increased cytoskeletal forces have dissipated, yielding to enhanced chromatin dynamics driven instead by large scale chromatin decondensation that make the nuclear interior more compliant. We confirm these temporal changes in chromatin condensation state using fluorescence lifetime imaging microscopy (FLIM). These findings uniquely identify the evolution of chromatin dynamics with established temporal expression profiles. Additionally, they build on our previous work identifying the primary pathway through which mechanical forces are transduced into the human nucleus for chromatin agitation specifically as it relates to chemically stimulated gene activation. These results shed light on mechanical signaling pathways for mechanotransduction, particularly its role in shear-responsive endothelial cells, as well as the precise role of chromatin dynamics and remodeling in transcriptional activation with implications for DNA replication and repair.

Methods

Cell Culture, Transfection and Drug Treatments

Human umbilical vein endothelial cells (HUV-EC-C, ATCC CRL1730, Manassas, VA) of passages 2-8 were cultured in endothelial basal media with growth supplements (Lonza, Hopkinton, MA). The cells were passaged to 35 mm μ-dishes with ibiTreat (ibidi, Verona, WI) and transfected with rDNA of GFP-Fib (kind gift from D. Discher, University of Pennsylvania) or with p^{CMV}LifeAct-TagRFP (S. Kumar, UC Berkeley) to visualize actin using Lipofectin transfection reagent (Life Technologies, Grand Island, NY) in Opti-MEM I Reduced Serum Medium (Life Technologies, Grand Island, NY). After five hours of incubation, the media was changed and the cells were incubated for 24-72 hours post-transfection prior to experiments in order to reach confluency and allow for adequate expression levels. For VEGF treatments, cells were exposed to 50 ng/mL of VEGF for the indicated times.

Particle Tracking Imaging and Analysis

Imaging for particle tracking experiments was done using a 63x (1.4 NA) oil immersion objective of an inverted microscope (DMI6000, Leica, Buffalo Grove, IL) in a controlled live-cell imaging chamber. Cell nuclei were labeled with 0.5 μg/mL Hoechst 33342 (Life Technologies, Grand Island, NY). Images were taken at multiple positions per plate at 3.0 minute intervals with 1-4 transfected cells per field of view and 4-10 particles per cell for GFP-Fib and 5-35 particles per cell for Hoechst 33342-stained DNA. Cells maintained viability well

beyond the duration of the experiment as confirmed by continued imaging for over an hour after the completion of data collection. Two-dimensional tracking of either GFP-Fib or punctate regions of Hoechst 33342-stained DNA was done using custom Laptrack71 programs designed in MATLAB (Natick, MA) as previously published.[40, 41] Briefly, images were cropped and aligned to remove artifacts including imaging drift, nuclear translation, and nuclear rotation. Particles were then detected through statistical algorithms after calibration of background noise parameters. Particle tracks were then determined by correspondence with succeeding frames. Only persistent tracks of particles present for the full duration of the experiment were used for further analysis.

The ensemble-averaged MSD was calculated from the particle tracks as shown in Equation 1,[42] where τ is the lag time. MSD magnitudes were compared at each time point using Student's t-test. Data were fit to a power-law rheological model as consistent for biological systems[43] and the nucleus in particular[44] as shown in Equation 4, where D_{eff} is the effective diffusivity and indicative of the chromatin compliance (where chromatin decondensation increases compliance and *vice versa*) and β is the power-law diffusive exponent which provides a measure of system forces including thermal forces and cytoskeletal forces. Calculation of D_{eff} was done by normalizing lag time, τ, to the sampling time step of three minutes. This allowed for enhanced accuracy in the fit calculation by using interpolation of the data rather than extrapolation. 95% confidence intervals for parameter values were used for statistical comparison. Since the MSD is an inherently positive quantity, outliers with large magnitudes may bias the resultant

ensemble average. Consequently, all outliers greater than three standard deviations from the mean were removed and the data were reanalyzed, though with little to no change in the trends. These cells generally had issues with alignment wherein nuclear rotation or translation was not properly removed.

$$MSD(\tau) = \langle (x_{t+\tau} - x_t)^2 + (y_{t+\tau} - y_t)^2 \rangle \quad (1)$$

Cell Fixation and Fluorescence Lifetime Imaging Microscopy

Following treatment, cells were fixed using 3.7% formaldehyde in phosphate buffered saline (PBS) solution. Cells were then permeabilized using 0.2% Triton X-100 in PBS. DNA was stained using Hoechst 33342 (Life Technologies, Grand Island, NY) for fluorescence lifetime imaging microscopy (FLIM). For fluorescence imaging, actin was stained using rhodamine phalloidin (Life Technologies, Grand Island, NY) and lamin A/C was immunostained using a primary mouse monoclonal lamin A/C antibody and a secondary goat anti-mouse antibody IgG-CFL Alexa Fluor 488 (Santa Cruz Biotechnology, Santa Cruz, CA).

FLIM measurements were obtained using a Leica TCS SP5 inverted laser scanning confocal microscope with a 100x (1.4 NA) oil immersion objective. The corresponding pixel resolution was 256 x 256 and the scan rate was 400 Hz. A Ti:sapphire mode-locked, pulsed infrared laser (Chameleon, Coherent) system was used for multiphoton excitation source (1 W, average). The laser was tuned to 825 nm (Hoechst) using pulse-widths of <140 fs delivered at 90 MHz. Emission

was detected from 404-536 nm (Hoechst) using a FLIM-specific photomultiplier tube (PMT), consistent with the complete emission spectra for those fluorophores.

Data acquisition and analysis were done using methods previously published.[45] Briefly, images were acquired for approximately ten minutes in order to minimize errors associated with photobleaching, low signal-to-noise ratios and pile-up effects as determined by maintaining rates of photons detected, converted, and stored between 1 x 10^4 and 1 x 10^6. A suite of software programs from Becker & Hickl SPC-830 was used for time-correlated single photon counting (TCSPC) with 10 ps resolution. Lifetime variance was minimized using 220 time channels and a measurement window of 10.8 ns.

The fluorescence lifetime can be modeled as the summation of exponential decay rates as shown in Equation 2. Here τ_n and a_n correspond to the lifetime and normalized amplitude, respectively, of the n^{th} exponential decay. I(t) is the number of photons detected per unit time, t, and I_0 is the background offset. When there are multiple exponential decays the mean fluorescence lifetime, τ_m, is determined from Equation 3.

$$I(t) = I_0 + \sum_n a_n e^{-t/\tau_n} \quad (2)$$

$$\tau_m = \frac{\sum_n a_n \tau_n}{\sum_n a_n} \quad (3)$$

Data were analyzed and fluorescence lifetime images created using the Becker & Hickl SPCImage software. For each data set, the instrument response functions were determined and the lifetime images were binned such that the peak photon count was ≥ 1000, as required for verification of double-exponential decay.[46] Using MATLAB, the nuclei were segmented to remove autofluorescence

and background. Then the average lifetimes and corresponding standard deviation for both a single and double exponential decay were determined for each experiment by averaging the value for each pixel. The respective fits were compared using a χ^2 test. Hoechst 33342 was modeled best as a double exponential decay.

Three-Dimensional Length Scales of Endothelial Cells

Subconfluent endothelial cells spread significantly on flat substrates and show distended nuclei and elongated actin stress fibers. We wanted to determine contributions from three-dimensional structures. We used confocal imaging of fixed cells to determine the relative spatial dimensions of cellular structures (Figure 4.1). Actin structures in adjacent cells abut and are difficult to segment. However, from the DNA and lamin channels (blue and red of Figure 4.1), the nucleus is easily visually segmented. As such, we observe that the nucleus is roughly 22 μm in the x-direction, 30 μm in the y-direction and less than 3 μm in the z-direction. Thus, we observe that there is a <1:10 aspect ratio for the height of nuclear structures compared with radial positions within spread endothelial cells.). Cells were imaged on a Nikon AZ100 C2 laser scanning confocal microscope at 63x magnification (1.40 NA).

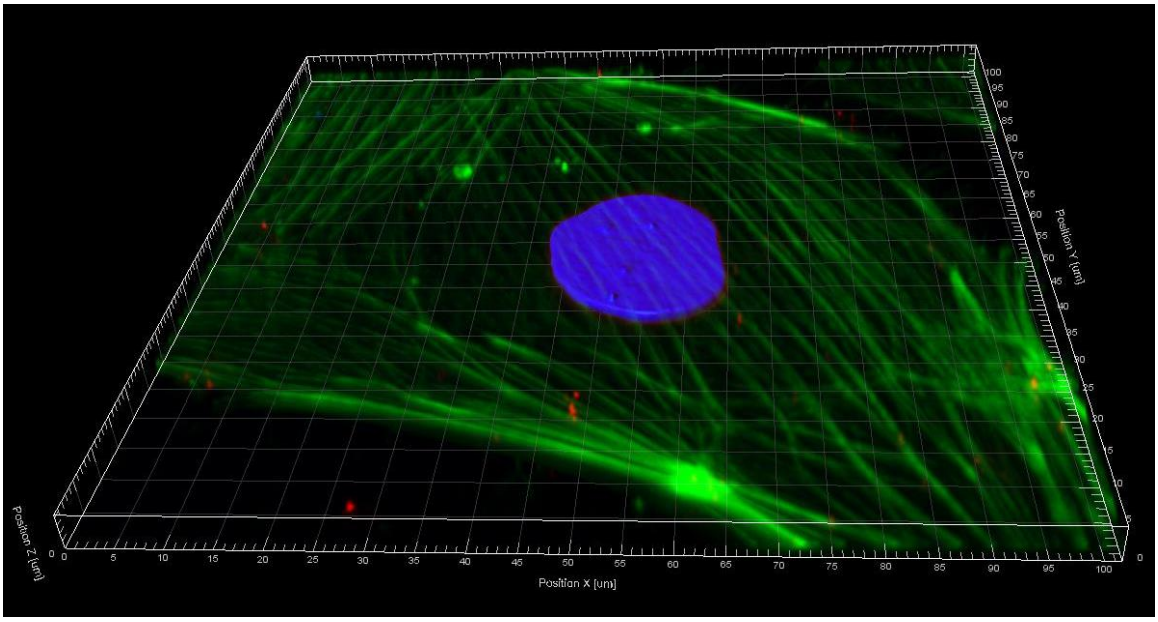

Figure 4.1: Confocal image of fixed endothelial cell allows visualization of cellular dimensions. *A fixed HUVEC labeled in green for F-actin (labeled with phalloidin), in red for lamin A (antibody to lamin A), and in blue for DNA (Hoechst 33342) shows a nuclear diameter of 20-30 μm but a nuclear height under 3 μm.*

Nuclear fluctuation

Nuclei, stained with Hoechst 33342 and in some cases GFP-fibrillarin were imaged every three minutes for two hours. We utilize the Hoechst 33342 signal for precisely segmented nuclear boundaries. Fluctuations of nuclear area were quantified using MATLAB's Image Processing Toolbox. The Hoechst 33342 DNA channel was thresholded using the Image Processing Toolbox's built-in Otzu's method to obtain nuclear area. Areas were confirmed by visual inspection. Nuclear areas for each cell were normalized to the area of the initial image and compiled for the control and VEGF treatment groups. To measure

intranuclear speeds, GFP-fibrillarin positions were calculated from the images after subtraction of rigid body rotation and translation of the nucleus using previously described image analysis in Matlab.[47-49]

Kymographs

Images were taken at three minute time intervals for two hours. Target nuclei were cropped and the images were aligned to remove image drift and nuclear translation and rotation using a custom Laptrack71 software.[47-49] Kymographs were then generated using ImageJ (NIH) and the Kymograph plugin (J. Rietdorf and A. Seitz). Regions of interest were determined to show the different time scales and length scales of deformations.

Statistics

Magnitudes of the ensemble-averaged mean squared displacement were statistically compared using Student's t-test. Fitting parameters and corresponding 95% confidence intervals were determined using the MATLAB for nonlinear least squares regression trust-region algorithm and verified using ANOVA ($p<0.001$). For FLIM experiments, the fits (single or double exponential decays) were determined using a χ^2 test, as discussed above. The mean fluorescence lifetimes were compared using Student's t-test and the variance compared using the F-test.

Results

Chromatin Fluctuations from VEGF-Stimulated Genome Reorganization

We aimed to investigate the impact of the dramatic changes in gene expression from VEGF stimulation on chromatin dynamics in live HUVECs. We have previously shown that ensemble probe motions of fibrillarin, upstream binding factor-1 and punctate Hoechst 33342 demonstrate physically uniform dynamics.[4, 41] Thus, we transfected cells with GFP-Fibrillarin (GFP-Fib) and track its motion in live cells to calculate the mean squared displacement (MSD) from Equation 1 as a measure of these dynamics. For extracting the physical parameters associated with these chromatin dynamics, we fit the MSD to the power-law equation (Equation 4). As we've previously shown D_{eff} is a measure of chromatin compliance which is dependent on condensation state and β is measure of system forces driven primarily by the active cytoskeleton.[4] An increase in D_{eff} is consistent with chromatin decondensation, and *vice versa*, through mechanically relaxing the local structure making it more compliant and flexible for chromatin fluctuations. By contrast, increased cytoskeletal forces act to enhance chromatin dynamics beyond thermal fluctuations through the power-law time dependence of the exponent β. These forces stem primarily from the actin motor protein myosin II and its mechanical connections to the nuclear interior through the LINC complex.

$$MSD = D_{eff}\tau^{\beta} \quad (4)$$

To investigate the role of VEGF stimulation on chromatin dynamics, we examined effects of the temporal expression profiles on chromatin dynamics after

one hour and after 2.5 hours. These time points were selected to match with microarray analysis that shows distinct temporal gene expression profiles corresponding to genes directly induced by VEGF at early times (<40% of total genes) and the remaining genes likely stimulated by secondary mechanisms involving the signaling and transcription factors upregulated in the first wave.[26] Our results show VEGF stimulation results in enhanced chromatin dynamics from VEGF stimulation for both the early and later responses, with a large increase in MSD (Figure 4.2A). Similar results were observed for particle tracking of punctate regions of Hoechst 33342-stained chromatin (data not shown). However, the chromatin dynamics exhibited distinct temporal behavior at these time points. During the early VEGF response, the increase in MSD stems primarily from a dramatic increase in β of 40% (Figure 4.2C), indicating increased active force propagation to the nuclear interior that is likely derived from the actin cytoskeleton. This increase in active forces appears to return to control levels at long times as evinced through β. Yet the enhanced chromatin dynamics persist due to an increase in D_{eff} (Figure 4.2B) corresponding to large scale chromatin decondensation that makes the network more compliant.

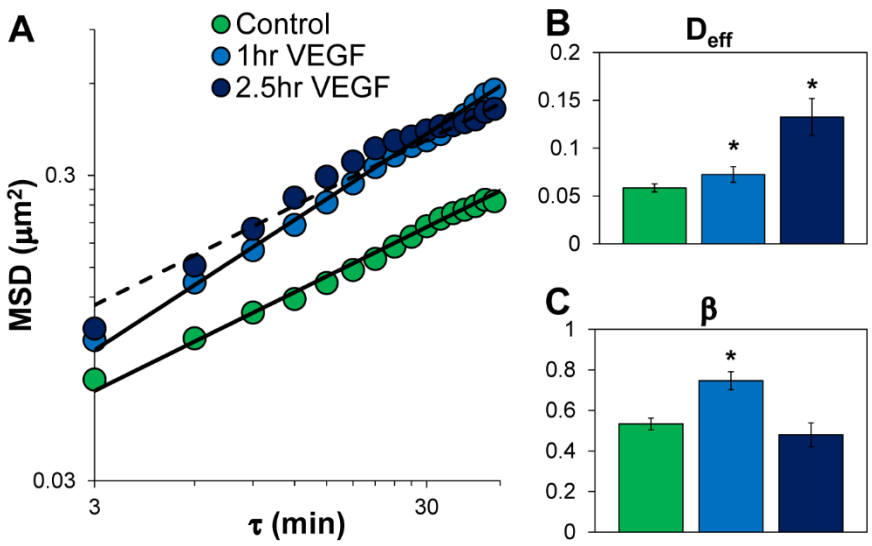

Figure 4.2: Chromatin dynamics from VEGF-stimulated genome reorganization exhibit distinct temporal behavior. *(A) Cells treated with VEGF had increased magnitudes of MSD ($p<0.01$). Fitting the data to Equation 4 showed (B) a statistically significant increase the prefactor D_{eff} for both time points, but more prominently at later times, indicating an effective softening of the nuclear interior consistent with chromatin decondensaiton ($p<0.05$) and (C) an increase in the diffusive exponent β following initial VEGF exposure ($p<0.05$) indicating increased active stresses (and no change at the later time) stemming primarily from the cytoskeleton. Error bars reflect 95% confidence intervals.*

Altered Chromatin Condensation State During Stimulated Gene Expression

Having established the temporal effects of VEGF stimulation on chromatin dynamics, we sought to confirm the changes in chromatin condensation state using fluorescence lifetime imaging microscopy (FLIM). FLIM provides a spatially resolved quantitative measure of the chromatin condensation state and

structural remodeling during physiological changes and within the context of functional nuclear processes. As such, we aimed to quantify VEGF-stimulated changes in chromatin condensation state *in situ* using the fluorescence lifetime as well as the spatial reorganization of these condensation states corresponding to underlying changes in gene expression.

As indicated in the mean fluorescence lifetime heat maps (Figure 4.3A), we observe an increasing number of high mean fluorescence lifetime regions within the nucleus with increasing duration of VEGF exposure consistent with a growing number of regions of decondensed chromatin. At later times, we qualitatively observe a combination of low and very high mean fluorescence lifetime regions consistent with both condensed chromatin and highly decondensed chromatin, respectively. We further quantify these changes in chromatin condensation state where we observe strongly significant step-wise increases in the mean fluorescence lifetime compared to control levels upon VEGF stimulation after 1 hour and 2.5 hours, respectively (Figure 4.3B). Interestingly, these trends align with the aforementioned mechanical measurements of chromatin condensation state from particle tracking of chromatin dynamics,[4] thereby confirming the changes in chromatin condensation state and highlighting the complementarity of this technique with particle tracking as a high-throughput alternative measure of the mechanical effects of chromatin condensation state on bulk and localized intranuclear mechanics.

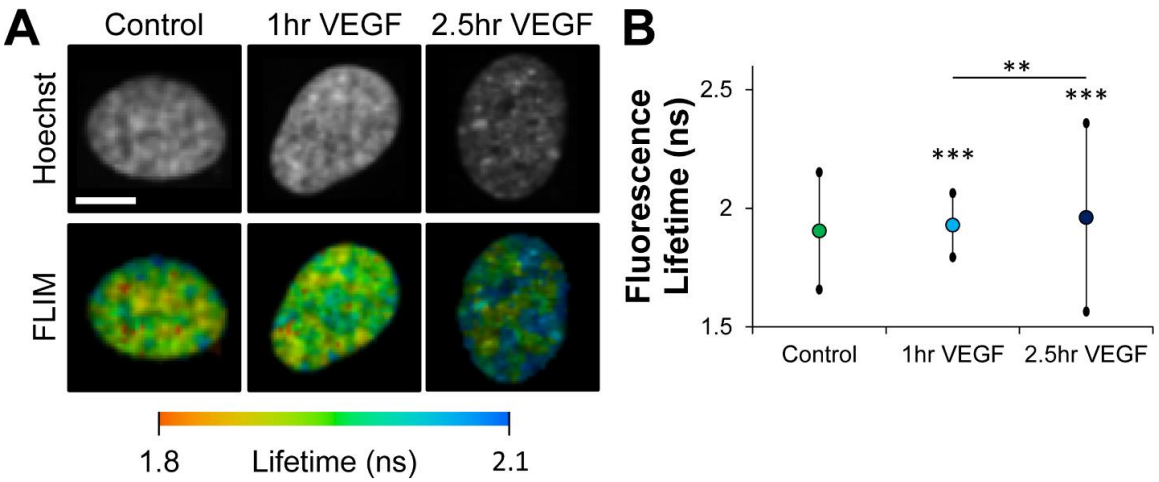

Figure 4.3: Fluorescence lifetime measurements of chromatin condensation state during stimulated gene activation in VEGF-stimulated endothelial cell nuclei. *(A) Fluorescence intensity confocal images (top) and mean fluorescence lifetime heat maps (bottom) of chromatin in endothelial cell nuclei labeled with Hoechst 33342 and treated with VEGF for 0, 1 or 2.5 hours. Mean fluorescence lifetime heat maps indicate spatial arrangement of local fluorophore environments for stained chromatin which is consistent with varying chromatin condensation state. Altered fluorescence intensity with treatments show differential chromatin condensation state, with more intense fluorescence arising from highly concentrated condensed chromatin. (B) Treatment with VEGF at both time points resulted in a strong and statistically significant increase the mean fluorescence lifetime relative to untreated controls (***p<<0.001), with a step-wise increase at each time point (**p<0.025). Analysis was done using 60-80 segmented nuclei for each treatment condition. Error bars indicate standard deviation of pixel-to-pixel mean fluorescence lifetime differences of segmented nuclei under each treatment condition. Scale bar is 10 μm.*

VEGF Stimulation Increases Actin Stress Fiber Colocalization with the Nucleus

The role of actin in chromatin dynamics has been previously established.[4, 31, 39] Additionally, actin plays a prominent role in driving cellular physiological changes associated with VEGF stimulation. Thus, given the enhanced chromatin dynamics observed early in the VEGF response stems from enhanced force-driven agitation, we aimed to determine how actin reorganizes in response to VEGF stimulation.

In both fixed and live cells we observed that actin reorganization in VEGF stimulated HUVECs. In live cells, we visualize actin with LifeAct and the nucleus with Hoechst 33342. In control cells, actin fibers were found primarily at the edge of the cell as part of the cortical network (Figure 4.4, Control). As cells crawled, actin moved primarily at the cortical regions of the cell. However, in VEGF stimulated cells, we observed distinct actin fibers near and above the nucleus (Figure 4.4, +VEGF).

In fixed imaging we grew cells to confluent monolayers and we visualized actin using phalloidin, the nucleoskeleton with immunocytochemistry and the nucleus with Hoechst 33342 for DNA (Figure 4.4). We quantified actin intensity close to the nucleus (Figure 4.5). In control cells, there was little to no actin fiber localization around the nucleus. By contrast, after VEGF stimulation we observed increased actin fiber fluorescence (visualized as intensity fluctuations) colocalized with and peripheral to the nucleus fluorescence (Figure 4.5).

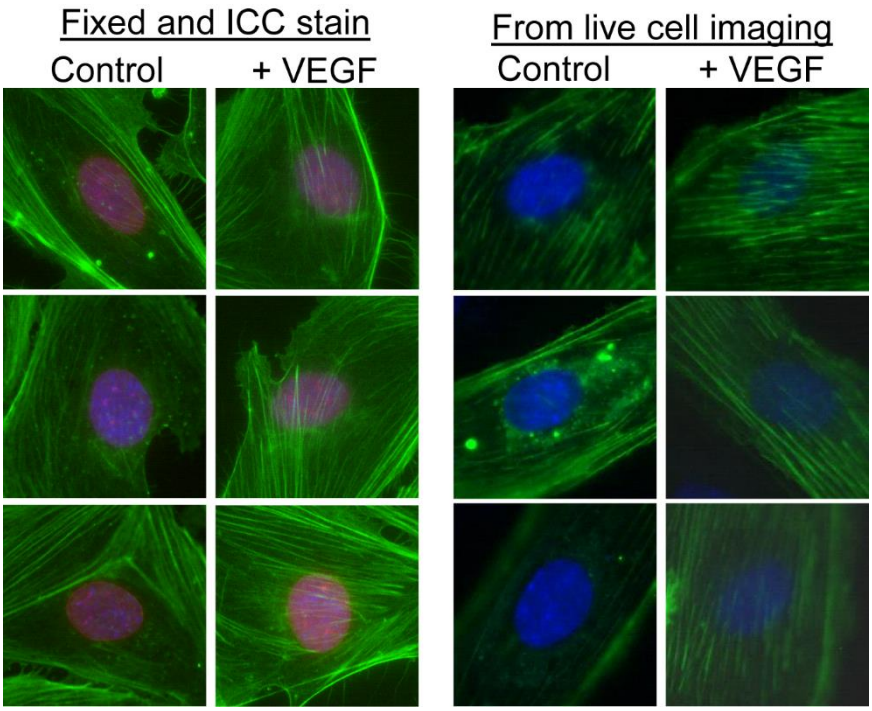

Figure 4.4: VEGF treatment shows actin stress fibers near the nucleus. Either in fixed, labeled cells or in live cells, control HUVEC show actin stress fibers near but separated from the nucleus. In HUVECs treated with VEGF, actin is found more closely localized with the nucleus.

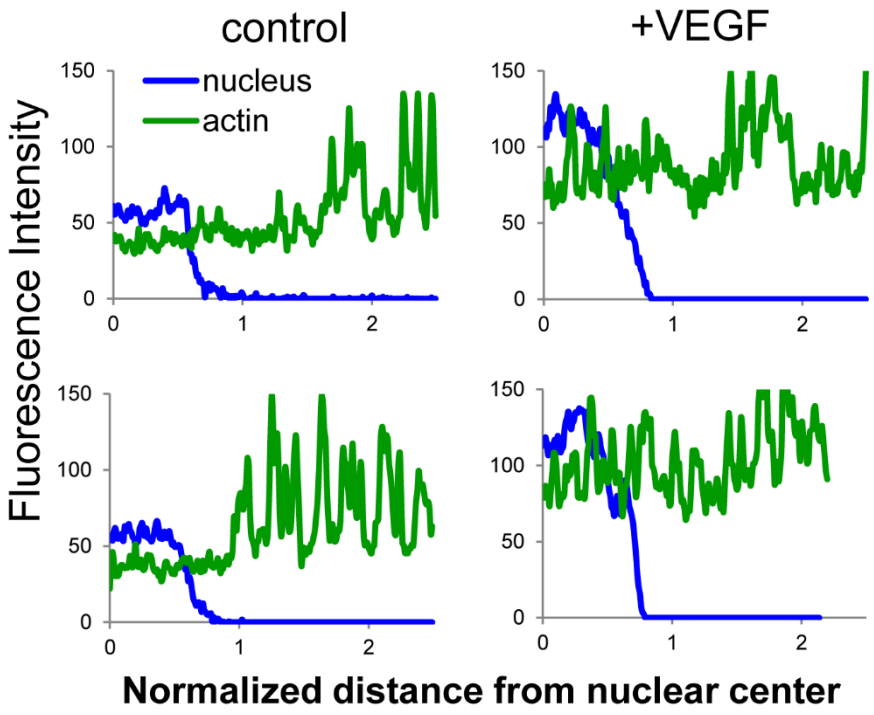

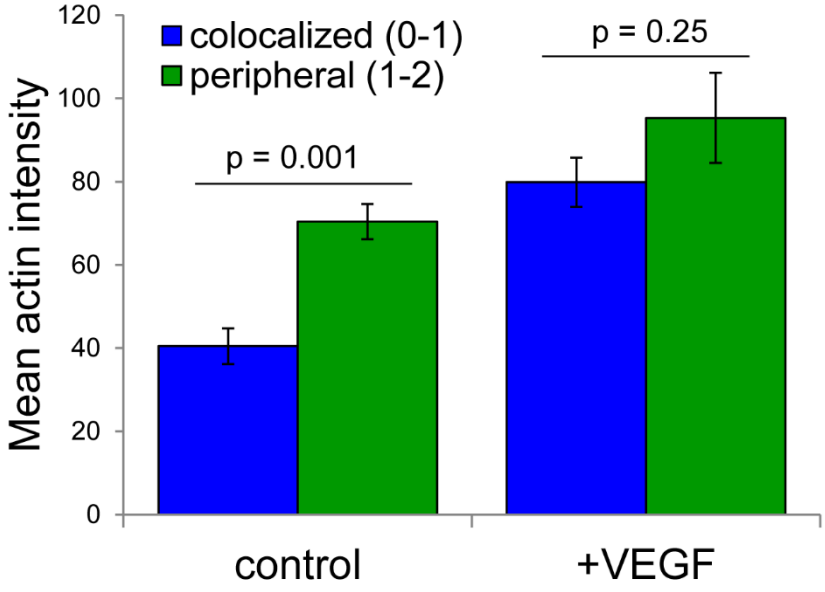

Figure 4.5: Colocalization of actin and nuclear fluorescence intensity. *We analyzed images of fixed HUVEC in confluent monolayers with labeled actin (phalloidin) and nuclei (Hoechst 33342), similar to fixed cells in Figure 4.1. Nuclear fluorescence was normalized to position 0-1 and histograms of actin*

fluorescence were determined normal to the actin fibers for more than double that length (position 0 – 2.5). Two representative cells are shown for each condition. The mean actin intensity was then considered for regions that overlapped with nuclear fluorescence intensity (0-1) and outside the nuclear intensity (1-2). Control cells showed a statistical difference in actin fluorescence based on localization, whereas VEGF-treated cells show statistically similar levels (n=5, for each condition).

VEGF Stimulation Increases Nuclear Envelope Fluctuations

Given that the early enhancement of chromatin dynamics upon VEGF stimulation are driven primarily by motor activity and that VEGF stimulation coincides with increased actin colocalization with the nucleus, we aimed to investigate and quantify the possibility of active cytoskeletal forces on the nucleus. We imaged nuclear deformability in HUVECs with the cell-permeable DNA dye Hoechst 33342. Control cells showed minimal fluctuations in nuclear area consistent with central rigid bodies (Figure 4.6). In contrast, nuclei in cells treated with VEGF showed large, inward fluctuations (Figure 4.6). To quantify these nuclear fluctuations, we calculated changes in nuclear area over time normalized to the initial nuclear area (Figure 4.7). The histogram of the VEGF treatment group had a smaller mean, depicting the greater tendency of the nuclei in the VEGF treatment group to get smaller, or fluctuate in the inward direction. The histogram was also broader highlighting the increase fluctuation of the VEGF treatment group through greater deviation in the normalized nuclear area. This

agrees with the observation that the VEGF treatment group tended to have larger and more frequent nuclear deformations than the control group. This increase in fluctuation, or variance in normalized nuclear area, was confirmed with an F-test with $p<<0.001$.

Visualization of nuclear fluctuations of VEGF-stimulated cells shows small deformations (short time and short length scale) and large deformations (long time and larger length scale). From kymographs, we observe deformations over minutes that are less than 1 μm (Figure 4.6, point 1) as well as large deformations nearing 4 μm that persist over tens of minutes (Figure 4.6, point 2). These small and medium fluctuations, together with the global fluctuations of Figure 4.7, suggest significant changes in nuclear-cytoskeletal coupling associated with VEGF treatment that likely facilitates the enhanced chromatin dynamics in the initial VEGF response.

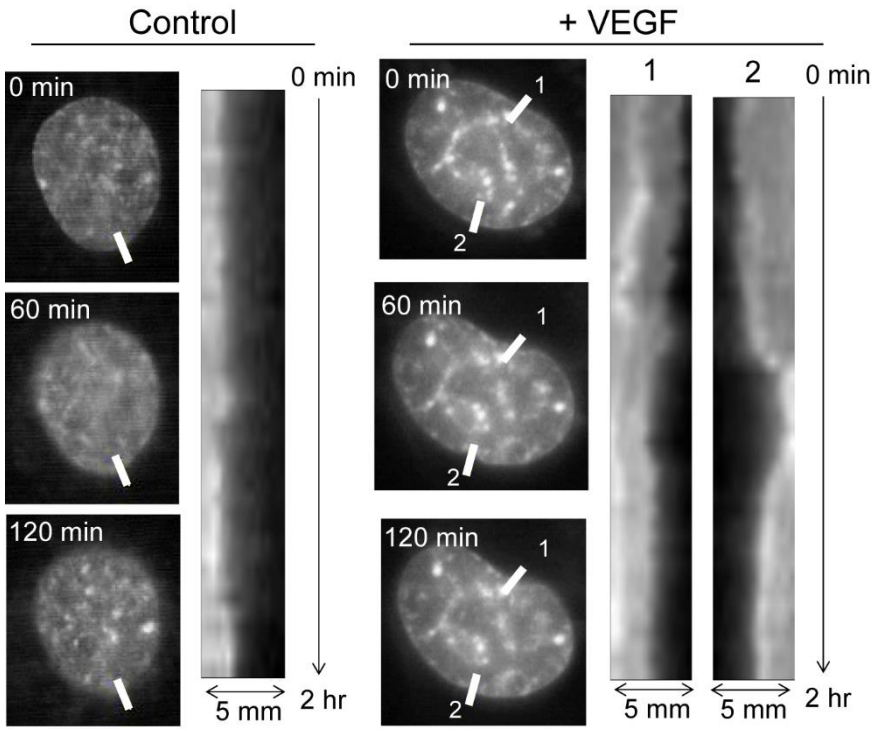

Figure 4.6: VEGF treatment is associated with fine fluctuations of the nuclear envelope. *We followed fluctuations at the nuclear envelope (imaged with the cell permeable DNA stain Hoechst 33342) over 5 μm length scales to highlight the impact of VEGF treatment. There are obvious regions wherein nuclei show gross distortions inward over long time as well as short distortions over short times.*

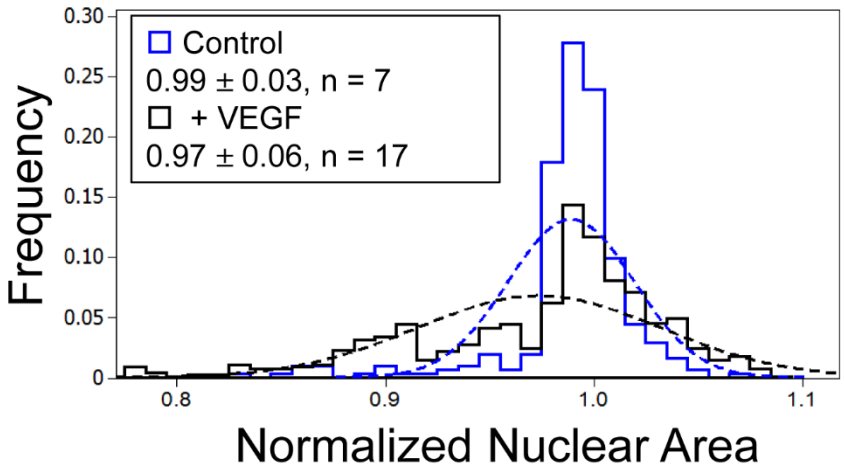

Figure 4.7: VEGF treatment is associated with gross area fluctuations of the nucleus. *We tracked the nuclear area of live cells (imaged with the cell permeable DNA stain Hoechst 33342) every 3 minutes for two hours. In control cells, nuclei maintained nearly constant area, showing mostly rigid body rotation and translation but little dilation or fluctuation. In contrast, VEGF-treated nuclei showed large-scale changes in area including invaginations and dilations. These changes are best quantified by the distribution of normalized area. VEGF-treated cells show a much broader distribution reflecting the larger fluctuations. A two tailed Student's t-test performed on the distributions of normalized nuclear areas*

indicates that these sampled populations are significantly different with a confidence level of 0.05. The variance of the two groups were found to be statistically different using an F-test with $p<<0.001$.

Discussion

Long missing in our understanding of the physiological effects of VEGF stimulation and the corresponding biochemical signaling cascades and the subsequent gene activation is the nuclear reorganization of chromatin associated with these changes. At its essence, the mechanism of transcriptional activation is well established, but not *in situ* within the context of nuclear organization of functional sites and chromatin dynamics. Here we demonstrate how chromatin dynamics are impacted by these ongoing processes during VEGF stimulation. Additionally, we show potential coordination of structural and mechanical changes of the cytoskeleton with the resulting chromatin dynamics through active force transduction to the nuclear interior for chromatin agitation.

A hallmark of our understanding of transcriptional activation is the need for chromatin remodeling and decondensation to allow access to transcriptional machinery. Our present work highlights the progression of VEGF-stimulated gene activation through the temporal increase in chromatin decondensation over time as measured by the increasing mean fluorescence lifetime. Further, we show the spatial distribution of these decondensed regions in endothelial cell nuclei over these time scales as more genes seemingly become activated. Yet, our previous work[4] and that of others[31] have shown more decondensed chromatin to be highly dynamic through an increase in compliance that accompanies decondensation

enhances its fluctuations. Thus, it seems likely that decondensation may not solely be a means of allowing accessibility, but also facilitating chromatin spatial and functional reorganization through enhanced compliance and mobility. This enhanced mobility would increase collision frequency and sampling radius for finding transcriptional machinery, at which time these fluctuations may become stabilized.

Beyond changes in chromatin condensation state, large scale changes in gene expression associated with major physiological events have been suggested to be aided by cytoskeleton-induced nuclear deformations to enhance chromatin agitation for reorganization.[31, 32, 39, 50] We previously demonstrated the role of ATP-dependent motor activity, and myosin II on actin specifically, in chromatin agitation of primary human cells.[4] Here we extend this finding to the specific case of VEGF-stimulated endothelial cells. Such motor activity likely facilitates the enhanced efficiency of binding events in the nucleus compared to *in vitro* studies by acting globally and nonspecifically to agitate chromatin and increase the mobility, collision frequency, remodeling and conformational turnover.[31, 32, 50] As discussed previously in Chapter III, by increasing the diffusive exponent, β, the effective sampling radius for finding binding partners increases to favor binding probabilities of more distantly positioned binding partners.[51] Thus, early in the VEGF response as transcription factors translocate to the nucleus, the binding probability is enhanced by this increase in motor activity. Similar effects associated with cytoskeletal force-induced chromatin agitation have been observed during development, including the establishment of specific chromatin

territories and promoting the pairing of homologous chromosomes during cell division.[32] This agitation also provides a mechanism for enhanced turnover and chromatin remodeling[31] during stimulated changes in expression. While chromatin exists in a distribution of intermediate states of condensation, previous work has shown opposing bivalent (i.e. both activating and repressing) chromatin modifications particularly at transcriptionally "competent" sites.[52] Our work suggests differential mobility at these sites may also play a role and that force-induced agitation may serve to facilitate unfolding, with more rapid unfolding at these less condensed, transcriptionally "competent" sites as has been suggested elsewhere.[31, 53]

Our previous work has highlighted the myosin II actin motor as one of the primary motor proteins impacting chromatin dynamics. This was supported by showing that abrogation of the cytoskeletal mechanical connections to the nuclear interior through the LINC complex results in quantitatively similar chromatin dynamics, as did global ATP depletion. Here we show that within the context of VEGF stimulation, early in the response the chromatin dynamics are largely influenced by enhanced motor activity. We similarly show coordinated colocalization of actin with the nucleus and increased nuclear deformations in response to VEGF. This seemingly points to an active role for actin force generation[54] in driving these dynamics and enhancing chromatin agitation[31, 32, 55, 56] possibly to facilitate remodeling. This is also consistent with previous observations of an increase in perinuclear actin cap formation and TAN line engagement associated with transitional states in cells.[57] Further, endothelial cells

express high levels of LINC proteins including nesprin 3[58] and transcription factor nuclear signaling in response to mechanical stimuli has been shown to depend on actin polymerization states.[31, 59, 60]

We suggest numerous hypotheses for the immediate change in intranuclear responsiveness from myosin II force generation followed by a second regime of chromatin decondensation. Mechanical forces may provide the impetus for the immediate responsiveness of the nuclear interior by enhancing chromatin mobility (increased β). Additionally, forces may facilitate genome remodeling and reorganization as part of the secondary mechanisms resulting in the dramatic chromatin decondensation (increase D_{eff}) for subsequent induction of the majority of VEGF-responsive genes at later times as shown in previous studies highlighting the role of external forces in inducing chromatin decondensation.[31] It is also possible that the increased nuclear deformations, including nuclear envelope fluctuations and intranuclear movements, may lead to a variety of downstream cellular changes including increased cytoplasmic-nuclear transport of biochemical factors through nuclear pores which are enhanced by stretching and fluctuation of the nuclear envelope.[61]

Our results are also supported by previous work on chemically-stimulated expression changes that have shown only moderate chromatin decondensation and low transcription efficiency on the time scales of ~20 minutes post stimulation, with maximal decondensation and peak transcriptional activity occurring >2 hours after exposure.[28] Thus, it seems likely that the early force-induced chromatin agitation facilitates the transport and kinetic events associated with stimulated

changes in gene expression. Consequently, our findings suggest a plausible mechanism wherein mechanics, through both force-induced chromatin agitation and chromatin decondensation, may play a role in the kinetic and transport mechanisms associated with stimulated changes in gene expression. This carries implications beyond transcriptional changes, where this understanding of the mechanisms of chromatin remodeling and dynamics also has implications for mechanotransduction[31] and the DNA damage response involving chromosome translocations and repair.[62, 63]

Acknowledgements

We gratefully acknowledge help with multiphoton confocal imaging and analysis by Brian Holt (Carnegie Mellon Biomedical Engineering) and Mohammad Islam (Carnegie Mellon Materials Science and Engineering). Additional thanks to James Weltz (Carnegie Mellon, Chemical Engineering and Biomedical Engineering) for his help with experimental design and image analysis; Elizabeth Booth-Gauthier (UC Berkeley) for her helpful discussion and input throughout; Ge Yang (Carnegie Mellon Biomedical Engineering, Lane Center for Computational Biology, and Biological Sciences) and Minhua Qui (Carnegie Mellon Biomedical Engineering) for development and assistance with the LAPtrack71 suite of particle tracking programs; Lynn Walker (Carnegie Mellon Chemical Engineering) for her insight into the polymer characterization and rheology (Carnegie Mellon Chemical Engineering); Gant Luxton (University of Minnesota Genetics, Cell Biology and Development) and Nathan Harris

(University of Minnesota Genetics, Cell Biology and Development) for providing the KASH constructs and helpful discussion; J. Szymanski and A. Feinberg (Carnegie Mellon University, Department of Biomedical Engineering) for help with confocal imaging; and S. Kumar (UC Berkeley, Department of Bioengineering) for reagents. This work is supported by the NSF (NSF-CBET-0954421, CMMI-1300476 to KND and DMR-0619424 to Mohammad Islam) and the ARCS Foundation (STS), Bertucci Fellowship (STS), and James C. Meade Fellowship (STS).

References

1. C. R. Clapier and B. R. Cairns, *Annu Rev Biochem*, 2009, **78**, 273-304.
2. M. R. Hubner and D. L. Spector, *Annu Rev Biophys*, 2010, **39**, 471-489.
3. L. Meldi and J. H. Brickner, *Trends in cell biology*, 2011, **21**, 701-708.
4. S. T. Spagnol and K. N. Dahl, *Integr Biol-Uk*, 2014, **6**, 523-531.
5. S. Kliche and J. Waltenberger, *IUBMB life*, 2001, **52**, 61-66.
6. S. Cebe-Suarez, A. Zehnder-Fjallman and K. Ballmer-Hofer, *Cellular and molecular life sciences : CMLS*, 2006, **63**, 601-615.
7. P. Carmeliet and R. K. Jain, *Nature*, 2011, **473**, 298-307.
8. M. J. Webber, J. Tongers, C. J. Newcomb, K. T. Marquardt, J. Bauersachs, D. W. Losordo and S. I. Stupp, *Proceedings of the National Academy of Sciences of the United States of America*, 2011, **108**, 13438-13443.
9. G. Gasparini, *The oncologist*, 2000, **5 Suppl 1**, 37-44.
10. A. O. Afuwape, S. Kiriakidis and E. M. Paleolog, *Histol Histopathol*, 2002, **17**, 961-972.
11. R. B. Caldwell, M. Bartoli, M. A. Behzadian, A. E. El-Remessy, M. Al-Shabrawey, D. H. Platt and R. W. Caldwell, *Diabetes/metabolism research and reviews*, 2003, **19**, 442-455.
12. C. Campa and S. P. Harding, *Current drug targets*, 2011, **12**, 173-181.
13. N. Ferrara and T. Davis-Smyth, *Endocrine reviews*, 1997, **18**, 4-25.
14. L. Lamalice, F. Le Boeuf and J. Huot, *Circulation research*, 2007, **100**, 782-794.
15. S. Yang, X. Xin, C. Zlot, G. Ingle, G. Fuh, B. Li, B. Moffat, A. M. de Vos and M. E. Gerritsen, *Arteriosclerosis, thrombosis, and vascular biology*, 2001, **21**, 1934-1940.
16. W. Risau, *Nature*, 1997, **386**, 671-674.

17. S. Esser, M. G. Lampugnani, M. Corada, E. Dejana and W. Risau, *Journal of cell science*, 1998, **111 (Pt 13)**, 1853-1865.
18. T. Matsumoto and L. Claesson-Welsh, *Science's STKE : signal transduction knowledge environment*, 2001, **2001**, re21.
19. T. Matsumoto and H. Mugishima, *Journal of atherosclerosis and thrombosis*, 2006, **13**, 130-135.
20. B. Kiec-Wilk, J. Grzybowska-Galuszka, A. Polus, J. Pryjma, A. Knapp and K. Kristiansen, *Journal of physiology and pharmacology : an official journal of the Polish Physiological Society*, 2010, **61**, 217-225.
21. S. Yang, K. Toy, G. Ingle, C. Zlot, P. M. Williams, G. Fuh, B. Li, A. de Vos and M. E. Gerritsen, *Arteriosclerosis, thrombosis, and vascular biology*, 2002, **22**, 1797-1803.
22. B. Vasir, J. C. Jonas, G. M. Steil, J. Hollister-Lock, W. Hasenkamp, A. Sharma, S. Bonner-Weir and G. C. Weir, *Transplantation*, 2001, **71**, 924-935.
23. B. Bussolati, C. Dunk, M. Grohman, C. D. Kontos, J. Mason and A. Ahmed, *The American journal of pathology*, 2001, **159**, 993-1008.
24. D. W. Leung, G. Cachianes, W. J. Kuang, D. V. Goeddel and N. Ferrara, *Science*, 1989, **246**, 1306-1309.
25. Y. H. Cao, J. Arbiser, R. J. D'Amato, P. A. D'Amore, D. E. Ingber, R. Kerbel, M. Klagsbrun, S. Lim, M. A. Moses, B. Zetter, H. Dvorak and R. Langer, *Sci Transl Med*, 2011, **3**.
26. M. Abe and Y. Sato, *Angiogenesis*, 2001, **4**, 289-298.
27. G. C. Weston, I. Haviv and P. A. Rogers, *Molecular human reproduction*, 2002, **8**, 855-863.
28. S. M. Janicki, T. Tsukamoto, S. E. Salghetti, W. P. Tansey, R. Sachidanandam, K. V. Prasanth, T. Ried, Y. Shav-Tal, E. Bertrand, R. H. Singer and D. L. Spector, *Cell*, 2004, **116**, 683-698.
29. C. H. Thomas, J. H. Collier, C. S. Sfeir and K. E. Healy, *Proceedings of the National Academy of Sciences of the United States of America*, 2002, **99**, 1972-1977.
30. C. Lanctot, T. Cheutin, M. Cremer, G. Cavalli and T. Cremer, *Nature reviews. Genetics*, 2007, **8**, 104-115.
31. K. V. Iyer, S. Pulford, A. Mogilner and G. V. Shivashankar, *Biophysical journal*, 2012, **103**, 1416-1428.
32. B. Hampoelz, Y. Azou-Gros, R. Fabre, O. Markova, P. H. Puech and T. Lecuit, *Development*, 2011, **138**, 3377-3386.
33. K. M. Stroka and H. Aranda-Espinoza, *Cellular and molecular bioengineering*, 2011, **4**, 9-27.
34. C. M. Nelson, D. M. Pirone, J. L. Tan and C. S. Chen, *Molecular biology of the cell*, 2004, **15**, 2943-2953.
35. M. Versaevel, T. Grevesse and S. Gabriele, *Nature communications*, 2012, **3**, 671.
36. C. A. Reinhart-King, M. Dembo and D. A. Hammer, *Biophysical journal*, 2005, **89**, 676-689.

37. Y. T. Shiu, J. A. Weiss, J. B. Hoying, M. N. Iwamoto, I. S. Joung and C. T. Quam, *Critical reviews in biomedical engineering*, 2005, **33**, 431-510.
38. J. R. Sims, S. Karp and D. E. Ingber, *Journal of cell science*, 1992, **103 (Pt 4)**, 1215-1222.
39. A. J. Maniotis, C. S. Chen and D. E. Ingber, *Proceedings of the National Academy of Sciences of the United States of America*, 1997, **94**, 849-854.
40. G. Yang, L. A. Cameron, P. S. Maddox, E. D. Salmon and G. Danuser, *Journal of Cell Biology*, 2008, **182**, 631-639.
41. E. A. Booth-Gauthier, T. Alcoser, K. N. Dahl and G. Yang, *Biophysical journal*, 2012.
42. X. Michalet, *Biophysical journal*, 2011, **100**, 252-252.
43. P. Kollmannsberger and B. Fabry, *Annu Rev Mater Res*, 2011, **41**, 75-97.
44. K. N. Dahl, A. J. Engler, J. D. Pajerowski and D. E. Discher, *Biophysical journal*, 2005, **89**, 2855-2864.
45. P. N. Yaron, B. D. Holt, P. A. Short, M. Losche, M. F. Islam and K. N. Dahl, *Journal of nanobiotechnology*, 2011, **9**, 45.
46. M. Kollner and J. Wolfrum, *Chem Phys Lett*, 1992, **200**, 199-204.
47. G. Yang, L. A. Cameron, P. S. Maddox, E. D. Salmon and G. Danuser, *The Journal of cell biology*, 2008, **182**, 631-639.
48. E. A. Booth-Gauthier, T. A. Alcoser, G. Yang and K. N. Dahl, *Biophysical journal*, 2012, **103**, 2423-2431.
49. G. Yang, A. Matov and D. Danuser, IEEE Computer Society Conference on Computer Vision and Pattern Recognition (CVPR'05), San Diego, CA, 2005.
50. Y. C. Poh, S. P. Shevtsov, F. Chowdhury, D. C. Wu, S. Na, M. Dundr and N. Wang, *Nature communications*, 2012, **3**.
51. G. Guigas and M. Weiss, *Biophysical journal*, 2008, **94**, 90-94.
52. O. Ram, A. Goren, I. Amit, N. Shoresh, N. Yosef, J. Ernst, M. Kellis, M. Gymrek, R. Issner, M. Coyne, T. Durham, X. L. Zhang, J. Donaghey, C. B. Epstein, A. Regev and B. E. Bernstein, *Cell*, 2011, **147**, 1628-1639.
53. Y. Cui and C. Bustamante, *Proceedings of the National Academy of Sciences of the United States of America*, 2000, **97**, 127-132.
54. C. Gong, K. V. Stoletov and B. I. Terman, *Angiogenesis*, 2004, **7**, 313-321.
55. T. J. Chancellor, J. Lee, C. K. Thodeti and T. Lele, *Biophysical journal*, 2010, **99**, 115-123.
56. S. B. Khatau, C. M. Hale, P. J. Stewart-Hutchinson, M. S. Patel, C. L. Stewart, P. C. Searson, D. Hodzic and D. Wirtz, *Proceedings of the National Academy of Sciences of the United States of America*, 2009, **106**, 19017-19022.
57. S. B. Khatau, S. Kusuma, D. Hanjaya-Putra, P. Mali, L. Cheng, J. S. Lee, S. Gerecht and D. Wirtz, *PloS one*, 2012, **7**, e36689.
58. J. T. Morgan, E. R. Pfeiffer, T. L. Thirkill, P. Kumar, G. Peng, H. N. Fridolfsson, G. C. Douglas, D. A. Starr and A. I. Barakat, *Molecular biology of the cell*, 2011, **22**, 4324-4334.

59. F. Miralles, G. Posern, A. I. Zaromytidou and R. Treisman, *Cell*, 2003, **113**, 329-342.
60. M. K. Vartiainen, S. Guettler, B. Larijani and R. Treisman, *Science*, 2007, **316**, 1749-1752.
61. T. Jamali, Y. Jamali, M. Mehrbod and M. R. Mofrad, *International review of cell and molecular biology*, 2011, **287**, 233-286.
62. V. Roukos, T. C. Voss, C. K. Schmidt, S. Lee, D. Wangsa and T. Misteli, *Science*, 2013, **341**, 660-664.
63. A. Zidovska, D. A. Weitz and T. J. Mitchison, *Proceedings of the National Academy of Sciences of the United States of America*, 2013, **110**, 15555-15560.

Chapter V

Nuclear Stiffening and Chromatin Softening with Progerin Expression Leads to an Attenuated Nuclear Response to Force

Introduction

Hutchinson-Gilford progeria syndrome (HGPS) is a premature aging disorder caused by a mutation in lamin A, a structural protein of the cell nucleus. The mutant lamin A, also called Δ50 lamin A or progerin, accumulates at the nuclear envelope[1] leading to downstream nuclear defects. These defects in nuclei of cells from patients with HGPS include abnormal morphology,[2] thickening of the nuclear lamina[1] and stiffening of the nucleus.[3] Additionally, these cells exhibit increased DNA damage[4] and altered chromatin modification patterns.[5] Specifically, heterochromatin appears to be decondensed in cells from patients with HGPS.[6] However, heterochromatin is a load-bearing element in nuclei[7] and, in some cases, dictates the stiffness of the entire nucleus.[8, 9] Thus, the precise nature of the nuclear stiffening from progerin within the context of the integrated nucleoskeleton and chromatin mechanical network is not well understood.

Systemically, effects of HGPS are most pronounced in structural and force-responsive tissues. These include endothelial cells exposed to shear stress[10] and skeletal tissues under compression[11] as well as many others. Shear stress is of particular interest for study in patients with progeria due to increased incidence of atherosclerosis[12] stemming from endothelial cell dysfunction and an improper

genetic response to shear stress.[13-15] However, it is unclear how a mutant protein expressed in most cells of the body has its most pronounced pathological effects primarily in force-responsive tissue types. Also, how nuclear stiffening could cause this progressive, segmented syndrome is currently unknown.

The role of physiological forces, including shear stress and compression, in stimulating changes in gene expression has been well established.[16-18] In addition to mechanotransduction in the cell membrane, focal adhesions and cytoskeleton, the nucleus acts as a mechanoresponsive element within the cell. Recent work suggests that direct mechanical force propagation from the cell into the nuclear interior alters nuclear structure and dynamics and may facilitate the underlying chemical signaling mechanisms.[19-22] Also, evidence of force-induced changes to chromatin condensation state[23] and enhanced force sensitivity in euchromatin relative to heterochromatin[19] provides plausible mechanisms for the role of mechanical force in chromatin reorganization.[24]

Here, we study the stiffness of nuclei using the traditional mechanical measurement technique micropipette aspiration (MPA) and find that nuclei of cells exogenously expressing progerin are stiffer than control counterparts, similar to cells from patients with HGPS. However, in measuring the compliance of the chromatin within the nucleus, we find that the chromatin is softer inside cells expressing progerin. Thus, the composite structure of the nucleus shows a stiffened nucleoskeleton, but softer chromatin interior with the expression of progerin. Further, we show that forces, from both the cytoskeletal molecular motors and from external stresses imposed on the cell, have a reduced effect on

chromatin movements in cells expressing progerin. This suggests that progerin expression in HGPS alters the mechanical connections of the cell, and may explain altered cell function and gene expression in the mechanical tissues of patients.

Materials and Methods

Cell Culture and Transfection

Human cervical cancer cells (HeLa, ATCC, Manassas, VA) and human osteosarcoma cells (Saos2, ATCC, Manassas, VA) were cultured using Dulbecco's modified Eagle's medium (DMEM, Thermo Scientific, Rockford, IL) with 10% fetal bovine serum (Life Technologies, Grand Island, NY) and 1% penicillin-streptomycin (Life Technologies, Grand Island, NY). Human umbilical vein endothelial cells (HUVECs, ATCC, Manassas, VA) were cultured using endothelial base media with growth supplements (Lonza, Hopkinton, MA). Fibroblasts were generously donated from the Progeria Research Foundation (Peabody, MA) and were cultured in DMEM with high glucose, 15% fetal bovine serum, 1% L-glutamine and 1% penicillin-streptomycin (Invitrogen, Carlsbad, CA). Two cells lines from the Progeria research foundation were used: an HGPS cell line (HGADFN167, referred to as HGPS) with the mutation CT608 in exon 11, and an adult control (HGADFN168, referred to as control) from a 40-year-old parent, negative for the point mutation.

Cells were transfected with recombinant DNA of fluorescent tagged upstream binding factor one (UBF1-GFP) or fibrillarin (Fib-GFP, a kind gift from

D. Discher, University of Pennsylvania). HeLa cells were transfected with Polyfect (Quiagen, Valencia, CA) per manufacturer's recommendations, media was changed, and cells were incubated an additional 24 hours before imaging. Saos2 cells and HUVECs were transfected with Lipofectin (Life Technologies, Grand Island, NY) and media was changed after 5-8hrs of transfection. All cells experienced 48 hrs of incubation post-transfection prior to imaging.

Micropipette Aspiration

MPA experiments were performed on wild type cells and cells expressing GFP-UBF1 and DsRed-progerin. Micropipettes were pulled from 1 mm glass capillaries using a PMP102 Micropipette puller (Microdata). The ends of the micropipette tips were between 3 and 10 μm in diameter. Cells were trypsized and resuspended in a PBS solution with 3 μM of cytoclasin D (Sigma-Aldrich), 0.125 μM of Nocodazole (Sigma-Aldrich) and 0.17 μg/mL of Hoescht 33342 to label the nuclei (Invitrogen). Nocodazole inhibits polymerization of microtubules and cytochalasin D inhibits actin polymerization. A micromanipulator (Narishige) was used to approach the cells of interest. A pressure was then applied and the cells were aspirated into the pipette. Pressure was applied through a syringe and passes from air to a water reservoir that runs parallel to a pressure transducer (Validyne) and the pipette that is in contact with the cell of interest. Any change in pressure was given time to equilibrate at which time an image was captured, then the pressure was increased and the process repeated. The effective whole nuclear

stiffness (E_{eff}) was computed from the micropipette radius (R_p), the change in pressure (ΔP), and the length of the cell up the pipette (L_P).

$$\Delta P \propto E_{eff} \frac{L_P}{R_P} \quad (1)$$

Shear and Compressive Force

For shear experiments, transfected cells were passed into a micro-slide VI flow chamber (ibidi, Verona, WI) 24 hours prior to a shear exposure. The shear stress was applied from a peristaltic pump (Instech, Plymouth Meeting, MA) through two media reservoirs to buffer the flow and then through the ibidi micro-slide. Media was pre-equilibrated to 37^{o}C and 5% CO_2 for a minimum of 30 minutes, and the entire flow apparatus was housed inside a Pecon live-cell imaging chamber on the microscope. Nuclei were labeled with 1 μg/mL Hoechst 33342 (Life Technologies, Grand Island, NY) and incubated for a minimum of 30 minutes. Images of cells were captured at multiple sites per experiment using an automated stage every 3 minutes. Cell viability was confirmed by continued imaging for over an hour after the completion of data collection. Shear stress of 20 dyn/cm^2 was used for all shear experiments.

During compression experiments, transfected cells were seeded into 35 mm MatTek dishes. The compressive force was applied by a 100 g weight set on top of a glass coverslip above the cells, leading to a total force of 1.0 N. Nuclei were labeled with 1 μg/mL Hoescht 33342 (Life Technologies, Grand Island, NY) and with 0.3 μg/ml propidium iodide (Life Technologies, Grand Island, NY) to indicate cell death and incubated for a minimum of 30 minutes prior to starting

the experiments. Images were acquired every 2 minutes, and cell viability was confirmed by propidium iodide staining and continued imaging for over an hour after the completion of data collection.

Cells were imaged on an inverted microscope (DMI6000, Leica, Buffalo Grove, IL) using a 63x (1.4 NA) oil immersion objective. During imaging the entire microscope environment was regulated by a Pecon live-cell imaging chamber heated to 37ºC (Pecon, Erbach, Germany). Cells were viable beyond 2 hours, the duration of the experiment. The time steps used in these experiments were determined in order to account for phototoxity and photobleaching over the course of the experiments.

Data Analysis

Data analysis was done as consistent with previous studies.[24-26] Particle tracking image analysis was done with custom Laptrack71 suite of programs designed in Matlab (Natick, Ma).[27] Images were initially aligned to remove noise caused by cellular drift, translocation, and rotation. The images were then statistically segmented to select for bright spots and the spot information was restructured into particle tracks. Mean squared displacement (MSD) was calculated for the first hour of data taken (Equation 2) where t is time, τ is the time lag, and x and y are the position coordinates at the given times. Between 5 and 15 different nuclei from 2-3 independent experiments were analyzed for each data set with when calculating MSD.

$$MSD = \langle (x_{t+\tau} - x_t)^2 + (y_{t+\tau} - y_t)^2 \rangle \quad (2)$$

$$MSD = D_{eff}\tau^{\beta} \quad (3)$$

The chromatin dynamics measured by MSD exhibit power-law time dependence (Equation 3). Further characterization of the nature of these dynamics comes from the fitting parameters. Here, D_{eff} is a measure of the effective compliance of the intranuclear chromatin network, where chromatin decondensation enhances the effective compliance and *vice versa* increasing the amplitudes of the motion within the nucleus.[24] By contrast, β indicates the level of system forces driving these dynamics including motor proteins that enhance motion beyond thermal energy and external force application.[24]

Results

Exogenous Progerin Expression Stiffens Nuclei

Previously, nuclei isolated from HGPS patient fibroblasts were shown to be stiffer than control nuclei.[3] To test if the exogenous expression of progerin has the same nuclear stiffening effect, we investigated the effect of DsRed-progerin expression in HeLa cells using the same technique: micropipette aspiration (MPA). The effect of exogenous UBF1-GFP (used in subsequent experiments) was monitored by co-transfection. Most human nuclei deform viscoelastically.[28] However, our results demonstrate that HeLa nuclei deform elastically under MPA-imposed forces on short time scales (on the order of seconds) with

increasing pressure causing increased deformation into the micropipette, as observed previously in HeLa cells.[29]

Control HeLa cells displayed an effective whole nuclear stiffness of ~4 kPa (Figure 5.1). In contrast, progerin expression resulted in an effective whole nuclear stiffness of more than double that of control cells of ~9 kPa**.** This suggests that the overexpression of progerin is sufficient to significantly stiffen the nucleus, as seen in patient cells.[3]

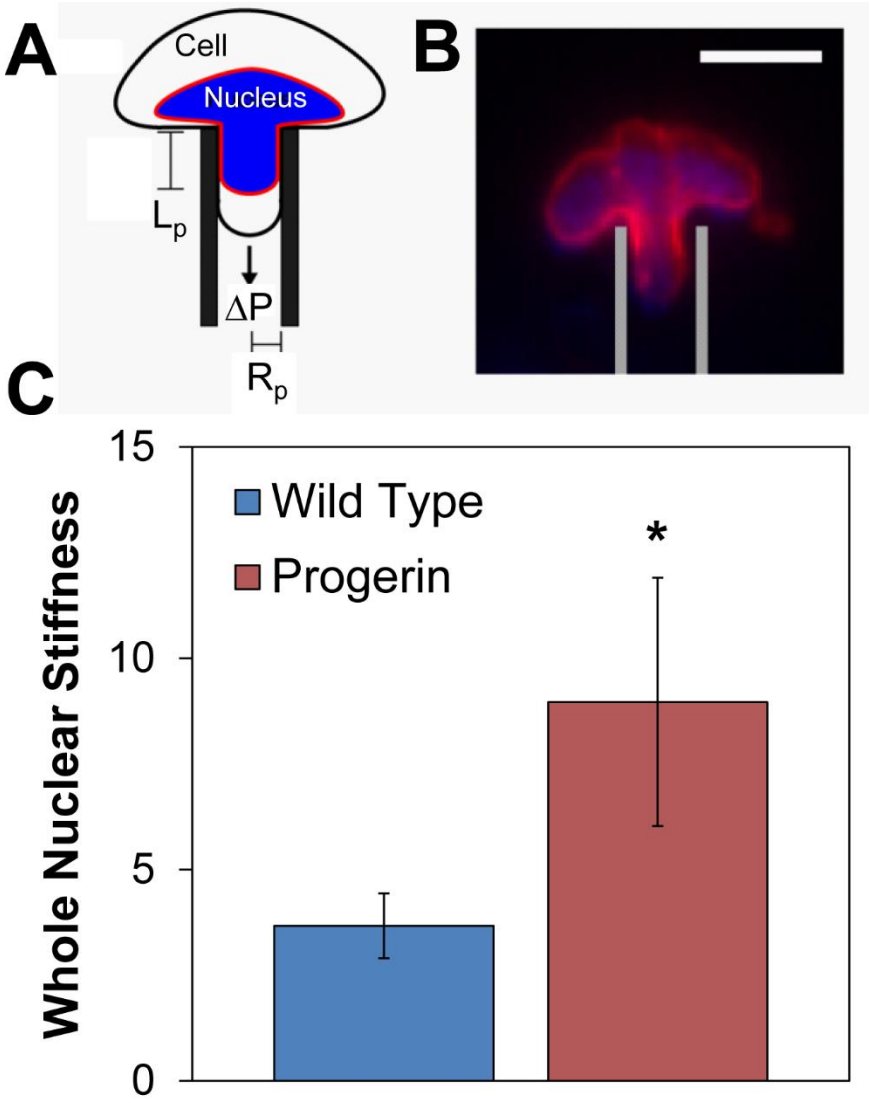

Figure 5.1: Exogenous progerin expression stiffens nuclei. *(A) Schematic of micropipette aspiration (MPA) of the nucleus within a cell. (B) MPA was performed on whole HeLa cells with depolymerized cytoskeleton and nuclei labeled with Hoechst 33342. An example aspirated nuclei expressing DsRed-progerin. Scale bar is 10 µm. (C) With increasing pressure, nuclear deformation was determined from nuclear stretch into the micropipette. DsRed-progerin-expressing cells are approximately 2.4 times stiffer than the other control cell populations. n>6 for all measurements. Error bars are mean squared error (SEM) *p<0.05.*

Progerin Expression Reduces Chromatin Condensation and Softens the Nuclear Interior

The stiffness of the nucleus is governed both by the stiffness of the lamina nucleoskeleton as well as the chromatin interior. Since progerin accumulates at the nuclear envelope,[1] we next sought to examine how progerin expression affects the chromatin dynamics and mechanics of the nuclear interior. To do this we expressed chromatin-bound, GFP-tagged probes (UBF1-GFP or Fib-GFP, having previously shown chromatin dynamics to be probe independent for several probes on these time scales[24, 26]) and tracked the movements in live cells (see Chapter III). With image processing to remove cellular movements, we were able to calculate the intranuclear dynamics of chromatin (mean squared displacement or MSD) in fibroblasts from patients with HGPS (Figure 5.2), as well as in the nuclei of cells expressing exogenous DsRed-progerin (Figure 5.3). MSD versus lag time values were then fit to the subdiffusion (Equation 3) to determine quantifiable

parameters for chromatin compliance (D_{eff}) and system forces driving chromatin movement (β).

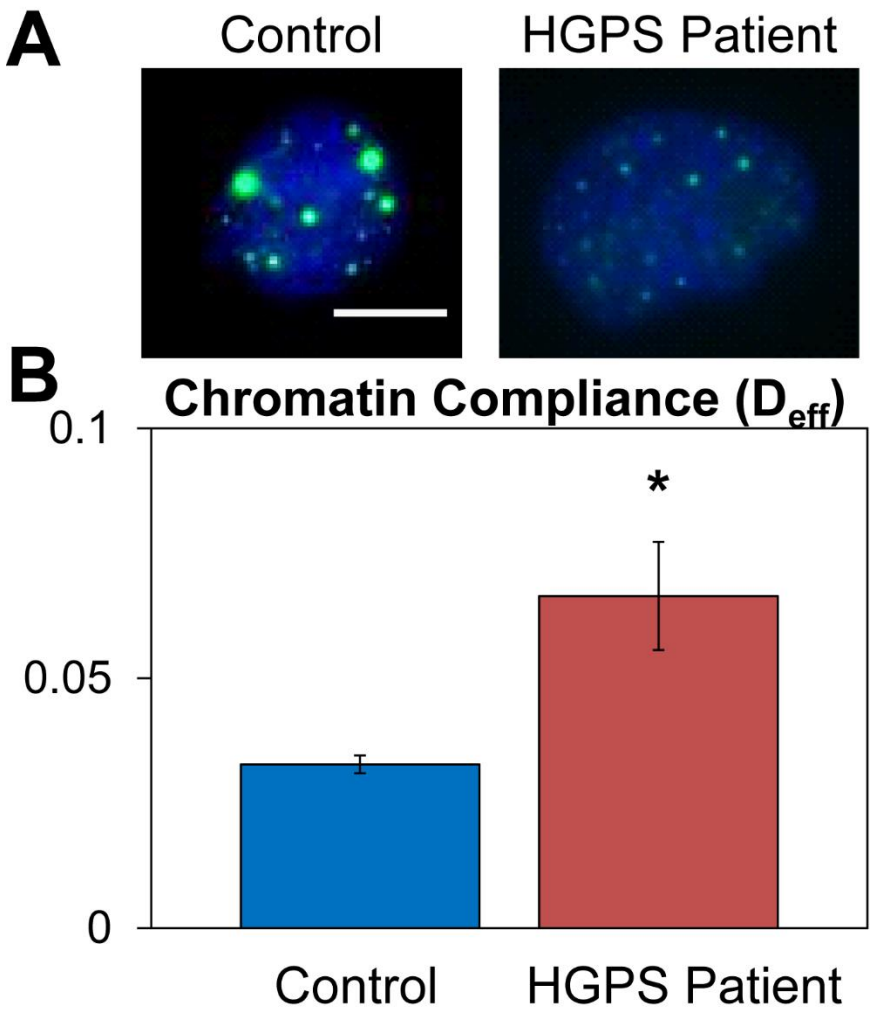

Figure 5.2: HGPS patient cells show enhanced chromatin compliance.

Punctate regions of GFP-tagged proteins used for particle tracking with Hoechst 33342-stained DNA in control patient (left) and HGPS patient (right) cells (A). Chromatin compliance is measured from the particle tracking experiments which is inversely proportional to chromatin condensation (B). HGPS patient cells have increased chromatin compliance relative to patient control cells ($p<0.05$)

indicating reduced chromatin condensation in HGPS patients. Error bars reflect 95% confidence intervals.

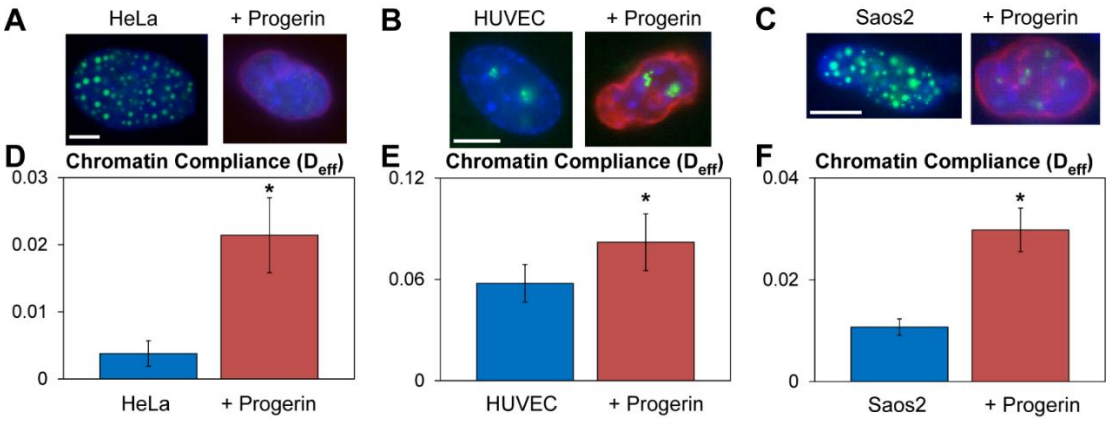

Figure 5.3: Exogenous expression of DsRed-Progerin enhances chromatin compliance in cells. *Punctate regions of GFP-tagged proteins used for particle tracking with Hoechst 33342-stained DNA in (A) HeLa cells (left) and HeLa cells transfected with DsRed-Progerin (right) cells, (B) HUVECs (left) and HUVECs transfected with DsRed-Progerin (right) cells as well as (C) Saos2 cells (left) and Saos2 cells transfected with DsRed-Progerin (right) cells. Exogenous progerin expression increased chromatin compliance in (D) HeLa cells, (E) HUVECs and (F) Saos2 cells relative to controls ($p<0.05$) indicating reduced chromatin condensation. Error bars reflect 95% confidence intervals.*

In cells from patients with HGPS, chromatin compliance was significantly increased compared with matched controls (Figure 5.2B). Exogenous expression of DsRed-progerin resulted in increased chromatin compliance for HeLa cells (Figure 5.3D), HUVECs (Figure 5.3E) and Saos2 cells (Figure 5.3F). Thus, our

results suggest progerin expression consistently causes increased compliance of the nuclear interior due to reduced chromatin condensation as measured by D_{eff}. Further, these results indicate that the stiffening of the nucleus in progerin-expressing cells is associated with a stiffened nucleoskeleton, while the nuclear interior becomes more compliant.

Progerin Expression Reduces Propagation of Cytoskeletal Forces to the Nuclear Interior

Also available from fitting the chromatin dynamics and calculating the MSD versus lag time is the role of system forces providing the driving force for chromatin dynamics (see Chapter III). In cells at rest these enhanced system forces beyond thermal motion are derived from molecular motors, primarily the cytoskeletal molecular motors myosin II, propagated to the nuclear interior that augment movements of the chromatin as well as mechanically communicating force from the cell to the nuclear interior [19, 24]. HGPS patient cells and exogenous progerin-expressing cells all showed a reduction in system forces, most of which were strongly significant (Figure 5.4). Thus, the stiffening of the nucleoskeleton associated with progerin-expression seemingly damps force propagation into the nuclear interior from the cytoskeleton.

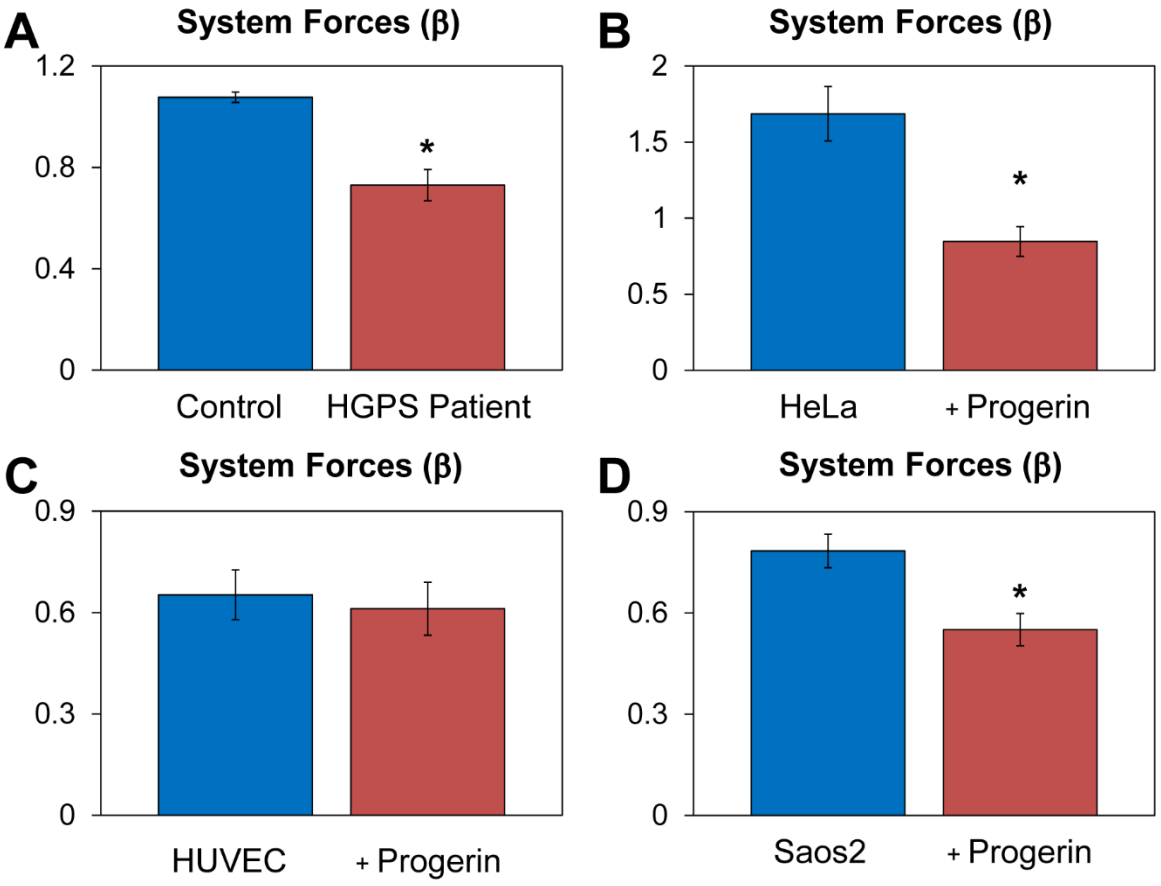

Figure 5.4: Progerin expression reduces cytoskeletal force propagation to the nuclear interior. *System forces as measured from the particle tracking experiments indicate the level of cytoskeletal forces and external forces propagated to the nuclear interior. Progerin expression in patient cells (A) as well as exogenous expression in HeLa cells (B), HUVECs (C) and Saos2 cells (D) results in reduced system forces from reduced force propagation to the nuclear interior. Error bars reflect 95% confidence intervals. *p<0.05.*

Progerin Expression also Reduces the Intranuclear Response to Extracellular Applied Force

HGPS pathology is most pronounced in mechanically active tissues where the progerin-induced dysfunction results in aberrant mechanosensing. As such, we aimed to investigate progerin-expressing cells under physiologically relevant force. Since progerin-expressing cells are less able to transduce force from the cytoskeleton to the nuclear interior, we were interested in how this affects the intranuclear response to external force. We tracked motion of chromatin in live cells under stress using fluid shear stress on endothelial cells (HUVEC) and compression on bone cells (Saos2). As expected, application of stress to control cells resulted in an increased in system forces driving enhanced chromatin movement compared to the stress-free cells (Figure 5.5C-D). In this case, the increased force propagation to the nuclear interior is derived from the applied stress. Application of stress also reduced chromatin compliance (Figure 5.5A-B). We suggest that this change occurs from nuclear compression and reduced nuclear volume [23] resulting from both applied shear and applied compression leading to chromatin condensation.

In progerin-expressing cells exposed to the same stresses, we observed an attenuated response. We again observed a decrease in chromatin compliance with applied stress (Figure 5.5A-B), but the progerin-expressing HUVEC cells were less responsive than control cells. More dramatically, the progerin-expressing HUVECs showed no statistical change in system forces with shear stress application (Figure 5.5C). This suggests these extracellular applied forces are not significantly transduced to the nuclear interior with exogenous progerin

expression. Progerin-expressing Saos2 cells under compression also showed a mild response with stress application that fails to recapitulate the system forces in control cells, indicating a similarly muted force transduction response. These results suggest that progerin expression results in an attenuated intranuclear mechanical response to external force likely due at least in part to nucleoskeletal stiffening.

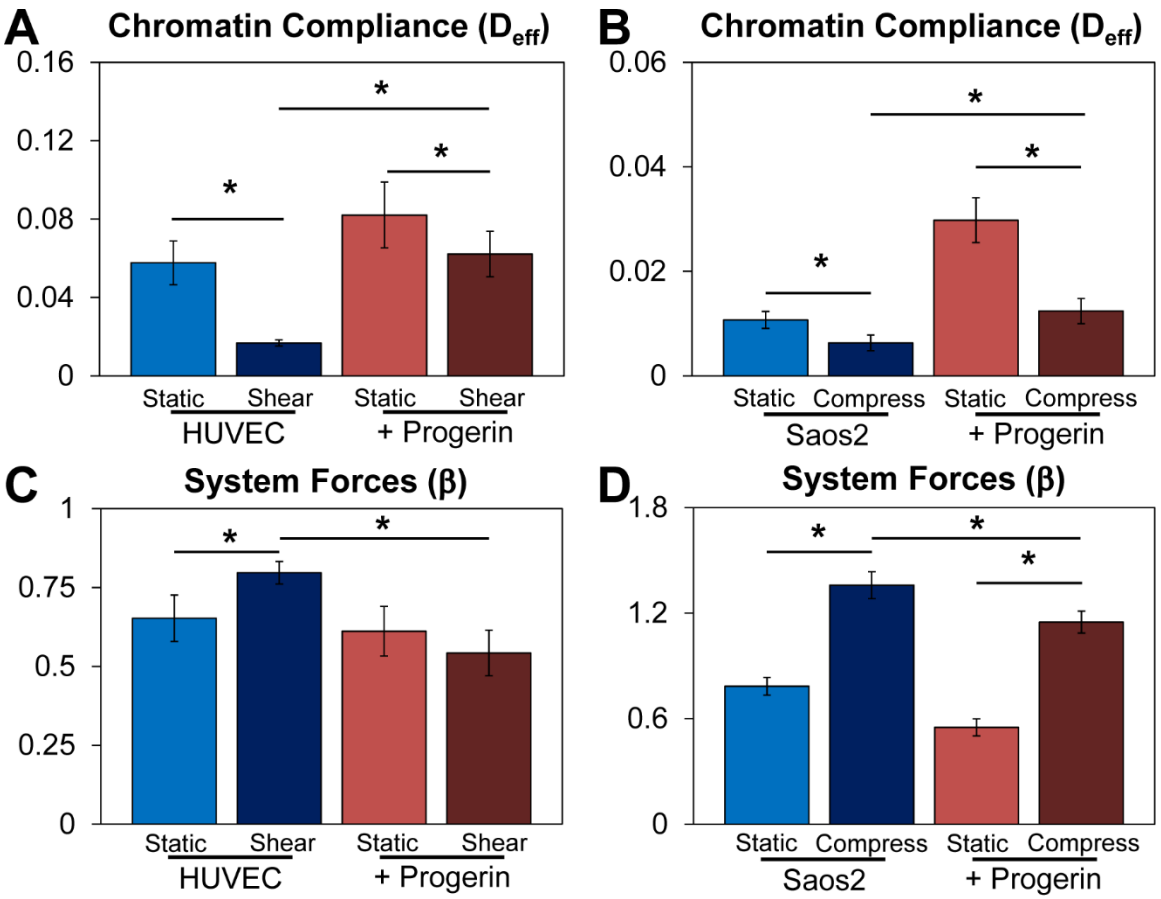

Figure 5.5: Progerin expression reduces intranuclear mechanical sensitivity to external force application. *External force application from 20 dyn/cm^2 shear stress to HUVECs or 1 N compression to Saos2 cells results in reduced chromatin*

*compliance (A and B, respectively) while increasing system forces propagated to the nuclear interior (C and D, respectively) in control cells. By contrast, while progerin-expressing cells experienced reduced chromatin compliance upon external force application relative to static progerin-expresssing cells, it fails to recapitulate the chromatin condensation state of control cells under shear (A) or compression (B). Further, progerin-expressing HUVECs under shear experience no increase in system forces relative to static progerin-expressing cells (C) while progerin-expressing Saos2 cells under compression do not experience the same degree of system forces propagated to the nuclear interior as control cells under compression (D). Error bars reflect 95% confidence intervals. *p<0.05.*

Discussion

Previously, nuclear stiffening has been observed in HGPS patient fibroblasts.[3, 30] Here, we show that exogenous progerin expression also causes stiffening of the whole nucleus, as measured by MPA. While progerin expression stiffens the nucleus when measured as a whole structure, particle tracking experiments of chromatin bound probes indicate the nuclear interior softens as a result of progerin expression in both patient cells and exogenously expressing cells. Thus, nucleoskeletal stiffening seems to be the predominant contributor to the increased nuclear stiffness observed in progerin-expressing cells. We suggest that this is consistent with the preferential localization of progerin to the nuclear envelope resulting from farnesyl tail association with the membrane,[3] whereas wild type lamin A can exchange between the nucleoplasm and the lamina.[3, 31]

Progerin expression has previously been shown to reduce chromatin condensation and alter the epigenetics of specific territories.[6] Progerin-induced dysregulation of genome organization includes altered chromatin tethering at the nuclear periphery,[32] the mislocalization of telomeres and the clustering of centromeres.[12] We similarly find an overall reduction in chromatin condensation associated with progerin expression, and our work highlights the impact on chromatin dynamics that may further impact this dysregulation. Analysis of our chromatin dynamics data suggests that the enhanced chromatin compliance we observe with progerin expression is a manifestation of the loss of higher order chromatin organization. This likely results in a loss of genome function, where aberrant transcriptional activity[33] and increased incidence of DNA damage and compromised repair are associated with progerin expression.[34-36] Enhanced chromatin compliance is of particular concern with DNA damage, where increased chromatin dynamics may be implicated in translocation frequency.[37, 38] Given HGPS patient cells exhibit elevated levels of reactive oxygen species (ROS) causing increased DNA damage,[36] further genomic instability imparted by increased chromatin dynamics may act to compound the problem.

HGPS patients experience dysfunction associated with mechanoresponsive tissues including bone degradation and cardiovascular complications, with heart attacks and strokes being the most common fatalities. Previous studies have shown that progerin-expressing cells are more mechanosensitive and prone to apoptosis in response to mechanical stress.[30] Our results provide some mechanistic details suggesting why mechanosensitive tissues show altered gene

expression patterns. Specifically, we find the nuclear interior of progerin expressing cells to have a reduced response to forces, either from the cell's own molecular motors or from extracellular applied force. In the most dramatic example, we observe no change in force propagation to the chromatin in progerin-expressing HUVECs under shear whereas control cells showed shear stress related changes.[26] Thus, it seems progerin expression reduces the natural mechanical force propagation to the nuclear interior that is necessary for the normal mechanical response.

In normal individuals, a number of genes expressed in endothelial cells and smooth muscle cells under shear stress are thought to confer an "atheroprotective" phenotype inhibiting atherosclerosis.[39] The attenuated intranuclear response to force (as evidenced in the muted chromatin dynamics) in progerin-expressing cells resulting from progerin accumulation may play a role by inhibiting the mechanical signaling required for chromatin reorganization and expression. To this end, recent work has highlighted the role of direct mechanical force transduction in mediating biochemical signaling cascades through force-induced chromatin decondensation and increased fluctuations.[19, 24] Further, nuclear transport of some transcription factors has been shown to depend on the presence of intact cytoskeletal-nuclear mechanical structures, with transport coinciding with cytoskeletal reorganization and chromatin remodeling.[19] Thus, it seems likely that the attenuated genetic response of progerin-expressing cells to mechanical stimulus may follow directly from the reduced force transduction into

the nuclear interior,[40] which we show definitively contributes to reduced chromatin dynamics relative to control cells.

The increased stiffness of the nucleoskeleton is the most obvious rationale for the reduced force transduction in progerin-expressing cells. We suggest that the presence of a disproportionately stiffer nucleoskeleton would damp forces transmitted from outside the nucleus. However, progerin expression also alters nucleoskeletal connections to the LINC complex, [41] which would further limit force transduction. We have also shown recently that HGPS patient cells have reduced traction force generation[42] and other studies indicate decreased cytoskeletal stiffness,[43, 44] both of which likely contribute to the loss of cell polarity observed and the reduced ability to align in the flow direction under shear. These hallmarks of the disease – reduced cytoskeletal force generation, loss of proper LINC connections and a stiffened nucleoskeleton – likely result in the reduced system forces driving chromatin dynamics in progerin-expressing cells even under static conditions where less cytoskeletal force is transmitted to the nuclear interior. More broadly, our findings suggest a complete collapse of mechanical integrity in progerin-expressing cells. These results highlight that the nucleus and cytoskeleton operate as a wholly-integrated mechanical network that operates bi-directionally to facilitate nuclear structure and genome function on one side and to balance force generation for adhesion and motility on the other. As such, dysfunction in a single component results in loss of proper chromatin organization and dynamics as well as nucleoskeletal and cytoskeletal mechanical integrity. Thus, HGPS provides a model system that demonstrates a necessary

role for mechanical mechanisms as regulators of genome function and stability, the absence of which provides insight into the pathologies of cardiovascular disease and DNA damage.

Acknowledgements

We gratefully acknowledge Elizabeth A. Booth for design and implementation of experiments for our analysis. Additional thanks to Ge Yang (Carnegie Mellon Biomedical Engineering, Lane Center for Computational Biology and Biological Sciences) and Minhua Qui (Carnegie Mellon Biomedical Engineering) for development and assistance with the LAPtrack71 suite of particle tracking programs. This work is supported by the NSF (CBET-0954421 and CMMI-1300476 to KND) and the ARCS Foundation (STS), Bertucci Fellowship (STS) and James C. Meade Fellowship (STS).

References

1. R. D. Goldman, D. K. Shumaker, M. R. Erdos, M. Eriksson, A. E. Goldman, L. B. Gordon, Y. Gruenbaum, S. Khuon, M. Mendez, R. Varga and F. S. Collins, *Proc Natl Acad Sci U S A*, 2004, **101**, 8963-8968.
2. P. Scaffidi and T. Misteli, *Science*, 2006, **312**, 1059-1063.
3. K. N. Dahl, P. Scaffidi, M. F. Islam, A. G. Yodh, K. L. Wilson and T. Misteli, *Proceedings of the National Academy of Sciences of the United States of America*, 2006, **103**, 10271-10276.
4. B. Liu, J. Wang, K. M. Chan, W. M. Tjia, W. Deng, X. Guan, J. D. Huang, K. M. Li, P. Y. Chau, D. J. Chen, D. Pei, A. M. Pendas, J. Cadinanos, C. Lopez-Otin, H. F. Tse, C. Hutchison, J. Chen, Y. Cao, K. S. Cheah, K. Tryggvason and Z. Zhou, *Nat Med*, 2005, **11**, 780-785.
5. Y. Gruenbaum, A. Margalit, R. D. Goldman, D. K. Shumaker and K. L. Wilson, *Nat Rev Mol Cell Biol*, 2005, **6**, 21-31.
6. D. K. Shumaker, T. Dechat, A. Kohlmaier, S. A. Adam, M. R. Bozovsky, M. R. Erdos, M. Eriksson, A. E. Goldman, S. Khuon, F. S. Collins, T. Jenuwein and R. D. Goldman, *Proceedings of the National Academy of Sciences of the United States of America*, 2006, **103**, 8703-8708.

7. A. Mazumder and G. V. Shivashankar, *Journal of the Royal Society, Interface / the Royal Society*, 2010, **7 Suppl 3**, S321-330.
8. K. N. Dahl, A. J. Engler, J. D. Pajerowski and D. E. Discher, *Biophysical journal*, 2005, **89**, 2855-2864.
9. A. Mazumder and G. V. Shivashankar, *Biophysical journal*, 2007, **93**, 2209-2216.
10. D. McClintock, L. B. Gordon and K. Djabali, *Proc Natl Acad Sci U S A*, 2006, **103**, 2154-2159.
11. C. Sanchez, L. Pesesse, O. Gabay, J. P. Delcour, P. Msika, C. Baudouin and Y. E. Henrotin, *Arthritis Rheum*, 2011, **64**, 1193-1203.
12. P. Taimen, K. Pfleghaar, T. Shimi, D. Moller, K. Ben-Harush, M. R. Erdos, S. A. Adam, H. Herrmann, O. Medalia, F. S. Collins, A. E. Goldman and R. D. Goldman, *Proc Natl Acad Sci U S A*, 2009.
13. R. M. Nerem, *J Biomech Eng*, 1992, **114**, 274-282.
14. O. Traub and B. C. Berk, *Arterioscler Thromb Vasc Biol*, 1998, **18**, 677-685.
15. K. M. Eyster, S. E. Appt, C. J. Mark-Kappeler, A. Chalpe, T. C. Register and T. B. Clarkson, *Menopause*, 2011, **18**, 1087-1095.
16. A. R. Brooks, P. I. Lelkes and G. M. Rubanyi, *Physiological genomics*, 2002, **9**, 27-41.
17. A. R. Brooks, P. I. Lelkes and G. M. Rubanyi, *Endothelium-J Endoth*, 2004, **11**, 45-57.
18. A. C. Shieh and K. A. Athanasiou, *Osteoarthr Cartilage*, 2007, **15**, 328-334.
19. K. V. Iyer, S. Pulford, A. Mogilner and G. V. Shivashankar, *Biophysical journal*, 2012, **103**, 1416-1428.
20. D. N. Simon and K. L. Wilson, *Nat Rev Mol Cell Bio*, 2011, **12**, 695-708.
21. N. Wang, J. D. Tytell and D. E. Ingber, *Nat Rev Mol Cell Bio*, 2009, **10**, 75-82.
22. A. J. Maniotis, C. S. Chen and D. E. Ingber, *Proceedings of the National Academy of Sciences of the United States of America*, 1997, **94**, 849-854.
23. M. Versaevel, T. Grevesse and S. Gabriele, *Nature communications*, 2012, **3**, 671.
24. S. T. Spagnol and K. N. Dahl, *Integr Biol-Uk*, 2014, **6**, 523-531.
25. G. Yang, L. A. Cameron, P. S. Maddox, E. D. Salmon and G. Danuser, *Journal of Cell Biology*, 2008, **182**, 631-639.
26. E. A. Booth-Gauthier, T. A. Alcoser, G. Yang and K. N. Dahl, *Biophysical journal*, 2012, **103**, 2423-2431.
27. G. Yang, A. Matov and G. Danuser, *IEEE Computer Society Conference on Computer Vision and Pattern Recognition (CVPR'05)*, 2005.
28. K. N. Dahl, S. M. Kahn, K. L. Wilson and D. E. Discher, *J Cell Sci*, 2004, **117**, 4779-4786.
29. A. C. Rowat, L. J. Foster, M. M. Nielsen, M. Weiss and J. H. Ipsen, *J R Soc Interface*, 2005, **2**, 63-69.
30. V. L. R. M. Verstraeten, J. Y. Ji, K. S. Cummings, R. T. Lee and J. Lammerding, *Aging Cell*, 2008, **7**, 383-393.

31. J. L. Broers, B. M. Machiels, G. J. van Eys, H. J. Kuijpers, E. M. Manders, R. van Driel and F. C. Ramaekers, *Journal of cell science*, 1999, **112 (Pt 20)**, 3463-3475.
32. N. Kubben, M. Adriaens, W. Meuleman, J. W. Voncken, B. van Steensel and T. Misteli, *Chromosoma*, 2012, **121**, 447-464.
33. M. Columbaro, C. Capanni, E. Mattioli, G. Novelli, V. K. Parnaik, S. Squarzoni, N. M. Maraldi and G. Lattanzi, *Cellular and Molecular Life Sciences*, 2005, **62**, 2669-2678.
34. P. Scaffidi and T. Misteli, *Nature cell biology*, 2008, **10**, 452-U167.
35. E. K. Benson, S. W. Lee and S. A. Aaronson, *Journal of cell science*, 2010, **123**, 2605-2612.
36. S. A. Richards, J. Muter, P. Ritchie, G. Lattanzi and C. J. Hutchison, *Human molecular genetics*, 2011, **20**, 3997-4004.
37. V. Roukos, T. C. Voss, C. K. Schmidt, S. Lee, D. Wangsa and T. Misteli, *Science*, 2013, **341**, 660-664.
38. V. Dion and S. M. Gasser, *Cell*, 2013, **152**, 1355-1364.
39. J. Zhou, Y. S. Li and S. Chien, *Arteriosclerosis, thrombosis, and vascular biology*, 2014, **34**, 2191-2198.
40. M. L. Lombardi and J. Lammerding, *Biochem Soc Trans*, 2011, **39**, 1729-1734.
41. F. Haque, D. Mazzeo, J. T. Patel, D. T. Smallwood, J. A. Ellis, C. M. Shanahan and S. Shackleton, *Journal of Biological Chemistry*, 2010, **285**, 3487-3498.
42. E. A. Booth-Gauthier, V. Du, M. Ghibaudo, A. D. Rape, K. N. Dahl and B. Ladoux, *Integr Biol-Uk*, 2013, **5**, 569-577.
43. C. M. Hale, A. L. Shrestha, S. B. Khatau, P. J. Stewart-Hutchinson, L. Hernandez, C. L. Stewart, D. Hodzic and D. Wirtz, *Biophys J*, 2008, **95**, 5462-5475.
44. C. Y. Ho, D. E. Jaalouk, M. K. Vartiainen and J. Lammerding, *Nature*, 2013, **497**, 507-+.

Chapter VI

Increased Chromatin Fluctuations are Localized to Regions of DNA Damage and Induced by Structural Relaxation

Introduction

The genome is continuously damaged within human cell nuclei in response to cellular processes and environmental agents including ionizing radiation. Fortunately, cells devote a large portion of energy and protein resources to DNA repair machinery making it a highly efficient process. Further, cells possess additional mechanisms that help guard against single point mutations in the linear sequence. Thus, of particular consequence are the incidents of DNA damage that give rise to double-strand breaks (DSBs), where the ligation of incorrect ends (termed translocations) pose a dire threat to genetic stability.[1] Evidence of the deleterious nature of translocations is seen in their recurring role in cancer pathogenesis, particularly in leukemias and lymphomas.[2, 3] The lethality of DSBs is also strategically leveraged for anticancer therapeutics. For instance, the goal of treating cancer cells with ionizing radiation is to induce DSBs and cause cell death. Although induction of DSBs is capable of eradicating tumor progression, off-target effects include death of noncancerous cells and potentially inducing new, secondary tumors. Thus, understanding DSB repair is critical to elucidating the pathways involved in the genesis and treatment of cancer.

Upon initiation of the DNA damage repair process by DSB formation, the defining step in the process is the locating and rejoining of complementary severed ends among multiple damage sites that commonly occur in response to DNA damaging agents.[1] As such, the mobility of severed ends appears to be critical to the repair process. In support of this, repair foci clustering (and with them DSBs) has been observed for some persistent DSBs.[4] Others have shown DSBs in condensed, heterochromatic chromatin may be differentially repaired from decondensed, transcriptionally active euchromatin, with heterochromatic DSBs undergoing an initial relocation to euchromatin regions for repair leading to unique kinetics.[5] Further, the correlation of translocation frequency with chromosome proximity[6] lends additional credence to the role of chromatin positioning, mobility and higher-order organization in DSB repair.

Despite this seemingly prominent role of mobility in DSB repair, the physical mechanisms driving chromatin dynamics at sites of DSBs remain to be the determined. Previous studies from our laboratory[7] and others[8, 9] have demonstrated that chromatin fluctuations undergo subdiffusive motion driven by molecular crowding, binding and obstruction as well as the viscoelasticity of the nuclear interior. Such dynamics curtail long range motion and enhance the probability of finding local binding partners over distant ones relative to normal Brownian diffusion.[10] Yet, a recent study observed that translocating arrays exhibit faster dynamics than typical DSBs.[11] Thus, chromatin dynamics of DSBs may directly influence translocation probabilities.[1] However, it seems unlikely that translocating pairs alone have unique mechanisms driving their dynamics

differentially from other DSBs (given that the deleterious consequences would seemingly inhibit that evolution) without stimulation of additional pathways, as is perhaps the case with difficult or persistent DSBs. This view is supported by studies demonstrating that DSBs do not have dramatic differences in their mobility relative to undamaged chromatin,[11-15] though this remains a point of contention with others observing conflicting results.[16-18] Part of this discrepancy may stem from the use of different techniques and time scales. These include tracking of photoactivated, fluorescently-tagged histones sampling on millisecond time scales[12, 14] versus sampling at intervals of minutes for the tracking of fluorescently-tagged transcriptional activators or repressors or fluorescently tagged repair machinery[11, 15, 16, 18, 19] as we do here. However, simple quantification of the extent of chromatin mobility following DSB induction is also limited by the fact that it gives no insight into the evolution of physiological states that may directly impact these movements through altering the associated physics – via either the amplitude or the time dependence of the dynamics – by remodeling the chromatin polymer network or changes to the underlying driving forces, respectively.[7]

Determining the nature and role of chromatin mobility following DSB induction is not likely to be obtained through biochemical means alone. Rather than merely quantifying the extent of movement, understanding the physical mechanisms (including the mechanical effects of DSB-induced chromatin remodeling on chromatin compliance and the role of molecular motor activity from that remodeling and other cellular processes)[1] can identify the effects of

specific biochemical factors in chromatin dynamics as they relate to translocation probabilities. This includes how the nucleus may organize DSB repair through regulation of these dynamics, as well as the extent to which the DNA damage response globally impacts chromatin dynamics versus the possibility that the nucleus may specifically modulate the dynamics DSB loci.[1] Additionally, a longstanding issue in understanding active chromatin remodeling complexes is the precise nature of its role in chromatin dynamics, particularly as it relates to the DNA repair processes where remodeling is extensive.

To this end, we investigate chromatin dynamics in live human cells in response to chemically-induced DNA damage using the genotoxic agent bleomycin. We track distinct markers within the chromatin of live human cell nuclei, including the telomeric protein TRF1 and the nucleolar protein fibrillarin for undamaged chromatin as well as the DSB marker 53BP1. We demonstrate that healthy human cells exhibit physical uniformity of ensemble chromatin dynamics. This physical uniformity is disrupted upon DNA damage induction at the DNA damage sites. While undamaged chromatin in bleomycin-treated cells shows no change in the characteristic behavior of its dynamics relative to controls, DSBs have demonstrably increased dynamics. This results from increased chromatin compliance that corresponds with large scale relaxation of chromatin structure at these damage sites, enhancing local chromatin dynamics in a time-independent manner. This chromatin relaxation coincides with a reduction in molecular motor activity (and, therefore, time-dependent mobility) experienced at these sites. The result is to curtail long range motion at longer time scales, while allowing for

enhanced local dynamics initially relative to undamaged chromatin. This directly impacts the probabilistic nature of the mobility as related to distal translocation partners.[10] Further, as part of collaboration with Professor L. Lan's Laboratory (University of Pittsburgh Medical Center – Hillman Cancer Center) we demonstrate distinct roles for the SSRP1 subunit of the FACT histone chaperone complex and the deacetylase SIRT6 in chromatin remodeling at the sites of DSB. These findings demonstrate that DNA damage may be a unique nuclear response that decouples DSB sites from undamaged chromatin dynamics. This would allow for mechanical isolation which may act to quarantine these sites in order to damp force propagation and effectively curtail long range mobility. This points directly to chromatin remodeling complexes as a means of relaxing chromatin to specifically tune the dynamics, which has implications for mobility-dependent translocation probabilities and highlights possible future chemotherapeutic targets associated with those functions.

Methods

Cell Culture, Transfection and Drug Treatments

The human osteosarcoma cell, U2OS, (kind gift from L. Lan, University of Pittsburgh Medical Center – Hillman Cancer Center) were cultured in DMEM low glucose media supplemented with 10% FBS and 1% penicillin-streptomycin (Life Technologies, Grand Island, NY). The cells were passaged to 35 mm μ-dishes with ibiTreat (ibidi, Verona, WI) and transfected with rDNA of GFP-Fib (kind gift from D. Discher, University of Pennsylvania), RFP-TRF1 (kind gift

constructed by P. Opresko and S. Watkins, University of Pittsburgh) and/or GFP-53BP1 (kind gift from L. Lan, University of Pittsburgh Medical Center – Hillman Cancer Center) to visualize chromatin dynamics of various sites (see Figures 6.1-6.3). Cells were transfected using Lipofectamine 3000 transfection reagent (Life Technologies, Grand Island, NY) in Opti-MEM I Reduced Serum Medium (Life Technologies, Grand Island, NY). Cells were washed with PBS and media was changed ~24 hours after incubation, and experiments were run 24-72 hours post-transfection initiation to allow for adequate expression levels. For bleomycin DNA damage experiments, cells were treated with 5 ng/mL for 2 hours, at which time cells were washed with PBS and media was changed. The human cervical adenocarcinoma cancer cell line, HeLa, and mouse embryonic fibroblast cell line (MEFs) were cultured, treated and stained by L. Lan's laboratory (University of Pittsburgh Medical Center – Hillman Cancer Center) and provided for fluorescence lifetime imaging microscopy (FLIM) experiments after fixation and staining (see below).

Photoactivation of TRF1-KR in MEF cells was done using established cell lines as described in previously published methods, verifying DSB formation and initiation of the repair process.[20] Briefly, KR photoactivation for bulk cells was done using a 15-W SYLVANIA cool white fluorescent bulb for 10 minutes of exposure in a stage UVP (Uvland, CA, USA). This yielded a rate of 15 J/m^2/s, which, for 10 minutes of exposure, resulted in 9000 J being delivered to the whole dish and a final power of ~9 mJ/μm^2 delivered to the KR (~1 μm^2) upon light

exposure. Accumulation of γH2AX or 53BP1 foci at sites of KR were observed to verify DSB formation (see Figures 6.11 and 6.12).

Particle Tracking Imaging and Analysis

Imaging for particle tracking experiments was done using a 63x (1.4 NA) oil immersion objective of an inverted microscope (DMI6000, Leica, Buffalo Grove, IL) in a controlled live-cell imaging chamber with humidified 5% CO_2 and held at 37°C. Cell nuclei were labeled with 0.5 μg/mL Hoechst 33342 (Life Technologies, Grand Island, NY). Images were taken at multiple positions per plate at 3.0 minute intervals with multiple transfected cells per field of view and multiple particles per cell (see Figures 6.1-6.3). Cells maintained viability well beyond the duration of the experiment as confirmed by continued imaging for over an hour after the completion of data collection. Two-dimensional tracking of either GFP-Fib, RFP-TRF1 or GFP-53BP1 chromatin regions was done using custom Laptrack71 programs designed in MATLAB (Natick, MA) as previously published.[21, 22] Briefly, images were cropped and aligned to remove artifacts including imaging drift, nuclear translation, and nuclear rotation. Particles were then detected through statistical algorithms after calibration of background noise parameters. Particle tracks were then determined by correspondence with succeeding frames. Only persistent tracks of particles present for the full duration of the experiment were used for further analysis.

The ensemble-averaged MSD was calculated from the particle tracks as shown in Equation 1,[23] where τ is the lag time. MSD magnitudes were compared

at each time point using Student's t-test. Data were fit to a power-law rheological model as consistent for biological systems[24] and the nucleus in particular[25] as shown in Equation 3, where D_{eff} is the effective diffusivity and indicative of the chromatin compliance (where chromatin decondensation increases compliance and *vice versa*) and β is the power-law diffusive exponent which provides a measure of system forces including thermal forces and cytoskeletal forces (see Chapter III).[7] Calculation of D_{eff} was done by normalizing lag time, τ, to the sampling time step of three minutes. This allowed for enhanced accuracy in the fit calculation by using interpolation of the data rather than extrapolation. 95% confidence intervals for parameter values were used for statistical comparison. Since the MSD is an inherently positive quantity, outliers with large magnitudes may bias the resultant ensemble average. Consequently, all outliers greater than three standard deviations from the mean were removed and the data were reanalyzed, though with little to no change in the trends. These cells generally had issues with alignment wherein nuclear rotation or translation was not properly removed.

$$MSD(\tau) = \langle (x_{t+\tau} - x_t)^2 + (y_{t+\tau} - y_t)^2 \rangle \quad (1)$$

Cell Fixation and Fluorescence Lifetime Imaging Microscopy

As described above, HeLa and MEF cells were cultured, treated and stained by L. Lan's laboratory (University of Pittsburgh Medical Center – Hillman Cancer Center) per their protocols. DNA was stained using DAPI (Life Technologies, Grand Island, NY) for fluorescence lifetime imaging microscopy

(FLIM). Cells were also labeled for a DNA DSB marker (either 53BP1 or γ-H2AX) and the MEF cells were labeled with telomeric protein TRF1-KR, which was used to induce DNA DSBs by photoactivation in those MEF cells. DNA damage was induced in HeLa cells using bleomycin as described above.

FLIM measurements were obtained as described previously (see Chapter II). Briefly, using a Leica TCS SP5 inverted laser scanning confocal microscope with a 100x (1.4 NA) oil immersion objective. The corresponding pixel resolution was 256 x 256 and the scan rate was 400 Hz. A Ti:sapphire mode-locked, pulsed infrared laser (Chameleon, Coherent) system was used for multiphoton excitation source (1 W, average). The laser was tuned to 825 nm (DAPI) using pulse-widths of <140 fs delivered at 90 MHz. Emission was detected from 404-536 nm (Hoechst) using a FLIM-specific photomultiplier tube (PMT), consistent with the complete emission spectra for those fluorophores.

Data acquisition and analysis were done using methods previously published[26] and described in Chapter II. Briefly, images were acquired for approximately ten minutes in order to minimize errors associated with photobleaching, low signal-to-noise ratios and pile-up effects as determined by maintaining rates of photons detected, converted, and stored between 1×10^4 and 1×10^6. A suite of software programs from Becker & Hickl SPC-830 was used for time-correlated single photon counting (TCSPC) with 10 ps resolution. Lifetime variance was minimized using 220 time channels and a measurement window of 10.8 ns.

The decay rate of the fluorescence lifetime can be modeled an exponential decay (Equation 2), where t is time, τ is the lifetime and I_0 is the number of photons at t = 0, respectively. I(t) is the number of photons detected per unit time, t.

$$I(t) = I_0 e^{-t/\tau} \quad (2)$$

Data were analyzed and fluorescence lifetime heat map images created using the Becker & Hickl SPCImage software. The software was also used for determination of the spatially resolved fluorescence lifetimes as distinct regions within the nucleus, including DNA DSB sites. For each data set, the instrument response functions were determined and the lifetime images were binned such that the peak photon count was ≥ 1000, as required for statistical verification of double-exponential decay.[27] Using MATLAB, the nuclei were segmented to remove autofluorescence and background. Then the average lifetimes and corresponding standard deviation for both a single and double exponential decay were determined for each experiment by averaging the value for each pixel. The respective fits were compared using a χ^2 test. Unlike Hoechst 33342 (but similar to PicoGreen), DAPI was modeled best as a single-exponential decay.

Statistics

Magnitudes of the ensemble-averaged mean squared displacement were statistically compared using Student's t-test. Fitting parameters and corresponding 95% confidence intervals were determined using the MATLAB for nonlinear least squares regression trust-region algorithm and verified using ANOVA ($p<<0.001$).

For FLIM experiments, the fits (single- or double-exponential decays) were determined using a χ^2 test, as discussed above. The mean fluorescence lifetimes were compared using Student's t-test and the variance compared using the F-test.

Results

DNA Damage Induces Decoupling of Chromatin Dynamics Coincident with Structural Relaxation

To investigate the physical mechanism of chromatin dynamics in response to DNA damage, we used fluorescently tagged proteins that bind within undamaged chromatin (nucleolar protein GFP-fibrillarin and the telomeric protein called telomeric repeat-binding factor 1, RFP-TRF1, as shown in Figures 6.1 and 6.2) in control and bleomycin-treated cells as well as a DSB marker (tumor suppressor p53-binding protein 1, GFP-53BP1, Figure 6.3) in bleomycin-treated cells to track these dynamics in a live human osteosarcoma cell line (U2OS).

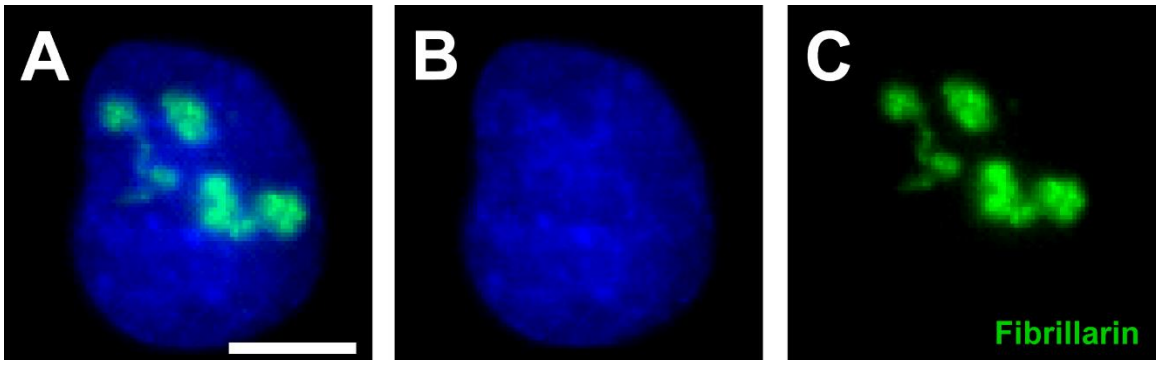

Figure 6.1: Particle tracking of nucleolar regions in U2OS cells. *(A) Merged image overlay of live U2OS cells labelled with individual fluorophores for (B)*

DNA (Hoechst 33342, blue) and (C) an exogenous nucleolar protein, fibrillarin (transfected, GFP-Fibrillarin or GFP-Fib). Scale bar is 10 μm.

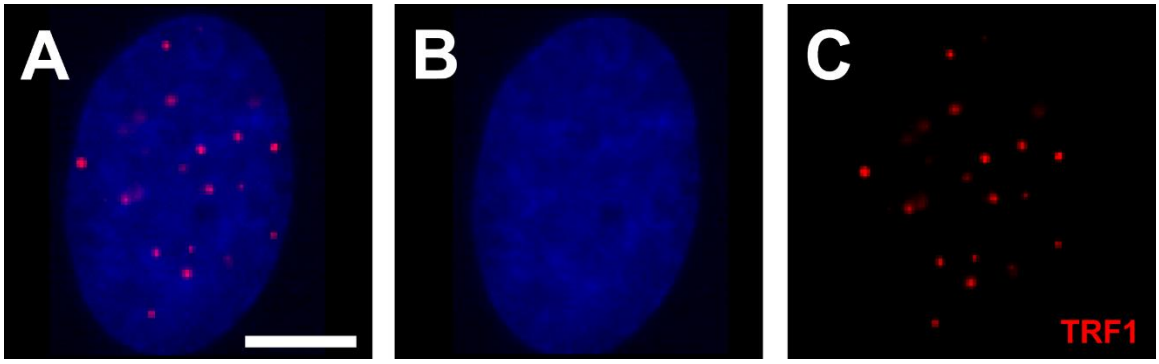

Figure 6.2: Particle tracking of telomeres in U2OS cells. *(A) Merged image overlay of live U2OS cells labelled with individual fluorophores for (B) DNA (Hoechst 33342, blue) and (C) an exogenous telomeric protein, telomeric repeat-binding factor 1 (transfected, RFP-TRF1). Scale bar is 10 μm.*

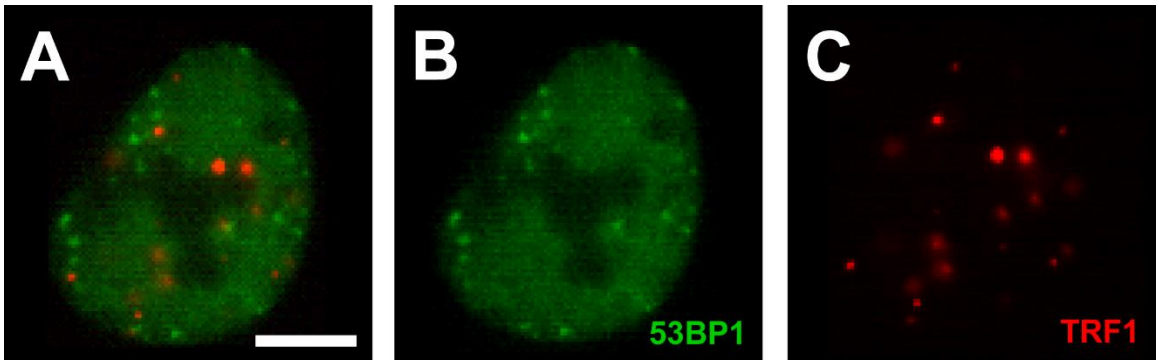

Figure 6.3: Particle tracking of chromatin in bleomycin-treated U2OS cells. *(A) Merged image overlay of live U2OS cells labelled with individual fluorophores for (B) DNA double-strand break (DSBs) marker and repair protein, tumor suppressor p53-binding protein 1 (transfected, GFP-53BP1) and (C) an exogenous telomeric protein, telomeric repeat-binding factor 1 (transfected, RFP-TRF1). Scale bar is 10 μm.*

From the live cell trajectories of these chromatin markers, we calculated the mean squared displacement (MSD) from Equation 1. We fit this to the characteristic power-law equation of anomalous subdiffusion (Equation 3), where we've previously shown D_{eff} to be a measure of chromatin compliance and β as a measure of molecular motor forces (see Chapter III).[7] As such, increasing D_{eff} is indicative of chromatin decondensation, with the relaxed chromatin structure increasing local compliance of the fiber. Further, molecular motor forces serve to drive the chromatin fluctuations beyond that of thermal energy to influence the diffusive exponent, β.

$$MSD = D_{eff}\tau^{\beta} \quad (3)$$

In control cells, we observe physical uniformity of ensemble chromatin dynamics with statistically indistinguishable MSD, D_{eff} and β for telomeric and nucleolar labels (Figure 6.4). This is consistent with our previous work demonstrating uniform ensemble chromatin dynamics across multiple cell lines for a variety of chromatin markers[7, 22] on these time scales, as well as other work demonstrating randomized, coherent motion of chromatin dynamics on short time scales (<10 seconds) of ~4-5 μm that likely facilitates the physical uniformity of these dynamics at our longer time scales.[28] The statistical similarity of D_{eff} and β also indicates these distinct nuclear functional sites – associated with unique components – experience similar chromatin compliance and forces transduced from motor protein activity.

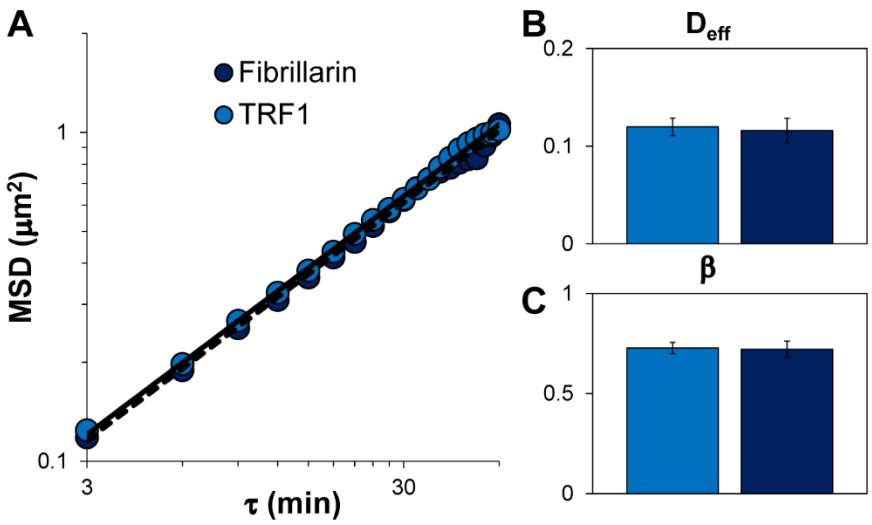

Figure 6.4: Chromatin dynamics of nucleolar and telomeric regions measured by ensemble averaged MSD are physically uniform. *Particle tracking measurements of nucleolar protein, GFP-Fib, and telomeric protein, RFP-TRF1, resulted in statistically indistinguishable magnitudes, trends and fits ($p>0.05$). (A) MSD versus lag time values, (B) the prefactor, D_{eff}, and (C) the diffusive exponent, β. Error bars reflect 95% confidence intervals.*

Following DNA damage induction, we still see physical uniformity of undamaged chromatin sites with their chromatin dynamics seemingly unaffected by bleomycin treatment relative to untreated cells. However, we observe enhanced chromatin dynamics of fluorescently tagged DSBs (DNA repair protein 53BP1, Figure 6.5). This indicates physical decoupling of DSB sites relative to undamaged loci following bleomycin treatment. Thus, while undamaged chromatin appears capable of maintaining the same behavior of control cells with statistically similar measures of chromatin compliance (D_{eff}) and molecular motor activity (β), damaged sites exhibit unique behavior resulting in increased

chromatin dynamics on these time scales. The increase in dynamics arises from chromatin relaxation, making chromatin more compliant as observed through an increase in D_{eff}. Interestingly, we see a decrease in molecular motor activity experienced at damage sites, corresponding to a reduction in β. Thus, while the local relaxation of chromatin structure and the concomitant increase in chromatin compliance increases the mobility of damage sites, the reduced molecular motor activity relative to undamaged chromatin makes this effect short lived by exerting its influence through the temporal nature of these dynamics. Thus, the enhanced chromatin dynamics of DSBs are only statistically significant for the first 30 minutes ($p<0.05$, with $p<0.01$ for the first 18 minutes). To characterize the temporal nature of this deviation from undamaged chromatin, we define a crossover time, τ_c, as shown in Equation 4 where we equate the characteristic power-law MSD equations of undamaged (U) and damaged (D) to obtain τ_c.

$$MSD_U = \ MSD_D = D_{eff,U} * {\tau_C}^{\beta_U} = \ D_{eff,D} * {\tau_C}^{\beta_D} \quad (4)$$

We find $\tau_c \sim 30$ minutes, before which the increased chromatin compliance from local chromatin decondensation of damage sites results in increased chromatin mobility relative to undamaged sites. However, beyond ~30 minutes, the enhanced molecular motor forces experienced at undamaged sites results in increased chromatin dynamics through its influence on the time dependence as a result of the larger diffusive exponent (β) relative to the damage sites. Thus, at longer time scales, the motion of damaged chromatin is effectively curtailed to

inhibit long range displacements. This has direct implications for translocation probabilities of DSBs that are not proximally located, and it points to the likelihood of "escape" of two complementary DSBs from each other as being most probable early in the response if left uncontrolled. However, certain protein components, including the MRN complex, have been observed to tether severed ends of DSB in a manner that has no effect on mobility, which may restrict this escape.[19]

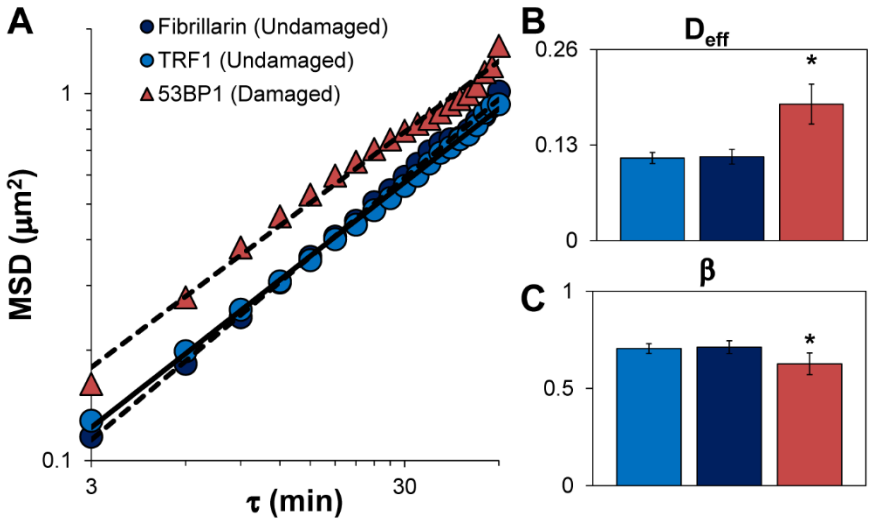

Figure 6.5: Chromatin dynamics in the presence of DNA double-strand breaks results in a physical decoupling of DNA damage dynamics from control behavior. *Cells are treated with bleomycin, with DNA DSBs monitored by GFP-53BP1 and undamaged sites monitored by GFP-Fib and RFP-TRF1. (A) Undamaged chromatin dynamics of GFP-Fib and RFP-TRF1 were statistically indistinguishable in bleomycin-treated cells with respect to MSD magnitudes, trends and fits ($p>0.05$). These trends were also statistically indistinguishable from their control counterparts ($p>0.05$). By contrast, DNA DSBs marked by GFP-53BP1 exhibited markedly enhanced chromatin dynamics particularly at*

early times ($p<0.01$ for first 18 minutes and $p<0.05$ for first 30 minutes). DNA DSBs marked by GFP-53BP1 demonstrated (B) increased chromatin compliance through D_{eff} and (C) reduced molecular motor activity experienced at sites of DSBs as evinced through the diffusive exponent, β. Error bars reflect 95% confidence intervals.

FACT Complex Subunit SSRP1 and SIRT6 Deacetylase Facilitate Chromatin Relaxation at Sites of Double-Strand Breaks

Given the pronounced effect of chromatin decondensation on the mobility of damage sites relative to undamaged and control chromatin dynamics, we sought to determine the roles of specific chromatin remodeling proteins that may impact chromatin relaxation at DSBs. We utilized fluorescence lifetime imaging microscopy (FLIM) as our quantitative measure of chromatin condensation state to investigate these effects. Previous studies in our laboratory and others have shown that the fluorescence lifetime is a quantitative and spatially resolved measure of chromatin condensation state for cell nuclei *in situ*.[7, 29, 30] The fluorescently-tagged chromatin of the interphase cell nucleus is associated with a spatially heterogeneous distribution of fluorescence lifetimes, indicating differential fluorophore environments corresponding to varying levels of chromatin condensation. Decondensed chromatin is associated with increased fluorescence lifetimes (and *vice versa*) due to mechanical changes to chromatin that accompany altered condensation state and impact the local fluorophore environment (on the scale of angstroms up to ~10 nm).[7, 29, 31]

Through collaboration with Professor Li Lan (M.D., Ph.D.) and her laboratory at the Hillman Cancer Center within the University of Pittsburgh Medical Center (UPMC), we identified several targets we hypothesized may be critical to the chromatin remodeling effects that would influence the chromatin dynamics through increased decondensation and compliance. Using fluorescence lifetime imaging microscopy (FLIM) of DAPI-labeled DNA, we examine the roles of the Facilitates Chromatin Transcription (FACT) complex subunit protein SSRP1 as well as the protein deacetylase and mono-ADP ribosyltransferase sirtuin-6 (SIRT6) in chromatin condensation during the DNA damage response.

The FACT complex is a heterodimer protein complex composed of a 140 kDa subunit, Spt16, and an 80 kDa subunit, SSRP1. The FACT complex is known to associate with RNA Polymerase II (Pol II) to facilitate transcription on *in vitro* chromatin.[32] However, it has also been shown to generally facilitate the remodeling of chromatin through its role as a histone chaperone. In this capacity, it facilitates both the dissociation and reassembly of nucleosomes on chromatin as observed during transcription. This function as a general chromatin remodeler has led to investigation and evidence of a role for the FACT complex in DNA repair processes.

In untreated cells with SSRP1 suppression, we observe a reduced fluorescence lifetime relative to control cell nuclei indicating that SSRP1 loss may promote global chromatin condensation (Figure 6.6). After inducing DNA damage with bleomycin treatment, all cells (control and SSRP1-suppressed cells) show an increase in fluorescence lifetime suggesting chromatin decondensation.

This confirms the chromatin decondensation effects evinced through particle tracking MSD measurements as quantified through chromatin compliance (D_{eff}), and further highlights that large scale DNA damage has a concomitant effect that can be measured through global chromatin condensation state changes. Bleomycin-treated cells with SSRP1 suppression show a modest increase in the fluorescence lifetime relative to the 3.6% increase in untreated cells and fail to recapitulate the chromatin remodeling accompanying DNA damage in control cells (13% lower fluorescence lifetimes than bleomycin-treated control cells). Since FLIM allows for spatial quantification of chromatin condensation, we analyzed the distinct chromatin condensation state changes at DNA damage sites. Qualitatively through heat maps of the mean fluorescence lifetime of DAPI-stained chromatin of nuclei with DNA damage sites labeled for 53BP1, we see increased fluorescence lifetimes associated with DNA damage sites (Figures 6.7 and 6.8), albeit with reduced capacity to fully remodel the chromatin following SSRP1 suppression (Figures 6.8). We quantify this by measuring the fluorescence lifetime solely at DNA damage sites for control and SSRP1 suppressed cells and observe reduced fluorescence lifetimes at DNA damage sites in cells with SSRP1 suppression relative to controls (Figure 6.9). This indicates that SSRP1 is necessary for the proper chromatin remodeling that accompanies the DNA damage response. This was consistent with additional SSRP1 suppression treatments we explored (data not shown). Thus, SSRP1 is associated with regulating chromatin condensation in control cells. Its suppression results in increased chromatin condensation and reduced capacity to remodel chromatin for

decondensation in response to DNA damage. However, it does not appear to hinder the upstream signaling of DSBs given the presence of the 53BP1 DSB marker. These findings were consistent with the findings of our collaborators at the UPMC Hillman Cancer Center.

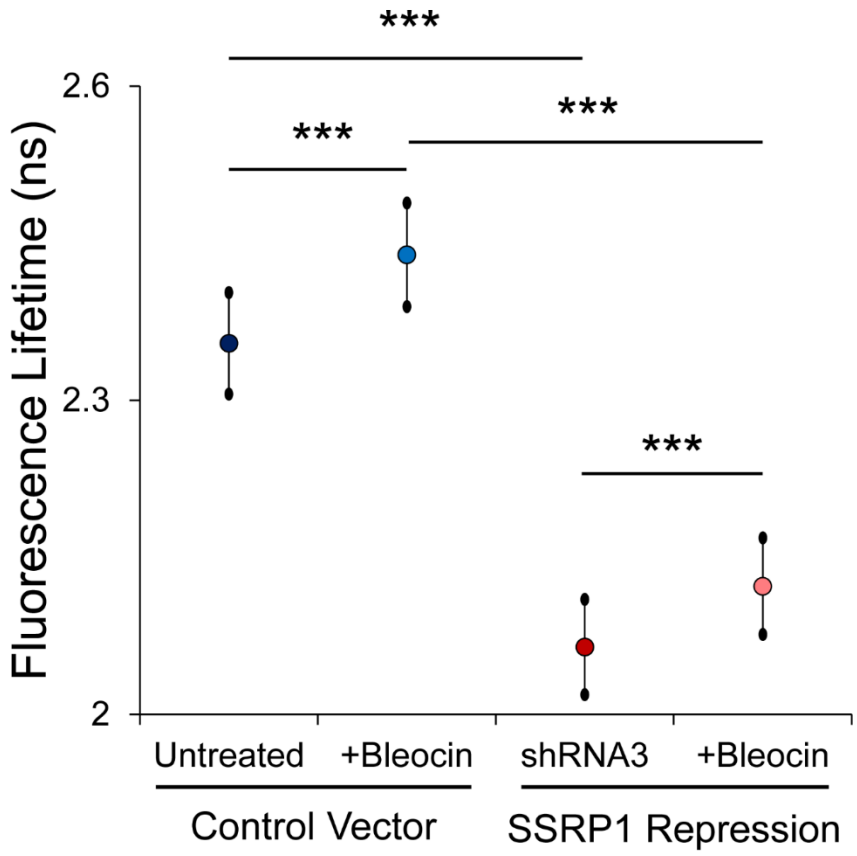

Figure 6.6: Fluorescence lifetime measurements of global chromatin condensation state in HeLa cell nuclei associated with FACT complex subunit SSRP1 and the DNA damage response from bleomycin treatment. *Inhibition of SSRP1 by small hairpin RNA (shRNA) resulted in strongly reduced fluorescence lifetimes (***p<<0.001) relative to the control vector. In response to DNA damage induced by bleomycin treatment, we see increased fluorescence lifetimes in cells treated with the control vector (***p<<0.001). SSRP1*

*suppression resulted in reduced capacity to properly decondense chromatin in response to DNA damage relative to cells treated with the control vector (***p<<0.001). Analysis was done using 60-120 segmented nuclei for each treatment condition. Error bars indicate standard deviation of pixel-to-pixel fluorescence lifetime differences of segmented nuclei under each treatment condition.*

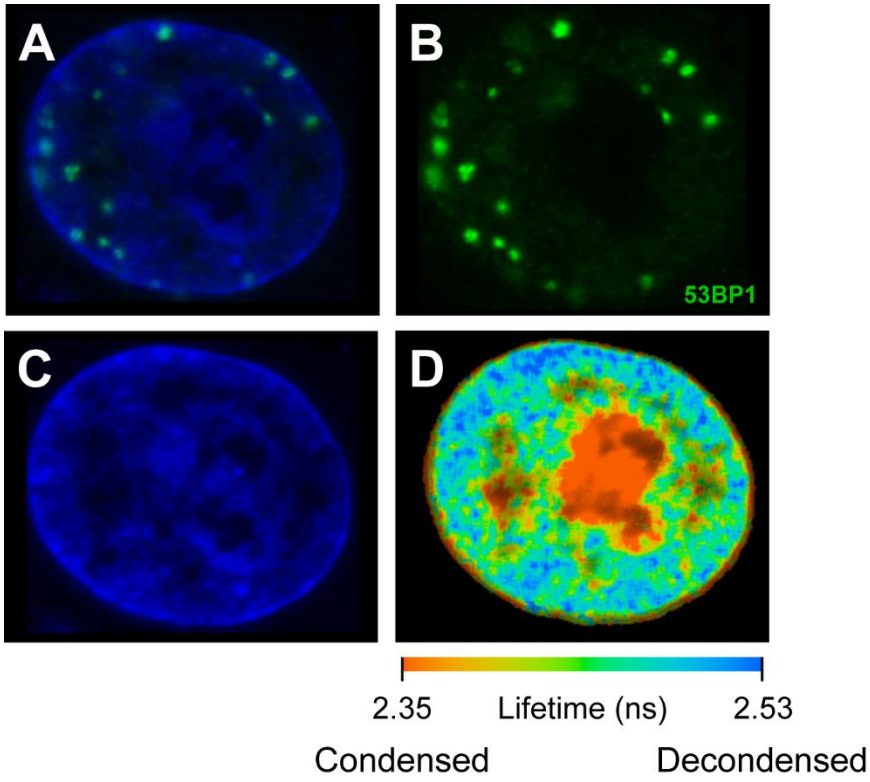

Figure 6.7: Fluorescence lifetime spatial distribution of HeLa cell nucleus treated with the control vector following bleomycin exposure. *(A) An overlay of a confocal image of a HeLa cell nucleus with DAPI-stained DNA (blue, B) and DNA DSB marker 53BP1 (green, C). (D) The spatially resolved fluorescence*

lifetime heat maps of the same nucleus shows chromatin decondensation localized to DNA DSB sites (deep blue regions).

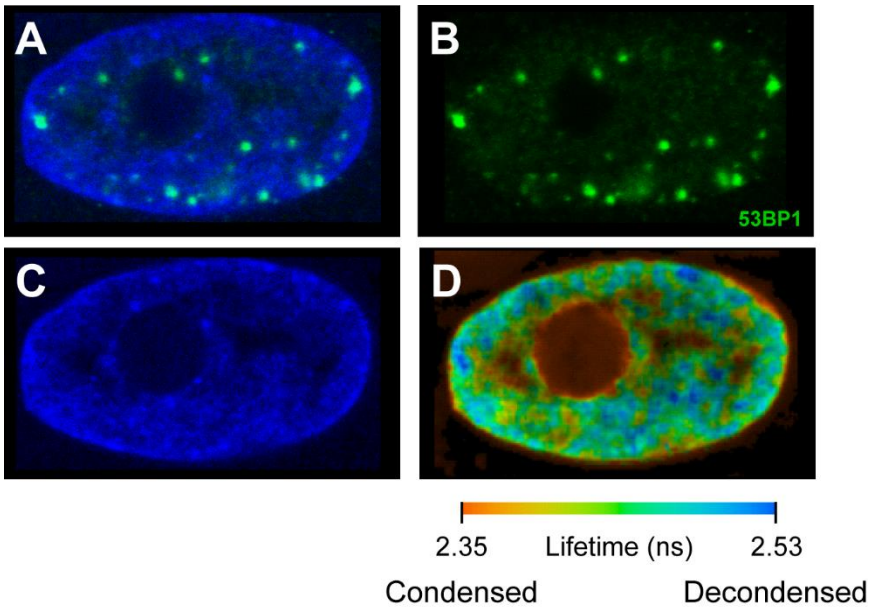

Figure 6.8: Fluorescence lifetime spatial distribution of HeLa cell nucleus with SSRP1 inhibition from short hairpin RNA (shRNA) following bleomycin exposure. *(A) An overlay of a confocal image of a HeLa cell nucleus with DAPI-stained DNA (blue, B) and DNA DSB marker 53BP1 (green, C). (D) The spatially resolved fluorescence lifetime heat maps of the same nucleus shows reduced capacity to decondensed chromatin at DNA DSB sites (green-red regions).*

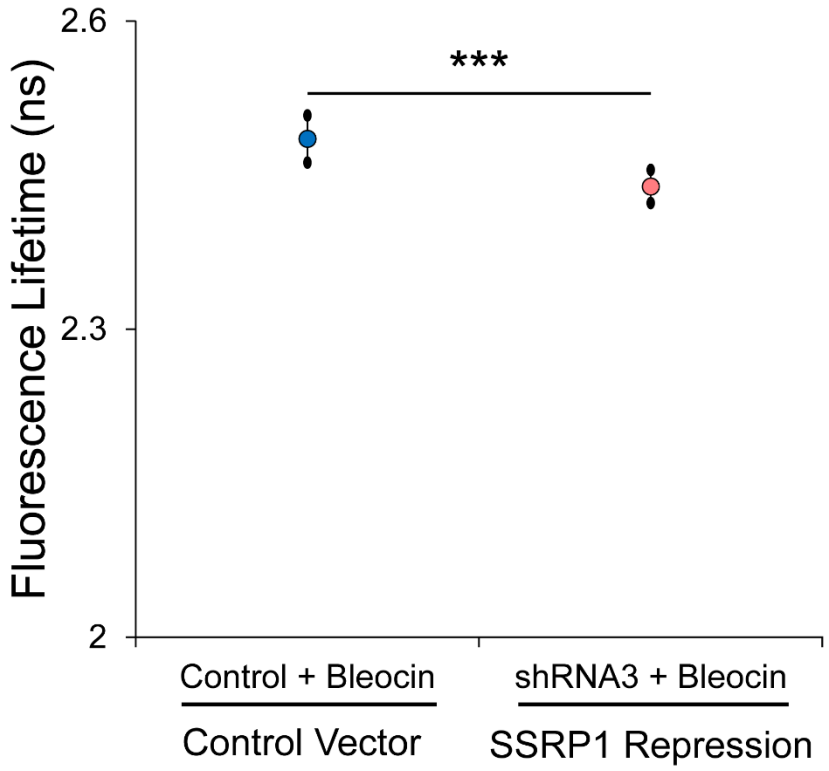

Figure 6.9: Fluorescence lifetime measurements of chromatin condensation state of DNA Damage foci in HeLa cells associated with FACT complex subunit SSRP1 activity following bleomycin treatment. *DNA DSB sites exhibit a noticeable increase in the fluorescence lifetime relative to the global averages indicating they are more decondensed chromatin, particularly for the control vector. However, inhibition of SSRP1 by small hairpin RNA (shRNA) resulted in a prominent reduction in the fluorescence lifetime at DNA DSB sites (***p<<0.001) relative to the control vector. This indicates an inability to properly remodel chromatin in response to DSBs without the SSRP1 subunit of the FACT complex. Analysis was done for multiple DNA damage sites across treatment conditions. Error bars indicate standard deviation.*

In addition to SSRP1, we investigated the role of SIRT6 in response to DNA damage. SIRT6 is from the sirtuin class of proteins that have mono-ADP-ribosyltransferase and/or deacylase activity which are involved in a variety of essential cellular processes. SIRT6 has been found to be a histone deacetylase involved in chromatin remodeling, particularly in stress response. It is also involved in telomere maintenance and DNA repair, but its precise role in chromatin remodeling in DNA repair is unclear.[33]

Here we use a stably transfected mouse embryonic fibroblast (MEF) cell line with the telomeric protein TRF1 fused to the fluorophore KillerRed (KR) developed by L. Lan's laboratory. Excitation of TRF1-KR results in the rapid generation of reactive oxygen species (ROS) at levels far exceeding that of other fluorophores. The result is ROS-induced DNA damage from these oxidative species at precise locations within the genome associated with the protein KR is fused to,[20] in this case at telomeric regions for TRF1-KR. As in the case of bleomycin-treated cells, we observe DNA damage induction by photoactivation of TRF1-KR expressing cells results in increased fluorescence lifetimes indicating corresponding chromatin decondensation in wild type cells (Figure 6.10). In SIRT6 knockout MEFs without photoactivation, we observe a modest increase in fluorescence lifetime relative to wild type cells that express SIRT6 (Figure 6.10). This finding is unsurprising given our previous work chemically simultaneously inhibiting multiple histone deacetylases (HDACs) where we observe increased

fluorescence lifetime resulting from the corresponding chromatin decondensation. It seems likely that SIRT6 is necessary but not sufficient for normal chromatin remodeling given its modest effect on chromatin condensation state relative to global HDAC inhibition we showed previously. Alternatively, SIRT6 may act solely at specific chromatin regions as it is speculated to operate most prominently at telomeres.

In SIRT6 knockout MEFs with photoactivated TRF1-KR, we observe no change in fluorescence lifetime which demonstrates that these cells are incapable of chromatin remodeling following DNA damage induction (Figure 6.10). We confirm these findings qualitatively in heat maps of wild type and SIRT6 knockout MEFs with photoactivated TRF1-KR co-labeled with the DNA damage marker γ-H2AX (Figures 6.11 and 6.12), and we find SIRT6 knockout cells have reduced fluorescence lifetimes at damage sites relative to wild type cells, which we quantified specifically at the DNA damage sites (Figure 6.13). Thus, while the deacetylase activity of SIRT6 seems to facilitate proper chromatin condensation in control cells, its role in the DNA damage response may be to facilitate decondensation, or, alternatively, that its role in condensing chromatin is necessary for later rounds of remodeling in the response. Regardless, we find that SIRT6 is necessary to induce the proper chromatin remodeling for the normal DNA damage response, but its absence does not seemingly affect upstream signaling components of the DNA damage response given the presence of the γ-H2AX labeled sites. Our results were consistent with the findings of our collaborators in L. Lan's laboratory.

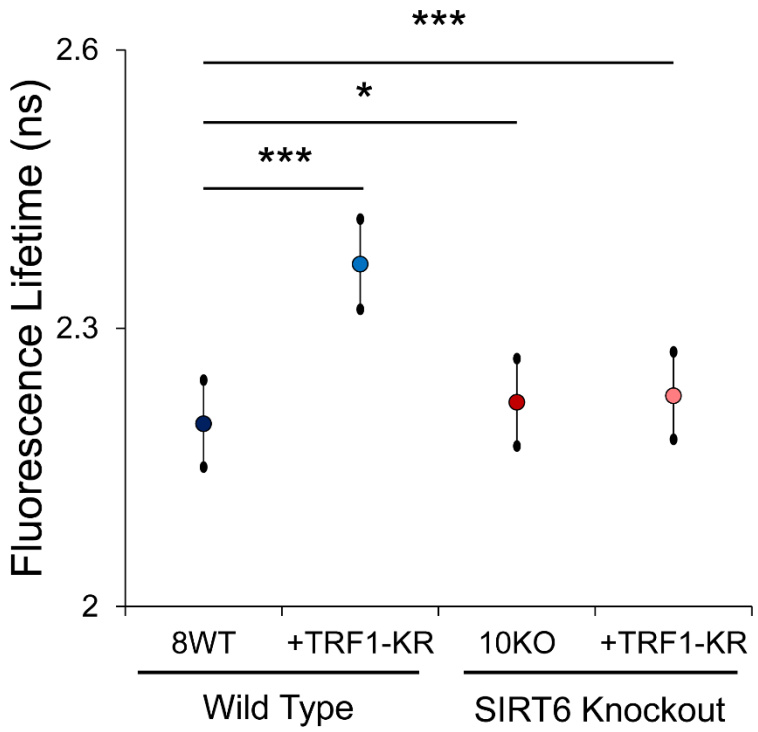

Figure 6.10: Fluorescence lifetime measurements of global chromatin condensation state in MEF cell nuclei associated the DNA DSB damage response. *SIRT6 knockout (10KO) MEF cells had a modestly increased fluorescence lifetime relative to wild type (8WT) controls ($p<0.05$), indicating a role in regulating chromatin condensation. Photoactivation of the KillerRed-fused telomeric protein (TRF1-KR) induced DNA DSBs, leading to an increase in fluorescence lifetime in wild type MEF cells but no change in SIRT6 knockout MEF cells. This points to an inability to remodel chromatin during the DNA repair process in SIRT6 knockout MEF cells. Analysis was done using 60-120 segmented nuclei for each treatment condition. Error bars indicate standard deviation of pixel-to-pixel fluorescence lifetime differences of segmented nuclei under each treatment condition.*

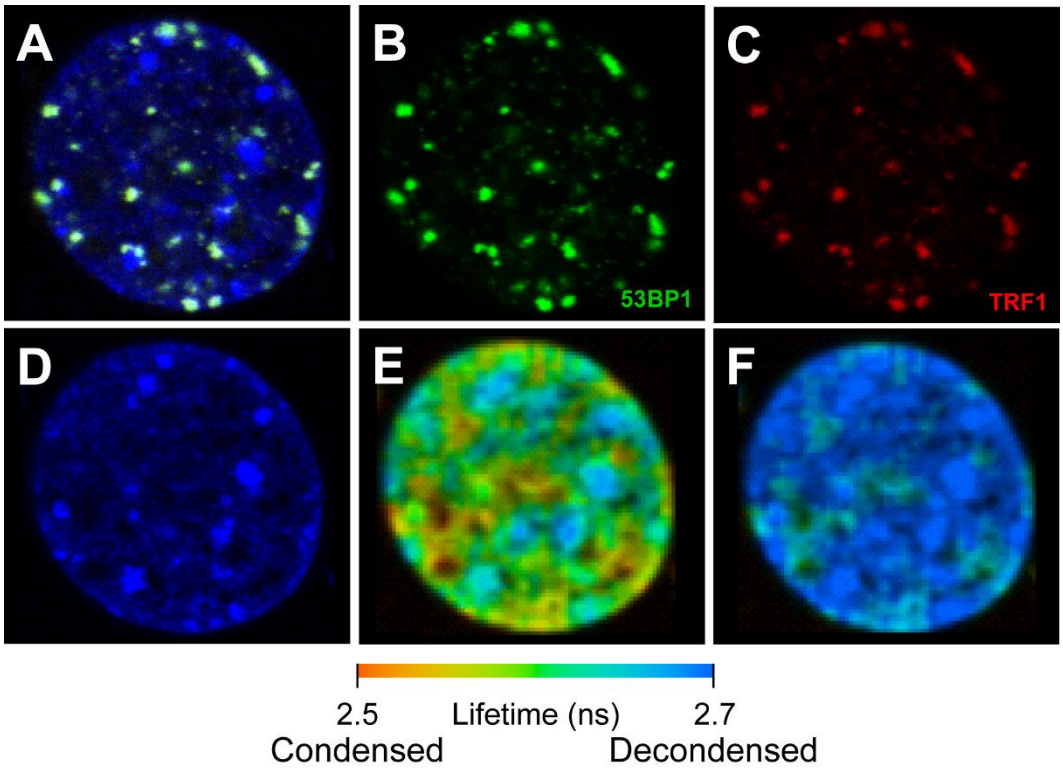

Figure 6.11: Fluorescence lifetime spatial distribution of wild type MEF cell nucleus with DNA damage induced by photoactivation of TRF1-KR. *(A) An overlay of a confocal image of a wild type MEF cell nucleus with DNA DSB marker γ-H2AX (green, B), telomeric protein TRF1-KR used to induce DSBs (red, C) and DAPI-stained DNA (blue, D). (E) The spatially resolved fluorescence lifetime heat maps of the same nucleus shows chromatin decondensation localized to DNA DSB sites (green-blue regions). (F) The spatially resolved fluorescence lifetime heat maps of the same nucleus on the same scale as the SIRT6 knockout cell in Figure 6.12 shows more decondensed chromatin as well (blue regions).*

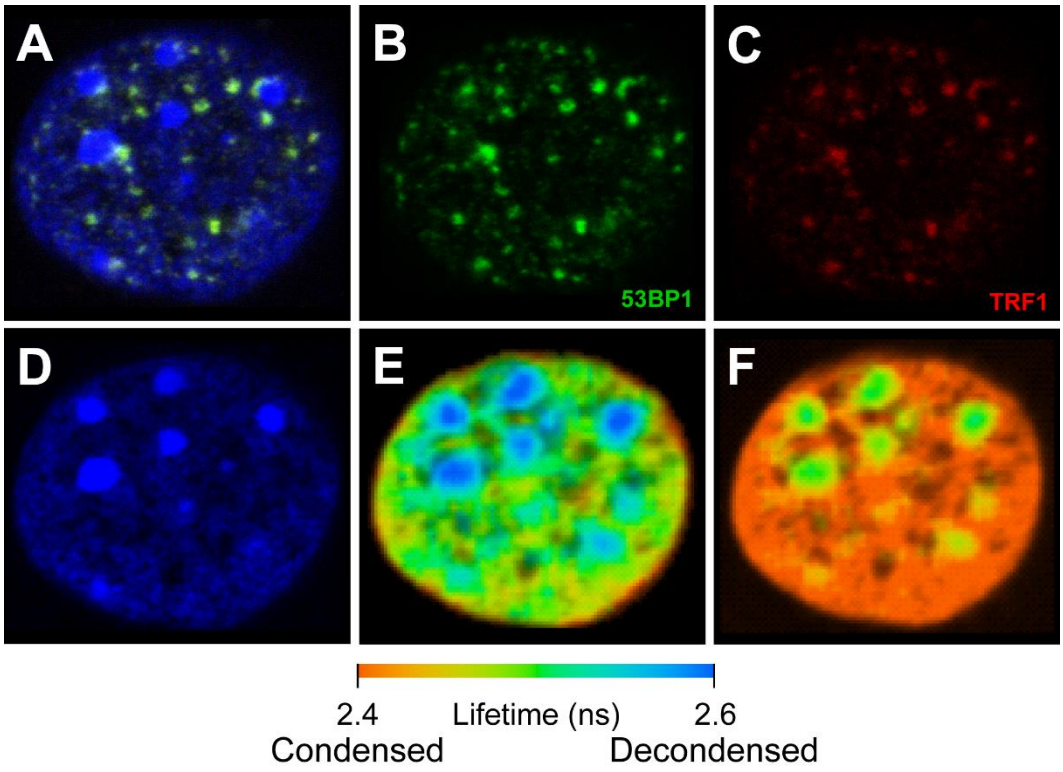

Figure 6.12: Fluorescence lifetime spatial distribution of SIRT6 knockout MEF cell nucleus with DNA damage induced by photoactivation of TRF1-KR. *(A) An overlay of a confocal image of a wild type MEF cell nucleus with DNA DSB marker γ-H2AX (green, B), telomeric protein TRF1-KR used to induce DSBs (red, C) and DAPI-stained DNA (blue, D). The spatially resolved fluorescence lifetime heat maps of the same nucleus shows reduced capacity to decondensed chromatin at DNA DSB sites as shown in the new range for heat map lifetime values (E, green-orange regions) or in the extreme values on the same scale as the wild type cell in Figure 6.11 (F, orange regions).*

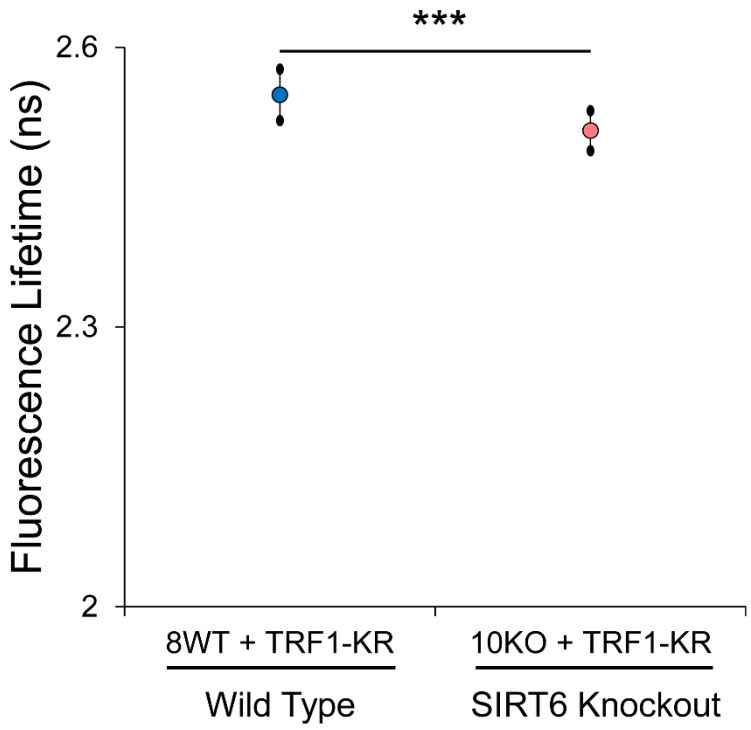

Figure 6.13: Fluorescence lifetime measurements of chromatin condensation state of DNA Damage foci in MEF cells associated with SIRT6 activity at following photoactivation of TRF1-KR. *DNA DSB sites (labelled by γ-H2AX) exhibit a noticeable increase in the fluorescence lifetime relative to the global averages indicating they are more decondensed chromatin, particularly for the wild type cells (8WT). However, SIRT6 knockouts (10KO) exhibited reduced fluorescence lifetime at DNA DSB sites (***p<<0.001) relative to the wild type cells (8WT). This indicates an inability to properly remodel chromatin in response to DSBs without SIRT6. Analysis was done for multiple DNA damage sites across treatment conditions. Error bars indicate standard deviation.*

Discussion

Decoupling of Chromatin Dynamics at DNA DSB Sites through Structural Relaxation Influences Translocation Probability

Here we demonstrate DSBs exhibit increased dynamics relative to undamaged chromatin sites of both bleomycin-treated and untreated cells. Given the congruence of undamaged sites in the presence or absence of DNA damage, it is evident that DNA damage sites are governed by distinct physical effects resulting in this decoupled behavior. Our work highlights the nature of these physical effects, and points to specific factors that give rise to these changes.

Specifically, we see DSBs are associated with a more compliant chromatin environment resulting from structural relaxation of the chromatin fiber which is confirmed through our chromatin dynamics measurements and FLIM measurements. This chromatin remodeling is consistent with other studies showing a need for decondensation to allow for the repair mechanism to proceed.[34] Yet, interestingly the increased chromatin dynamics we observe is not buoyed by molecular motor activity, with DNA damage sites experiencing reduced molecular motor activity driving their dynamics.

Whether the molecular motor activity of chromatin remodeling complexes involved in active decondensation processes impacts the mobility, or if the changes result solely from the altered chromatin fiber flexibility that accompanies decondensation has been a source of contention.[1] Our work demonstrates that on these time scales it is the altered chromatin compliance accompanying changes in condensation state that influences the dynamics, not the associated molecular motor activity of remodeling complexes. Specifically, we see increased

compliance from chromatin decondensation that enhances chromatin dynamics while the molecular motor activity experienced at DNA damage sites is reduced. While we cannot completely rule out that the molecular motor activity of remodeling complexes plays a role, our previous work[7] and that of others[28] have shown these forces to be relatively transient and small in magnitude. Thus, the molecular motor activity of chromatin remodeling complexes is effectively dwarfed by the much larger and more pervasive cytoskeletal motor forces despite the longer length scales they need to be transduced, particularly for ensemble probe motions.[7]

We suggest that the dramatic decondensation at DNA damage sites, and the corresponding decoupling from the physical uniformity of dynamics of undamaged chromatin, serves to mechanically isolate DNA damage sites allowing for strict control over the mobility. This idea is supported by recent work demonstrating the loss of "elastic coupling" of chromatin dynamics in response to DNA damage. In this study, normal chromatin exhibited randomized, transient (<10 seconds) coherent motion for stretches of noncontiguous chromatin spanning ~4-5 μm, which was lost upon large scale DNA damage induction.[28] While these time scales are much shorter than those in this present work, it seems likely that the phenomena at short time scales give rise to the observed physical uniformity of undamaged sites and decoupling of damage sites at our longer time scales. Such mechanical decoupling would effectively restrict the role of large length scale force transduction (including from the cytoskeleton) on DNA damage sites, possibly allowing for more precise regulation of the mobility of these sites. This

previous study pointed to nuclear motor proteins as a potential source of this elastic coupling, but our work shows this may require condensed chromatin domains for its propagation. While decondensed chromatin is a natural feature of human nuclei, it is likely that either the extent of structural relaxation at DSB sites or the potential presence of distinct mechanistic features associated with repair results in this decoupling. Future work should be aimed at identifying factors associated with this elastic coupling and how DSB sites gain this seeming mechanical isolation.

Even in the presence of DNA damage, the nucleus appears capable of maintaining the chromatin dynamics of ongoing processes as undamaged sites were unaffected by the presence of damage, consistent with another recent study that looked at telomeres in irradiated cells specifically.[18] While the coherent chromatin dynamics observed previously found genome-wide loss of this coherent motion upon DNA damage induction, we believe that this was the result of larger doses of DNA damage qualitatively observed in that treatment[28, 35] than we observe in our experiments where we see no deviation from control behavior in undamaged sites. We speculate that a threshold amount of DNA damage exists wherein the dynamics of undamaged sites may be similarly compromised. We suggest future work aimed at investigating the dose-dependence of the DNA damage response in chromatin dynamics.

Models of DNA DSB Dynamics and Repair Probabilities

The nature and extent of chromatin dynamics at DNA damage has been a major source of controversy. Specifically, two models of DSB repair have been posed that highlight a prominent point of contention. The "contact-first" model holds that translocation is most probable for proximally-located DSBs, requiring (or at least favoring) translocating chromosomes to be in close contact prior to DSB induction due to the restrictive mobility of chromatin dynamics. By contrast, the "break-first" model suggests DSB induction precedes a dramatic increase in mobility of damaged chromatin capable of moving several microns in minutes in search of a translocating partner. Such partners may include distantly positioned nuclear territories, with the possible presence of mechanisms directing this large scale motion. Evidence for both these models has been observed via enhanced[16-18] or restricted[11-15] mobility of chromatin in response to DNA damage. While we observe enhanced chromatin dynamics on our time scale of interest, we highlight that damage site dynamics are still relegated to the subdiffusive regime which is not consistent with the large scale motion of the "break-first" model.

The careful delineation of the unique physical environment of DSB dynamics shown here demonstrates that the convergence of aspects of these two models is not incompatible. While translocations between proximally-located DSBs is heavily favored by the subdiffusive motion we observe in these experiments, the enhanced mobility driven by a decondensation-induced increase in chromatin compliance shows DSBs have heightened mobility at short time scales. This increases the potential "escape" of complementary ends early in the

response. However, at time scales beyond the crossover time of ~30 minutes, the reduced temporal dependence of DSB dynamics from decreased molecular motor activity experienced at these sites acts to restrict motion to a narrower search radius than undamaged chromatin dynamics, as evinced in Figure 6.15. This reduced time-dependence of damage sites favors the rejoining probability for complementary ends through the decreased subdiffusive exponent which further curtails long range motion in favor of nearby binding targets (and much more so than for normal Brownian diffusion) given the limitations in possible deviations for its trajectory.[36]

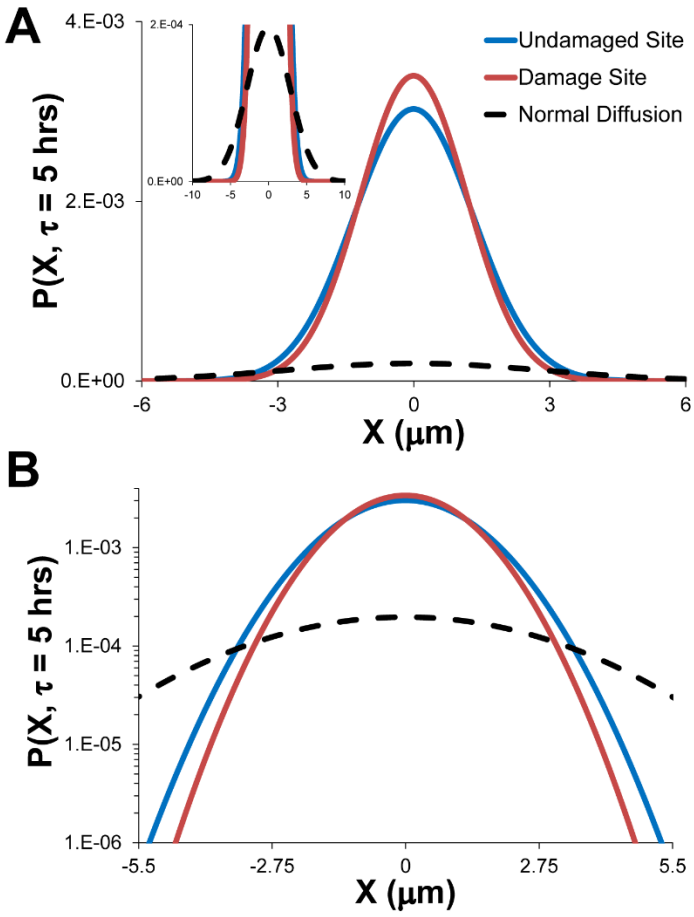

Figure 6.14: Probability distribution of 1D random walk displacements for undamaged and damaged chromatin. *Chromatin associated with DSBs exhibit restricted motion relative to undamaged chromatin beyond the crossover time of ~30 minutes. At five hours we see a noticeable narrowing of the probability distribution for DSBs in comparison to undamaged chromatin (and much more so than normal Brownian diffusion) (A, B). The heightened probability of restricted motion is shown in the cusps of the linear plot (A, with normal Brownian diffusion shown in the inset), while the longer tails of the distribution for the undamaged chromatin and normal Brownian diffusion are exemplified in the log-linear plot of the distributions (B).*

Mechanistic Effects of Chromatin Remodeling in the Context of Ongoing Repair

Recent works have aimed to elucidate the chromatin remodeling complexes associated with DSB repair. Here we demonstrate a role for the SSRP1 subunit of the FACT histone chaperone complex and the sirtuin family deacetylase, SIRT6. In both cases, loss of their remodeling capacity resulted in the inability to properly decondense chromatin at sites of DSBs. This was also true independent of DNA damage for SSRP1. By contrast, untreated SIRT6 knockout MEFs had a moderate level of chromatin decondensation consistent with our work with global inhibition of histone deacetylase activity[7] as well as the known effect of SIRT6 on telomeric chromatin condensation. This seeming contradiction in behavior for SIRT6 is rectified by recent work highlighting rapid and transient rounds of condensation and decondensation immediately following

DNA damage induction[34] that may serve to restrict transcription. Thus, we suggest the inability to properly remodel chromatin in either direction during DNA damage repair may inhibit assembly and function of repair machinery, particularly given the observation that condensing chromatin serves to initiate upstream repair signaling.[34] Our results with SIRT6 knockout MEFs lend further credibility to this view. Further, a growing body of evidence points to chromatin condensation state, including histone modifications, as a possible source of DNA damage signaling.[34] We highlight that in both SSRP1 suppression and SIRT6 knockout, initial DNA damage signaling appears to be unhampered given the presence of DNA damage foci despite this inability to properly remodel chromatin in the damage response. Thus, these effects appear to act further downstream in the repair process.

Mechanistically, the crossover time of ~30 minutes (below which DSBs have enhanced mobility relative to undamaged sites and after which they have restricted mobility) aligns with other temporal events associated with DSB repair. It has been demonstrated that DSBs formed within condensed heterochromatin regions are decondensed and relocated to nearby decondensed, euchromatin regions by ~30 minutes. Thus, the enhanced mobility afforded by decondensation shown here may likely facilitate this relocation, and previous models have shown that entropy and physical effects are capable driving forces for this relocation which is consistent with our understanding.[17] Additionally, severed complementary ends of DSBs have been shown undergo an initial separation of

roughly ~100-220 nm that coincides with ~30 minutes in a manner dependent on the DSB repair protein Ku80.[37]

Allowing this initial mobility of DSBs poses a threat to the integrity of the repair process as it raises the probability that complementary severed ends may "escape" from each other, particularly in light of the relationship between increased movements and translocations.[11] However, there is evidence that distinct repair factors, including the MRN complex (and the Mre11 component of the complex in particular), may tether severed ends in a manner that has been shown to have no effect on mobility.[11, 19] Additionally, it appears as though large displacements of complementary severed ends in and of itself may not be what gives rise to translocations as these severed ends do not appear to yield distinct repair foci following DSB induction in a wide variety of experiments,[11, 16] though it may be that it does occur below the resolution of these techniques. However, the dynamics of complementary ends of DSBs may be synchronized (with repair foci clustering) for reciprocal translocations underlying some cancers, though non-reciprocal translocations are seemingly more common particularly with cancer progression.[3] Reciprocity in translocations may be explained by evidence showing reduced repair foci fusion correlates with treatments that decrease mobility.[16] Additionally, inhibition of the downstream DNA damage response (which has no effect on colocalization) increases translocation frequency, while inhibition of colocalization reduces it in a manner that depends on Mre11.[11]

Our work demonstrates unique mobility characteristics, including physical decoupling and structural relaxation, associated with chromatin of DSBs that may

likely correlate with the probability of translocations. From our findings with SSRP1 and SIRT6, it also appears possible to isolate the factors impacting chromatin mobility as potential targets for reducing (or, in the case of eradicating tumors, increasing) translocations. Future studies aimed at further delineation of the role of these protein factors in the repair mechanism is necessary to understand the complete response. Additionally, our work points to a definitive link between higher-order chromatin organization and structural state with chromatin mobility in the DNA damage repair process, which builds on previous work demonstrating transient condensation state changes as necessary for the repair mechanism and serving a possible signaling role. Future work is currently under way in our lab aimed at carefully investigating this response in heterochromatin versus euchromatin as it relates to chromatin mobility and structural remodeling. The cell line capable of doing these experiments was established by L. Lan and colleagues, who have shown differential recruitment of repair factors to differential states of chromatin condensation.[20] Further elucidation of the mechanisms and factors regulating chromatin structure and dynamics in the DNA damage repair is a promising avenue for the discovery of new cancer therapies.

Acknowledgements

We gratefully acknowledge the work and extensive intellectual insight of our University of Pittsburgh Medical Center – Hillman Cancer Center collaborators Li Lan (M.D., Ph.D.) and Ying Gao, with their specific

experimental contributions listed above. We gratefully acknowledge use of the multiphoton confocal imaging system from Mohammad Islam and help with use and analysis by Brian Holt (Carnegie Mellon, Biomedical Engineering). Additional thanks to Elizabeth Booth-Gauthier (UC Berkeley) for her helpful discussion and input throughout; Ge Yang (Carnegie Mellon Biomedical Engineering, Lane Center for Computational Biology, and Biological Sciences) and Minhua Qui (Carnegie Mellon Biomedical Engineering) for development and assistance with the LAPtrack71 suite of particle tracking programs; and Lynn Walker (Carnegie Mellon Chemical Engineering) for her insight into the polymer characterization and rheology (Carnegie Mellon Chemical Engineering. This work is supported by the NSF (NSF-CBET-0954421, CMMI-1300476 to KND and DMR-0619424 to Mohammad Islam) and the ARCS Foundation (STS), Bertucci Fellowship (STS), and James C. Meade Fellowship (STS).

References

1. V. Dion and S. M. Gasser, *Cell*, 2013, **152**, 1355-1364.
2. M. Nambiar, V. Kari and S. C. Raghavan, *Bba-Rev Cancer*, 2008, **1786**, 139-152.
3. O. V. Iarovaia, M. Rubtsov, E. Ioudinkova, T. Tsfasman, S. V. Razin and Y. S. Vassetzky, *Molecular cancer*, 2014, **13**.
4. J. A. Aten, J. Stap, P. M. Krawczyk, C. H. van Oven, R. A. Hoebe, J. Essers and R. Kanaar, *Science*, 2004, **303**, 92-95.
5. B. Jakob, J. Splinter, S. Conrad, K. O. Voss, D. Zink, M. Durante, M. Lobrich and G. Taucher-Scholz, *Nucleic Acids Res*, 2011, **39**, 6489-6499.
6. Y. Zhang, R. P. McCord, Y. J. Ho, B. R. Lajoie, D. G. Hildebrand, A. C. Simon, M. S. Becker, F. W. Alt and J. Dekker, *Cell*, 2012, **148**, 908-921.
7. S. T. Spagnol and K. N. Dahl, *Integr Biol-Uk*, 2014, **6**, 523-531.
8. B. Albert, I. Leger-Silvestre, C. Normand and O. Gadal, *Bba-Gene Regul Mech*, 2012, **1819**, 468-481.

9. S. C. Weber, A. J. Spakowitz and J. A. Theriot, *Proceedings of the National Academy of Sciences of the United States of America*, 2012, **109**, 7338-7343.
10. G. Guigas and M. Weiss, *Biophysical journal*, 2008, **94**, 90-94.
11. V. Roukos, T. C. Voss, C. K. Schmidt, S. Lee, D. Wangsa and T. Misteli, *Science*, 2013, **341**, 660-664.
12. M. J. Kruhlak, A. Celeste, G. Dellaire, O. Fernandez-Capetillo, W. G. Muller, J. G. McNally, D. P. Bazett-Jones and A. Nussenzweig, *Journal of Cell Biology*, 2006, **172**, 823-834.
13. B. Jakob, J. Splinter and G. Taucher-Scholz, *Radiat Res*, 2009, **171**, 405-418.
14. J. Liu, P. A. Vidi, S. A. Lelievre and J. M. K. Irudayaraj, *Journal of cell science*, 2015, **128**, 599-604.
15. B. Jakob, J. Splinter, M. Durante and G. Taucher-Schoiz, *Proceedings of the National Academy of Sciences of the United States of America*, 2009, **106**, 3172-3177.
16. P. M. Krawczyk, T. Borovski, J. Stap, T. Cijsouw, R. ten Cate, J. P. Medema, R. Kanaar, N. A. P. Franken and J. A. Aten, *Journal of cell science*, 2012, **125**, 2127-2133.
17. Y. Zhang and D. W. Heermann, *Chromosoma*, 2014, **123**, 103-115.
18. N. Dimitrova, Y. C. M. Chen, D. L. Spector and T. de Lange, *Nature*, 2008, **456**, 524-U551.
19. A. Becker, M. Durante, G. Taucher-Scholz and B. Jakob, *PloS one*, 2014, **9**.
20. L. Lan, S. Nakajima, L. Z. Wei, L. X. Sun, C. L. Hsieh, R. W. Sobol, M. Bruchez, B. Van Houten, A. Yasui and A. S. Levine, *Nucleic Acids Res*, 2014, **42**, 2330-2345.
21. G. Yang, L. A. Cameron, P. S. Maddox, E. D. Salmon and G. Danuser, *Journal of Cell Biology*, 2008, **182**, 631-639.
22. E. A. Booth-Gauthier, T. Alcoser, K. N. Dahl and G. Yang, *Biophysical journal*, 2012.
23. X. Michalet, *Biophysical journal*, 2011, **100**, 252-252.
24. P. Kollmannsberger and B. Fabry, *Annu Rev Mater Res*, 2011, **41**, 75-97.
25. K. N. Dahl, A. J. Engler, J. D. Pajerowski and D. E. Discher, *Biophysical journal*, 2005, **89**, 2855-2864.
26. P. N. Yaron, B. D. Holt, P. A. Short, M. Losche, M. F. Islam and K. N. Dahl, *Journal of nanobiotechnology*, 2011, **9**, 45.
27. M. Kollner and J. Wolfrum, *Chem Phys Lett*, 1992, **200**, 199-204.
28. A. Zidovska, D. A. Weitz and T. J. Mitchison, *Proceedings of the National Academy of Sciences of the United States of America*, 2013, **110**, 15555-15560.
29. S. T. Spagnol and K. N. Dahl, *Integr Biol-Uk*, 2015, **Manuscript In Review**.
30. D. Lleres, J. James, S. Swift, D. G. Norman and A. I. Lamond, *Journal of Cell Biology*, 2009, **187**, 481-496.
31. M. Y. Berezin and S. Achilefu, *Chem Rev*, 2010, **110**, 2641-2684.

32. D. D. Winkler and K. Luger, *Journal of Biological Chemistry*, 2011, **286**, 18369-18374.
33. M. Van Meter, Z. Y. Mao, V. Gorbunova and A. Seluanov, *Aging-Us*, 2011, **3**, 829-835.
34. R. C. Burgess, B. Burman, M. J. Kruhlak and T. Misteli, *Cell Rep*, 2014, **9**, 1703-1717.
35. J. H. Lee, Y. Kang, V. Khare, Z. Y. Jin, M. Y. Kang, Y. Yoon, J. W. Hyun, M. H. Chung, S. I. Cho, J. Y. Jun, I. Y. Chang and H. J. You, *Oncogene*, 2010, **29**, 1431-1450.
36. S. C. Weber, A. J. Spakowitz and J. A. Theriot, *Physical review letters*, 2010, **104**.
37. E. Soutoglou, J. F. Dorn, K. Sengupta, M. Jasin, A. Nussenzweig, T. Ried, G. Danuser and T. Misteli, *Nature cell biology*, 2007, **9**, 675-U121.

Chapter VII

Early Passage Dependence of Mesenchymal Stem Cell Mechanics Influences Cellular Invasion and Migration

Introduction

Human mesenchymal stem cells (hMSC), also known as multipotent mesenchymal stromal cells, are stromal-derived adherent cells originally identified by Friedenstein and colleagues.[1-4] These unique cells appear to be pericytes,[5] which arise from a lineage different than hematopoietic cells. Their myriad of unique properties include: marked self-renewal/*ex vivo* expansion from bone marrow, adipose tissue and umbilical cords; differentiation into bone, cartilage and adipose tissue; selective (not global) immunomodulatory properties; the production of bioactive cytokines and proteins and secretion of antimicrobial peptides; facilitation of engraftment and suppression of rejection; and migration to sites of inflammation.[6-11] These varied properties make them ideal for use in a variety of clinical investigations involving cell replacement, tissue repair and regeneration, as well as immunomodulation. Many thousands of patients now have received these cells for a variety of indications.[12-14]

Many groups continue to explore optimization of techniques for collection, expansion and administration of hMSCs based on the desired application. Intravenous administration raises numerous mechanical considerations for optimal clinical performance. Injected hMSCs entering tissues

must be sufficiently robust to survive the shear stress of a non-adherent fluid-phase injection.[15] Following injection, hMSCs must be able to invade and translocate tight interstitial spaces of extracellular matrix.[16] This combination of mechanical states requires a cell to exhibit complex set of viscous flow, elastic stretch and recovery as well as cellular force generation.[17]

Complex cellular viscoelastic mechanics is a function of complex, integrated intracellular structures, primarily actin cytoskeletal networks, as well as their reorganization in response to applied stress. hMSCs are well-spread cells with fine actin filament structures,[18] and the cytoskeleton is not strongly integrated with other rigid cell structures such as the nucleus.[19] Structurally, there are numerous changes within hMSCs observed during differentiation including a coarsening of the actin stress fibers[18, 20] and stiffening of actin cytoskeletal network.[21] Cellular mechanics, however, is governed not only by the cytoskeletal structure but also by the molecular motor force generation and the resulting tension imposed on the network.[17, 22] There have been numerous studies looking at the role of extracellular matrix (ECM) mechanical properties and endogenous cell forces during differentiation.[23, 24]

Previous studies of hMSCs have provided conflicting accounts of the stiffness of adhered hMSCs in both form (viscoelastic model) and magnitude. Also, comparisons of early passage and later passage hMSCs showed varying mechanical changes. In one study using AFM of adhered cells, the stiffness (reported as Young's modulus) decreased during differentiation.[25] In another study using similar methodologies, the stiffness (reported as the inverse mechanical

compliance) increased during differentiation.[18] Low-strain deformation of non-adherent cells using optical stretching showed no change in stiffness during differentiation.[18] Measurements of cell mechanics are prone to these inconsistencies due to different preparations, measurement types, mechanical models and analyses.[26]

As such, in this study, we have examined mechanics of non-adherent cells since we are most concerned with the stiffness of cells in suspension during the injection procedure. We examine viscoelasticity of early passage hMSCs isolated for clinical use using micropipette aspiration. This non-adherent, high-strain technique is able to measure the innate material mechanics of cells and changes during differentiation. Also in line with application, we examine the ability of adherent hMSCs to invade and move through micropillar arrays, which mimic extracellular matrix spaces. Together these measurements provide a more clinically-relevant set of assays to quantify hMSC behavior that, when taken in consort with previous studies, show the resilient nature of the hMSC and its efficacy in therapeutic use.

Material and methods

Cell isolation and Culture

Samples of bone marrow aspirates from the posterior iliac crests of subjects were obtained as the starting material for isolating and *ex vivo* expansion of the hMSCs in tissue culture using previously published methods.[27-29] The hMSCs were cultured in DMEM low glucose supplemented with 10% FBS, 1%

L-glutamine and 1% Penicillin-Streptomycin. Human foreskin fibroblasts, HFF (SCRC-1041, ATCC), are a pooled sample of non-immortalized fibroblasts and were cultured in DMEM high glucose supplemented with 15% FBS and 1% Penicillin-Streptomycin.

Micropipette Aspiration

Cells were trypsized and resuspended in a PBS solution with 3 μM cytochlasin D (Sigma-Aldrich), 0.125 μM nocodazole (Sigma-Aldrich) with 0.3 μg/mL propidium iodide (Invitrogen). Micropipettes were pulled from 1 mm glass capillaries (WPI) using a PMP102 Micropipette puller (Microdata) with ends of the micropipette tips between 6 and 10 μm in diameter. Micropipettes were backfilled with phosphate buffered saline (PBS) and 2% bovine serum albumin (BSA) and attached to a water-filled reservoir. A micromanipulator (Narishige) was used to move the micropipette to the cells of interest. A set pressure (ΔP) was applied through a syringe to the micropipette in parallel with a pressure transducer (WPI). A set pressure was applied and maintained with a ball valve (McMaster-Carr) and the deformation of the cell into the pipette was tracked over time $L(t)$. A schematic is provided in Figure 7.1. Imaging was done using a 63x (1.4 NA) oil immersion objective of an inverted microscope (DMI6000, Leica, Buffalo Grove, IL) in a controlled live-cell imaging chamber.

Mechanical Analysis

From the known constant applied pressure, ΔP, and deformation over time, $L(t)$, normalized to the radius of the pipette, R_p, we determine a creep compliance, $J(t)$ as shown in Figure 7.1. The prefactor, α, is determined from non-dimensional shape factors[19] and is set to 4.1.

$$J(t) = \alpha \frac{L(t)}{R_p} \frac{1}{\Delta P} \tag{1}$$

Plotting the deformation over time, where $J(t)$ versus t is a straight line with a y-axis offset, suggests that hMSCs are viscoelastic fluids. From the model of creep compliance of an instantaneous stress for a linear viscoelastic fluid (Maxwell model), we can extract the elastic stiffness or Young's modulus, E, and the viscosity, μ.

$$J_{fluid}(t) = \frac{1}{E} + \frac{t}{\mu} \tag{2}$$

With increased passage, the hMSCs mechanics transitions to a viscoelastic solid (Voigt model) wherein $J(t)$ exhibits an exponential dependence on t reaching an asymptote.

$$J_{solid}(t) = \frac{1}{E}(1 - e^{-\frac{E}{\mu}t}) \tag{3}$$

Comparisons of a viscoelastic fluid (Equation 2) and a viscoelastic solid (Equation 3) typically involve the calculation of a crossover time, τ, wherein $J_{fluid} = J_{solid}$.

$$\tau = \left(\frac{E}{\mu}\right)^{-1} = \frac{\mu}{E} \tag{4}$$

PDMS Micropillars

Polydimethylsiloxane (PDMS) micropillar arrays were prepared for the studies similar to previous methods.[30, 31] Micropillar size was held constant with a 10 μm diameter and 20 μm height, but the distance between micropillars was altered: 8 μm, 10 μm, and 12 μm spacing. Polydimethylsiloxane (PDMS, Sylgard 184, Dow Corning, Midland, MI) micropillar arrays were prepared over a silicon wafer using a 10:1 solution of PDMS to curing agent, incubating at 60ºC for 8-12 hrs and removed. Solid PDMS pillars were plasma treated (Harrick Plasma Cleaner and Sterilizer PDC-32G, Ithaca, NY) and coated with fibronectin (20 μg/mL in PBS, Sigma Aldrich) for 20 min at room temperature. Cells were seeded on the micropillar array at 20% confluency and incubated for 24 hours.

Invasion Analysis

Micropillar invasion was quantified by counting the numbers of cells growing inside the micropillars normalized by the number growing outside the micropillars. Statistical significance was determined by Student's t-test between individual samples with $p < 0.05$. More than 100 cells per condition were considered. Within the pillars, we measured persistence length of the cell as the longest length of the cell in the 8 μm micropillars before cells turn or branch within the pillars (Figure 7.1 for schematic).

Cell Labeling and Imaging

After 24 hours culture in the PDMS micropillars, cells were washed with PBS to remove culture media and non-adherent cells. Cells were fixed with 3.7% formaldehyde in PBS for 20 min and permeabilized with 0.2% Triton X-100 in PBS for 20 min. Cells were labeled with rhodamine phallodin for F-actin (165 nM, Invitrogen) and DAPI for DNA (300 nM, Invitrogen). Samples were imaged on a Nikon Eclipse TS100 with a 20x (0.4 NA) dry objective for fixed cell experiments. Image analysis of micropipette aspiration deformation and cell invasion into the micropillars was performed using ImageJ.

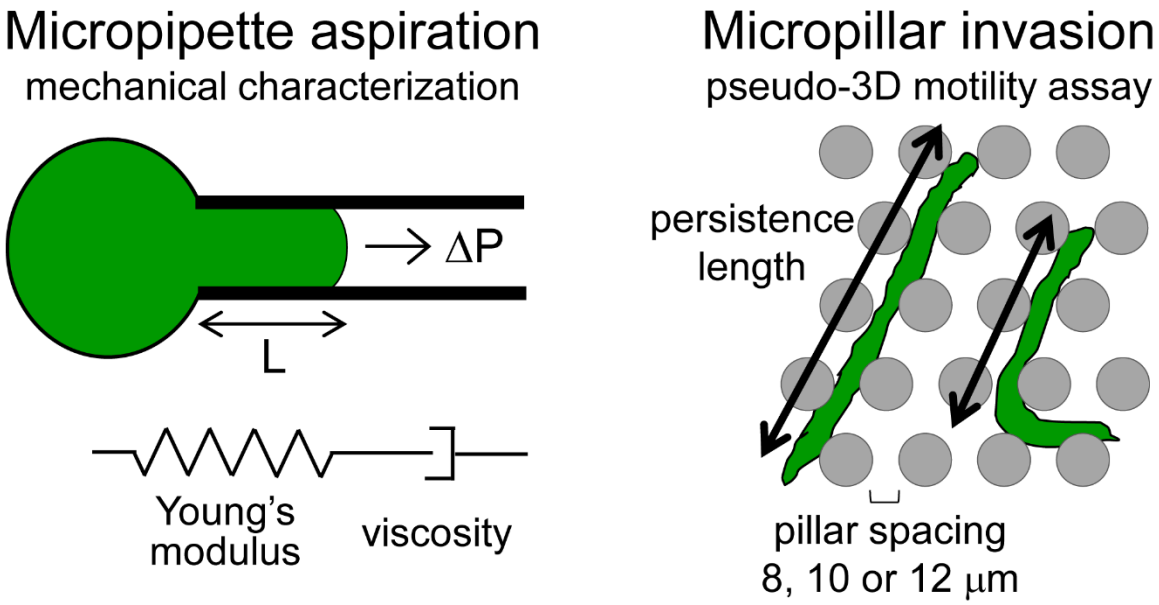

Figure 7.1: Schematics of methodologies for cellular analysis. *Viscoelastic cell creep is measured by micropipette aspiration by pulling a cell into a micropipette with a constant, instantaneous aspiration pressure and following the projection length over time. From plots of aspiration data, we observe that primary hMSCs can be modeled mechanically as viscoelastic fluids. The micropillar invasion*

assay allows quantification of cellular motility into small, pseudo-three dimensional extracellular spaces. The pillar spacing refers to the edge-to-edge spacing between the pillars. Also, cellular morphology can be determined while cells are deformed in the micropillars.

Results

Measuring Mechanics of Primary hMSCs Measured by Micropipette Aspiration

We first measured the viscoelastic properties of early passage hMSCs using micropipette aspiration. With instantaneous applied pressure, we followed the deformability of cells over time (see Methods and Figure 7.1). The hMSCs deformed nearly indefinitely with the application of applied force (Figure 7.2).

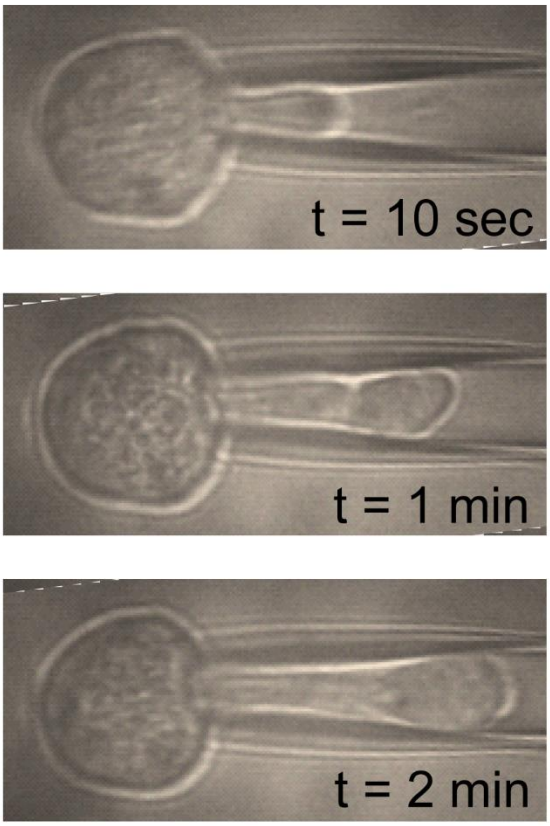

Figure 7.2: Micropipette aspiration of hMSCs. *Sample images of micropipette aspiration of hMSC with a set pressure of 3.8 kPa show the increased deformation of the cell into the pipette with increased time.*

This increase in deformability, normalized to pressure as creep compliance (*J*, see Methods) is a straight line with time for all of the samples considered (Figure 7.3). At least five cells were measured for each sample, and there was extremely small variability between cells. Comparison of different patient samples (labeled A, B and C) showed statistically different responsiveness (Figure 7.3). However, while the differences are statistically different, there is still small variability between samples compared to deviations from other cell types.

Fibroblast deformability regime, characterized previously using identical methodologies [32] are shown in gray in Figure 7.3.

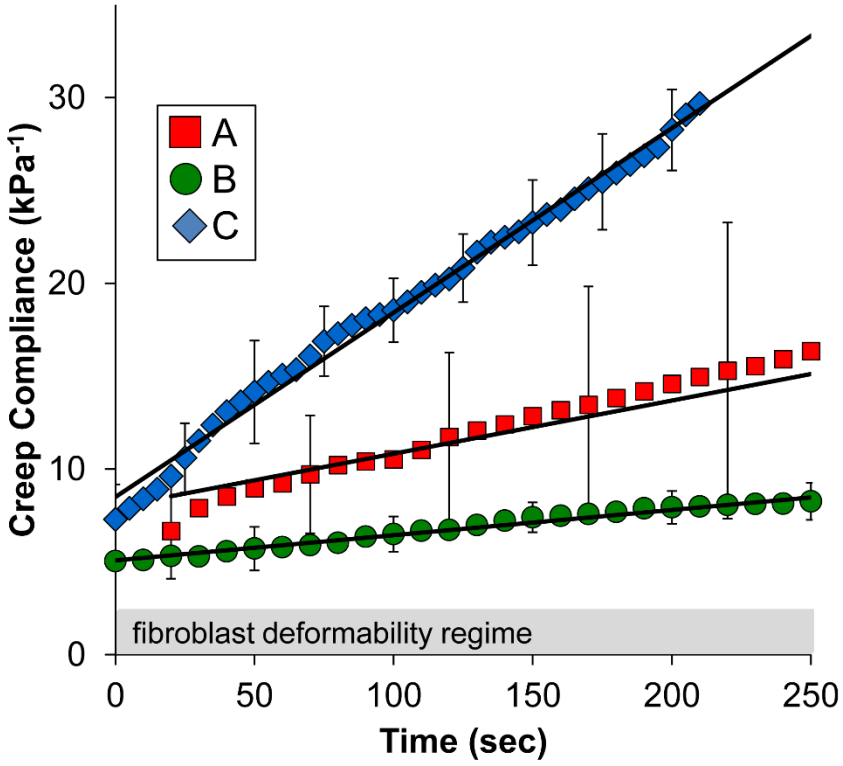

Figure 7.3: Quantification of creep compliance of hMSCs for three patient samples. *Creep compliance, J, plotted over time for the mean of at least five cells per sample (error bars are SEM) show the statistical variation between samples. Higher creep compliance represents more deformability of the cells per applied stress, while cells with a lower creep compliance are less deformable. Linear fits are shown to the data. For contrast, deformability of fibroblasts occurs in the gray region, but both the magnitude and form of the fibroblast creep compliance are strikingly dissimilar from the hMSCs; fibroblasts are grossly less deformable than hMSCs.*

When creep compliance was fit to a model of a viscoelastic fluid (see Methods, Equation 2), we are able to determine the Young's modulus of elasticity and Newtonian viscosity (Figure 7.4). Although there is no major difference in the Young's modulus across different patient cells, the viscosity is higher for patient B's sample (Figure 7.4). Thus, the reduction in deformability of patient B's sample (from Figure 7.3) arises from the increased cellular viscosity (Figure 7.4).

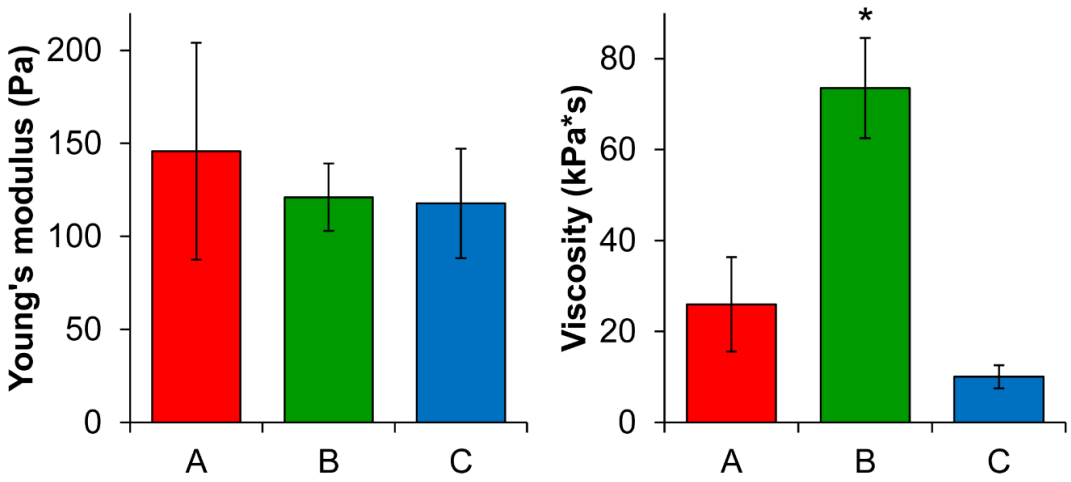

Figure 7.4: Mechanical parameters of hMSCs determined from creep compliance data. *Fitting creep compliance data to a model of a linear viscoelastic fluid allows determination of elasticity (Young's modulus) and viscosity. The least deformable patient cells (sample B) show no difference in elasticity, only an increase in viscosity. All samples are statistically similar ($p > 0.05$) except for viscosity of sample B (* $p < 0.01$).*

hMSCs Grow into Micropillars

In addition to characterizing the cell deformability and mechanics, we also

examined *in situ* cellular deformability. Investigating cell crawling into differentially spaced micropillars allows for visualization of functional deformability as well as mimicking extracellular matrix invasion. Fibroblasts (primary human foreskin fibroblasts, HFFs, see Methods) were considered due to their ability to invade the extracellular matrix during wound healing.[33] When cells are cultured on flat portions outside of the micropillar arrays, hMSCs have a much larger spread area than primary human fibroblasts, with finer actin filaments.[18] Despite their larger size, hMSCs invade into tight micropillars as do HFFs (8 μm between micropillars, Figure 7.5).

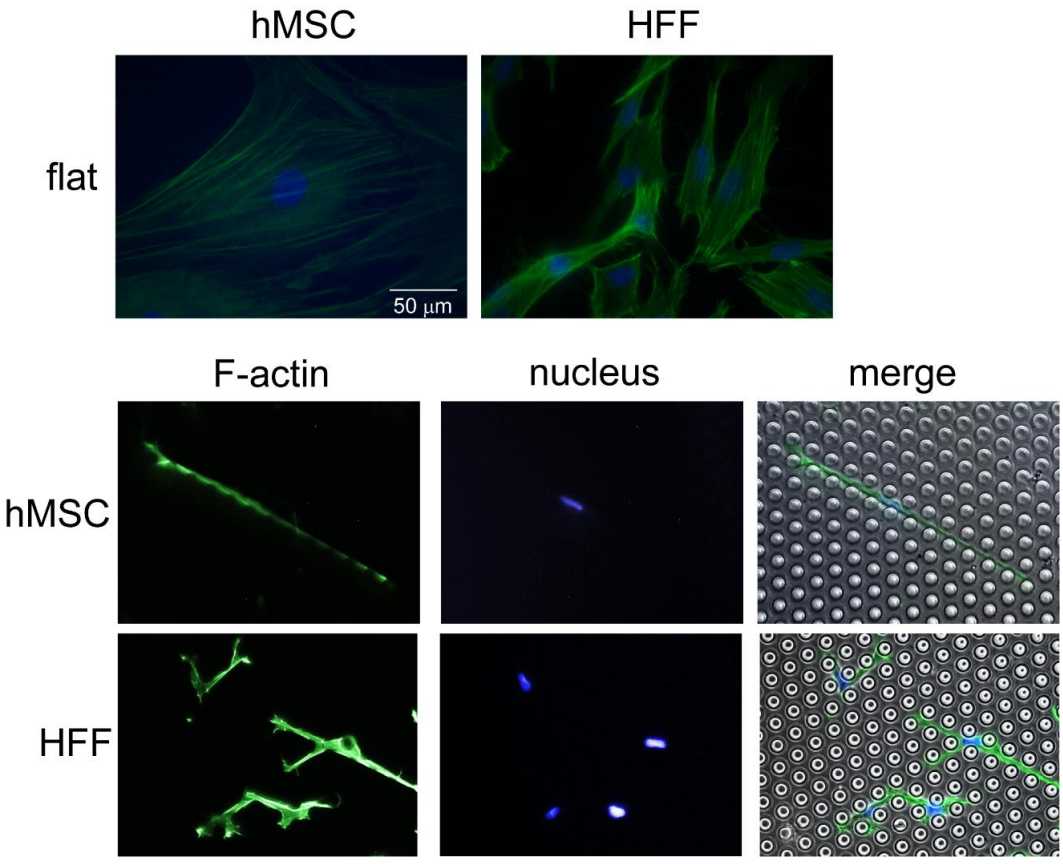

Figure 7.5: hMSCs and fibroblasts grown on flat surfaces and 8 μm spaced micropillars. *Labeling of the F-actin (green) cytoskeletal structures shows the organization of the cytoskeleton, polarization of the cell and general cell boundaries. Labeling of DNA (blue) inside the nucleus provides an idea of cell number and general idea of centroid. In the absence of pillars (flat), hMSCs are far larger and more spread with finer cytoskeletal features. Within 8 μm (spacing edge-to-edge) micropillars, hMSCs elongate along the pillars whereas fibroblasts (HFF) tend to branch. All images are to scale with one another.*

We quantified the probability of invasion into micropillars (see Methods) for differentially spaced micropillars (8, 10 and 12 μm spacing). As expected, there was a higher probability for cells to enter larger spaced micropillars (Figure 7.6). Interestingly, the patient cell line that was the least mechanically deformable (patient B) had the best probability of entering micropillars with small spacing (Figure 7.6), invading micropillars of all size spacing relatively uniformly.

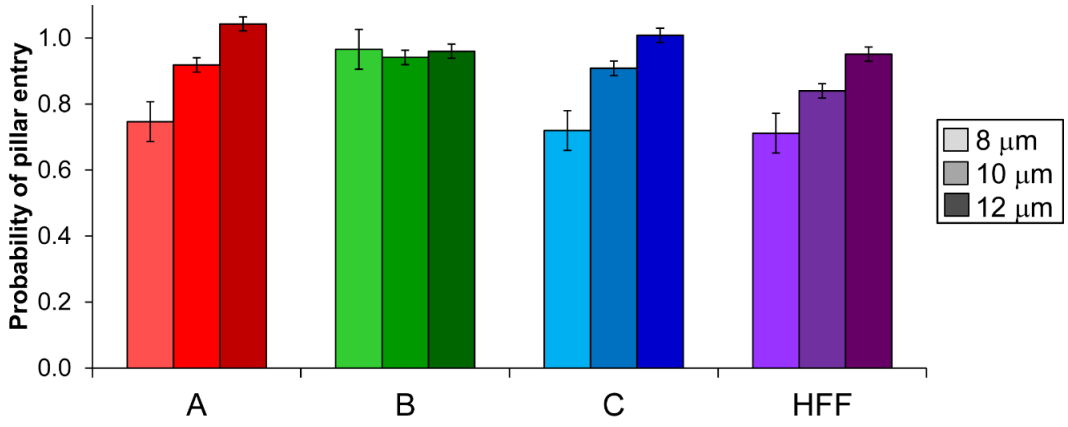

Figure 7.6: Entry of cells into differentially spaced micropillars. *Small pillar spacing (lighter colors) had a significantly reduced probability of cell entry into the micropillars based on pillar spacing except for sample B (error is SEM, n > 100 cells). Samples are statistically different from 8, 10, 12 μm by Student t-test p < 0.01 except for sample B.*

Differential Cell Elongation in Micropillars

In addition to quantifying cell entry into micropillars, we also examined morphology of cells within the micropillars. From the actin labeled cytoskeleton (Figure 7.5), we measured persistence of the cells (see Methods and Figure 7.1); higher persistence length suggests a longer extension and no branching. This was the most dramatic in the tightest pillar spacing, 8 μm. From morphological examination, we see that hMSCs are more elongated and less branched than fibroblasts (Figure 7.7). Fibroblast branching is likely associated with a stiff, solid-like cytoskeleton and leading edge force generation.[34] Since hMSCs branch less and are mechanically viscoelastic fluids (Figures 7.3 and 7.4), we suggests a potentially different mode of invasion into pillars by hMSCs. That is, it is possible that the hMSCs "flow" between the micropillars.

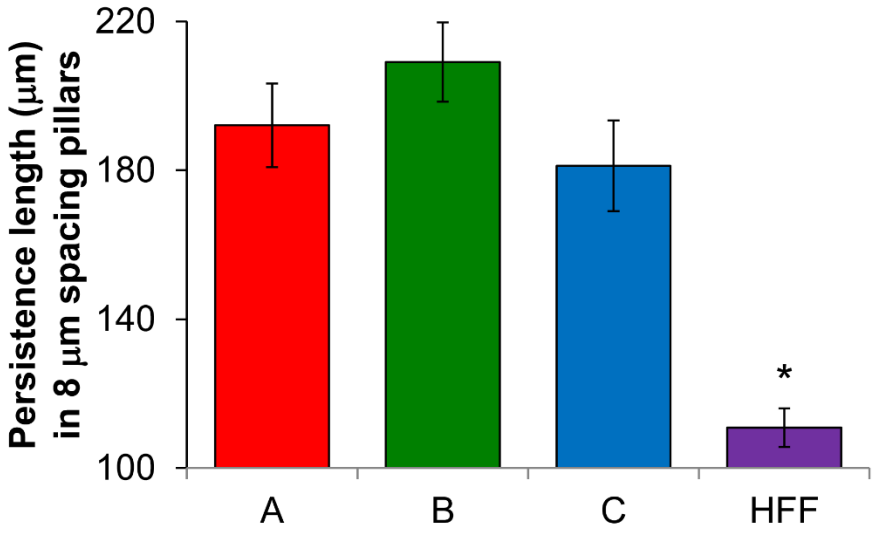

Figure 7.7: Persistence length of cells within 8 μm micropillars. *Persistence length in this case is the length of a cell without a branch. hMSCs are consistent with one another ($p > 0.07$) but significantly different (* $p < 10^{-6}$) than the highly branched fibroblasts in the micropillars (Figure 7.5).*

Increased Cell Passage Alters Cell Mechanics and Invasion Potential

Previous reports of hMSCs from our group and others have shown that commercial hMSCs behave as viscoelastic solids[19, 25] rather than as viscoelastic fluids observed here. To test the possible differences we passaged one line of hMSCs and measured mechanics by micropipette aspiration. We observed a dramatic change from a viscoelastic fluid (a straight line of creep compliance with time) to a viscoelastic solid (exponential increase to a plateau value) as observed in Figure 7.8. While this makes the parameters poorly comparable, there is a crossover time $\tau = 23$ minutes (see Methods, Equation 4). Before ~20 minutes, the late passage cells are more deformable, but the time dependence of the mechanics suggests that after ~20 minutes these cells will be less deformable. We similarly

tested these passaged cells (C-2) in the micropillar invasion assay. The effective stiffening and transition to viscoelastic solid cells also leads to an increase in micropillar invasion (Figure 7.8).

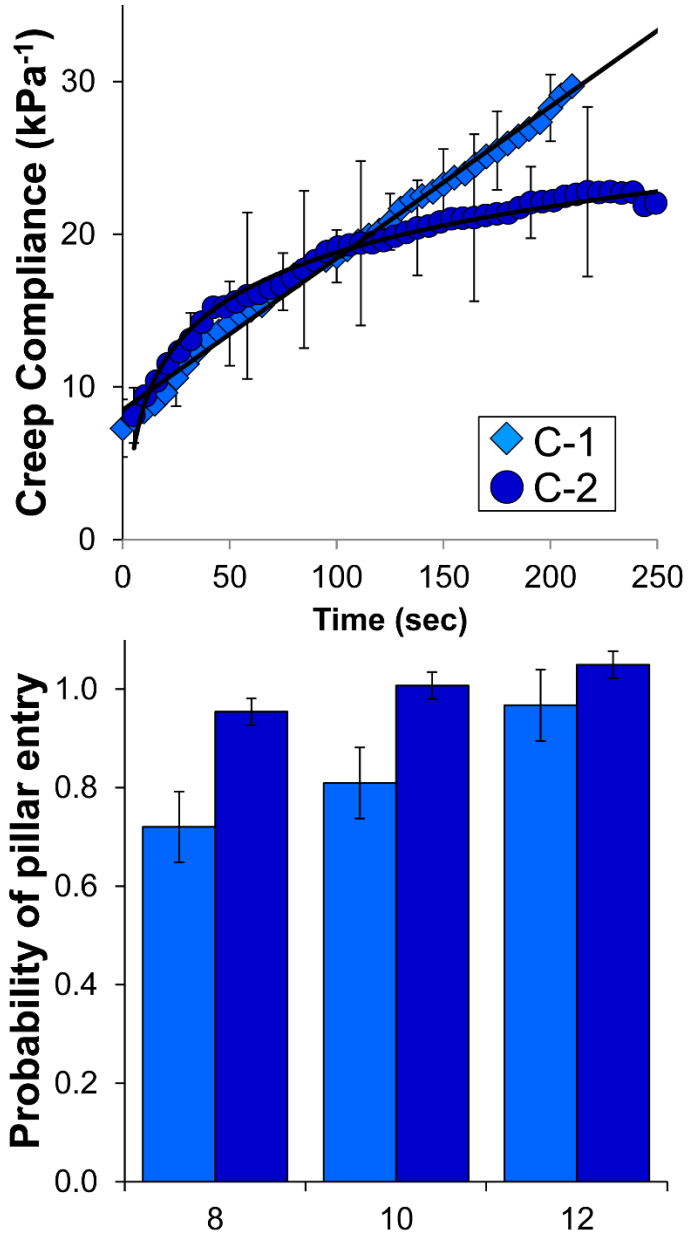

Figure 7.8: Increased passage alters cell mechanics and invasion into micropillars. *We passaged hMSC patient cell line C multiple times (C-2) and measured cell mechanics using micropipette aspiration. Plotted together with*

data from Figure 7.2 (C-1), the creep versus time shows a functional transition from a viscoelastic fluid (linear fit shown) to a viscoelastic solid (exponential fit shown). Invasion data of (C-2) plotted with data from Figure 7.6 (C-1) shows an enhancement of hMSC invasion in to 8 μm spaced micropillar arrays.

Discussion

Using complementary techniques we are able to assess mechanics of cells in solution as well as cell deformability of cells within tight interstitial spaces. In comparison to previous micropipette aspiration mechanical measurements, we observe that the hMSCs passaged 2-3 times here are similarly deformable as commercially available hMSCs with comparable elastic and viscous parameters.[19] Importantly, extremely low passage hMSCs examined here deform as viscoelastic fluids. This suggests that only a few passages of hMSCs are sufficient to greatly alter the mechanical nature of the cells. This phenomena has also been observed by AFM and by thickening of stress fibers within hMSCs with increased passage.[18]

We suggest that hMSCs deforming as viscoelastic fluids when suspended is a benefit for clinical injection. Most adherent cells deform as viscoelastic solids. However, leukocytes have been shown for decades to deform as Maxwell fluids,[35] the model that fit the data here. There are several analogies that can be drawn between a circulating leukocyte and an injected hMSC. Both cell types must survive the harsh fluid dynamics of the circulation and tight regions of the capillaries. Both cell types home to sites of inflammation[9, 11, 27] or damage and

must transition to a phenotype that invades into extracellular matrix. Thus, the best hMSCs for clinical injection survival are likely the most early passage cells. We considered the survival of cells through a 30 gauge needle at 100 μL/min, and we found 83 +/- 17% cell survived. This was compared to similar methodologies we previously published with commercial hMSCs (Lonza) wherein 1.0 +/- 0.2% survived.[19]

Contrary to likely survival by injection, we found that the increased elasticity associated with increased passage does not inhibit, but rather improves, the invasion of cells into micropillars. It may appear contradictory that more elastic cells have a greater ability to enter tight spaces; we tend to think that viscous fluid could more easily flow in. However, within micropillars the same contractility that induces increased cell stiffness simultaneously provides the driving force for invasion from molecular machinery within the cells from these same cytoskeletal filaments.[17, 30] Thus, independent characterization through MPA and the micropillar invasion assay allows us to suggest mechanisms of cellular invasion, and we suggest that it is the driving force from motor activity leading to enhanced contractility that simultaneously increases cell stiffness measured by MPA. As measured by persistence length, the hMSCs are mostly elongated within the structures, limiting their resistance. Additionally, previous work has also shown that stiffer cells more readily fluidize upon stress application and deformation.[17] Generally, through this study we find that overly soft cells deform poorly into tight spaces.

We suggest that mechanical tools could be used to select cells prior to

clinical use. Currently, cells are screened for biological characteristics including stem-ness, etc. It may prove useful for clinical applications to select for mechanically "optimal" cells from a pool delivery to the patient to reduce mechanically-induced necrosis or cell lysis. Recently, microfluidic devices with the capability of measuring cell mechanics have shown promise for larger-scale operations.[36-38]

Acknowledgements

We gratefully acknowledge use of microfabrication facilities of Shelley Anna and help from Sharon Vuong (Carnegie Mellon, Chemical Engineering) as well as specific insight for use of micropillars with cells by Benoit Ladoux (Université Paris Diderot, Physics). This work is supported by the NSF (NSF-CBET-0954421 and CMMI-1300476 to KND), fellowships from ARCS, Bertucci, and James C. Meade (STS) and National Center for Regenerative Medicine and Cell Therapy Integrated Services (CTIS) Core Facility of the Case Comprehensive Cancer Center (P30 CA43703 to HML). BL acknowledges financial supports from the Agence Nationale de la Recherche (Program Nanotechnologies & Nanosystems 2013 ANR 13-NANO-0011), the Human Frontier Science Program (grant RGP0040/2012), the Institut Universitaire de France and the Mechanobiology Institute (Singapore).

References

1. M. Dominici, K. Le Blanc, I. Mueller, I. Slaper-Cortenbach, F. Marini, D. Krause, R. Deans, A. Keating, D. Prockop and E. Horwitz, *Cytotherapy*, 2006, **8**, 315-317.
2. A. J. Friedenstein, R. K. Chailakhyan, N. V. Latsinik, A. F. Panasyuk and I. V. Keiliss-Borok, *Transplantation*, 1974, **17**, 331-340.
3. A. J. Friedenstein, A. A. Ivanov-Smolenski, R. K. Chajlakjan, U. F. Gorskaya, A. I. Kuralesova, N. W. Latzinik and U. W. Gerasimow, *Experimental hematology*, 1978, **6**, 440-444.
4. M. F. Pittenger, A. M. Mackay, S. C. Beck, R. K. Jaiswal, R. Douglas, J. D. Mosca, M. A. Moorman, D. W. Simonetti, S. Craig and D. R. Marshak, *Science*, 1999, **284**, 143-147.
5. A. I. Caplan, *Cell stem cell*, 2008, **3**, 229-230.
6. P. Bianco, P. G. Robey and P. J. Simmons, *Cell stem cell*, 2008, **2**, 313-319.
7. S. P. Bruder, N. Jaiswal and S. E. Haynesworth, *Journal of cellular biochemistry*, 1997, **64**, 278-294.
8. A. I. Caplan, *Journal of cellular physiology*, 2007, **213**, 341-347.
9. G. Chamberlain, J. Fox, B. Ashton and J. Middleton, *Stem cells*, 2007, **25**, 2739-2749.
10. J. M. Karp and G. S. Leng Teo, *Cell stem cell*, 2009, **4**, 206-216.
11. M. B. Murphy, K. Moncivais and A. I. Caplan, *Experimental & molecular medicine*, 2013, **45**, e54.
12. J. Ankrum and J. M. Karp, *Trends in molecular medicine*, 2010, **16**, 203-209.
13. E. J. Culme-Seymour, N. L. Davie, D. A. Brindley, S. Edwards-Parton and C. Mason, *Regenerative medicine*, 2012, **7**, 455-462.
14. L. Sensebe, M. Krampera, H. Schrezenmeier, P. Bourin and R. Giordano, *Vox sanguinis*, 2010, **98**, 93-107.
15. B. D. Riehl, J. S. Lee, L. Ha and J. Y. Lim, *Journal of the Royal Society, Interface / the Royal Society*, 2015, **12**.
16. K. Wolf and P. Friedl, *Trends in cell biology*, 2011, **21**, 736-744.
17. P. Kollmannsberger, C. T. Mierke and B. Fabry, *Soft Matter*, 2011, **7**, 3127-3132.
18. J. M. Maloney, D. Nikova, F. Lautenschlager, E. Clarke, R. Langer, J. Guck and K. J. Van Vliet, *Biophysical journal*, 2010, **99**, 2479-2487.
19. A. J. Ribeiro, S. Tottey, R. W. Taylor, R. Bise, T. Kanade, S. F. Badylak and K. N. Dahl, *Journal of biomechanics*, 2012, **45**, 1280-1287.
20. P. S. Mathieu and E. G. Loboa, *Tissue engineering. Part B, Reviews*, 2012, **18**, 436-444.
21. K. M. McAndrews, D. J. McGrail, N. D. Quach and M. R. Dawson, *Physical biology*, 2014, **11**, 056004.
22. B. D. Hoffman and J. C. Crocker, *Annual review of biomedical engineering*, 2009, **11**, 259-288.

23. Y. Sun, C. S. Chen and J. Fu, *Annual review of biophysics*, 2012, **41**, 519-542.
24. A. J. Engler, S. Sen, H. L. Sweeney and D. E. Discher, *Cell*, 2006, **126**, 677-689.
25. T. Bongiorno, J. Kazlow, R. Mezencev, S. Griffiths, R. Olivares-Navarrete, J. F. McDonald, Z. Schwartz, B. D. Boyan, T. C. McDevitt and T. Sulchek, *Journal of biomechanics*, 2014, **47**, 2197-2204.
26. Y.-l. Wang and D. E. Discher, *Cell mechanics*, Elsevier Academic Press, Amsterdam ; Boston, 2007.
27. O. N. Koc, S. L. Gerson, B. W. Cooper, S. M. Dyhouse, S. E. Haynesworth, A. I. Caplan and H. M. Lazarus, *Journal of clinical oncology : official journal of the American Society of Clinical Oncology*, 2000, **18**, 307-316.
28. H. M. Lazarus, S. E. Haynesworth, S. L. Gerson, N. S. Rosenthal and A. I. Caplan, *Bone marrow transplantation*, 1995, **16**, 557-564.
29. H. M. Lazarus, O. N. Koc, S. M. Devine, P. Curtin, R. T. Maziarz, H. K. Holland, E. J. Shpall, P. McCarthy, K. Atkinson, B. W. Cooper, S. L. Gerson, M. J. Laughlin, F. R. Loberiza, Jr., A. B. Moseley and A. Bacigalupo, *Biology of blood and marrow transplantation : journal of the American Society for Blood and Marrow Transplantation*, 2005, **11**, 389-398.
30. E. A. Booth-Gauthier, V. Du, M. Ghibaudo, A. D. Rape, K. N. Dahl and B. Ladoux, *Integrative biology : quantitative biosciences from nano to macro*, 2013, **5**, 569-577.
31. M. Ghibaudo, J. M. Di Meglio, P. Hersen and B. Ladoux, *Lab on a chip*, 2011, **11**, 805-812.
32. K. N. Dahl, P. Scaffidi, M. F. Islam, A. G. Yodh, K. L. Wilson and T. Misteli, *Proceedings of the National Academy of Sciences of the United States of America*, 2006, **103**, 10271-10276.
33. W. U. Hassan, U. Greiser and W. Wang, *Wound repair and regeneration : official publication of the Wound Healing Society [and] the European Tissue Repair Society*, 2014, **22**, 313-325.
34. T. M. Freyman, I. V. Yannas, R. Yokoo and L. J. Gibson, *Experimental cell research*, 2002, **272**, 153-162.
35. C. Dong, R. Skalak and K. L. Sung, *Biorheology*, 1991, **28**, 557-567.
36. I. Sraj, C. D. Eggleton, R. Jimenez, E. Hoover, J. Squier, J. Chichester and D. W. Marr, *Journal of biomedical optics*, 2010, **15**, 047010.
37. B. Lincoln, F. Wottawah, S. Schinkinger, S. Ebert and J. Guck, *Methods in cell biology*, 2007, **83**, 397-423.
38. A. J. Mach, O. B. Adeyiga and D. Di Carlo, *Lab on a chip*, 2013, **13**, 1011-1026.

Chapter VIII

Conclusions

Summation and Conclusions

From chromosome positioning and movement within the nucleus to its continuous structural remodeling, it is evident that these biological features are underwritten in no small part by the physical properties of chromatin. In this Thesis, we aimed to elucidate the physical underpinnings of genome function and organization related to normal nuclear processes as well as during physiological and pathological changes. To that end, we develop techniques that enable investigation of the genome as a dynamic entity. Further, we illuminate how the cell harnesses the complex physical properties of macromolecules to deliver genome functions necessary for survival.

Structural remodeling of chromatin is a continuous process in human cell nuclei. This forms the basis for evolving functional needs requiring access to the linear sequence and, further, impacts the dynamic mobility of chromatin through altered mechanical compliance. In Chapter II we develop fluorescence lifetime imaging microscopy (FLIM) as a high-throughput technique for quantifying and spatially resolving chromatin condensation state in human cell nuclei. Through a series of experiments with nuclear chromatin *in situ* and DNA solutions *in vitro*, we demonstrate that the fluorescence lifetime is acutely sensitive to local solution viscosity on length scales of angstroms up to < 10 nm in a manner that is dependent on condensation state. In the decondensed state, we observe a more

compliant and flexible chromatin fiber whose fluctuations depend on local solution viscosity. Further, decondensation within the nucleus serves to enhance the surrounding viscosity itself, thereby compounding this effect. Leveraging these measureable changes to chromatin mechanical state that accompany functional changes, we can spatially resolve regions of differential condensation within nuclei as well as global changes through high-throughput measurements of many nuclei under varying conditions. We demonstrate the utility of this technique for physiological and pathological scenarios throughout other Chapters.

The physical mechanisms regulating chromatin dynamics in human cell nuclei are illuminated in Chapter III. We show that chromatin undergoes "active" subdiffusion within the human cell nucleus as shown in Equation 1. The temporal dependence quantified in the diffusive exponent (β) is dictated by the baseline viscoelasticity, crowding, binding and obstruction of chromatin within the nucleus, but enhanced by the presence of molecular motor proteins to drive it out of equilibrium and beyond simple thermal energy. Further, we highlight that cytoskeletal motor forces propagated through the Linker of Nucleoskeleton and Cytoskeleton (LINC) complex are a primary source of these active forces. By contrast, we show alterations to chromatin compliance through condensation state changes (as measured in Chapter II) are decoupled from molecular motor effects, influencing in the amplitudes of the motion (D_{eff}) in a manner conceptually similar to changes to the effective "tube size" in polymer reptation. These results are summarized in Figure 8.1, outlining a physiological regime over which the cell may tune chromatin dynamics for functional changes.

$$MSD = D_{eff}\tau^{\beta} \quad (1)$$

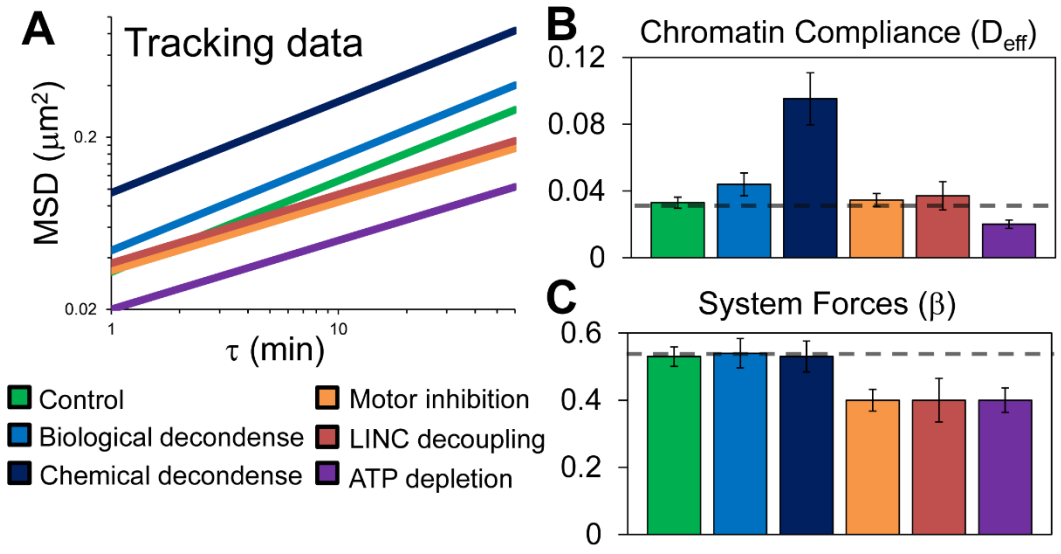

Figure 8.1: Summary of previous control studies of nuclear particle tracking and discrete impacts on chromatin compliance and system forces. *(A) Fits of experimental data to mean squared displacement (MSD) versus τ on a log-log graph yield straight lines. (B) The intercept, D_{eff} from Equation 1, is modulated by decondensation of chromatin by trichostatin A (biological) and daunomycin (chemical). (C) Conversely, system forces, β from Equation 1, are altered by myosin inhibiting Blebbistatin, altered LINC complex protein expression and ATP depletion.*

In Chapter IV we begin to investigate dynamic chromatin remodeling and mobility in the context of physiological processes, specifically for vascular endothelial growth factor (VEGF) stimulated changes in nuclear organization and gene expression in endothelial cells. We show VEGF stimulation enhances

chromatin dynamics in a manner that evolves with duration in the response. Initially, chromatin dynamics are driven primarily by molecular motor forces exerting temporal influence through the diffusive exponent. Consistent with this, we show an increase in actin fibers around the nucleus and increased nuclear deformations that collectively point to cytoskeletal forces as the likely source for enhanced dynamics (consistent with Chapter III). After this initial response, we observe these increased molecular motor forces dissipate and return to control levels, with enhanced chromatin dynamics driven instead by large scale chromatin decondensation. We verify the step-wise increase in chromatin decondensation using FLIM, highlighting the mechanical link and complementarity of FLIM and particle tracking. These results are consistent with the known temporal changes in the stimulated gene expression profile for VEGF stimulation, where maximal chromatin decondensation and transcriptional activation occurs hours after stimulation. These findings also point to a role for mechanical force propagation as a means of enhancing the transport and kinetic events associated with nuclear reorganization and possible chromatin decondensation, with implications for gene activation by mechanical stimuli (termed mechanotransduction) in addition to the obvious role observed here for chemical stimuli.

Building on mechanical pathways that influence chromatin dynamics, in Chapter V we investigate a disease pathology associated with a mutated version of the structural and mechanical protein of the nucleoskeleton, lamin A. The effects of the mutated protein, called progerin, clinically manifest most prominently in the force-responsive tissues of the cardiovascular and skeletal

systems. We show that dysfunction in this prominent structural and mechanical protein of the nucleus results in nucleoskeletal stiffening due to its accumulation at the periphery as well as a more compliant nuclear interior resulting from chromatin decondensation. In response to physiological forces, including shear stress in endothelial cells and compression in bones, we see a loss of mechanical integrity from progerin expression as evinced by reduced or completely absent sensitivity of chromatin dynamics to external force. This likely plays into the altered transcriptional profile of progerin-expressing cells and an inability to express mechanoresponsive genes due to this loss in chromatin mechanical sensitivity. Most prominently, Chapter V demonstrates a definitive link between cell mechanics, structure and genome organization and dynamics.

In Chapter VI, we explore the physical mechanisms regulating chromatin mobility at sites of a specific type of DNA damage called a double-strand break (DSB), which poses a dire threat to genetic stability and is implicated in cancer pathogenesis including leukemias and lymphomas. Chromatin mobility at DSBs is suggested to play a role in the likelihood of incorrect ligation of severed ends (translocation) given the correlation of translocation frequency with chromosome proximity. We examined the physical nature of DSB mobility in order to further elucidate the underlying mechanism regulating it. Undamaged chromatin exhibits physical uniformity in its dynamics. By contrast, chromatin dynamics at DSBs become decoupled from the broader chromatin dynamics, coinciding with structural relaxation of chromatin that makes it more compliant for enhanced mobility at short time scales through its effect on D_{eff}. A coincident reduction in

molecular motor activity experienced at DSB sites decreases the time-dependence of the mobility through β, which curtails long range motion at longer time scales beyond a crossover time of ~30 minutes. This has consequences for the likelihood of translocations through the probabilistic effect on chromatin mobility. It also suggests chromatin remodeling complexes (through their effect on chromatin compliance) may act directly to mechanically isolate DSB sites, and we identify two proteins involved in that process (the SSRP1 subunit of the FACT complex and SIRT6). This work points to a promising avenue for the discovery of future cancer therapies associated with this maintenance of higher-order chromatin organization in the DNA damage response.

Chapter VII serves to incorporate our work more broadly on cell mechanics and how it is implicated in physiological processes. Specifically we focus on cytoskeletal force generation and cell deformability – of which the nucleus provides the most formidable obstacle – as related to stem cell injection and subsequent migration for therapies. As we show in previous Chapters, these phenomena are implicated in nuclear organization and chromatin maintenance.

Through the course of this Thesis, we develop an understanding of biological phenomena behind normal physiology and disease pathologies in a physical context. We find that the physical properties of the genome can be leveraged to resolve changes in its structure and organization through FLIM. Further, we demonstrate that alterations to the physical properties of chromatin accompanying biologically-derived changes influence the dynamics necessary for movement and reorganization to drive function. The intricacy of this physical

system is highlighted by contrasting features associated with dysfunction. We see the mere loss of normal function in a primary structural and mechanical element of the nucleus (lamin A) leads to complete loss in the integrity of chromatin higher-order organization and dynamics. Further, DNA damage – at least for DSBs – results in a decoupling of the chromatin network that otherwise attempts to transduce and uniformly distribute forces for ensemble motions. By contrast, in physiological changes, including stimulated reorganization for transcriptional activation, we see these forces serve to act globally and nonspecifically for enhancement of chromatin dynamics and to possibly drive remodeling. Thus, the cell can effectively exert control over chromatin structure and dynamics to appropriately tune the response for function. Our work reveals the dynamic, physical properties of the genome that illuminate integral aspects of its function with implications for human health and disease.

Future Outlook

This Thesis develops the physical understanding and framework for investigating dynamic aspects of genome regulation associated with higher-order structure and spatial organization within the nucleus. We aimed to unify the biological understanding of structure, organization and dynamics of the genome with its physical properties as a polymer.

With respect to chromatin dynamics, our work has mostly focused on ensemble averaged effects to develop this understanding without focusing on the subtle nuances that play out for individual particles. Yet, there is much

information to be gained in developing an understanding of single particle trajectories, where transient effects get averaged out in the ensemble. For instance, it is likely that local nuclear motors fleetingly exert their minute forces (relative to their cytoskeletal counterparts) on nearby chromatin loci – or even directly on a specific locus. While this has not been of interest to us in developing these techniques and the conceptual framework of the underlying physics, it is nonetheless of functional importance for specific biological scenarios. Additionally, single particle analysis would allow us to more comprehensively map nuclear organization of the genome as well as the local obstacles to chromatin fluctuations and dynamics that trap its motion. Investigating how this changes during functionally-derived condensation state alterations, among other physiological effects, would also lend better understanding of specific properties of distinct regions within the genome. Other work investigating more homogeneous and uniform ensemble probes of very similar chromatin domains could also serve to distinguish unique features of different chromatin environments. The time scale-dependent behavior associated with different sampling times, and resolving at which time scales certain biological phenomena come into play in the dynamics, would also be of interest.

The emergence of super-resolution fluorescence microscopy and its application to live-cell experiments will provide additional opportunities to advance our understanding of chromatin structure and dynamics. In particular, it will enable more precise investigation of distinct chromatin loci, where we currently require fluorescent tags (often repressor or activator proteins) covering

larger stretches of the linear sequence. For instance, we currently largely rely on the dissolution of DNA DSB repair foci as our measure of process completion, but single particle tracking coupled with super-resolution fluorescence microscopy may serve to provide a better understanding of the finer points of DSB mobility and end-to-end ligation.

The physical coupling and uniformity of chromatin dynamics also merits future investigation. While nuclear motor proteins are suggested to play a role in the transduction and coupling of these forces, we also point to chromatin structure itself as a mechanical element that facilitates this process. If nuclear motor proteins are the source, how they enable and control this physical coupling remains to be determined.

The precise cause-and-effect relationship of large scale forces, including those derived from the cytoskeleton, on driving chromatin remodeling also deserves attention. We showed VEGF stimulation drives enhanced chromatin dynamics early on through molecular motors. The cytoskeleton appears to facilitate this process based on our work with VEGF stimulation as well as by serving as a primary driving force of baseline chromatin dynamics in human cell nuclei. However, whether the cytoskeletal forces merely act to enhance chromatin mobility to enable coalescing with binding partners, or if these forces themselves also drive chromatin remodeling as suggested elsewhere, remains to be determined. Determination of how the biochemical factors behind this cytoskeletal reorganization play into the resulting chromatin dynamics would also yield meaningful mechanistic understanding, particularly for mechanical stimuli.

To this end, the diffusive exponent of chromatin dynamics (β) may serve as an intranuclear force sensor for investigating cytoskeletal or external forces. More broadly, determining how external or cytoskeletal mechanical forces fit into the coupling of chromatin dynamics remains important for understanding mechanoresponsive tissues as well as disease pathologies associated with dysfunction like progeria.

Our work has done much to develop the techniques to investigate the genome as a physical entity and build an understanding of its dynamic properties in the context of normal physiology and disease pathology. Yet, this field still remains a frontier where our understanding of the dynamic and physical genome developed here must be more unified with observations in biology. Unifying the theories of polymer physics, structure and rheology with biology will enable us to finally unveil the full complexity of genome function.

Appendix

Publications and Conference Proceedings Resulting from Thesis

Publications

Sairaam Ganesh, Zhao Qin, **Stephen T. Spagnol**, Matthew T. Biegler, Kelli A. Coffey, Agnieszka Kalinowski, Markus J. Buehler and Kris Noel Dahl.
"The tail domain of lamin B1 is more strongly modulated by divalent cations than lamin A"
Nucleus, Epub ahead of print (2015).

Elizabeth A. Booth-Gauthier, **Stephen T. Spagnol** and Kris Noel Dahl
"Mechanobiology of the Endothelial Nucleus"
Book Chapter in *Mechanobiology of the Endothelium*, CRC Press 2015, 23-46.

Stephen T. Spagnol, Travis J. Armiger, Li Lan and Kris Noel Dahl
"Increased Chromatin Fluctuations are Localized to Regions of DNA Damage and Induced by Structural Relaxation"
Manuscript in Preparation (2015).

Stephen T. Spagnol and Kris Noel Dahl
"Spatially resolved quantification of chromatin condensation through differential local rheology in cell nuclei fluorescence lifetime imaging"
Invited Manuscript in Review (2015).

Stephen T. Spagnol, Weichun Lin, Elizabeth A. Booth, Benoit Ladoux, Hillard M. Lazarus and Kris Noel Dahl
"Early passage dependence of mesenchymal stem cell mechanics influences cellular invasion and migration"
Manuscript in Review (2015)

Elizabeth A. Booth*, **Stephen T. Spagnol*** and Kris Noel Dahl
"Nuclear stiffening and chromatin softening with progerin expression leads to an attenuated nuclear response to force"
Manuscript in Review (2015).
*These Authors contributed equally

Stephen T. Spagnol*, James S. Weltz*, Yongqiang Xue* and Kris Noel Dahl
"Mechanical Coupling of the Endothelial Cytoskeleton and Nucleus with VEGF Stimulation"
Cellular and Molecular Bioengineering, 7(2) 2014, 225-230.
*These Authors contributed equally

Stephen T. Spagnol and Kris Noel Dahl
"Active cytoskeletal force and chromatin condensation independently modulate intranuclear network fluctuations"
Integrative Biology, 6(5) 2014, 523-531.

Podium Presentations

Stephen T. Spagnol and Kris Noel Dahl
"Quantification of *in situ* chromatin condensation using fluorescence lifetime imaging (FLIM)"
Biomedical Engineering Society Annual Meeting, Tampa Bay, FL, October 7-10, 2015.

Stephen T. Spagnol, Elizabeth A. Booth and Kris Noel Dahl
"Altered Nuclear Rheology and Cellular Force Transduction Highlight Reduced Mechanosensitivity in Premature Aging"
American Institute of Chemical Engineers Annual Meeting, Atlanta, GA, Thursday, November 20, 2014.

Stephen T. Spagnol and Kris Noel Dahl
"Alterations of Structure and Mechanics in Endothelial Cells Treated with VEGF"
American Institute of Chemical Engineers Annual Meeting, Atlanta, GA, Thursday, November 20, 2014.

Alexandre Ribeiro, **Stephen T. Spagnol**, Hillard Lazarus, Stephen Badylak and Kris Noel Dahl
"Characterization of stem cell mechanical structures and the role of stiffness in survival and invasion"
Invited Keynote Lecture in "Stem Cell Mechanics" session at the 7th World Congress of Biomechanics in July 6-11, 2014.

Stephen T. Spagnol, Elizabeth A. Booth and Kris Noel Dahl
"Nuclear Structure and Reorganization in Endothelial Cell Responsiveness to VEGF"
American Institute of Chemical Engineers Annual Meeting, San Francisco, CA, Friday, November 8, 2013.

Stephen T. Spagnol and Kris Noel Dahl
"Mechanical Enhancement of VEGF Intracellular Signaling in Endothelial Cells"
American Institute of Chemical Engineers Annual Meeting, San Francisco, CA, Thursday, November 7, 2013.

Stephen T. Spagnol, James S. Weltz and Kris Noel Dahl
"Microrheology of VEGF-Stimulated Nuclear Reorganization in Endothelial Cells"
American Institute of Chemical Engineers Annual Meeting, Pittsburgh, PA, Thursday, November 1, 2012.

Stephen T. Spagnol, James S. Weltz and Kris Noel Dahl
"Nuclear Mechanics of VEGF-Stimulated Endothelial Cells"
American Institute of Chemical Engineers Annual Meeting, Pittsburgh, PA, Monday, October 29, 2012.

Kris Noel Dahl, **Stephen T. Spagnol** and Elizabeth A. Booth
"Multiscale Engineering Analysis of Nuclear Structure"
Invited lecture at The American Society for Cell Biology Annual Meeting, Denver, Colorado, December 3-7, 2011.

Poster Presentations

Stephen T. Spagnol, Elizabeth A. Booth, Turi Alcoser and Kris Noel Dahl
"Progerin-Induced Reduction of Nuclear Territories"
Progeria Research Foundation Scientific Workshop, Bethesda, Maryland, April 24-26, 2013.

Stephen T. Spagnol, Elizabeth A. Booth and Kris Noel Dahl
"Temporal alteration of nuclear structure and stiffness accompany gene expression changes from force and cytokine treatment"
American Society for Cell Biology Annual Meeting, San Francisco, California, December 15-19, 2012.

Kris Noel Dahl, **Stephen T. Spagnol** and James S. Weltz
"Extracellular Chemical Stimuli and Mechanotransduction"
American Institute of Chemical Engineers Annual Meeting, Pittsburgh, PA, October 2012.

Elizabeth A. Booth, **Stephen T. Spagnol** and Kris Noel Dahl
"Cells Exhibit a Threshold Dependent Nuclear Reorganization Response to Shear Stress"
Poster presentation at The American Society for Cell Biology Annual Meeting, Denver, Colorado, December 6, 2011.